BETA-ADRENERGIC RECEPTOR SIGNALLING AND EXCITATION-CONTRACTION COUPLING IN THE HEART:
IMPACT OF CIRCADIAN RHYTHMS AND BETA-3 RECEPTORS

Thesis submitted for the degree of Doctor of Philosophy at the University of Leicester

by

Hayley Elizabeth Crumbie BSc (Hons), MSc

Department of Cardiovascular Sciences

University of Leicester

September 2015

BETA-ADRENERGIC RECEPTOR SIGNALLING AND EXCITATION-CONTRACTION COUPLING IN THE HEART: IMPACT OF CIRCADIAN RHYTHMS AND BETA-3 RECEPTORS

Hayley Crumbie

A time-of-day variation in myocardial contraction and its response to sympathetic stimulation of β-adrenoceptors (b-ADR) exists, which is reflected by time-of-day variations in intracellular calcium $[Ca^{2+}]_i$ regulation and electrical activity. There are three isoforms of β-ADR ($β_1/β_2/β_3$) and the functional outcome of each receptor differs. $β_1/β_2$-ADRs result in positive inotropism, whereas $β_3$-ADR induces a negative inotropic effect, associated with nitric oxide (NO) signalling.

The aims of this thesis were to determine the role of the $β_3$-ADR in the time-of-day variation in the response to sympathetic stimulation previously shown by our group and to investigate the role $β_1$-ADR, $β_2$-ADR and $β_3$-ADR play the control of Ca^{2+} regulation in isolated ventricular myocytes.

Ventricular myocytes were isolated during the rest-period (ZT3) and active-period (ZT15) of male Wistar rats by enzymatic digestion. $[Ca^{2+}]i$ was measured in myocytes loaded with Fura-2. Arrhythmic activity was determined from video imaging, myocytes were electrically field-stimulated at 1Hz. Measurement of action potentials, transient outward (I_{to}) and L-type calcium (LTCC) currents were made using whole-cell patch-clamp recordings.

Investigation of the time-of-day variation in response to sympathetic stimulation revealed a time-of-day variation in basal systolic $[Ca^{2+}]_i$ and in the increase in systolic $[Ca^{2+}]_i$ following β-ADR activation with ISO, greatest in rest-period (ZT3) myocytes. This did not appear to be governed by the time-of-day variation in action potential duration I observed or in the response of $β_3$-ADR agonist-induced stimulation.

Unlike conventional $β_1$-ADR, $β_2$-ADRs are tightly coupled to phosphodiesterase's (PDE) through the inhibitory G-protein (G_i). Our data suggests this coupling to G_i and PDE activation is responsible for the reduced response of systolic Ca^{2+} to $β_2$-ADR agonists, reducing the arrhythmic potential of $β_2$-ADR activation.

The reduction in systolic $[Ca^{2+}]_i$ by $β_3$-ADR activation with BRL_{37344} shows a time-of-day variation, with a greater negative inotropic response in rest-period (ZT3) myocytes, mediated via NO and PDE, leading to an increase in Sarco/Endoplasmic Reticulum Calcium ATPase (SERCA) activity but a reduction in SR Ca^{2+} content. This action contributes to an anti-arrhythmic action of the $β_3$-ADR agonist BRL_{37344} against $β_1$-ADR agonist induced arrhythmia.

The ability of $β_3$-ADR activation to reduce arrhythmic activity in response to further sympathetic stimulation is likely to exhibit a time-of-day variation. This work highlights the importance of chrono-pharmacology in the use of $β_3$-ADR agonists as a treatment in arrhythmia management.

Acknowledgements

Publications

In addition to the work presented in this thesis, I have contributed to a publication investigating remote ischemic preconditioning of cardiomyocytes. In brief, I determined the RMP of cardiomyocytes in response to a range of potassium concentrations to construct a calibration curve of the $DiBac_4(3)$ fluorescent signal used in the investigation.

Turrell HE, Thaitirarot C, Crumbie H and Rodrigo G. 2014. Remote ischemic preconditioning of cardiomyocytes inhibits the mitochondrial permeability transition pore independently of reduced calcium-loading or sarcKATP channel activation. *Physiol Rep*. 26;2(11).

Conference Abstracts

Physiology 2015, Cardiff, UK, 6th-8th July 2015
- The anti-arrhythmic role of β_3 adrenoceptors. Crumbie HE, Squires I. and Rodrigo G.

Joint British Society for Cardiovascular Research and British Atherosclerosis Society Spring meeting 2014, Manchester, UK, 2nd-3rd June 2014
- Diurnal Variation in Sympathetic Control of Excitation-Contraction coupling: The role of β3 Adrenoceptors and Nitric Oxide. Crumbie HE, Squires I. and Rodrigo G

IUPS 2013, Birmingham, UK, 21st-26th July 2013
- Diurnal Variation in Sympathetic Control of Excitation-Contraction coupling: The role of β3 Adrenoceptors and Nitric Oxide. Crumbie HE, Squires I. and Rodrigo G.
- The role of Nitric Oxide and calcium regulation in cardio-protection from remote ischaemic preconditioning. Thaitirarot C, Crumbie H and Rodrigo G.

Joint British Society for Cardiovascular Research and British Atherosclerosis Society Spring meeting 2013, London, UK, 3rd – 4th June 2013
- The depressed response of rat ventricular myocytes isolated during the active period to Isoproterenol does not reflect β3 adrenoceptor activity. Crumbie HE, Squires I. and Rodrigo G.
- The role of Nitric Oxide and calcium regulation in cardio-protection from remote ischaemic preconditioning. Thaitirarot C, Crumbie H and Rodrigo G.

Abbreviations

AC	Adenylate cyclase
Ach	Acetylcholine
AM	Acetoxymethyl
AMP	Adenosine monophosphate
ANOVA	Analysis of variance
ANS	Autonomic nervous system
APD	Action potential duration
APD30	Repolarisation of action potential to 30%
APD50	Repolarisation of action potential to 50%
APD90	Repolarisation of action potential to 90%
ARVM	Adult rat ventricular myocytes
ATP	Adenosine triphosphate
AV-node	Atrioventricular node
β-ADR	β- adrenoceptor
β$_1$-ADR	β-adrenoceptor 1
β$_2$-ADR	β-adrenoceptor 2
β$_3$-ADR	β-adrenoceptor 3
β$_4$-ADR	β-adrenoceptor 4
BP	Blood pressure
BSA	Bovine serum albumin
Ca^{2+}	Calcium ion
Ca^{2+}/CaM	Calcium-bound Calmodulin
[Ca^{2+}]$_i$	Intracellular calcium concentration
[Ca^{2+}]$_{SR}$	Sarcoplasmic reticulum calcium concentration
CaCl$_2$	Calcium chloride
CaM	Calmodulin
cAMP	Cyclic AMP
CBK	Cardiomyocyte-specific BMAL1 KO
CCD	Charge coupled device
CCM	Cardiomyocyte-specific CLOCK mutant
cDNA	Complementary DNA
cGMP	Cyclic GMP
CICR	Calcium-induced calcium release
Cl$^-$	Chlorine ion
CO	Cardiac output
CT	Crossing threshold
CVS	Cardiovascular system
DAD	Delayed after-depolarisation
DMSO	Dimethyl sulfoxide

DNA	Deoxyribonucleic acid
EAD	Early after-depolarisation
EC-Coupling	Excitation-contraction coupling
E_K	Equilibrium potential for K^+
E_{Na}	Equilibrium potential for Na^+
eNOS/NOS3	Endothelial nitric oxide synthase
FCS	Foetal calf serum
GHK	Goldman-Hodgkin-Katz
G_i	Inhibitory GTP binding protein
GPCR	G-protein coupled receptor
GRK	G-protein coupled receptor kinase
G_s	Stimulatory GTP binding protein
HCN	Hyperpolarisation-activated cyclic nucleotide-gated channels
HEPES	4-(2-Hydroxyethyl)piperazine-l-ethanesulfonic acid
HF	Heart failure
HR	Heart rate
I/R	Ischaemia/reperfusion
I_{Ca}	Calcium current
$I_{Cl(Ca)}$	Calcium activated chlorine current
I_{K1}	Inward rectifier potassium current
I_{Kr}	Delayed outward rectifier K^+ current, rapid
I_{Ks}	Delayed outward rectifier K^+ current, slow
I_{Kur}	Delayed outward rectifier K^+ current, ultra-rapid
I_{Na}	Inward sodium current
I_{NCX}	Reversible sodium/calcium current
iNOS/NOS2	Inducible Nitric oxide synthase
$I_{NS(Ca)}$	Non-selective calcium activated current
ISO	Isoproterenol
I_{to}	Transient outward K^+ current
K^+	Potassium ion
KO	Knock-out
L-NNA	N^G-nitro-L-arginine
LTCC	L-type Ca^{2+} channel
LV	Left ventricular
MI	Myocardial infarction
mRNA	Messenger RNA
Na^+	Sodium ion
$Na^+/K^+ATPase$	Sodium/potassium ATPase
NaCl	Sodium chloride
NaH_2PO_4	Sodium phosphate monobasic

NaOH	Sodium hydroxide
Na-pyruvate	Sodium pyruvate
NCX	Sodium/ Calcium exchanger
NHE	Sodium/ Hydrogen exchanger
nNOS/NOS1	Neuronal Nitric oxide synthase
NO	Nitric oxide
NOS	Nitric oxide synthase
OE	Overexpression
PCMA	Sarcolemmal Ca^{2+} ATPase
PCR	Polymerase chain reaction
PDE	Cyclic nucleotide Phosphodiesterase
PKA	Protein kinase A
PKG	Protein kinase G
PLB	Phospholamban
P_o	Open probability
PTx	Pertussis toxin
RMP	Resting membrane potential
RNA	Ribonucleic acid
ROS	Reactive oxygen species
RT	Reverse transcription
RT-qPCR	Quantitative real-time polymerase chain reaction
RyR2	Ryanodine receptor (Cardiac isoform)
SAN	Sino-atrial node
SCD	Sudden cardiac death
SCN	Suprachiasmatic nucleus
SEM	Standard error of the mean
SERCA	Sarcoplasmic/endoplasmic reticulum calcium ATPase
sGC	Soluble Guanylate cyclase
SR	Sarcoplasmic reticulum
SV	Stroke volume
TnC	Troponin C
TnI	Troponin I
TnT	Troponin T
T-tubules	Transverse tubules
WT	Wild type
ZT	Zeitgeber time
ZT15	Zeitgeber time 15 (Active-period)
ZT3	Zeitgeber time 3 (Rest-period)

Table of Contents

Chapter 3: Time-of-day variation in Excitation-Contraction coupling in ventricular myocytes

Chapter 1: Introduction

1.1 Cellular mechanisms of cardiac Excitation-Contraction Coupling

Excitation-contraction coupling (E-C coupling), a term first coined in 1952, describes the cellular process underlying a single heartbeat. It is a rapid process, which begins with an electrical depolarisation and concludes with contraction and subsequent relaxation of the myocyte (Bers 2002). During E-C coupling, a transient increase in the intracellular concentration of calcium ions (Ca^{2+}) during the cardiac action potential is essential, as Ca^{2+} are the activators of contraction (Aaronson and Ward 2007).

1.1.1 The Ventricular Cardiac Action Potential

E-C coupling in the myocyte begins with an action potential and concludes with contraction of the heart. The action potential originates from pacemaker sinoatrial node (SAN) cells in the heart, and propagates excitation from myocyte to myocyte, allowing the heart to function in a syncytium both electrically and mechanically (Bers 2006). The ionic currents underlying the cardiac action potential are the potassium ion (K^+), sodium ion (Na^+), chloride ion (Cl^-) and Ca^{2+}, and the configuration of the action potential is governed by the movement of these ions through the their specific ion channels currents.

The configuration of the action potential varies across the ventricular myocardium, with shortest action potential duration (APD) at the apex and longest in cells located in the septum (Schram, Pourrier et al. 2002). The ventricular action potential displays a characteristic plateau phase, which results in a prolonged APD.

Species variation in ventricular action potential configuration and duration also exist (See Figure 1.1A), largely due to the expression of K^+ ion channels and to the relative contributions of these repolarising currents. Large mammals, for example guinea pigs and rabbits, have delayed repolarisation due to slow activating delayed rectifier currents, leading to a dome shaped action potential which is longer in duration. In smaller mammals such as the mouse and rat, the action potential has a more triangular morphology, due to a prominent transient outward current and a less defined plateau phase, leading to a shorter APD. The rat also displays lower amplitude delayed rectifier currents, I_{Kr} and I_{Ks}, during repolarisation as compared to the larger mammals.

A.

Rabbit   Guinea Pig   Rat

B.

C.

I_{Na} / Nav1.5

I_{CaL} / Cav1.2

$I_{Na/Ca}$

I_{to1} / Kv4.2/Kv4.3

I_{Ks} / Kv7.7

I_{Kr} / Kv11.1

I_{Kur} / Kv1.5

I_{K1} / Kir2.1
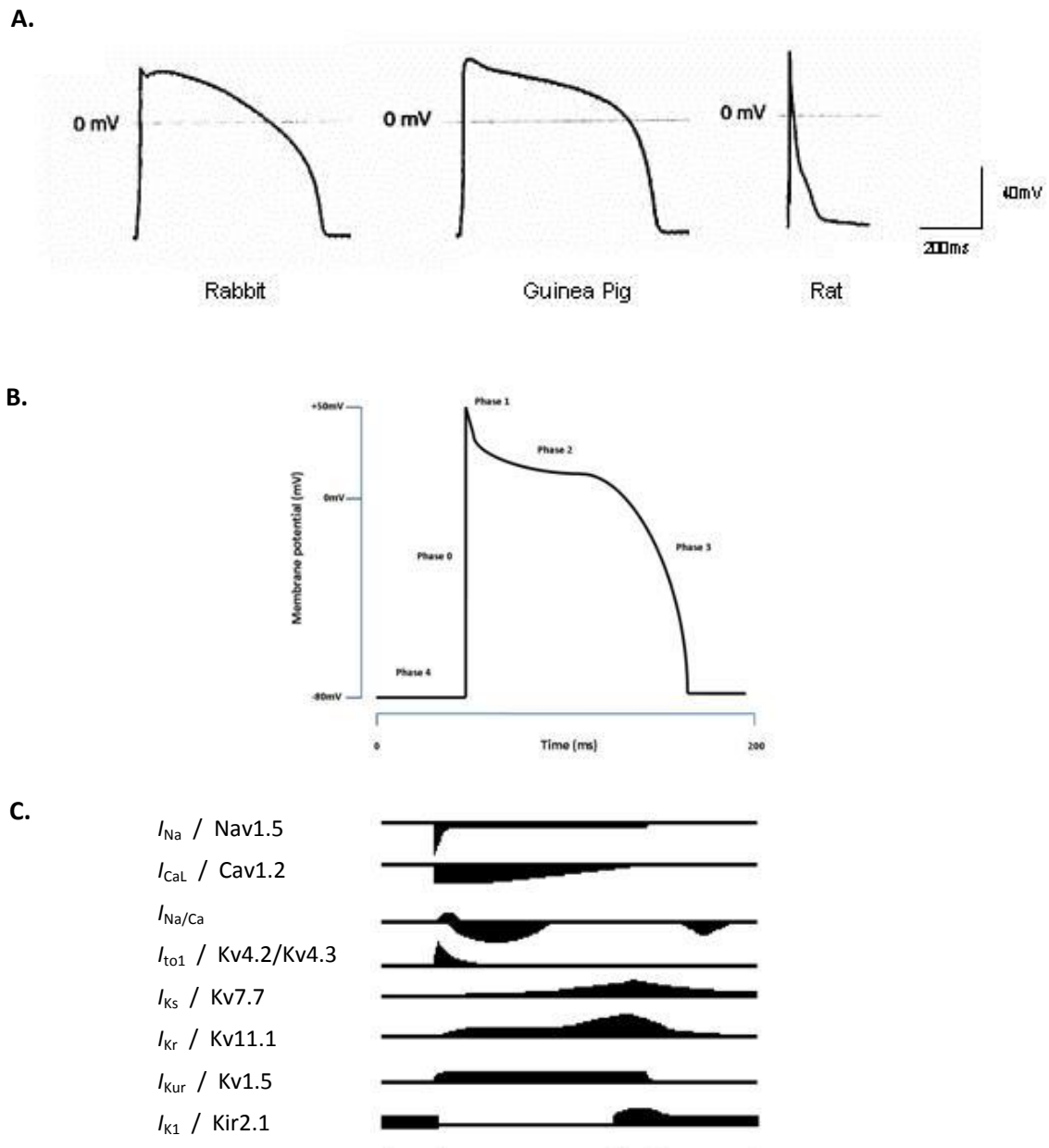
Figure 1.1   **The cardiac ventricular action potential (adapted from Varro *et al.* 1993 and Tamargo *et al.* 2004).**

A. This figure shows the configuration of the ventricular action potential (AP) in Rabbit, Guinea Pig and Rat isolated myocytes, adapted from (Varro, Lathrop et al. 1993).

B. This figure shows a schematic of the ventricular action potential, defining the 5 phases of the action potential (phase 0, 1, 2, 3, 4). Phase 4. The resting membrane potential (RMP) maintained by I_{K1}. Phase 0. The rapid upstroke phase, governed by I_{Na}. Phase 1. Early repolarisation phase, governed by I_{to}. Phase 2. The plateau phase, the balance between inward I_{Ca} and outward rectifying K$^+$ currents, I_{Kr} and I_{Ks}. Phase 3. Late repolarisation phase, governed by repolarising K$^+$ currents I_{K1}, I_{Kr} and I_{Ks}.

C. This figure shows the underlying ionic currents contributing to the cardiac action potential. This is illustrative only, to show the relative time course of currents and not the relative amplitudes. Adapted from (Tamargo, Caballero et al. 2004).

7

Despite the less defined plateau phase of the ventricular action potential in rat myocytes, there are no apparent differences in the amplitude and voltage dependence of the calcium current between the rabbit, guinea pig and rat (Varro, Lathrop et al. 1993). It is important to consider these variations in channel expression and current densities when selecting an animal model as the individual currents involved and resulting morphology of the action potential will differ between species.

Generation of the action potential marks the initiation phase of E-C coupling. The ventricular action potential is shown in Figure 1.1B and the underlying currents responsible for the different phases are shown in Figure 1.1C. action potential configuration is defined by 5 phases (phase 0, 1, 2, 3, 4).

Phase 4: The resting membrane potential (RMP) maintained by inward rectifier current, I_{K1}.

Phase 0: The rapid upstroke phase, governed by rapid inward Na$^+$ current, I_{Na}.

Phase 1: Early repolarisation phase, governed by the transient outward potassium current, I_{to}.

Phase 2: The plateau phase, a balance between an inward calcium current through L-type Calcium channels (LTCC), and outward rectifying K$^+$ currents, I_{Kr} and I_{Ks}.

Phase 3: Late repolarisation phase, governed by repolarising K$^+$ currents, the inward rectifier current, I_{K1}, and the outward rectifying I_{Kr} and I_{Ks} currents.

The individual phases of the action potential will be discussed in greater detail below.

Phase 4:   **Resting membrane potential**

This phase represents cardiac diastole, where electrical and contractile activity of the myocyte is at rest.

RMP is generated by the difference Na$^+$, K$^+$, Cl$^-$ and Ca^{2+} ion concentrations across the myocyte membrane. At rest extracellular Na$^+$ and Ca^{2+} concentration are relatively high and K$^+$ concentration is low, whereas intracellular concentrations of K$^+$ are relatively high and levels of Na$^+$ and Ca^{2+} are low.

The RMP of the ventricular myocyte is approximately -70 to -80mV, a figure close to the equilibrium potential for K$^+$ (E_K) (Bers 2001). The E_K is calculated by the Nernst equation, which determines the membrane potential at which no net movement of ions will occur (Hille 2001):

$$E_K = \frac{RT}{zF} \ln \frac{[K^+]_o}{[K^+]_i}$$

E_K *= Equilibrium potential of potassium*

R *= Gas constant*

T *= Absolute temperature*

z *= Ionic valency*

F *= Faradays constant (9.65 x 10^4 mol^{-1})*

$[K^+]_o$ *= Extracellular potassium concentration*

$[K^+]_i$ *= Intracellular potassium concentration*

Ion	Nernst equilibrium potential (mV)
K$^+$	-89
Na$^+$	+70
Cl-	-55
Ca^{2+}	+125

Table 1.1 Nernst equilibrium potentials for potassium (K$^+$), sodium (Na$^+$) chloride (Cl$^-$) and calcium (Ca^{2+}) ions (Bers 2001).

It is the difference between the Nernst equilibrium potential (see Table 1.1) and the cells actual membrane potential which is the driving force for ion movement across the cell membrane down its electrochemical gradient via ion specific channels during the action potential (Bers 2001).

However, the Nernst equation cannot be used to determine the RMP within the myocyte as the membrane also is permeable to Na$^+$ and Cl$^-$ at rest. The Goldman-Hodgkin-Katz equation can be used to calculate the membrane potential developed in a membrane permeable to more than one ion, as the equation takes into account the ionic currents and

the relative permeability for ion for which specific ion channels are open (Levick 2003), taking in to account the membranes permeability to K$^+$, Na$^+$ and Cl$^-$ at rest (Hille 2001):

$$V_m = \frac{RT}{F} \, log_{10} \, pK \frac{[K^+]_o}{[K^+]_i} + pNa \frac{[Na^+]_o}{[Na^+]_i} + pCl \frac{[Cl^-]_i}{[Cl^-]_o}$$

R   *= Gas constant*

T   *= Absolute temperature*

F   *= Faradays constant (9.65 x 10^4 mol^{-1})*

pNa   *= Relative membrane permeability for sodium*

pK   *= Relative membrane permeability for potassium*

pCl   *= Relative membrane permeability for chloride*

V_m   *= Membrane potential*

$[K^+]_o$ *= Extracellular potassium concentration*

$[K^+]_i$ *= Intracellular potassium concentration*

$[Na^+]_o$ *= Extracellular sodium concentration*

$[Na^+]_i$ *= Intracellular sodium concentration*

$[Cl^-]_o$ *= Extracellular chloride concentration*

$[Cl^-]_i$ *= Intracellular chloride concentration*

The resting myocyte is preferentially permeable to K$^+$ due to the open state of the channels of the inward rectifier current, I_{K1}, so called due to their ability to pass larger inward currents at membrane potentials negative to E_K than outward currents at membrane potentials positive to E_K (Lu 2004). K$^+$ flow down their chemical gradient out of the myocyte through open I_{K1} channels (Kir2.1) (Tristani-Firouzi, Chen et al. 2001), driving membrane potential towards the equilibrium potential for K$^+$ (E_K), -89mV (Bers 2001). However, RMP never reaches E_K due to the cell membrane being slightly permeable to Na$^+$, 1/100th of its permeability to K$^+$, but it is sufficient to cause a very small, inward background Na$^+$ current which raises membrane potential 10-20mV positive to E_K (Levick 2003). The Na$^+$/K$^+$-ATPase pump in the sarcolemma is electrogenic, driving 2 K$^+$ into the cell for every 3 Na$^+$ extruded, removing more positive charge from the cell than it drives into the cell, creating a hyperpolarising current, which may be up to -10mV depending on the activity of the pump (Klabunde 2005).

Phase 0:   The rapid upstroke of the action potential

Membrane depolarisation leads to the opening fast Na^+ channels (Nav1.5) once membrane potential is positive of -55mV (Nerbonne and Kass 2005). Once threshold is reached and channels open, the membrane becomes more permeable to Na^+, increasing conductance 100 fold (Levick 2003). This generates a large and rapid inward Na^+ current (I_{Na}) resulting in the rapid upward stroke of the cardiac action potential and contributes to an overshoot as the movement of Na^+ down their electrochemical gradient driving the membrane potential towards the Na^+ equilibrium potential (E_{Na}) of +70mV. However the Na^+ channels activate and inactivate rapidly (Nerbonne and Kass 2005), only remaining open for ~1 millisecond (Grant 2009), preventing the membrane potential from reaching E_{Na} (Bers 2001). During this rapid upstroke of the action potential a small outward I_{K1} current remains active which also prevents membrane potential reaching E_{Na} (Levick 2003). The inactivation of Na^+ channels indicates the end of rapid depolarisation and the membrane potential peaks between +30mV and +50mV (Bers 2001). As Na^+ channels close, and conductance of the channels reaches zero, the K^+ current dominates and begins to repolarise the cell, which signals the beginning of the early repolarisation phase of the action potential (Bers 2001).

Phase 1:   The early repolarisation phase of the action potential

The early repolarisation phase of the action potential, during which the cell membrane undergoes a rapid but incomplete repolarisation, is the result of the closure of Na^+ channels and activation of the transient outward current (I_{to}), a K^+ outward current. The I_{to} activates rapidly at potentials positive to -30mV and is comprised two current types, based on the kinetics of current inactivation and recovery from steady-state inactivation, a fast component ($I_{to,fast}$), current flow mediated by Kv4.2 and Kv4.3 channels, and a slow component ($I_{to,slow}$), current flow mediated by Kv1.4 channels (Nerbonne and Kass 2005; Grant 2009). Pharmacological studies have revealed that the current is composed of K^+ current (I_{to1}) and a Ca^{2+} activated Cl^- current (I_{to2}) in the ventricle (Grant 2009), however the existence of I_{to2} is controversial (Nerbonne and Kass 2005).

I_{to} is quickly inactivated, and so repolarisation is brief but does not return the membrane potential to resting levels (Bers 2001). The I_{to} is important for setting the level at which the plateau phase of the action potential occurs, with early repolarisation setting the driving

force for Ca^{2+} entry and I_{Ca} in the myocyte, enhancing Ca^{2+} influx though the LTCC and Sodium Calcium Exchanger (NCX) (Grant 2009). The rat myocardium expresses a high number of Kv4.2 channels (Schram, Pourrier et al. 2002), and has a strong I_{to} (Varro, Lathrop et al. 1993), this causes the plateau phase to occur at a more negative membrane potential than in species with a lower expression of Kv4.2 channels (Nerbonne and Kass 2005).

Phase 2: **The plateau phase**

The cardiac action potential is longer in duration than a skeletal muscle action potential due to the unique presence of the plateau phase (Grant 2009) during which there is little change in membrane potential. The long APD results in a delayed on set of repolarisation, preventing electrical re-excitation before full relaxation has occurred, thereby preventing tetanisation of the cardiac muscle (Bers 2001).

During the plateau phase, there is a small, but prolonged inward flux of Ca^{2+} down their concentration gradient through voltage gated L-type Ca^{2+} channels (LTCC/Cav1.2 channels), giving rise to a Ca^{2+} current. The LTCC are located in the T-tubules, they activate rapidly and the current is long lasting due to the slow inactivation of LTCC (Grant 2009). The LTCC are activated by depolarisation of the membrane at potentials positive to -40mV, however little Ca^{2+} entry via the LTCC occurs during the upstroke of the action potential or during early repolarisation, despite membrane potentials positive to -40mV and so does not contribute to the rapid upstroke phase of the action potential. The LTCC are unable to pass current near the peak of the action potential as LTCC are slow to activate, but also due to a low I_{Ca} driving force at potentials close to the reversal potential for I_{Ca}, ~+50mV. At the peak of the action potential, ~+40mV, the driving force for Ca^{2+} entry is low. The I_{to} and early repolarisation phase of the action potential is essential to increase the driving force of I_{Ca} during the plateau phase of the action potential (Bers 2008).

Ca^{2+} entry during this plateau phase is essential for E-C coupling, as Ca^{2+} entry through LTCC is the main trigger for release of Ca^{2+} from the sarcoplasmic reticulum (SR) which inititates contraction (Bers 2002).

Cardiac cells also express transient type (T-type) channels, found in the atrial and pacemaker cells of the SAN, but are absent from ventricular cells and so do not contribute to Ca^{2+} entry in the ventricular myocyte (Grant 2009).

The NCX an electro-genic plasma membrane transport protein located on the sarcolemma of the ventricular myocardium, can also contribute to Ca^{2+} entry during the early portion of the plateau phase of the action potential, but plays a lesser role than the LTCC. The stoichiometry of the NCX is 3 Na^+ for 1 Ca^{2+}, creating a net movement of positive charge (I_{NCX}). The NCX can function in a "forward-mode"; extruding Ca^{2+} from the cell in exchange for Na^+, creating an inward I_{NCX}, or in "reverse-mode"; extruding Na^+ from the cell in exchange for Ca^{2+}, generating an outward I_{NCX} (Bers 2002). The direction and amplitude of the I_{NCX} is dependent upon the membrane potential and on the transmembrane concentration gradients of Na^+ and Ca^{2+}, which sets the reversal potential of the NCX (Sher, Noble et al. 2008). Following the depolarisation phase of the action potential, the intracellular concentration of Na^+ ($[Na^+]_i$) in the space just beneath the membrane, termed the "fuzzy space", is high. This rapid increase in $[Na^+]_i$ and the more positive membrane potential causes the NCX to work in "reverse-mode", extruding Na^+ from the cell, leading to an influx of Ca^{2+}, contributing to the enhanced $[Ca^{2+}]_i$ (Bers 2002).

During the plateau phase of the action potential there is little change in membrane potential as the inward I_{Ca} is balanced by outward delayed rectifier K^+ currents, the rapid delayed rectifier current, I_{Kr}, and the slow delayed rectifier current, I_{Ks} (Bers 2001). Cardiac cells also express an ultra-rapid delayed rectifier current, I_{Kur}, however this is absent in the ventricle and so does not contribute to repolarisation of the ventricular action potential (Nerbonne and Kass 2005). The delayed rectifiers are named due to their delayed activation following a membrane depolarisation (Manis 2014). The I_{Kr}, despite its name, activates relatively slowly upon membrane depolarisation, although faster than I_{Ks}, and activates at relatively negative potentials, inwardly rectifying membrane potential at positive potentials (Veldkamp, van Ginneken et al. 1995). Conducted by the Kv11.1/hERG channels, I_{Kr} recovers from inactivation quickly (Schmitt, Grunnet et al. 2014) and the current is small in amplitude (Nerbonne and Kass 2005). I_{Ks}, conducted by Kv7.7/minK channels, activate at a slower rate than I_{Kr}, as the β-subunit of the minK channel inhibits activation (Barhanin, Lesage et al. 1996) and at more positive potentials (Veldkamp, van Ginneken et al. 1995). The delayed rectifier K^+ currents are activated at ~-30mV, but due to their relatively slow activation do not contribute to the early repolarisation phase of the action potential (phase 1), instead playing a role in opposing the inward I_{Ca} during the plateau phase of the action potential. However the current densities of I_{Kr}/I_{Ks} are small and so have little ability to repolarise the membrane (Nerbonne and Kass 2005) but the

matched inward and outward currents slow repolarisation until membrane potential reaches ~-20mV (Aaronson and Ward 2007), at which point repolarisation accelerates toward resting membrane potential as LTCC inactivate and the sustained I_{Kr}/I_{Ks} promote repolarisation (Bers 2001; Nerbonne and Kass 2005).

The opposing currents, I_{Ca} and I_{Kr}/I_{Ks}, and the resulting plateau phase of the action potential exists in a delicate balance, and any change in the conductivity of any one of the ion channels or the current density of the currents will affect the APD as the length of the plateau phase is altered (Bers 2001).

Phase 3:   **The late/rapid repolarisation phase**

Phase 3 represents the repolarisation phase of the AP from the plateau to RMP. It is due to a combination of inactivation of LTCC and a rise in K^+ conductance.

During the late/rapid repolarisation phase of the action potential, the inward I_{Ca} falls off as LTCC are inactivated and the driving force for net Ca^{2+} movement declines. In addition the conductance of the K^+ ion channels increase so that K^+ conductance dominates, driving the membrane potential towards E_K (Bers 2001).

Due to the slow inactivation of the I_{Kr} and I_{Ks} channels, the currents remain active during phase 3 repolarisation (Grant 2009), but the inward rectifier current, $I_{K1,}$ also becomes active as membrane potential declines towards resting levels. The I_{K1} does not possess a voltage-sensor, but at positive potentials little current passes due to a block of channels by to intracellular Mg^+. The I_{K1} does not pass current at voltages positive of -20mV (Schmitt, Grunnet et al. 2014). As the delayed rectifier currents I_{Kr} and I_{Ks} drive membrane potential to more negative potentials this blockade is removed and the I_{K1} current increases in amplitude (Grant 2009), accelerating repolarisation towards E_K and restoring RMP.

The NCX is also thought to contribute to repolarisation during phase 3 of the action potential (Sher, Noble et al. 2008). As mentioned previously, the direction and amplitude of the I_{NCX} is dependent upon the membrane potential and on the transmembrane concentrations of Na^+ and Ca^{2+}. Following the plateau phase of the action potential, the concentration $[Ca^{2+}]_i$ is high, inducing the NCX to work in "forward-mode", extruding Ca^{2+} from the cell, causing an outward I_{Ca} during the rapid repolarisation phase of the action potential (Bers 2001).

1.1.2 Cardiac contraction

An influx of Ca^{2+} via the LTCC during the plateau phase of the action potential is essential for successful E-C coupling, as an increase in $[Ca^{2+}]_i$ is the initiator of contraction (See Figure 1.2A).

The structural unit of the myocyte responsible for contraction is the sarcomere, which contains thick and thin myofilaments, composed of myosin and actin respectively. The myosin filament contains myosin heads, which extend outward to form complexes (cross-bridges) with the actin myofilament. The actin myofilament is coupled to tropomyosin, which interacts with the troponin complex (Gaine 2014), comprised of troponin C (TnC), a Ca^{2+} receptor, troponin I (TnI), an actin-myosin reaction inhibitor, and troponin T (TnT), a binding protein which interacts with TnI. The cardiac isoform of TnC contains two high affinity and one low affinity Ca^{2+} binding sites. The high affinity sites are always bound to Ca^{2+}, providing a structural anchoring of TnC to the troponin complex, allowing for interaction with TnI (de Tombe 2003). During resting states, when $[Ca^{2+}]_i$ is low, contraction is inhibited as the low affinity Ca^{2+} binding sites of TnC are unoccupied causing the interaction between TnC and TnI to be weak. This weakened interaction allows the interaction between TnI and actin to be strengthened, causing the troponin-tropomyosin complex to lie between the actin and myosin filaments, blocking myosin binding sites preventing cross-bridge formation (Bers 2001; Bers 2008; Gaine 2014). For contraction to occur Ca^{2+} must bind to the low affinity Ca^{2+} binding site of TnC. When $[Ca^{2+}]_i$ is raised above diastolic levels, >100nM, Ca^{2+} binds to the low affinity Ca^{2+} binding sites on TnC, strengthening the interaction with TnI, leading to a conformational change in the troponin-tropomyosin complex, freeing up the myosin actin binding site. This promotes actin and myosin cross-bridge formation, sliding the myofilaments across one another using Adenosine triphosphate (ATP) as an energy source, shortening the sarcomere resulting in shortening of the muscle, increased force and a contraction (Bers 2001; Bers 2008; Gaine 2014).

Cardiac contraction is regulated by Ca^{2+}, which in the majority of mammals is released from the sarcoplasmic reticulum (SR) in a phenomenon known as calcium-induced calcium-release (CICR), following a trigger from an influx of Ca^{2+} through the LTCC and by "reverse-mode" NCX during the cardiac action potential (Cannell and Kong 2012). Depolarisation of the membrane to potentials positive of -40mV activates the LTCC (See

figure 1.2). During the plateau phase, membrane potential of the myocyte remains close to 0mV, during which Ca^{2+} enters the intracellular space via LTCC, generating an inward LTCC (Bers 2002).

LTCC is the main mechanism of Ca^{2+} entry during E-C coupling, however small amounts of Ca^{2+} can also enter the cell via the NCX. As previously described (See Introduction 1.1.1) Ca^{2+} influx on the NCX occurs early in the action potential and may contribute to CICR (Bers 2002; Bers 2008). Ca^{2+} entry via the NCX is thought to be small in amplitude and short-lived, as Ca^{2+} entry via LTCC and Ca^{2+} release from the SR increases local $[Ca^{2+}]_i$, promoting "forward-mode" I_{NCX} and Ca^{2+} efflux (Bers 2008). The role of the NCX in triggering CICR is still debated (Bers 2008; Sher, Noble et al. 2008; Cannell and Kong 2012), with some experimenters finding the NCX is able to induce Ca^{2+} release from the SR (Goldhaber 1999), and others unable to detect Ca^{2+} release from the SR in the absence of LTCC (Adachi-Akahane, Lu et al. 1997). Up to 50-70% NCX are situated in the T-tubules (Sher, Noble et al. 2008), as so are well placed to affect Ca^{2+} release from SR stores, however co-localisation to SR Ca^{2+} release channels, ryanodine receptors (RyR2), is not well established, with estimates of only 6% of NCX co-localised to RyR2 in rat myocytes (Scriven, Dan et al. 2000).

The LTCC channels are mainly located in the T-tubular system of the myocytes sarcolemmal - SR junction, where the cardiac isoform of SR Ca^{2+} release channels, ryanodine receptors (RyR2) are located (Bers 2002). Each myocyte has around 20,000 junctions, with between 10 to 25 LTCC and 45 to 100 RyR2 which are densely clustered into groups between the surface membrane and the SR, known "couplons" (Cannell and Kong 2012). The entry of Ca^{2+} at the junction between the sarcolemma and the SR due to I_{Ca} through the LTCC triggers a co-ordinated opening of RyR2 and Ca^{2+} release from the SR, flooding the cytoplasm with Ca^{2+}; CICR (Bers 2008).

The release of Ca^{2+} through a cluster of RyR2 is known as a "Ca^{2+} spark". In the absence of an electrical impulse from an action potential, un-coordinated Ca^{2+} sparks naturally occur in quiescent cells, releasing Ca^{2+} from the SR though a cluster of RyR2. These Ca^{2+} sparks are not dependent upon an increase in $[Ca^{2+}]_i$ through the LTCC to initiate. The action potential co-ordinates these Ca^{2+} sparks, opening thousands of RyR2 simultaneously, giving rise to a synchronised Ca^{2+} release from the SR, which results in the Ca^{2+} transient

A.

200ms

B.
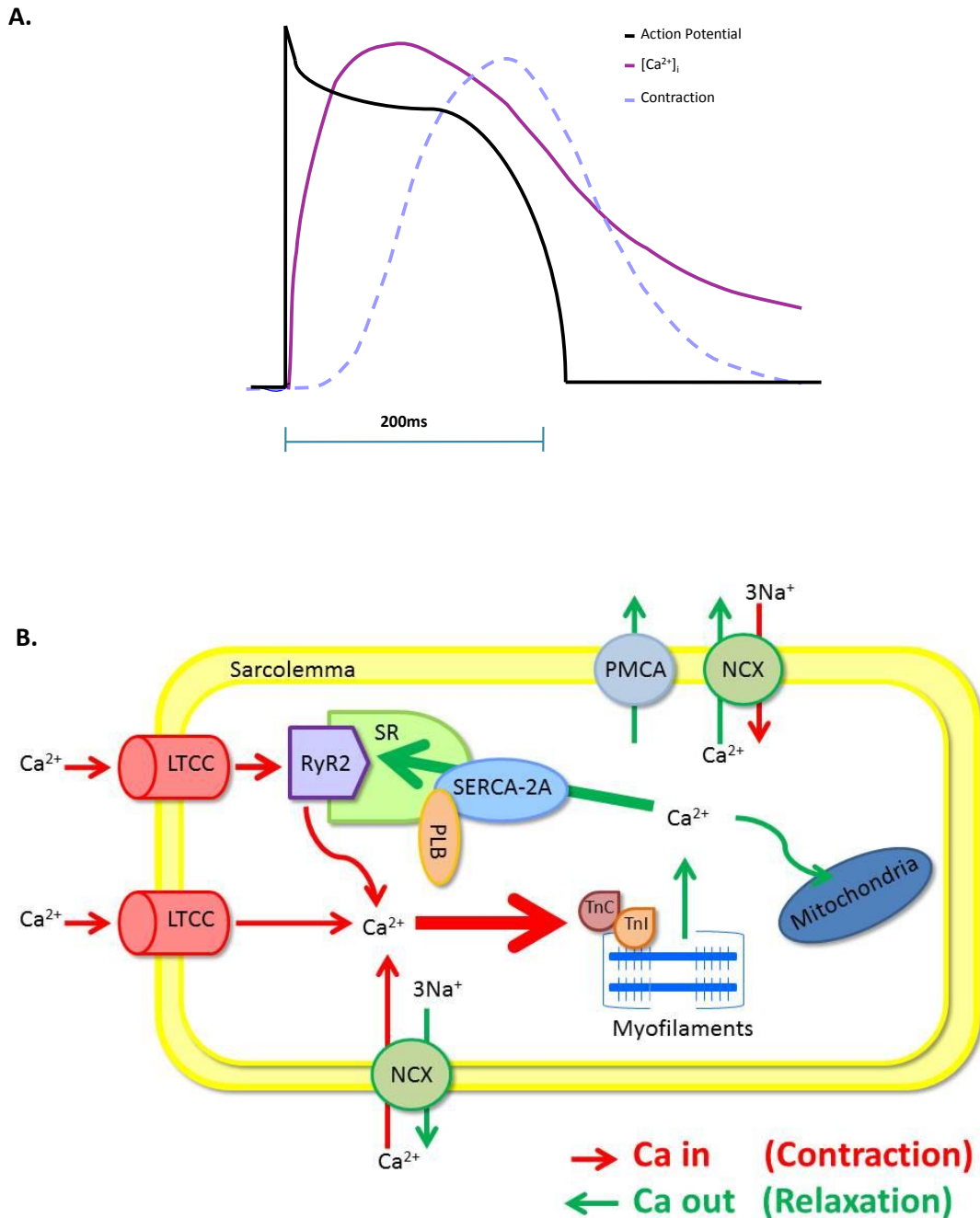
Figure 1.2 **A schematic showing the time course of a cardiac action potential, intracellular calcium ([Ca^{2+}]$_i$ transient and contraction of the heart and of Ca^{2+} transport processes involved in E-C coupling during a single heartbeat. Adapted from (Bers 2001).**

A. A schematic showing the time course of a cardiac action potential, intracellular calcium ([Ca^{2+}]$_i$ transient and contraction of the heart.

B. A schematic of Ca^{2+} transport processes involved in E-C coupling during a single heartbeat, showing the L-type calcium channels (LTCC), sarcoplasmic reticulum (SR), ryanodine receptors (RyR2), Troponin C (TnC), Troponin I (TnI), Sarcoplasmic Reticulum Calcium ATPase pump (SERCA-2A), sodium calcium exchanger (NCX), the sarcolemmal ATPase pump (PMCA) and the mitochondrial uniporter.

Routes of Ca^{2+} entry and release in the cell during contraction, in systole, are shown in red.
Routes of Ca^{2+} removal from the cytosol during relaxation in diastole are shown in green.

17

and leads to contraction (Cheng and Lederer 2008).

The close grouping of LTCC and RyR2 in "couplons" means a space of only 12nm exists between LTCC and RyR2, facilitating the action potential co-ordinated CICR in a process known as local control. The I_{Ca} through LTCC during the plateau phase of the action potential causes a local increase in $[Ca^{2+}]_i$. This leads to a rapid response of local RyR2, increasing their open probability (P_o) leading to CICR. The RyR2 are relatively insensitive to Ca^{2+}, providing stability for the CICR, ensuring RyR2 P_o is low at resting levels, preventing CICR in diastole (Cannell and Kong 2012).

CICR floods the cytoplasm with Ca^{2+} from stores in the SR, initiating contraction by allowing the binding of Ca^{2+} to TnC and causes the conformational changes in the contractile myofilaments generating force (Bers 2001). CICR also contributes to the closure of LTCC. Inactivation of the LTCC is both voltage- and Ca^{2+} dependant, and impairment off either type of inactivation can prolong the APD (Yamada, Ohta et al. 2008). Voltage-dependant inactivation is slower than Ca^{2+}-dependant inactivation and as a consequence, Ca^{2+}-dependant inactivation is the main source of inactivation of LTCC during E-C coupling (Zipes 2014), with SR release of Ca^{2+} responsible for inactivation of 90-95% LTCCs (Bers 2008). Ca^{2+}-dependant inactivation is modulated by CaM. When levels of $[Ca^{2+}]_i$ are high, following CICR, Ca^{2+} binds to high affinity sites on CaM, which interacts with LTCC channel, thereby accelerating deactivation of the LTCC and limiting I_{Ca} (Bers 2008).

Release of Ca^{2+} from stores in the SR during CICR are responsible for 90% of the $[Ca^{2+}]_i$ in the rat (Wier, Egan et al. 1994), however the amount of Ca^{2+} released via the RyR2 is dependent upon a number of factors including the stores of Ca^{2+} in the SR ($[Ca^{2+}]_{SR}$) (Bers 2002), on the amount of Ca^{2+} entering the cell via I_{Ca} (Bassani, Yuan et al. 1995), which is indirectly linked to the amplitude and kinetics of the action potential, and on the activity of the RyR2 and its regulatory proteins (Bers, 2008).

The $[Ca^{2+}]_{SR}$ stores are rarely emptied during CICR and it is reported only 50%-90% of $[Ca^{2+}]_{SR}$ is released (Bassani, Yuan et al. 1995; Bers 2008), although this is species dependant. The mechanism preventing the total depletion of SR Ca^{2+} stores is not yet fully determined and a number of mechanisms have been proposed.

It has been traditionally thought that as $[Ca^{2+}]_{SR}$ declines, the release gates of RyR2 favour closure (Bers 2008). More recently Calsequestrin (CASQ) has been proposed as a molecular basis for deactivation of the RyR2 following a release of Ca^{2+} from the SR, acting as a luminal Ca^{2+} sensor. CASQ is a Ca^{2+}-dependant regulatory protein localised to the SR (Gyorke and Terentyev 2008), which is bound to approximately 50-75% of Ca^{2+} taken up by the SR in the rat (Bers 2001; Gyorke and Terentyev 2008). CASQ has been proposed to inhibit P_o of the RyR2 when SR Ca^{2+} levels are low i.e. following CICR, due to its interaction with junctin (Gyorke and Terentyev 2008). Junctin is an intra-SR protein which forms a complex with CASQ and RyR2 at the SR membrane (Altschafl, Arvanitis et al. 2011). It has been proposed that at low luminal concentrations of Ca^{2+}, following CICR, CASQ binds to junctin, inhibiting RyR2 P_o, but as the luminal concentration of Ca^{2+} increases following the reuptake of Ca^{2+}, Ca^{2+} concentration inhibits CASQ binding to junctin, relieving CASQ inhibition on the RyR2, increasing their P_o (Gyorke and Terentyev 2008). However, at any one time the P_o of the RyR2 is determined by luminal and cytoplasmic concentrations of Ca^{2+} and so CASQ may not be the only mechanism for RyR2 closure.

Another suggestion for the mechanism of RyR2 closure of is 'stochastic attrition', an all-or-none behaviour, whereby the closure of a number of one or more RyR2 allows local $[Ca^{2+}]_i$ to decline to a level whereby the remaining RyR2 in the "couplon" favour closure. However, this model of RyR2 closure becomes problematic when considering the number of RyR2 present in a "couplon". It is possible that the lattice formation of RyR2 helps to overcome this problem via 'coupled gating', which is the theory that the physical state of one RyR2 within a cluster can affect the gating of adjacent channels, making the cluster behave as if it were comprised of a smaller number of RyR2 (Cannell and Kong 2012).

1.1.3 Cardiac relaxation

In order for the heart to function optimally, relaxation of the myocyte during diastole must occur, to allow adequate time for ventricular filling prior to subsequent contraction during systole. For relaxation to occur Ca^{2+} must first dissociate from the low affinity binding site on TnC, which occurs in response to a decline in $[Ca^{2+}]_i$ during the repolarisation phase of the action potential, and the dissociated Ca^{2+} must then be removed from the cytosol. Relaxation is initiated by the closure of LTCCs, reducing I_{Ca} and thereby inhibiting the

release of Ca^{2+} from SR via RyR2, allowing time for replenishment of SR Ca^{2+} stores (Bers 2001).

There are a number of routes by which Ca^{2+} can be transported out of the cytosol; Sarco-endoplasmic reticulum Ca^{2+} pump (SERCA), the NCX, the plasmalemmal ATPase pump (PMCA) and the mitochondrial Ca^{2+} uniporter (See figure 1.2).

SERCA is a Ca^{2+} transport pump present in skeletal and cardiac muscle, and removes Ca^{2+} from the cytosol by sequestering Ca^{2+} back to the SR. SERCA returns Ca^{2+} to the lumen of the SR from the cytosol using ATP as an energy source. For Ca^{2+} transport to occur, two Ca^{2+} and one molecule of ATP are required to bind to high affinity binding sites on the cytosolic membrane of SERCA. Binding of Ca^{2+} to the transmembrane regions of SERCA creates a pore for Ca^{2+} to enter the SR, and addition of a phosphate to SERCA by the transfer of the terminal phosphate from ATP induces "ion occlusion", preventing Ca^{2+} from returning back to the cytosol. This ATP phosphorylation of SERCA also reduces the affinity of the Ca^{2+} binding site for Ca^{2+}, allowing Ca^{2+} to be released into the lumen of the SR, thereby increasing $[Ca^{2+}]_{SR}$. (Bers 2001). The activity of cardiac SERCA isoform (SERCA-2A), unlike the skeletal muscle isoform, is regulated by Phospholamban (PLB), an endogenous inhibitor of SERCA in its unphosphorylated state, slowing the removal of Ca^{2+} from the cytoplasm. Phosphorylation of PLB, by cyclic-AMP dependant protein kinase (PKA) during β-adrenergic stimulation for example, relieves it's inhibition of PLB of SERCA, increasing the Ca^{2+} affinity of SERCA 2-3 fold and thereby increasing the activity of SERCA, allowing for a faster decline of $[Ca^{2+}]_i$ (Bers 2002; Zipes 2012). SERCA is considered a 'fast' system of Ca^{2+} removal during the repolarisation phase of the action potential (Bers 2002; Bers 2008) and is the primary Ca^{2+} extrusion mechanism in mammals, although the reliance on SERCA is species dependant. In the rat, SERCA is responsible for approximately 90-95% of the decline of Ca^{2+} due to a greater density of SERCA in the rat cardiac tissue (Bers 2008), however SERCA is responsible for only 70% Ca^{2+} removal in large mammals such as rabbits, guinea pig, and humans (Bers 2008).

Ca^{2+} can also be transported out of the cytosol by removal from the myocyte by the NCX, accounting for approximately 5-8% of Ca^{2+} extrusion in rats and mice (Bers 2008). The exchange of Ca^{2+} for Na by the NCX is reversible and is dependent upon membrane potential and Na^+ and Ca^{2+} concentration gradient across the sarcolemma. Immediately

following contraction, the levels of $[Ca^{2+}]_i$ are high and membrane potential is repolarising, this favours "forward-mode" of the NCX to work in extruding Ca^{2+} from the cell contributing to a decline in cytosolic $[Ca^{2+}]$ (Bers 2001).

Ca^{2+} removal from the cytosol by the activity of SERCA and NCX combined accounts for 98-99% of Ca^{2+} decline across most species (Bers 2002; Bers 2008). The remaining Ca^{2+} extrusion from the cytosol is completed by the 'slow' systems; sarcolemmal ATPase pump (PMCA) and mitochondrial Ca^{2+} uniporter, responsible for only 1-2% of Ca^{2+} removal and are unlikely to significantly contribute to the decline in Ca^{2+} during normal E-C coupling (Bers 2002).

To maintain steady state E-C coupling, over time it is crucial for Ca^{2+} influx to equal Ca^{2+} efflux over a number of cardiac beats to maintain stable Ca^{2+} homeostasis (Bers 2002; Eisner, Kashimura et al. 2009). Ca^{2+} efflux via NCX during relaxation must equal Ca^{2+} influx via the LTCC and the NCX during the plateau phase of the action potential, and Ca^{2+} returned to the SR via SERCA must equal Ca^{2+} originally released by the RyR2 in order to maintain SR stores of Ca^{2+} (Bers 2002). The consequence of an imbalance between Ca^{2+} influx and efflux, and/or transport into the SR (Bers 2002) can lead to cytosolic, SR and/or mitochondrial Ca^{2+} overload, leading to myocyte damage and can contribute to arrhythmia generation.

1.1.4 Calcium mismanagement and arrhythmia generation

Cardiac myocytes are highly specialised contractile cells, which conduct electrical impulses between cells enabling the heart to work as syncytium. Action potential generation from the SAN is a tightly regulated cellular process, triggering a co-ordinated contraction of the atria followed by the ventricles, providing a rhythmic pulsing of the heart propelling blood out of the ventricle and around the body. If this rhythm becomes irregular or unstable it is categorised as an arrhythmia. An arrhythmia can span the spectrum from a single isolated event in a single myocyte to uncoordinated disordered signalling in the whole heart. Ventricular arrhythmias are significantly more lethal than atrial arrhythmia as they directly affect the pumping capacity of the heart (Schmitt, Grunnet et al. 2014).

Arrhythmias can be classified as either abnormal depolarisations of the cell (spontaneous or triggered arrhythmias) or as re-entry arrhytmias. Re-entry arrhythmia occurs when a

propogating impulse fails to diminish after normal activation by the action potential and continues to re-excite the heart and activate contraction after refactory periods and before the next action potenital is fired, initiating extra beats, which can be continually propogated (Antzelevitch 2001). Triggered arrhythmias are abnormal depolarisations of the membrane that do not result from a normal action potential triggered by a wave originating from the SAN and can be classified as an early or delayed after-depolariasion, depending on the time frame of when the after depolarisation occurs (Bers 2001). Early after-depolarisations (EADs) occur during the plateau or repolarising phase of an action potential, whereas delayed after-depolarisations (DADs) occur after repolarisation is complete, before the next action potential is propagated (Bers 2001) and both are associated with an abnormal Ca^{2+} signalling and/or transport (Bers 2002) (See figure 1.3).

EADs and DADs generated in a single myocyte are not usually able to contribute to an arrhythmic depolarising wave of excitation, able to induce activation in well coupled tissue, as the depolarising current of a single myocyte is not of sufficient magnitude to depolarise the neighbouring myocytes. In normal tissue, the neighbouring myocytes which are not prone to after-depolarisations will cause the depolarising arrhythmic myocyte to repolarise alongside them, preventing propagation of a depolarising wave (Weiss, Garfinkel et al. 2010). However, if the after-depolarisation occurs in a cluster of cells, the magnitude of the depolarising current can be great enough to pass through the tissue causing a whole heart arrhythmia (Bers 2008).
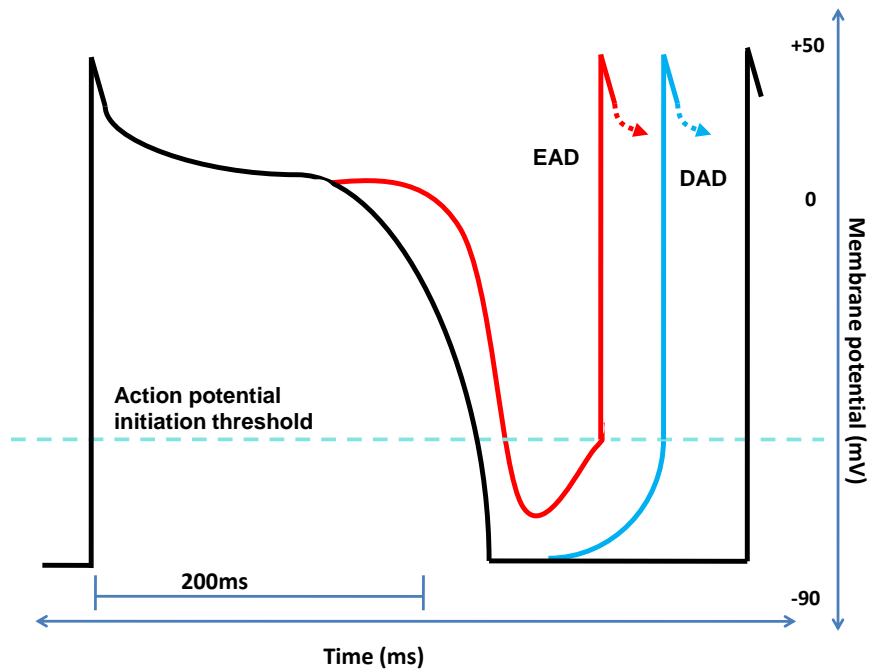
Figure 1.3   A schematic of the cardiac action potential, showing the initiation of early- and delayed- after depolariations, adapted from (Aaronson and Ward 2007).

This is a schematic showing the relationship between the normal action potential, early after-depolarisations (EADs) and delayed after-depolarisations (DADs).

The normal ventricular cardiac action potential is shown in black.

EADs (Red) are caused by a slowing or reversal of normal action potential repolarisation during the plateau or repolarising phase of an action potential.

DADs (Blue) occur after the action potential has fully repolarised.

1.1.4. Early after-depolarisations

EADs, defined as a secondary depolarisation during the plateau or repolarisation phase of the normal action potential (Schmitt, Grunnet et al. 2014). EADs occurring in the plateau phase of an action potential (phase 2) arise due to reactivation of LTCC, which are able to recover from voltage- and Ca^{2+}-dependant inactivation during long APDs (Bers 2001), and reactivate before the action potential is fully repolarised (Bers 2002). Work by January and Riddle, who were among the first groups to identify the role of LTCC in EADs, have shown there is a "vunerable window" during the plateau and repolarising phase of the action potential, whereby recovery from inactivation followed by depolarisation is possible, leading to an inward I_{Ca} current and development of an EAD. They showed that the amplitude of an induced EAD is enhanced by LTCC agonists and blocked by Ca^{2+} channel antagonists (January and Riddle 1989). The "vunerable window" lies between 30-90% of full repolarisation (APD_{30}-ADP_{90}) (Schmitt, Grunnet et al. 2014). Weiss *et al*. have shown that this re-depolarising window current occurs between -30mV and 0mV (Weiss, Garfinkel et al. 2010) which corrolates with the activation voltage of LTCC channels open, more positive than -40mV. As a consequence, EADs are more prone in cardiac cells with a long APD, such as ventricular myocytes (Bers 2001). This is due to a delayed repolarization in cells with a long APD, increasing the time interval of the "vulnerable window", increasing the probability of an EAD (Schmitt, Grunnet et al. 2014).

The NCX is also believed to be involved in facilitiaing a phase 2 EAD, but is not thought to able to induce a reversal of repolarisation by itself (Weiss, Garfinkel et al. 2010). As the largest proportion of Ca^{2+} removal from the cell during repolarisation is driven by SERCA, (90-95%) (Bers 2002), the NCX has little scope to innitiate an EAD. Instead the NCX is thought to crerate conditions whereby generation of an EAD is more probable.

Following the upstroke of the action potential (phase 0), Na^+ levels are high and membrane potential is positive, causing the NCX to favour "reverse-mode", extruding Na^+ from the cell and causing a Ca^{2+} influx. However, during the plateau phase (phase 2) and repolarisation (phase 3) of the action potential the NCX favours "forward-mode", extruding Ca^{2+} from the cell, replaced by a Na^+ influx, which becomes larger as repolarisation continues. In conditions of Ca^{2+} overload, e.g. heart failure (HF) or during β-adreneric stimulation, where $[Ca^{2+}]_i$ remains high during repolarisation, the NCX continues to favour "forward-mode", creating an Na^+ depolarising current which opposes

reolarisation. The influx of Na$^+$ by NCX cannot reverse repolarisation alone, however if [Ca^{2+}]$_i$ increases further, for example if the LTCC recover from inactivation and stimulate Ca^{2+} release from the SR, and the NCX continues to favour "forward-mode" this would increase the pobability of an EAD-triggered action potential (Weiss, Garfinkel et al. 2010).

An EAD can also occur during the repolarisation phase of an action potential (phase 3) when the membrane is undergoing repolarisation. Unlike EADs occuring in the plateau phase, EADs occuring during repolariastion cannot be attributed to LTCC as during repolarisation membrane potential falls below -40mV and the voltage-activated LTCC remain closed (Bers 2001). EADs initiated during a membrane potential below -40mV are thought to be caused by spontaneous CICR from the SR before the membrane has fully repolarised, appearing mechanistically similar to DADs (see below) (Bers 2008). A spontaneous CICR from the SR would cause the NCX to favour "forward-mode" and Ca^{2+} efflux, creating a Na$^+$ influx during the repolarisation phase resisting repolariastion. However, this is not thought to be suffcient to reverse repolarisation, but rather delays repolarisation sufficiently to to allow LTCC time to recover from inactivation (Weiss, Garfinkel et al. 2010).

1.1.4.2 Delayed after-depolarisations

DADs occur after an action potential has fully repolarised (phase 4), initiated by a spontaneous Ca^{2+} spark from the SR, elevating [Ca^{2+}]$_i$ and activating Ca^{2+} dependant depolarising currents during diastole, initiating a spontaneous action potential during diastole (Venetucci, Trafford et al. 2008). DADs are unable to initiate during phase 2 and 3 of the action potential due to the low availability SR Ca^{2+} after a CICR activated by an action potential (Bers 2001).

Cellular conditions which favour DAD are a high [Ca^{2+}]$_{SR}$ and a fast heart rate (HR) (Venetucci, Trafford et al. 2008), which are both a consequence of β-ADR (Bers 2001). An increased Ca^{2+} influx, e.g. via β-ADR increased LTCC, or a reduced Ca^{2+} efflux from the cell, leads to an increase in SR Ca^{2+} content. When [Ca^{2+}]$_{SR}$ is high, the likelihood of spontaneous Ca^{2+} sparks increases spark frequency and amplitude. If [Ca^{2+}]$_{SR}$ is sufficiently high, Ca^{2+} sparks can initiate Ca^{2+} waves which can propagate in myocytes, initiating a Ca^{2+}-activated transient inward depolarising current, depolarising the membrane (Venetucci,

Trafford et al. 2008; Eisner, Kashimura et al. 2009). If depolarising current is sufficient to reach threshold a spontaneous action potential initiates, a DAD (Bers 2008). There appears to be a 'threshold' SR Ca^{2+} content at which Ca^{2+} sparks will occur, which depends on the gating of the RyR2 (Venetucci, Trafford et al. 2008; Eisner, Kashimura et al. 2009). Conditions that favour RyR2 P_o will increase the likelihood of a Ca^{2+} spark. The P_o of the RyR2 is known to depend on both cytoplasmic and luminal $[Ca^{2+}]$. CASQ has been proposed to inhibit P_o of the RyR2 when $[Ca^{2+}]_{SR}$ levels are low, however in conditions of SR Ca^{2+} overload, the high luminal concentration of Ca^{2+} relieves CASQ inhibition on the RyR2, increasing their P_o (Gyorke and Terentyev 2008) which may increase DAD probability. Sympathetic stimulation also increases the likelihood of DAD development due to the increased SR Ca^{2+} load due to the increase LTCC and phosphorylation of PLB, increasing the activity of SERCA. The combination of increased Ca^{2+} influx and increased Ca^{2+} sequester back to the SR causes a loading of the SR (De Ferrari, Viola et al. 1995).

The Ca^{2+} spark does not initiate a DAD alone; it is the resulting Ca^{2+}-activated inward depolarising current which initiates the spontaneous action potential. There are 3 candidates proposed to be responsible for the transient inward depolarising current; NCX inward current, a Ca^{2+}-activated Cl^- current ($I_{Cl(Ca)}$) and a Ca^{2+}-activated non-selective cation current ($I_{NS(Ca)}$) (Schlotthauer and Bers 2000).

NCX inward current

During diastole, due to the negative membrane potential and low $[Na^+]_i$, the NCX favours "forward-mode", Ca^{2+} extrusion and Na^+ influx, causing a depolarising current which opposes RMP (Bers 2002). Following a spontaneous Ca^{2+} release from the SR the "forward-mode" I_{NCX} current increases, extruding Ca^{2+} from the cell causing an inward depolarising I_{Na} (Bers 2002).

Ca^{2+}-activated Cl^- current

Ca^{2+}-activated Cl^- current ($I_{Cl(Ca)}$) is an ionic channel with a low Ca^{2+} sensitivity, only activated at high $[Ca^{2+}]_i$. It has a reversal potential of approximately -50mV, which means it can be responsible for both a depolarising and a repolarising current through the movement of Cl^-. An efflux at -80mV would be sufficient to cause membrane depolarisation (Bers 2002).

Ca^{2+}-activated non-selective cation current

Ca^{2+}-activated non-selective cation current ($I_{NS(Ca)}$) has a reversal potential of approximately 0mV and so could also be responsible for a depolarising or a repolarising current, however there is little functional evidence for the contribution of the $I_{NS(Ca)}$ in ventricular myocytes (Bers 2002).

Schlotthauer and Bers propose the NCX to be responsible for >90% of DADs in rabbit ventricular myocytes, with the remaining 10% attributable to the $I_{Cl(Ca)}$ and suggesting no involvement of the $I_{NS(Ca)}$ (Schlotthauer and Bers 2000). However these findings are not conclusive as Wu and Anderson demonstrated that during blockade of the NCX and $I_{Cl(Ca)}$ currents, a residual transient inward depolarising current existed, which was sensitive to removal of extracellular cations, attributed to the $I_{NS(Ca)}$ (Wu and Anderson 2000).

The consensus is that the depolarising current is driven by the exchange of Ca^{2+} for Na^+ by the NCX (Venetucci, Trafford et al. 2008). The stoichiometry of the NCX, 3 Na^+ entering the cell in exchange for 1 Ca^{2+} leaving, leads to an influx of postive depolarising Na^+ current following a Ca^{2+} spark. If the Ca^{2+} release during the spark is small it can be balanced by a NCX efflux, maintaining the cyctolic $[Ca^{2+}]_i$ and therefore SR content, without creating a large depolarising current. However, when SR load and LTCC is high and the size of a Ca^{2+} spark increases. If suffciently large, the NCX will create a a large depolarising Na^+ current in an attempt to maintain the cyctolic $[Ca^{2+}]_i$, causing an upstroke of the action potential and initiation of a DAD (Venetucci, Trafford et al. 2008).

1.2   β-adrenergic control of cardiac Excitation-Contraction Coupling

The autonomic nervous system (ANS) consists of two opposing branches, the sympathetic and parasympathetic branches, which are a collection of neurons, originating from *the autonomic ganglia*. The sympathetic nervous system (SNS) is involved in the "fight-or-flight" response to stimuli, inducing in the myocardium an increase in HR (positive chronotropic effect), contraction (positive inotropic effect) and the rate of relaxation (positive lusitropic effect). The SNS regulates myocardial function, allowing the heart to respond to a stimulus within a matter of seconds. These changes in myocardial function are elicited by the binding of circulating catecholamines to adrenergic receptors (ADR) in the heart, particularly the beta-adrenoceptors (β-ADR) (Port and Bristow 2001).

1.2.1   β-adrenoceptors in the heart

The β-ADRs are G-protein-coupled receptors (GPCRs) located on the surface of cardiomyocytes. GPCRs are characterised by a 7 transmembrane domain structure, forming 3 intracellular and 3 extracellular loops. The N-terminal region of the receptor is extracellular and glycosylated with an intracellular C- terminus region (Strosberg 1997). The G-protein is a heterodimer consisting of G_α, G_β, G_γ sub-units. Agonist induced activation catalyses the exchange of guanosine tri-phosphate (GTP) for guanosine di-phosphate (GDP) on the G_α, resulting in the dissociation of the G_α and $G_{\beta\gamma}$ subunits, which are able to signal independently to induce changes in cardiac contractility and function. There are a number of β-ADRs expressed in the human heart: beta$_1$ (β_1-ADR), beta$_2$ (β_2-ADR), beta$_3$ (β_3-ADR) and beta$_4$ (β_4-ADR) (Moens, Yang et al. 2010), however levels of expression and functional outcomes of the receptors differ. The human heart expresses β_1-ADR, β_2-ADR and β_3-ADR subtypes, with a β_1-ADR : β_2-ADR/β_3-ADR ratio of 70:30 the atria and 80:20 ratio in the ventricle (Brodde, Bruck et al. 2006). Stimulation of the β_1-ADR and β_2-ADR subtypes induces a positive inotropic, chronotropic and lusitropic effect in cardiomyocytes and a positive dromotropic effect at the AV node (increased conduction velocity), whereas the β_3-ADR subtype activation induces a negative inotropic effect. Little is known about the β_4-ADR receptor subtype, but is thought to induce a positive inotropic effect. The β_1-ADR, β_2-ADR and β_3-ADR isoforms of β-ADR and their intracellular downstream cascades are shown in Figure 1.5 and will be discussed in greater detail.
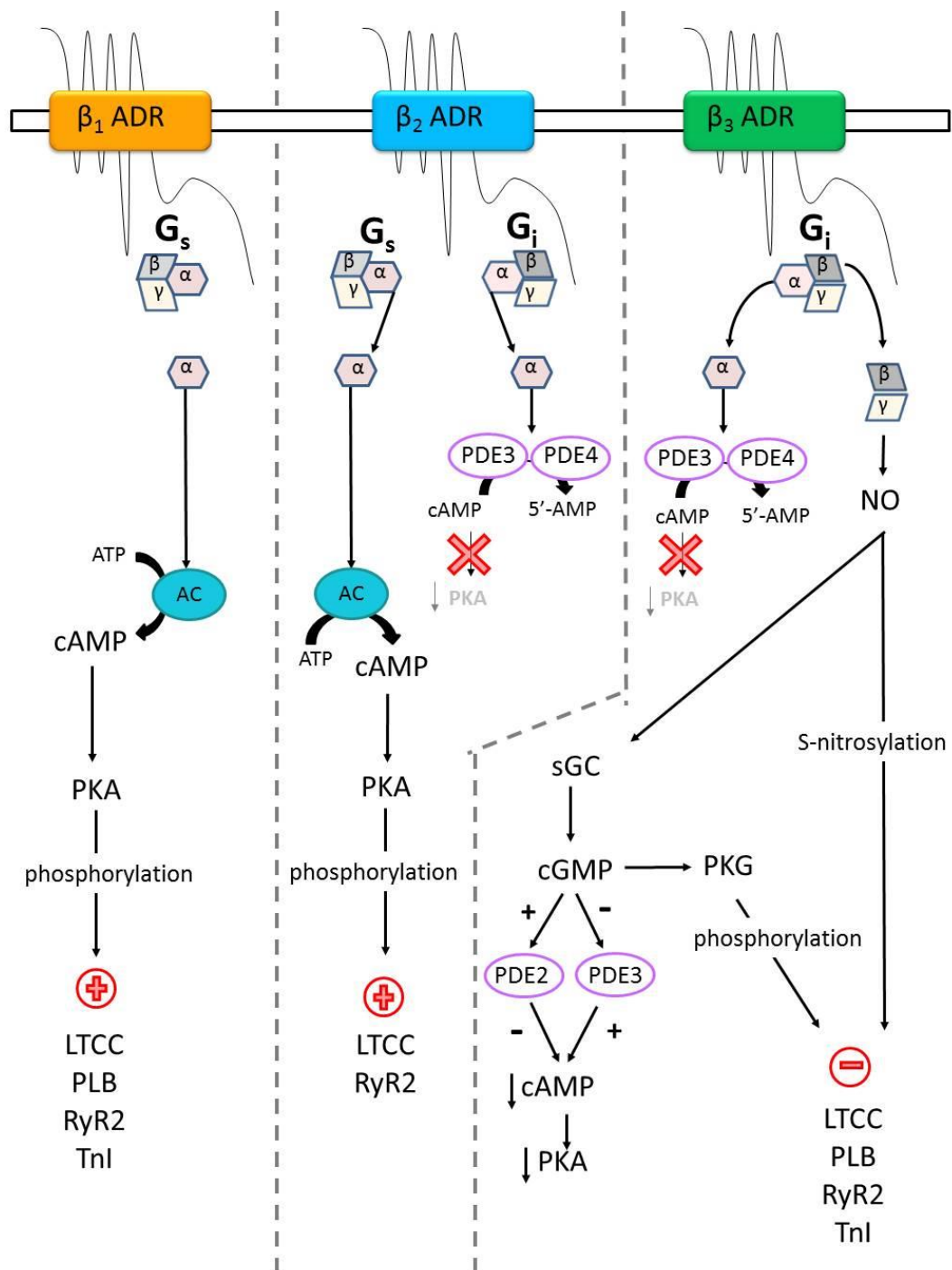
Figure 1.4   **A schematic of the β-adrenergic receptors in the ventricular myocardium**.
The figure shows the coupling of β_1-ADR, β_2-ADR and β_3-ADR isoforms of the β-adrenergic receptors (ADR) in the ventricular myocardium. The β_1-ADR is coupled to the stimulatory G-protein (G_s), inducing a positive inotropic effect. The β_2-ADR is bound to both G_S and the inhibitory G-protein (G_i). The β_3-ADR is coupled to G_i, inducing a negative inotropic effect.

Cell type	β_1-ADR	β_2-ADR	β_3-ADR
Atria	62%	30%	8%
Ventricle	73%	20%	7%
Aorta	25%	25%	50%
Mesenteric resistance artery	49%	49%	2%

Table 1.2 β-ADR expression in cell types of the heart and circulatory system. Estimated from (Brodde, Bruck et al. 2006), (Flacco, Segura et al. 2013) and (Dessy and Balligand, 2010).

The impact of sympathetic stimulation on ventricular myocytes, which results from binding of adrenaline and nor-adrenaline bind to β-ADRs, can be mimicked by the exogenous administration of the non-selective β-ADR agonist, isoproterenol (ISO). ISO preferentially activates β-ADR over α-ADR, and is a full agonist at all 3 β-ADR (Alexander, Benson et al. 2013). In fact, all 3 β-ADRs preferentially bind ISO over adrenaline and nor-adrenaline (Vrydag and Michel 2007). These agonists have different affinities for the β-ADR, adrenaline is preferential for the β_2-ADR ($\beta_2 > \beta_1 > \beta_3$) whereas nor-adrenaline ($\beta_1 = \beta_3 > \beta_2$) and ISO ($\beta_1 > \beta_2 > \beta_3$) are preferential for the β_1-ADR (Vrydag and Michel 2007). As the endogenous catecholamines and ISO, bind to all 3 β-ADR and so the effect of adrenaline, nor-adrenaline or ISO are the result of the combined activation of β_1–ADR, β_2–ADR and β_3-ADR (Bers 2001).

1.2.2 The β_1-adrenoceptor

Stimulation of the β_1-ADR produces positive inotropic and lusitropic effects in the myocyte and mediates its effect via the classical β-ADR/cAMP/PKA pathway.

The β_1-ADR is coupled to the stimulatory G_S, which as mentioned previously is comprised of G_α, G_β and G_γ subunits. Upon activation of the β_1-ADR by the binding of catecholamines' the G_α subunit dissociates and activates adenylate cyclase (AC). AC5 and AC6 are the dominant cardiac isoforms of AC (Defer, Best-Belpomme et al. 2000). AC catalyses the conversion of ATP to its second messenger; cyclic adenosine monophosphate (cAMP) whose primary target is protein kinase A (PKA). Once activated PKA phosphorylates several

target proteins in the ventricular myocyte involved in E-C coupling at specific serine and threonine residues, including LTCC, PLB, RyR2 and TnI (Bers 2001) (See Figure 1.5).

The increase in I_{Ca} following β-ADR stimulation is a classic observation, which is brought about by PKA phosphorylation of the LTCC at Ser1928 on the α-subunit and Ser478 and Ser479 of the β-subunit (Kamp and Hell 2000). PKA mediated phosphorylation increases the P_o and shifts the voltage-dependant activation to a more negative E_m. This increases I_{Ca} 2-4 fold during the action potential resulting in a larger Ca^{2+} influx (Bers 2001), providing a larger trigger for CICR, enhancing the amplitude of the Ca^{2+} transient (Bers 2002). PKA phosphorylation also slows inactivation of the LTCC, but functionally this is reversed Ca-dependant inactivation due to the larger I_{Ca}, and so overall, the LTCC inactivate faster (Bers 2002). The enhanced in I_{Ca} during β-ADR also tends to elevate the E_m of the plateau of the action potential (Bers 2001), however, β-ADR also increases I_{Ks} conductance (Walsh, Begenisich et al. 1988; Walsh and Kass 1988), and so the overall effect of β-ADR stimulation is a shortened APD with an elevated plateau phase E_m (Bers 2001).

PKA phosphorylation of RyR2 during $β_1$-ADR stimulation at Ser2808 (Marx, Reiken et al. 2000) and Ser2030 (Xiao, Jiang et al. 2005) increases sensitivity to activation by a Ca^{2+} trigger from the LTCC, increasing their P_o and increasing fractional release from the SR increasing systolic $[Ca^{2+}]_i$ (Bers 2001).

PKA phosphorylation of PLB at Ser16 reduces the inhibitory effect of PLB on the activity of SERCA, increasing SERCA activity by 2-3 fold increasing Ca^{2+} uptake into the SR, causing a faster decline in $[Ca^{2+}]_i$ (Bers 2001). The increased activity of SERCA increases the competition between SERCA and NCX for Ca^{2+} extrusion, and as SERCA dominates in the rat also results in greater amounts of Ca^{2+} sequestered back to the SR, resulting in an increase in SR Ca^{2+} content (Bers 2001).

The combined action of LTCC, RyR2 and PLB phosphorylation gives rise to the positive inotropic effect of $β_1$-ADR stimulation as the greater I_{Ca} results in a greater trigger for CICR, and the greater SR Ca^{2+} content and increased RyR2 sensitivity to Ca^{2+} allows for greater Ca^{2+} release by the RyR2 (Bers 2002).

As described above, the phosphorylation of PLB increases SERCA activity and therefore increasing the rate of Ca^{2+} sequester back to the SR leading to faster $[Ca^{2+}]_i$ decline (Bers 2001). TnI phosphorylation by PKA at Ser23 and Ser24 (Kobayashi and Solaro 2005)
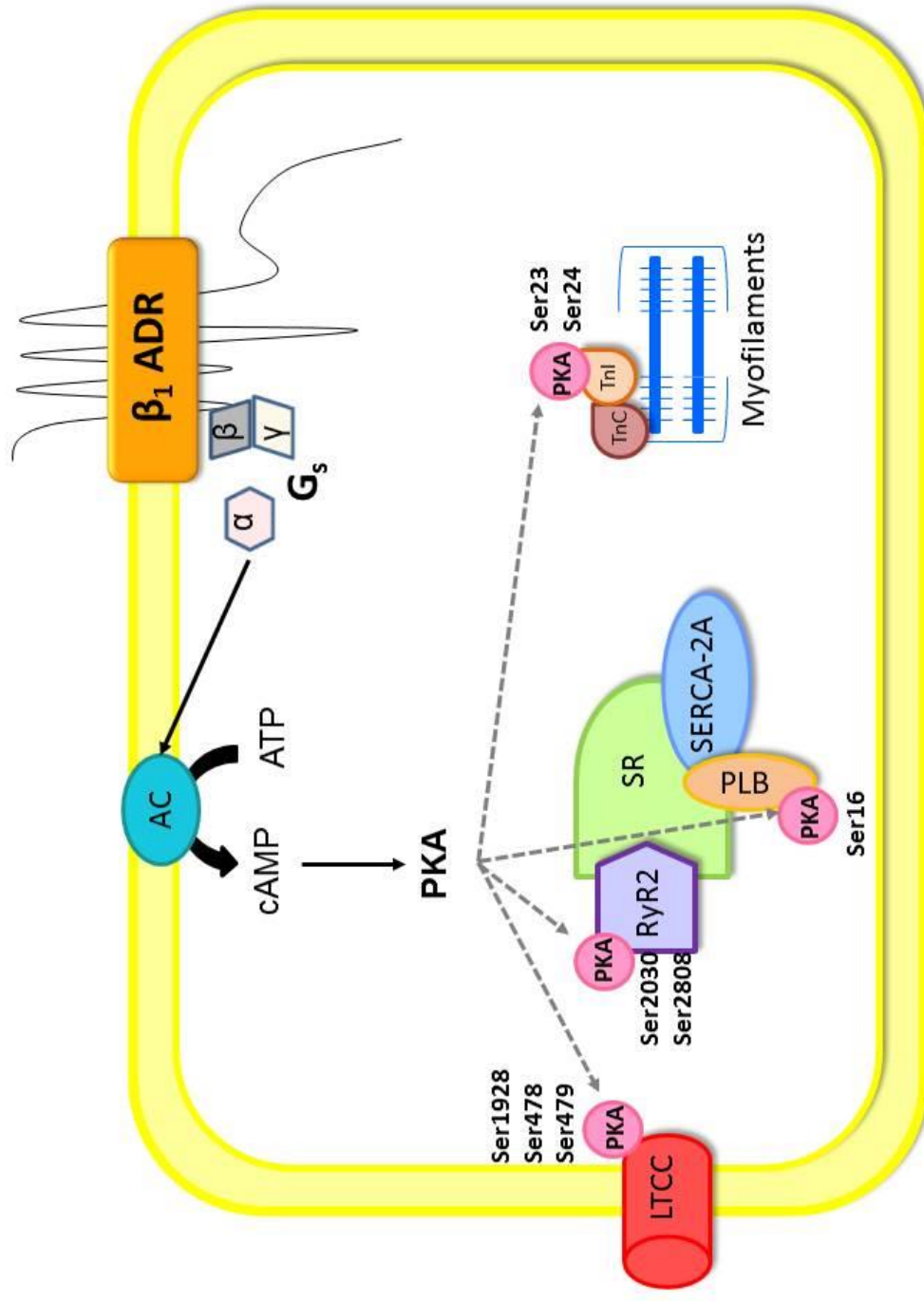
Figure 1.5   A schematic of β₁ -Adrenergic receptor activation and phosphorylation of targets relevant to excitation–contraction coupling.

Stimulation of the β₁ -Adrenergic receptor leads to the activation of PKA, able to phosphorylate a number of key E-C coupling proteins; L-type calcium channels (LTCC), Ryanodine receptors (RyR2), Phospholamban (PLB) and Troponin I (TnI), leading to the inotropic and lusitropic effects of β₁ -Adrenergic receptor stimulation.

decreases myofilament sensitivity to Ca^{2+}, promoting the release of Ca^{2+} from its binding site on TnC increasing the rate at which Ca^{2+} is released back into the cytoplasm for extrusion (by SERCA or NCX) facilitating an increased lusitropic effect (Solaro 2011). Alone this would reduce the force of contraction; however the increase in the Ca^{2+} transient (LTCC, RyR2 and increased SR Ca^{2+} loading) is sufficient to offset this (Bers 2002). Together the phosphorylation of PLB and TnI accelerate relaxation of the myocyte; the lusitropic effects of β_1-ADR stimulation.

The NCX is also affected by β-ADR stimulation however this is not due to PKA phosphorylation of the NCX , but instead due to the increased $[Ca^{2+}]_i$ following LTCC and Ca^{2+} release from the SR during CICR, stimulating Ca^{2+} extrusion from the cell in "forward-mode" (Bers 2001).

In the whole heart, β_1-ADR stimulation is associated with a chronotropic effect due to the effect on the SAN, increasing its firing rate and thereby increasing HR (Bers 2001), however this will not be discussed in detail here as this is not the brief for this investigation or introduction which concentrates on inotropism in ventricular myocytes.

1.2.3   The β_2-adrenoceptor

Like the β_1-ADR, β_2-ADR activation induces a positive inotropic response in the myocyte mediated via the β-ADR/cAMP/PKA pathway. β_2-ADR activation though its action on AC/cAMP/PKA can act upon the same components of E-C coupling as stimulation of the β_1-ADR. However β_2-ADR stimulation is unable to induce maximal inotropic contraction in the ventricle (Brodde, Bruck et al. 2006). Despite β_2-ADR stimulation inducing a greater AC activation (Lohse, Engelhardt et al. 2003), the inotropic effect of β_2-ADR stimulation is depressed as compared to β_1-ADR stimulation. Stimulation of β_1-ADR induces a global rise in cAMP in the myocyte, whereas β_2-ADR fails to induce a global rise, instead only inducing a local rise in cAMP levels, and so, all distal E-C coupling targets (PLB, TnI and possibly RyR2) are not phosphorylated (Xiao, Ji et al. 1995; Xiao, Avdonin et al. 1999; Xiao 2001; Heijman, Volders et al. 2011; Cros and Brette 2013).

β_2-ADR are coupled to the G_s mediated β-ADR/cAMP/PKA pathway but also to an inhibitory G-protein, G_i (Xiao and Lakatta 1993; Xiao, Ji et al. 1995). The dual coupling of
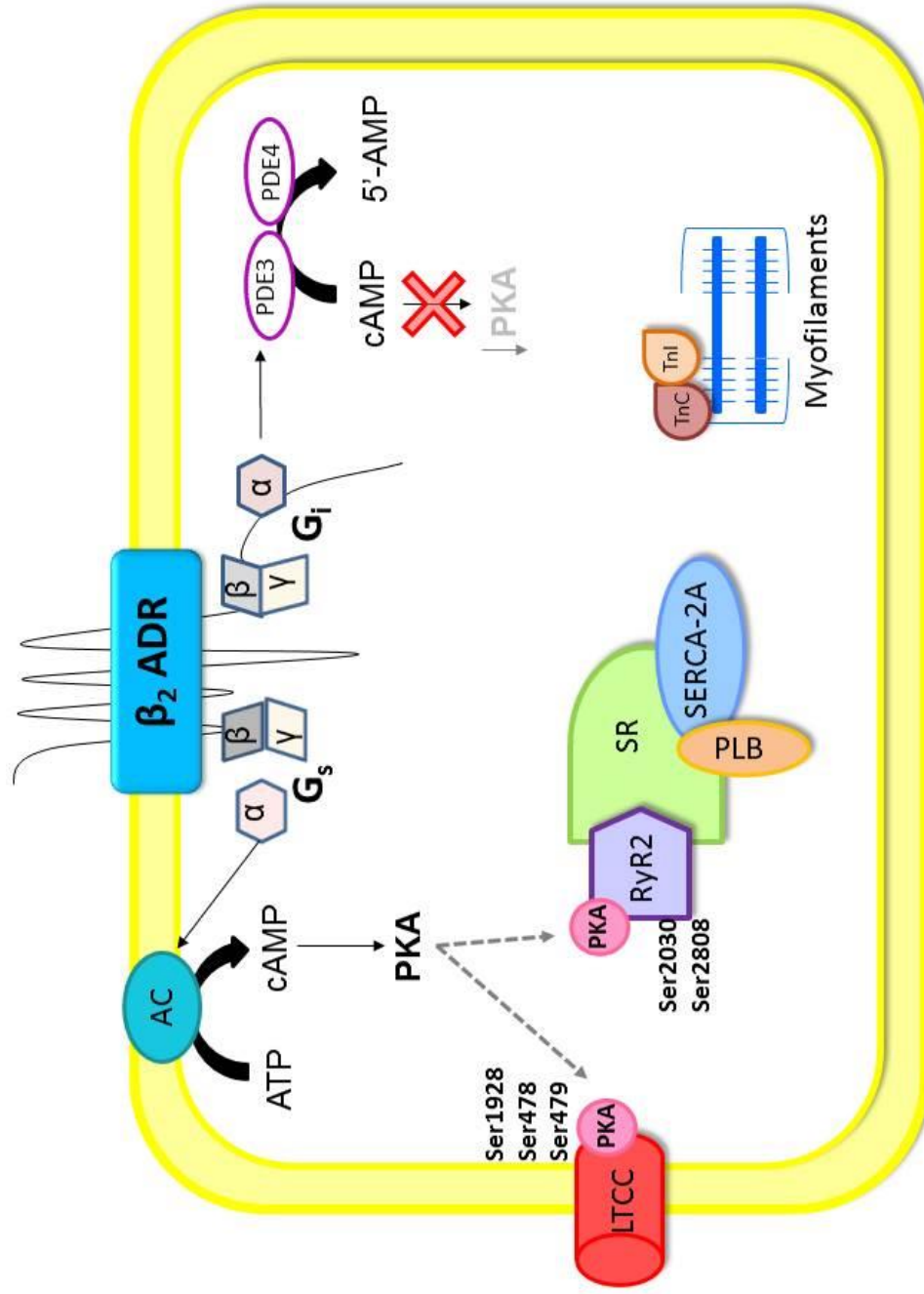
Figure 1.6   A schematic of β₂ -Adrenergic receptor activation and phosphorylation of targets relevant to excitation–contraction coupling.

The β_2-Adrenergic receptor (β_2-ADR) is dual coupled to G_s and G_i G-proteins. Stimulation of the β_2 -Adrenergic receptor leads to the activation of PKA via the G_s pathway which is able to phosphorylate local targets the L-type calcium channels (LTCC) leading to the inotropic effects of β_2 -Adrenergic receptor stimulation. Activation of the G_i pathway leads to activation of phosphodiesterase (PDE) PDE3 and PDE4 which hydrolyse cAMP, reducing levels of cAMP and PKA activation.

the β_2-ADR to has been described in a number of mammalian species, including rats (Xiao, Ji et al. 1995), mice (Sabri, Pak et al. 2000), sheep (Borea, Amerini et al. 1992), canines (Altschuld, Starling et al. 1995) and humans (Kilts, Gerhardt et al. 2000). Upon stimulation, the α-subunit of Gi ($G_{i\alpha}$) activates a number of phosphodiesterase (PDE) involved in the breakdown of cAMP. PDE3 and PDE4 are activated which hydrolyse cAMP to the inactive 5'-AMP (Berthouze, Laurent et al. 2011), limiting diffusion of cAMP into the cytosol and preventing PKA activation, limiting the inotropic effects of β_2-ADR stimulation.

1.2.3.1 Phosphodiesterases

PDE are enzymes which regulate the cellular levels of the second messengers cAMP and cyclic guanosine monophosphate (cGMP). The PDE selectively catalyse the hydrolysis of the 3'cyclic phosphate bonds of cAMP and cGMP. The PDE play an important role in modulating cellular function by controlling the rates of degradation of cAMP and cGMP, allowing for compartmentalisation of cAMP/cGMP signalling and therefore signal specificity (Bender and Beavo 2006).

Mammalian PDEs are encoded by 21 genes and are classified into eleven broad families (PDE1-11) based on the enzymatic properties, kinetic properties and sensitivity to inhibitors (Takimoto 2012). Genes within each family generate multiple isoforms and splice variants, each with a unique structure, regulatory and kinetic properties, cellular expression, and intracellular localization (Beca, Aschars-Sobbi et al. 2011).

The individual PDE families differ in multiple ways, including substrate specificity, regulation and tissue expression (Maurice et al., 2003) and this variation in substrate specificity and regulatory mechanisms allows for a cross talk between signalling pathways. Some PDE are specific for hydrolysis of cAMP (PDEs 4, 7 and 8), some are cGMP-specific (PDEs 5, 6 and 9) and others have dual specificity for cAMP and cGMP (PDEs 1-3, 10 and 11) (Bender and Beavo 2006).

The regulation of each PDE family also differs. PDE1 are the only PDE that are directly regulated by Ca^{2+}, through interaction with the Ca^{2+}/CaM complex. PDEs 2, 5 and 6 are activated via increases in cGMP levels, whereas PDE3 is inhibited by increases in cGMP levels (Francis, Blount et al. 2011).

Expression differs across tissue types, with the expression levels and subcellular distribution varying greatly between species. PDE 1-5 and 8 are expressed in the mammalian heart (Beca, Aschars-Sobbi et al. 2011).

PDE family	Substrate specificity	Regulation mechanism	Human tissue expression
PDE1	Dual cAMP/cGMP specificity	Ca^{2+}/CaM activated	**Heart**; Cardiomyocytes, Vascular smooth muscle and vascular endothelial cells. Brain, Kidney, Live, Pancreas, Thyroid
PDE2	Dual cAMP/cGMP specificity	cGMP stimulated	**Heart**; Cardiomyocytes and vascular endothelial cells) Brain, Endothelial cells
PDE3	Dual cAMP/cGMP specificity	cGMP inhibited	**Heart**; Cardiomyocytes, Vascular smooth muscle Platelets, White/Brown adipose tissue, Liver
PDE4	cAMP specific		**Heart**, Cardiomyocytes, Vascular smooth muscle Also Brain, Small intestine, Liver, Lung, Skeletal muscle, Reproductive system
PDE5	cGMP specific	cGMP stimulated	**Heart**; Cardiomyocytes, Vascular smooth muscle Also Vascular smooth muscle, Platelets
PDE6	cGMP specific	cGMP stimulated	Eye
PDE7	cAMP specific		Skeletal muscle, Brain, Kidney, Spleen, Reproductive system, Lungs, Thyroid
PDE8	cAMP specific		**Heart**; Cardiomyocytes Brain, Liver, Thyroid, Reproductive system
PDE9	cGMP specific		Brain, Kidney, Small intestine, Colon, Spleen
PDE10	Dual cAMP/cGMP specificity		Brain, Reproductive system
PDE11	Dual cAMP/cGMP specificity		Skeletal muscle, Reproductive system

Table 1.3 Summary of phosphodiesterase substrate specificity, isoform regulation and tissue expression in humans. Adapted from (Takimoto 2012) and (Francis, Blount et al. 2011).

1.2.3.2   β₂-adrenoceptor activation and phosphodiesterase activity

Upon stimulation of $G_{i\alpha}$, PDE3 and PDE4 are activated and modify the inotropic response of β₂-ADR stimulation in the heart (Bender and Beavo 2006; Rochais, Abi-Gerges et al. 2006; Gonzalez-Munoz, Fuente et al. 2009). PDE4 is cAMP specific and PDE3 has dual specificity for cAMP and cGMP. The affinity of PDE3 for cAMP and cGMP are similar, however the rate of cGMP hydrolysis is ~10% of the rate of cAMP breakdown (Francis, Blount et al. 2011).

In the heart, PDE3 and PDE4 mainly exist in the cytoplasm, thereby limiting cAMP diffusion though the cytoplasm and limiting the reach of cAMP and therefore PKA activation. However PDE are anchored to proteins of E-C coupling which may also limit the rise in cAMP around the protein, further limiting the inotropic response of the β₂-ADR, for example a splice variant of PDE3, PDE3A-135 is localized to the SR (Movsesian 2002) and a splice variant of PDE4, PDE4D3, is co-localised with RyR2 (Kass 2008), which will limit a rise in cAMP close to SR and may explain the inability of β₂-ADR mediated cAMP to phosphorylate the targets local to the SR (RyR2/PLB).

The level of positive inotropism achieved by the β₂-ADR stimulation appears to be species dependant. In humans, β₂-ADR are able to increase cAMP levels and PKA phosphorylation of distant targets (Kaumann and Molenaar 1997), whereas only minimal increases in cAMP, PKA activity or phosphorylation of PLB or TnI were induced by β₂-ADR stimulation in canine and mouse hearts (Altschuld, Starling et al. 1995; Sabri, Pak et al. 2000). In the rat heart, the effect of β₂-ADR stimulation appears to lie between these findings, with a local increase in cAMP and phosphorylation of LTCC, but no PKA-mediated phosphorylation of PLB or TnI (Xiao 2001). These species differences may be due to the strength of G_i coupling to the β₂-ADR or due to the activity of PDE3 and PDE4 in each species. For example, in the rat heart, 60% of cAMP degradation is mediated by PDE4 however in humans PDE4 only accounts for 10% cAMP degradation (Mika, Leroy et al. 2012), and so it may be that the activity of these PDE and the species dependence on cAMP by PDE3 and PDE4 accounts for the species differences observed.

The outcome of the dual coupling of β₂-ADR to G_s and $G_{i\alpha}$ proteins can result in a null inotropic effect (Xiao, Ji et al. 1995) as two opposing effects are activated; G_s promoting positive inotropism and $G_{i\alpha}$ which limits the inotropic effect of G_s. The full inotropic effect of β₂-ADR signalling can be revealed by uncoupling of the G_i protein with Pertussis toxin

(PTx) or inhibition of PDE3 and PDE4, which increases cAMP levels globally (Chen-Izu, Xiao et al. 2000) and enabling phosphorylation of distal targets of E-C coupling including PLB, causing a positive lusitropic on contractile relaxation effect which was absent previously (Xiao 2001).

1.2.4 The involvement of calmodulin and Epac in the β-ADR response

Although PKA is widely recognised as the primary effector of cAMP signalling, other effectors activated by cAMP and PKA have emerged as important modulators of cardiac Ca2+ homeostasis including PDEs (discussed in section 1.2.3.1), calmodulin and calcium/calmodulin-dependent protein kinase II and Epac.

1.2.4.1 Calmodulin and calcium/calmodulin-dependent protein kinase II

Calmodulin (CaM) is a ubiquitous, Ca^{2+}-binding protein which transduces Ca^{2+} signals by binding Ca^{2+} and modifying its own interaction with various target proteins. CaM is highly expressed in the heart, acting as a Ca^{2+} sensor, containing four Ca^{2+} binding sites. Upon binding of Ca^{2+}, CaM undergoes a significant conformational change which exposes a hydrophobic surface which can interact with its target proteins, such as Ca^{2+}/calmodulin-dependent protein kinase II (CaMKII) (Zipes 2014).

CaMKII is a multifunctional serine/threonine kinase with diverse roles in heart, providing a means by which the frequency/amplitude of Ca^{2+} signals can be translated into alterations in channel activity (Zipes 2014). CaMKII targets a number of Ca^{2+} homeostatic proteins including ion channels, transporters, SR accessory proteins, sarcomere contractile machinery, transcription factors and signaling molecules (Grimm and Brown 2010). Activation of CaMKII occurs 'locally', in restricted compartments of the myocyte and not globally in the cytosol during E-C coupling, namely the dyadic cleft (Bartel, Vetter et al. 2000; Song, Saucerman et al. 2008) and many of the targets of CaMKII are also the targets of PKA during β-ADR stimulation, including RyR2 (Ferrero, Said et al. 2007) and PLB (Said, Mundina-Weilenmann et al. 2002) mediating Ca^{2+} release from the SR (Curran, Hinton et al. 2007; Ferrero, Said et al. 2007) and increasing contractility (Wang, Zhu et al. 2004).

CaMKII regulation of LTCC:

CaMKII mediated phosphorylation of the LTCC lead to an increase in Ca+ influx, as phosphorylation of Ser1512 and Ser1570 on the α-subunit of the LTCC and/or Thr498 on the β-subunit of the LTCC induce the LTCC to open more frequently and to remain open for longer periods. However, the role of phosphorylation of the β-subunit remains controversial (Zipes 2014).

CaMKII regulation of Na$^+$ channels:

CaMKII mediated phosphorylation of the Nav1.5 channel reduced it availability and increase the Na+ 'late' current in cardiomyocytes (Zipes 2014), but binding sites for CaMKII remain undetermined, with Hund et al. suggesting Ser571 (Hund, Koval et al. 2010) and Ashpole suggesting a number of possible sites; Ser483, Ser483, Ser483 and/or Thr594 (Ashpole, Herren et al. 2012).

CaMKII regulation of K$^+$ channels:

The K+ channels responsible for RMP (I_{K1}/Kir2.1) and the I_{to} (Kv4.2/4.3) are also regulated by CaMKII, slowing inactivation of the Kv4.3 channel, leading to a greater I_{to} current density, and reducing the size of the I_{K1} current (Zipes 2014).

CaMKII regulation of RyR2:

CaMKII is associated with RyR2 and is able to phosphorylate the RyR2 increasing its open probability in much the same way as PKA. The phosphorylation site of CaMKII on the RyR2 is still somewhat under debate, with reports of phosphorylation at Ser2808 in rats, however this is also considered a PKA specific site by many investigators, and at Ser2814, a CaMKII specific phosphorylation site (Zipes 2014).

CaMKII regulation of PLB:

CaMKII is able to phosphorylate PLB at Thr17, the same phosphorylation site as PKA, also acting to increase the rate of Ca^{2+} resequester to the SR and contributing to a greater SR Ca^{2+} load (Mattiazzi and Kranias 2011).

During β-ADR stimulation there is an increase in Ca^{2+} entry via the LTCC and an increased SR Ca^{2+} release. In the dyadic cleft there is an increase in Ca^{2+} beyond the level maintained during normal beat-to-beat E-C coupling, and this increase in Ca^{2+} may be the trigger for CaMKII activation. Baltas et al. were the first to demonstrate that β-ADR stimulation can activate CaMKII in the intact rat heart (Baltas, Karczewski et al. 1997) and has since been reported by other groups (Kuschel, Karczewski et al. 1999; Said, Mundina-Weilenmann et al. 2002; Ferrero, Said et al. 2007; Song, Saucerman et al. 2008).

1.2.4.2 Epac

Epac (Exchange protein directly activated by cAMP) is a guanine nucleotide exchange factor which has recently emerged as an important regulator of cardiac function and Ca^{2+} homeostasis (Ruiz-Hurtado, Morel et al. 2013).

Two isoforms of Epac exist, Epac1, predominately expressed in the kidney and heart, and Epac2, predominately expressed in the brain and adrenal gland. Epac responds to physiologically relevant cAMP concentrations and can also be activated β-ADRs in cardiac myocytes (Berthouze, Laurent et al. 2011). Binding of cAMP to Epac induces a conformational change in the Epac protein, leading to the activation of Rap proteins, phospholipase Cε (PLCε) and/or protein kinase Cε (PKCε) and in turn the activation of CaMKII, however the exact mechanism of CaMKII activation has not been fully eluded (Ruiz-Hurtado, Morel et al. 2013).

It has been shown that Epac activation does not lead to a change in the LTCC, but rather induces phosphorylation of RyR2 at the CaMKII phosphorylation site, Ser2815, which was absent upon CaMKII inhibition (Pereira, Metrich et al. 2007). Recent data has shown that direct activation of Epac in cardiomyocytes with an Epac agonist (8-pCPT) is able to increase Ca^{2+} release from the SR in mouse myocytes in response to electrical stimulation during β-ADR stimulation, which was absent in PLCε KO mice. PLCε is important for the integrated signalling of G-coupled protein receptors to their downstream kinases, and therefore identified Epac as an important component of the β-ADR positive inotropic response (Oestreich, Wang et al. 2007). Epac activation has also been shown to increase the frequency of spontaneous Ca^{2+} sparks which was CaMKII dependant, increasing the Ca^{2+} leak and leading to a reduction in SR Ca^{2+} content and therefore a reduction in the

Figure 1.7 A schematic of β-Adrenergic receptor activation, PKG phosphorylation targets and CaMKII/Epac targets relevant to excitation–contraction coupling.

Activation of PKA and Epac/CaMKII by β-adrenergic receptor stimulation and phosphorylation of their targets. Abbreviations: β-AR, β-adrenergic receptor; LTCC, L-type Ca²⁺ channel; Gsα, α subunit of the Gs-protein; AC, adenylyl cyclase; cAMP, cyclic adenosine monophosphate; PKA, protein kinase A; Epac, exchange protein activated by cAMP; SR, sarcoplasmic reticulum; PLB, phospholamban; SERCA=2A, SR Ca²⁺-ATPase; RyR2, ryanodine receptor; CaM, Calmodulin; CaMKII, Ca²⁺ and calmodulin-dependent kinase II; Rap, a RAS-related GTP-binding protein; PLCε, phospholipase Cε; PKCε, protein kinase Cε.

41

amplitude of Ca^{2+} transients in rat cardiomyocytes and systolic Ca^{2+} and an increase in diastolic Ca^{2+} (Pereira, Metrich et al. 2007). These confounding effects of Epac activation on the Ca^{2+} transient has led to controversy over the exact effect of Epac, depicting either an increase, decrease or no change in the amplitude of Ca^{2+} transients, however these differences may be explained by the experimental models used, species differences and the time of 8-pCPT application. The current pool of data suggests that in the rat Epac may respond to the fast increase in cAMP levels upon β-ADR stimulation, mobilising Ca^{2+} from stores in the SR into the cytosol, however the effect on contractility may be null despite an increase in diastolic Ca^{2+} , and this may be involved in actions other than E-C coupling (Ruiz-Hurtado, Morel et al. 2013).

1.2.5   The β₃-adrenoceptor

$β_3$-ADR are a third type of β-ADR which are expressed in a number of laboratory animals including mice, rats, guinea pigs, rabbits (Gauthier, Tavernier et al. 1999) and also in humans (Rozec and Gauthier 2006) . The gene encoding the human $β_3$-ADR was discovered in 1989 (Emorine, Marullo et al. 1989) and has since been shown to be expressed in a number of tissues including the gastrointestinal tract inhibiting the contractile activity (Gauthier, Tavernier et al. 1996), white and brown adipose tissue mediating thermogenic and lipolytic effects (Gauthier, Langin et al. 2000), blood vessels mediating vasodilatation (Gauthier, Langin et al. 2000), and in the heart (Gauthier, Tavernier et al. 1996).

The $β_3$-ADR are GPCRs coupled to the inhibitory G-protein, G_i (Gauthier, Tavernier et al. 1996), and like $β_1$-ADR and $β_2$-ADR are activated by catecholamines, however they have a lower affinity for catecholamines and so a greater concentration of catecholamines are required for $β_3$-ADR stimulation (Strosberg 1997).The presence of $β_3$-ADR in the heart was suggested by the observation of a negative inotropic effect caused by β-ADR stimulation with nor-adrenaline at near pathophysiological levels under $β_1$-ADR and $β_2$-ADR blockade, which could be abolished by bupranolol, a $β_1$-ADR, $β_2$-ADR and $β_3$-ADR agonist (Gauthier, Tavernier et al. 1996). This was further strengthened by the observation of a negative inotropic response to stimulation of the $β_3$-ADR with the specific agonist, BRL_{37344} (Gauthier, Tavernier et al. 1996; Gauthier, Leblais et al. 1998) and following detection of mRNA in the heart (Gauthier, Tavernier et al. 1996) and later detection of the $β_3$-ADR

protein in the ventricle (Moniotte, Kobzik et al. 2001). It is thought that the β_3-ADR pathway may act as a negative feedback mechanism in the heart, preventing damage from excessive $\beta_{1/2}$-ADR stimulation during periods of high levels of circulating catecholamines. In contrast to the β_1-ADR and β_2-ADR, β_3-ADR activation leads to a marked negative inotropy response via PDE and NO signalling (Gauthier, Tavernier et al. 1996; Gauthier, Leblais et al. 1998; Gauthier, Tavernier et al. 1999; Gauthier, Langin et al. 2000; Rozec and Gauthier 2006) (See Figure 1.4 and Figure 1.8).

The inhibitory G_i protein is composed of $G_{i\alpha}$ and $G_{i\beta}$ subunits, which have differing effects on E-C coupling. The $G_{i\alpha}$ subunit activates PDE3 and PDE4 which hydrolyse cAMP and oppose the positive inotropic action of cAMP and PKA activation in the same manner as the $G_{i\alpha}$ subunit of the β_2-ADR (See Introduction 1.2.3). The $G_{i\beta}$ subunit activates nitric oxide synthase (NOS) enzymes leading to the production of NO.

1.2.5.1   Nitric Oxide in the myocardium

NO is synthesized by the group of nitric oxide synthase (NOS) enzymes which catalyse the oxygen- and NADPH-dependant oxidation of L-arginine, forming NO and L-citrulline (Gauthier, Leblais et al. 1998), a reaction requiring oxygen and other co-factors (Zhang and Casadei 2012). NO is a reactive oxygen species, containing one nitrogen atom covalently bonded to an oxygen atom with an unpaired electron (Danson 2005). Gaseous in nature and highly diffusible (Belge, Massion et al. 2005) the bioavailability of NO is limited, with a half-life of approximately 5 seconds (Treuer and Gonzalez 2015), and so the biological reactions are restricted temporally and spatially (Danson 2005). NO is particularly reactive with oxygen and haem containing groups and is known to react with the high myoglobin content of cardiac myocytes (Hammond and Balligand 2011) and superoxide anions produced by NOS, and therefore the source of NO is critical on its functional impact and will be discussed in below (See Introduction 1.2.4.1).

In the myocardium, NO exerts its biological effects on E-C coupling in the myocyte via both cGMP-dependent and cGMP -independent mechanisms.

cGMP-dependent action of NO:

Upon production of NO by NOS enzymes, NO binds to the heme group of soluble guanylyl cyclase (sGC) leading to the production of 3',5'-cyclic guanosine monophosphate (cGMP) from guanosine triphosphate (GTP) (Hammond and Balligand 2011). cGMP activates protein kinase G (PKG), which is able to directly phosphorylate the components of E-C coupling. PKG phosphorylation of the LTCC at Ser1928 on the α-subunit (same site as PKA phosphorylation) and Ser496 of the β-subunit (Yang, Liu et al. 2007) inhibiting the LTCC (Mery, Lohmann et al. 1991) and reducing the size of $[Ca^{2+}]_i$ (Kitamura, Onishi et al. 2000; Cheng, Zhang et al. 2001; Zhang, Cheng et al. 2005). Phosphorylation of the RyR2 by PKG also targets the same target sites as PKA, at Ser2808 and weakly at Ser2030 (Xiao, Zhong et al. 2006), increasing their P_o and facilitating Ca^{2+} leak. PKG phosphorylation of PLB at Ser16 and Thr17 (Wang, Kohr et al. 2008; Zhang, Zhang et al. 2008) which will enhance Ca^{2+} sequester back to the SR during contractile relaxation in the same manner as PKA. PKG also reducing myofilament sensitivity and the contractile response of myofilaments by phosphorylation of TnI at Ser23 and Ser24 (Layland, Solaro et al. 2005), the same residues as PKA.

cGMP also activates PDE2 and PDE3 cGMP-dependent PDEs, which are important in providing a 'cross-talk' between cGMP and cAMP (Hammond and Balligand 2011). PDE2 and 3 have dual specificity for cAMP and cGMP (Bender and Beavo 2006) and allows for cross-talk between cAMP and cGMP within the cell.

PDE2 is stimulated by cGMP, inducing hydrolysis of cAMP, leading to a local reduction in cAMP and thereby reducing its downstream effects. PDE2 is mainly associated with the plasma membrane, the SR and the golgi apparatus (Mika, Leroy et al. 2012).

On the other hand, cGMP inhibits PDE3 activity, which can lead to a local increase in cAMP resulting in an increase LTCC (Loscalzo and Vita 2000).

The opposing effect of PDE2 activation and PDE3 inhibition by cGMP allows cross talk between cGMP and cAMP signalling, and can either elevate or reduce cAMP levels depending upon cell specific expression of PDEs (Loscalzo and Vita 2000).

cGMP-independent action of NO:

NO can also set off a cascade of cGMP-independent signalling, namely via a S-nitrosylation reaction, which involves the covalent modification of a protein at cysteine-thiol residues generating an *S*-nitrosothiol (Hare 2003). S-nitrosylation has been found to cause a post-
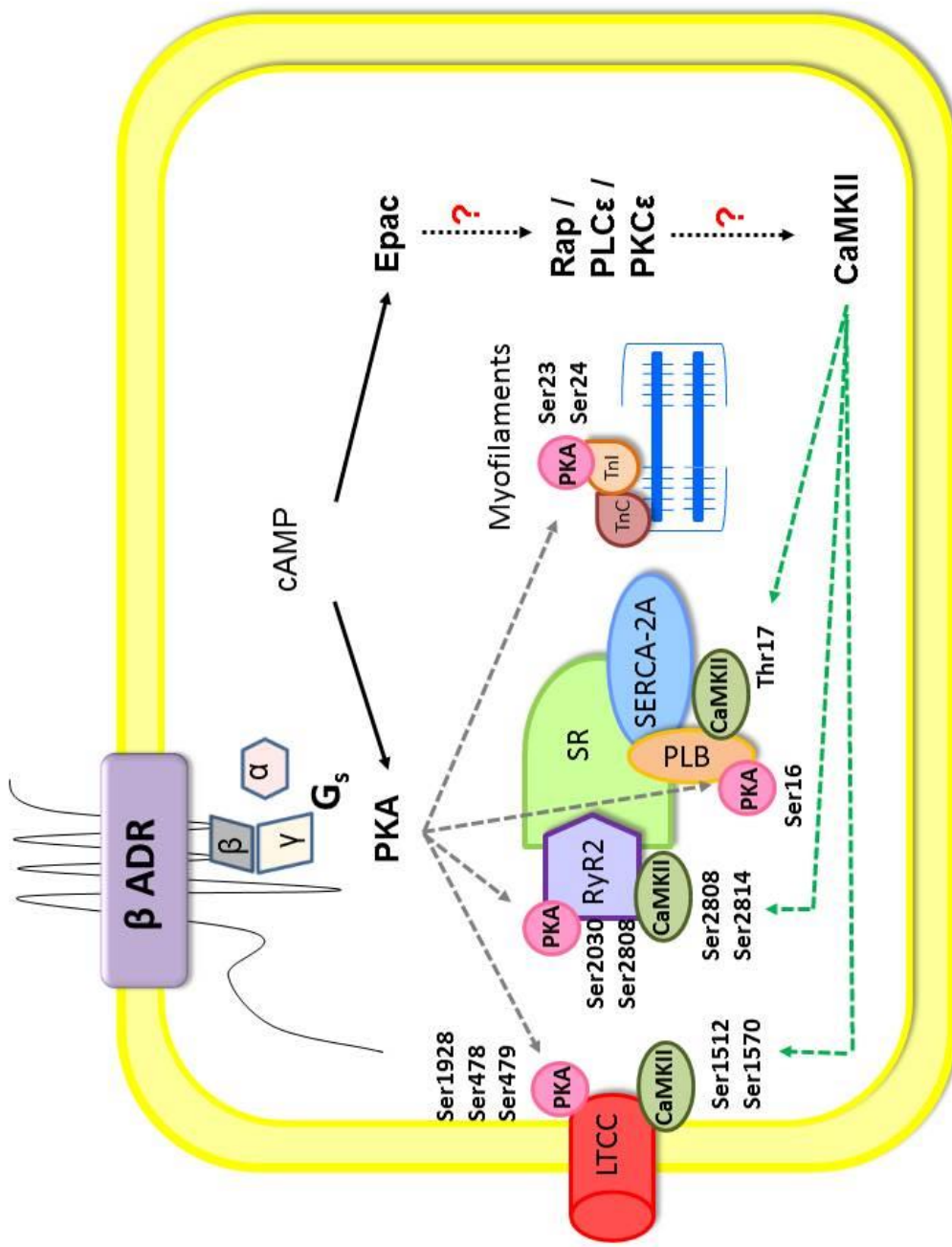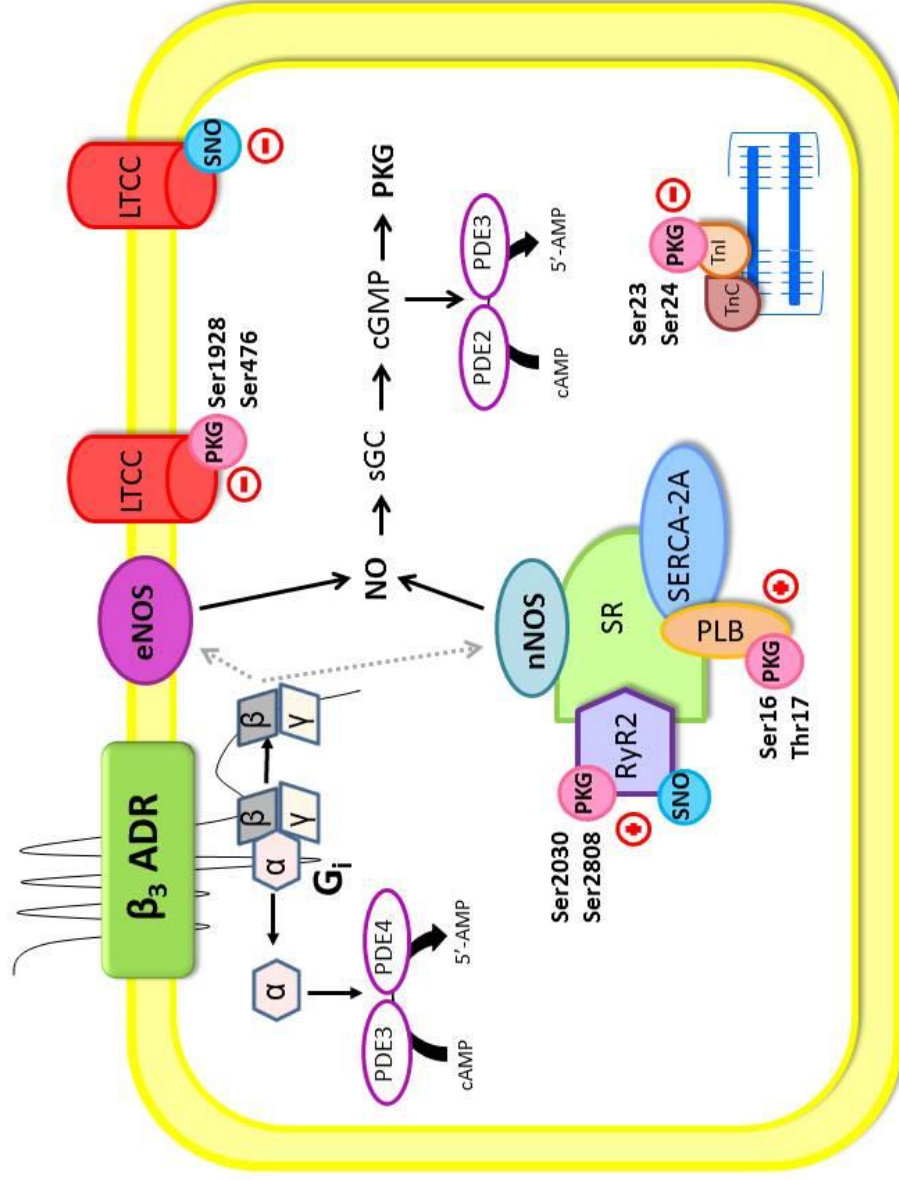
Figure 1.8   A schematic of β₃ -Adrenergic receptor activation, PKG phosphorylation targets and S-nitrosylation targets relevant to excitation– contraction coupling.

The β_3-Adrenergic receptor (β_3-ADR) is coupled to G_i proteins. The α subunit activates phosphodiesterase (PDE) PDE3 and PDE4 which leads a reduction in cAMP levels. The β subunit activates endothelial Nitric Oxide Synthase (eNOS) and/or neuronal Nitric Oxide Synthase (nNOS) which produce Nitric Oxide (NO). NO stimulates soluble guanylyl cyclase (sGC) which converts guanosine triphosphate (GTP) to 3',5'-cyclic guanosine monophosphate (cGMP) which in turn activates protein kinase G (PKG). PKG phosphorylates a number of targets of E-C coupling (indicated by a pink PKG). cGMP also governs activity of PDE2 and PDE3. NO is able to S-nitrolyslate a number of E-C coupling proteins directly (indicated by a blue SNO) including.

45

translational modification of a number of proteins involved in E-C coupling.

S-nitrosylation of LTCC inhibits current flux and reduces the current density of LTCC (Poteser, Romanin et al. 2001; Sun, Picht et al. 2006; Sun, Steenbergen et al. 2006) and S-nitrosylation of RyR2, which have a number of cysteine-thiol residues, increases the P_o of the RyR2 and leads to an enhanced Ca^{2+} leak from the myocyte (Gonzalez, Beigi et al. 2007; Sun, Yamaguchi et al. 2008). S-nitrosylation can occur at much lower concentrations of NO than required for cGMP production (Gonzalez, Fernandez et al. 2008; Treuer and Gonzalez 2015). NO has also been implicated in S-nitrosylation of a number of K^+ ion channels shortening APD, including channels for I_{to} at Cys331 and Cys346 (Gomez, Nunez et al. 2008), I_{Ks} at Cys445 (Asada, Kurokawa et al. 2009) and I_{K1} at Cys76 (Gomez, Caballero et al. 2009). It is thought that NO acts as a second messenger in the heart, opposing the positive inotropic action of catecholamines (Gauthier, Leblais et al. 1998), and this result from both the cGMP-dependent and cGMP-independent in the myocardium (Hare 2003).

1.2.5.2 Nitric Oxide Synthase

As mentioned previously NO is synthesized by the group of NOS enzymes which catalyse the conversion of L-arginine to NO (Gauthier, Leblais et al. 1998). The mammalian heart expresses all three of the NOS isoforms; endothelial NOS (eNOS), neuronal NOS (nNOS) and inducible NOS (iNOS) each utilising the same co-factors and substrates however they differ in their localisation, regulation and the effect they exert on the myocardium (Zhang and Casadei 2012). eNOS and nNOS are constitutively expressed in the myocardium, are modulated by Ca^{2+} and are considered low output enzymes as compared to iNOS, which is only expressed in the myocardium during inflammatory responses and produce much higher levels of NO independent to Ca^{2+} signalling (Ziolo, Kohr et al. 2008).

eNOS and nNOS trigger specific signalling pathways due to subcellular compartmentalisation of the NOS enzymes and the spatiotemporal reach of the NO produced, and so each isoform will be discussed individually below.

Despite almost three decades of investigation into the effects of NO on the myocardium, the complexity the NOS isoforms, NO downstream signalling and the full range of intracellular targets for NO in the heart are only just beginning to come to light and are still somewhat unknown. Part of the problem has been the assumption for many years that eNOS was the only NOS enzyme constitutively expressed in the myocardium and therefore

the theory that the effects of a non-specific NOS inhibitor was due solely to inhibition of the eNOS enzyme, however it is now known nNOS is expressed in myocytes (Balligand, Kobzik et al. 1995; Xu, Huso et al. 1999) this began a new era of research.

1.2.5.2.1   Endothelial NOS

eNOS was first identified in the vascular endothelium (Palmer, Ashton et al. 1988) and is encoded for by the NOS3 gene. eNOS is localised to the caveolae of the sarcolemma and T-tubules, co-immunoprecipitates to caveolin-3 and has been shown to be coupled to a number of receptors, including muscarinic, bradykinin and β-ADR receptors (Barouch, Harrison et al. 2002).

eNOS and basal contraction and E-C coupling:

The basal effects of eNOS appear to be very minimal as the specific inhibition of eNOS, genetic deletion or overexpression of the eNOS gene has little effect on basal systolic and diastolic properties in the mammalian heart or in isolated cardiomyocyte including I_{Ca}, Ca^{2+} transient amplitude or contraction (Han, Kubota et al. 1998; Barouch, Harrison et al. 2002; Khan, Skaf et al. 2003; Martin, Emanuel et al. 2006).

eNOS and contraction and E-C coupling in response to β-ADR stimulation:

Despite the inability of eNOS to act upon basal contractility, eNOS has been shown to modulate β-ADR increases in inotropy and chronotrophy. eNOS KO mice have been shown to exhibit greater increases in the Ca^{2+} transient, cell shortening (Barouch, Harrison et al. 2002) and an increased LTCC in myocytes isolated from eNOS KO mice (Wang, Kohr et al. 2008), in response to β-ADR stimulation with ISO as compared to WT mice. Interestingly, Wang *et al.* also observed an increased APD and a greater propensity for EAD arrhythmia generation in myocytes isolated from eNOS KO mice. The enhanced response to β-ADR stimulation has also demonstrated to similar level with eNOS inhibitors in WT isolated myocytes (Wang, Kohr et al. 2008).

eNOS overexpression studies have also provided evidence of the effect of eNOS signalling on the β-ADR response, as eNOS overexpression has been shown in the whole heart to prevent the inotropic increase in HR, systolic and diastolic function in response to ISO which is present in WT mice (Janssens, Pokreisz et al. 2004). Massion *et al.* have also shown an attenuation of the beta-adrenergic positive inotropic response in the whole

heart assessed by video microscopy, which corresponded with lower incidence of spontaneous after-contractions (Massion, Dessy et al. 2004).

However, the evidence is not clear cut, as other groups have found no effect of eNOS KO on sarcomere shortening and contractility in response to ISO between KO and WT (Martin, Emanuel et al. 2006). Zhang and Casadei have also recently observed that the increase in I_{Ca} in response to β-ADR stimulation in eNOS KO mice was not different to WT mice, suggesting eNOS may not be involved in the control of β-ADR stimulation.

eNOS E-C coupling targets:

eNOS is localised to the caveolin and so is well placed to affect the LTCC, indeed eNOS has been shown to localise to the LTCC (Balijepalli, Foell et al. 2006). eNOS derived NO can diffuse rapidly to the LTCC, and either via PKG phosphorylation (Jiang, Gawler et al. 2000; Yang, Liu et al. 2007) or S-nitrosylation (Dudzinski and Michel 2007), has been shown to reduce the size of the LTCC and decrease contraction by reducing the trigger for CICR (Wang, Kohr et al. 2008).

Recent work has shown that the effect of eNOS-derived NO is to enhance relaxation; an effect attributed to the action of cGMP-dependent PKG phosphorylation of TnI. Phosphorylation of TnI increases the off rate of Ca^{2+} from TnC, allowing for a faster relaxation as Ca^{2+} is available for removal from the cytoplasm (Seddon, Shah et al. 2007).

It has also been demonstrated that eNOS signalling exerts control over repolarisation and APD via the I_{Ks} channels. eNOS signalling has been shown to enhance the slow component of I_{Ks} leading to a faster repolarisation, shortening APD (Bai, Namekata et al. 2005). eNOS KO mice exhibit a greater lengthening of APD in response to ISO than WT (Wang, Kohr et al. 2008; Tang, Wang et al. 2014).

1.2.5.2.2   Neuronal NOS

nNOS is named due to its first identification in the neurone (Knowles, Palacios et al. 1989) and has since been identified to a number of tissue types including the myocardium, first identified in the heart in 1999 (Xu, Huso et al. 1999). nNOS is localised to the SR and co-immunoprecipitates with the RyR2 (Xu, Huso et al. 1999; Barouch, Harrison et al. 2002)

and mitochondria (Massion, Pelat et al. 2005), and so nNOS is well placed to affect a number of the components of E-C coupling including PLB and RyR2 (Hare 2003).

nNOS and basal contraction and E-C coupling:

Unlike eNOS, nNOS has been shown to affect the myocardium in basal conditions. In both nNOS KO ventricular myocytes and following nNOS inhibition in WT myocytes there is an increase in basal contractility, suggesting that constitutively active nNOS inhibits contraction (Schulz, Rassaf et al. 2005). Seddon *et al.* have shown that cardiomyocytes from nNOS$^{-/-}$ mice have greater basal cell shortening and a slower relaxation time than WT animals and similar effects could be seen in WT upon nNOS inhibition. *In vivo,* nNOS KO causes a greater contractile function and a prolonged LV relaxation compared to WT animals (Seddon, Shah et al. 2007) and exhibit a greater LV ejection fraction (Sears, Bryant et al. 2003). This evidence leads to the conclusion that nNOS-derived NO in basal conditions inhibits contraction whilst supporting relaxation.

nNOS and contraction and E-C coupling in response to β-ADR stimulation:

As well as modulating basal contractility and E-C coupling, nNOS signalling has also been implicated in the modulation of the contractile response to β-ADR stimulation.

The genetic deletion of nNOS in mouse cardiomyocytes have shown a reduced contractile response to β-ADR stimulation measured *in vivo* (Barouch, Harrison et al. 2002; Dawson, Lygate et al. 2005; Vandsburger, French et al. 2007) and a similar response was seen with nNOS inhibition in the whole heart (Schulz, Rassaf et al. 2005). However, as with eNOS, the story is not simple as conflicting results have been witnessed, with some finding genetic deletion of nNOS resulting in an augmented response to β-ADR stimulation, finding an increase in $[Ca^{2+}]_i$ transients and cell shortening (Ziolo, Kohr et al. 2008). The various methodologies used to investigate nNOS have led to variable results, however the majority of reports indicate an enhanced β-ADR response at cellular, tissue and whole animal level upon nNOS inhibition (Danson 2005).

nNOS E-C coupling targets:

nNOS is localised to the SR and co-immunoprecipitates with the RyR2 (Xu, Huso et al. 1999; Barouch, Harrison et al. 2002) and so nNOS well placed to affect a number of the components of E-C coupling including PLB and RyR2.

PLB is a key target of nNOS, and it has been shown that nNOS inhibition leads to a reduction in phosphorylation of PLB (Ziolo, Kohr et al. 2008). It is proposed that nNOS acts on PLB by promoting its phosphorylation, acting as a negative feedback mechanism, preventing $[Ca^{2+}]_i$ overload and Ca^{2+} fluxes, protecting the heart from triggered arrhythmias during states of high β-ADR stimulation (Sears, Bryant et al. 2003).

nNOS is also thought to target RyR2 in the myocardium, as nNOS has been shown to be able to co-immunoprecipitate with RyR2 and is thought to reversibly increase RyR2 P_o (Seddon, Shah et al. 2007). If this were to occur it could lead to a leak of $[Ca^{2+}]$ during relaxation, reducing $[Ca^{2+}]_{SR}$, which is consistent with the increased $[Ca^{2+}]_{SR}$ observed in nNOS$^{-/-}$ models. The increased contractility observed in nNOS KO animals and during nNOS inhibition in wild-type animals, is associated with an increase in I_{Ca}, a larger SR Ca^{2+} content and a greater $[Ca^{2+}]_i$ amplitude in myocytes (Sears, Bryant et al. 2003). It is thought that under basal conditions nNOS-derived NO reduces contractility through inhibition of LTCC and therefore reducing LTCC (Seddon, Shah et al. 2007). nNOS-derived NO may act as a negative feedback on Ca^{2+} entry via LTCC, as a rise in $[Ca^{2+}]_i$ may stimulate nNOS to produce NO, which in turn inhibits the LTCC (Casadei 2006).

nNOS has also been shown to interact with PMCA, modulating $[Ca^{2+}]_i$ levels. (Ziolo, Kohr et al. 2008). The increased $[Ca^{2+}]_{SR}$ observed in nNOS$^{-/-}$ myocytes is also thought to be due to a reduction in the rate of the slow time constant of I_{Ca} decay, this leads to an inward I_{Ca} current during the slow time constant which may explain the increased SR load in nNOS$^{-/-}$ models (Sears, Bryant et al. 2003).

1.2.5.2.3 Inducible NOS

Inducible NOS (iNOS), produced by the NOS2 enzyme, is only expressed in the myocardium in conditions of inflammation, produced in response to inflammatory cytokines infiltrating the myocardium (Massion, Pelat et al. 2005) in conditions such as ischemia-reperfusion injury, septicaemia, aging and HF. iNOS is not dependant on $[Ca^{2+}]_i$, and produces much greater levels of NO compared to eNOS or nNOS as once expressed iNOS remains continuously activated (Sears, Ashley et al. 2004). It is thought iNOS signalling is not compartmentalised as with eNOS and nNOS, due to the high volume of NO produced (Ziolo, Kohr et al. 2008).

As iNOS is only expressed in the heart during pathological conditions, it has been shown to have little effect on the basal contractile function (Massion, Pelat et al. 2005). However, many studies have shown that the cardiac dysfunction in many pathological conditions may be partly due to the expression of iNOS, for example genetic deletion or inhibition of iNOS offered protection against the myocardial dysfunction in sepsis in mice (Ziolo, Kohr et al. 2008). The expression of iNOS can be viewed as both a cardio-protective and a detrimental mechanism. iNOS is able to improve left ventricular function and reduce myocardial oxygen consumption, via a reduction in contractility, however in the majority of end-stage HF patients, iNOS expression is associated with a reduced response to β-ADR, which can be normalised with iNOS inhibition (Schulz, Rassaf et al. 2005), thereby acting as a permanent cardio-depressive agent.

1.2.5.3 Nitric Oxide in the vasculature

Nitric oxide was first discovered in 1980 in the vasculature, originally termed as endothelium-derived relaxing factor (Furchgott and Zawadzki 1980). It has since been renamed NO and is now recognised as a major regulator of vascular tone. Constriction and dilation of blood vessels in response to environmental demands are controlled by changes in the $[Ca^{2+}]_i$ in the vascular smooth muscle cell (VSMC) (Van Hove, Van der Donckt et al. 2009). NO is a potent vasodilator in the vasculature, and the balance between NO and endothelial derived vasoconstrictors and sympathetic stimulation maintains vascular tone.

Vascular smooth muscle contraction and relaxation:

Unlike cardiomyocytes, contraction in VSMC is slow, sustained and tonic, and VSMC do not express the regulatory protein troponin, instead contraction is regulated by the phosphorylation state of another protein, Myosin Light Chain (MLC). Contraction in VSMC is initiated upon a rise in cytosolic $[Ca^{2+}]$, either an increase in the size of the LTCC current or an increased Ca^{2+} release from the SR. This increase in $[Ca^{2+}]$ leads to binding of free Ca^{2+} to CaM. The Ca^{2+}/CaM complex activates the myosin light chain kinase (MLCK) enzyme, which in the presence of ATP phosphorylates MLC. Phosphorylation of MLC allows cross bridge formation between actin and myosin, facilitating contraction.

VSMC relaxation is initiated under conditions of reduced MLC phosphorylation, which can result from a reduction in the size of the LTCC current and/or a reduction in SR Ca^{2+} release
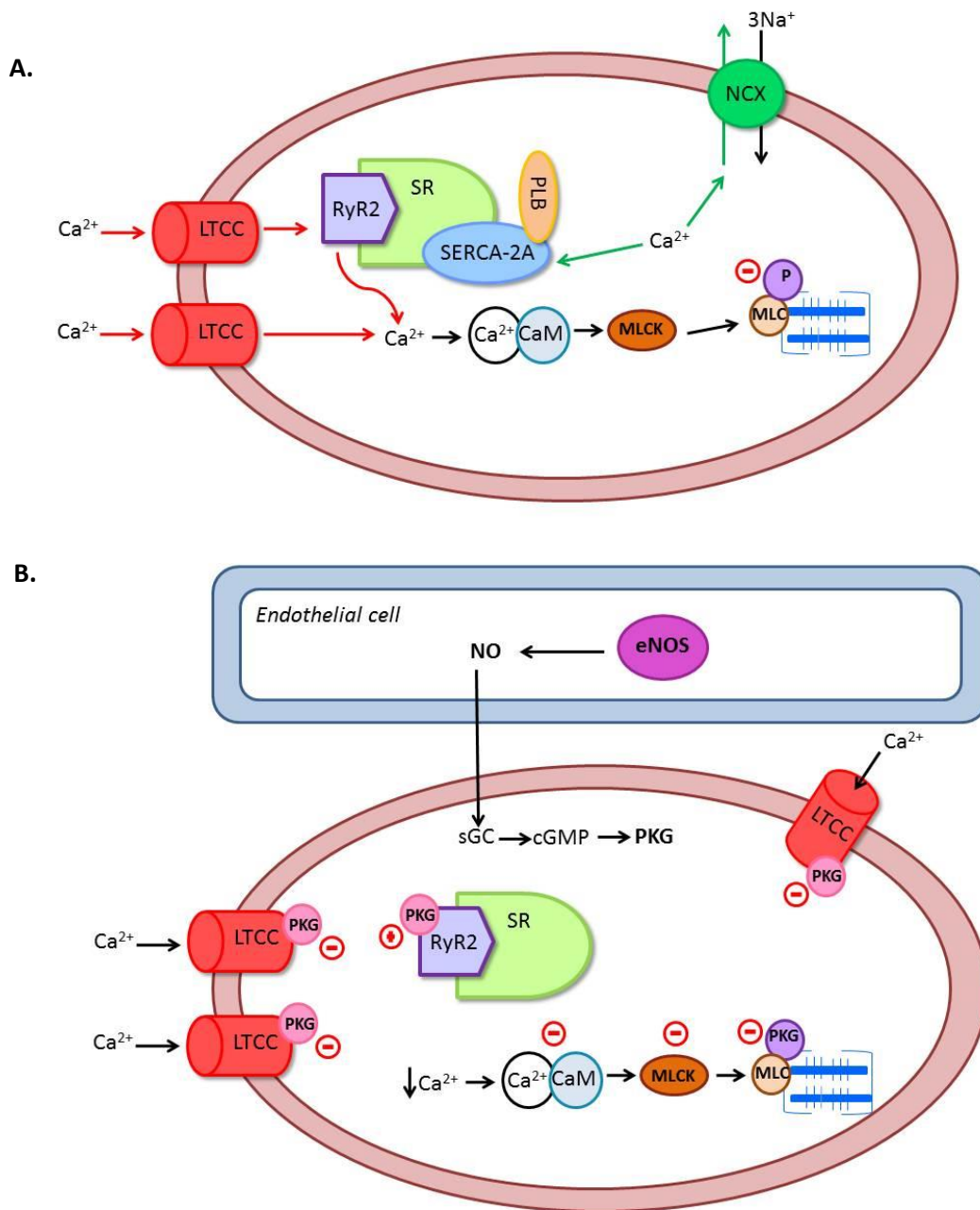
Figure 1.9   A schematic showing processes involved in vascular smooth muscle contraction and how this can be affected by nitric oxide. Adapted from (Golan 2008).

A. A schematic of Ca^{2+} transport processes involved in vascular smooth muscle contraction, showing the L-type calcium channels (LTCC), sarcoplasmic reticulum (SR), ryanodine receptors (RyR2), Sarcoplasmic Reticulum Calcium ATPase pump (SERCA-2A), sodium calcium exchanger (NCX), Ca^{2+}/calmodulin complex (Ca^{2+}/CaM), Myosin Light chain (MLC) and MLC kinase (MLCK). An increase in [Ca^{2+}] causes free Ca^{2+} to bind to CaM, activating MLCK and leading to phosphorylation of MLC (indicated by a purple P). Routes of Ca^{2+} entry and release in the cell during contraction are shown in red. Routes of Ca^{2+} removal from the cytosol during relaxation are shown in green.

B.   A schematic to show the effect of nitric oxide (NO) on the VSMC following activation of endothelial Nitric Oxide Synthase (eNOS), showing activation of soluble soluble guanylyl cyclase (sGC) which converts guanosine triphosphate (GTP) to 3',5'-cyclic guanosine monophosphate (cGMP) which in turn activates protein kinase G (PKG). PKG phosphorylates a number of targets of E-C coupling (indicated by a pink PKG).

and an activation of K^+ channels (Van Hove, Van der Donckt et al. 2009). The degree of MLC phosphorylation is regulated by G-protein-coupled signal transduction pathways e.g. β-ADR signaling and also by nitric oxide.There is a continual synthesis of NO by NOS in endothelial cells at rest, which maintain vascular tone by acting on VSMC, altering their contractile state (Vallance and Chan 2001). However, a number of biochemical (e.g. thrombin, adenosine, acetylcholine, bradykinin) and mechanical stimuli (e.g. shear stress) can activate eNOS and lead to an increase in NO production (Jin and Loscalzo 2010).

Within the resistance vessels, basal low levels of NO is produced within endothelial cells, which diffuses rapidly into adjacent VSMCs, activating sGC and leading to an increase in cGMP levels. In a similar manner to the action of NO in cardiomyocytes, NO leads to a reduction in cytosolic $[Ca^{2+}]$ through the inhibition of LTCC and via the activation of PKG, promotes phosphorylation of RyR reducing SR Ca^{2+} content. The resulting reduced cytosolic $[Ca^{2+}]$ inhibits the Ca^{2+}/CaM complex formation, reducing activation of myosin light chain kinase in the VSMC, which promotes relaxation of VSMC, promoting vascular dilatation and increased blood flow. cGMP also stimulates a cGMP-dependant protein kinase which activates myosin light chain phosphatase, which dephosphorylates the MLC, further promoting relaxation of VSMC (Jin and Loscalzo 2010).

Under basal conditions the generation of NO by endothelial cells allows for maintenance of basal vascular tone, crucial in maintaining peripheral vasodilatation. This basal nitric oxide mediated dilatation has been seen in every arterial bed studied, including cerebral, pulmonary, renal and coronary vasculature. In contrast, basal nitric oxide production does not have a major role in the maintenance of the resting tone in veins (Vallance and Chan 2001).

1.3   Circadian rhythms and E-C coupling

Despite variation in the environment and the demands placed on an individual over the course of a day, biological processes must remain within strict physiological limits to maintain normal physiology. Virtually all organisms have evolved a mechanism to enable the anticipation of environmental fluctuations over the course of the day; the circadian clock (Young 2006).

The circadian clock is a transcriptional-translational auto-regulatory loop which generates oscillations in clock regulated genes at a cellular level (Ko and Takahashi 2006). The clock is a set of proteins which is self-sustained by transcriptional positive and negative feedback loops, that generate an oscillator with a running period of around 24 hours, which needs to be entrained daily to maintain a 24 hour rhythm (Edery 2000).

The circadian clock is comprised of three components; (1) the clock mechanism, (2) zeitgebers, which are external factors which reset/entrain the circadian clock, and (3) the outputs from the clock, which influence gene expression, cell growth and cell division (Young 2003). The central circadian clock is located in the Suprechiasmic Nucleus (SCN) in the brain and responds to light signals for entraining. Mammals also possess peripheral circadian clocks, which are clocks found in almost every other cell of the body, including cells of the cardiovascular system (Dibner, Schibler et al. 2010; Albrecht 2012; Mohawk, Green et al. 2012). These peripheral clocks are entrained by the central circadian clock and also by neurohumoural factors, the exact identity of which have not yet been fully identified, however glucocorticoids, retinoic acid, melatonin and feeding have been suggested as possible candidates (Young 2003). Although the peripheral clocks are entrained by differing zeitgebers to the central clock, they must be synchronized to the central clock for normal functioning (Young 2006).

The circadian clock enables the cell to anticipate an event so that it can respond to a signal at the appropriate time of day, and so it is reasonable to assume that a disruption or loss synchronicity between the CVS and diurnal variations in the environment could impair the ability of the CVS to respond appropriately to stimuli. This would be maladaptive, possibility leading to contractile dysfunction in the heart or cardiovascular disease (Young 2003; Young 2006). It has also been suggested that zeitgebers act in a cell specific manner, and therefore the loss of synchronisation between two peripheral clocks could also become maladaptive, for example a dyscynchronisation between the circadian clocks in endothelial cells and VSMS would affect BP regulation in the vasculature (Young 2006).

1.3.1 Molecular mechanism of the circadian clock

The core components of the clock are defined as *"genes whose protein products are necessary for the generation and regulation of circadian rhythms within individual cells throughout the organism"* (Ko and Takahashi 2006).

The molecular basis of the central and peripheral clocks are similar and consists of the core transcriptional genes *clock* (Circadian Locomotor Output Cycles Kaput) and *bmal1* (Aryl hydrocarbon receptor nuclear translocator-like protein 1). Their protein products regulate the expression of the *period (per1, per2, per3)*, *cryptochrome (cry1, cry2)* and *rev-erbα* (nuclear receptor subfamily 1, group D, member 1) (See Figure 1.10).

The protein products of *clock* and *bmal1*, CLOCK and BMAL1 heterodimerize (CLOCK:BMAL1) and induce the transcription of target genes by binding to E-box cis-regulatory enhancer sequences in the promoter region of target genes, increasing levels of PER1, PER2, PER3, CRY1, CRY2 and REV-ERBα, which leave the nucleus and enter the cytoplasm.

Once in the cytoplasm, PER and CRY proteins heterodimerize and translocate back to the nucleus, providing negative feedback on the CLOCK:BMAL1, repressing heterodimerization of CLOCK and BMAL1.

A second regulatory loop of the CLOCK:BMAL1 heterodimer is achieved by REV-ERBα, which translocate back to the nucleus, repressing *bmal1* transcription, leading to oscillations in BMAL1 protein.

PER2 acts differently to the other PER proteins, instead of heterodimerizing with CRY proteins, PER2 translocates back into the nucleus and promotes *bmal1* transcription, initiating a positive feedback loop.

A delay of approximately 6 hours between peak gene expression and peak protein expression provides the phasic nature of the positive and negative feedback loops of the circadian clock. These feedback loops take approximately 24 hours to complete a cycle. (Portman 2001; Ko and Takahashi 2006; Dibner, Schibler et al. 2010; Albrecht 2012; Mohawk, Green et al. 2012).

1.3.2 Circadian clocks within the cardiovascular system

Circadian clocks have been identified in a number of components of the CVS, including cardiomyocytes and vascular smooth muscle cells (VSMC), and circadian rhythms, also known as diurnal or time-of-day variations, have historically been described in a number of CV parameters, including BP and HR, as well as in a number of pathophysiological conditions.

Martin Young et al. (2001) was the first to identify and characterise the presence of mammalian homologues of known *Drosophila* clock genes in the rat heart (*bmal1, clock, cry1, cry2, per1, per2, per3, dbp, hlf* and *tef*) demonstrating that the level of gene expression fluctuate dramatically over a period of 24 hours (Young, Razeghi et al. 2001). Within the heart, 10-15% of genes have been shown to exhibit diurnal cycling and many of these are involved in transcription, translation, protein turnover, ion homeostasis and metabolism (Durgan, Hotze et al. 2005). The circadian clock within the heart is able to potentially affect the responsiveness to sympathetic stimulation, electrical properties of the heart, Ca^{2+} homeostasis, contractile function, antioxidant capacity, signalling cascades and metabolism, allowing the heart to respond appropriately to changes in workload, substrate availability or the energy supply: demand ratio (Young 2006).

The zeitgeber which entrain the peripheral clock within the cardiomyocyte have not been fully established. However, alongside the possible candidates described by Young et al. (glucocorticoids, retinoic acid, melatonin) (Young 2003), sympathetic stimulation and noradrenaline levels are thought to zeitgebers for the circadian clock intrinsic to myocytes, due to the dramatic morning peak observed in sympathetic activity (Durgan, Hotze et al. 2005).

Young *et al*. have demonstrated significant variations in cardiac contractility and metabolism in the myocardium. Young has shown gene expression of a number of myocardial contractile proteins display circadian cycling, with expression highest during the active period of the rat. This was coupled with an increased contractility, CO and gene expression of myosin heavy chain α and β isoforms during the animals' active phase (Young 2006).

Time-of-day dependant variations have also been found in cardiac K^+ channel gene expression. Yamashita *et al.* have shown that a significant time of day variation in the gene
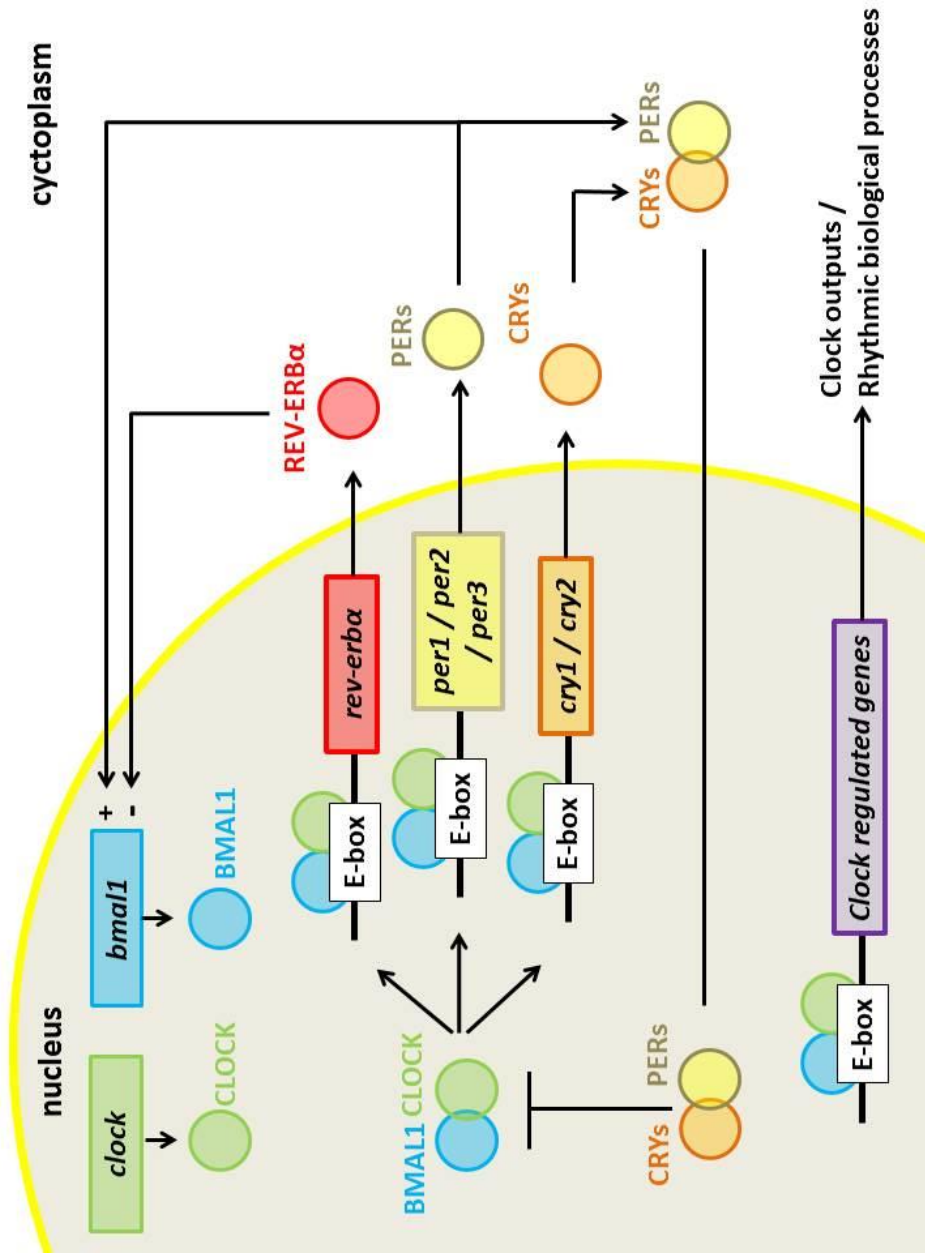
Figure 1.10   A schematic of the molecular mechanism of the circadian clock in mammals, adapted from (Mohawk, Green et al. 2012).
The molecular mechanism of the circadian clock displaying the heterodimerization of BMAL1 and CLOCK proteins, their target genes; *per1*, *per2*, *per3*, *cry1* and *cry2*, and their gene products; PER1, PER2, PER3, CRY1 and CRY2, which provide an auto-regulatory transcriptional feedback loop inhibiting BMAL1:CLOCK heterodimerization. PER2 feeds back and promotes *bmal1* transcription. BMAL1:CLOCK also targets the gene *rev-erbα* which in turn represses *bmal1* transcription, leading to an oscillation in BMAL1 expression. BMAL1:CLOCK also regulates a number of clock controlled output genes.

expression of the Kv4.2 channel, which partially encodes the I_{to}. mRNA levels of the Kv4.2 channel were found to increase two-fold from the trough at ZT18, the midpoint of the active phase in the rat, to the peak at ZT6, the midpoint of the resting phase. Functionally, the I_{to} current was also found to be greatest during the midpoint of the resting phase although this was not found to be significant. (Yamashita, Sekiguchi et al. 2003). More recently, Jeyaraj *et al.* examined the true circadian rhythmicity of these fluctuations in cardiac K^+ channel expression by placing male rats in constant darkness and it was found that expression of the α (Kcnd2) and β (KChIP2) subunits of I_{to} displayed circadian rhythm (Jeyaraj, Haldar et al. 2012).

1.3.3   The Circadian clock and Excitation-Contraction Coupling

Recent work by Collins and Rodrigo has highlighted for the first time a diurnal variation in E-C coupling in isolated cardiomyocytes, comparing 'rest period' myocytes (ZT3) to 'active period' myocytes (ZT15) in the nocturnal rat.   Basal systolic and diastolic $[Ca^{2+}]_i$, cell shortening, the rate of relaxation and $[Ca^{2+}]_{SR}$ were all found to be greater in myocytes isolated during the rest period of the rat. Rest period myocytes also exhibited a greater responsiveness to ISO, displaying a greater maximum systolic $[Ca^{2+}]_i$ and $[Ca^{2+}]_{SR}$, corresponding to a greater development of arrhythmias, specifically DADs, in rest-period myocytes compared to myocytes isolated in the active-period. Inhibition of NOS with a non-specific NOS inhibitor, L-NNA, had little effect on the contractility of rest-period myocytes, measured via $[Ca^{2+}]_i$, however administration of L-NNA significantly increased ISO induced systolic $[Ca^{2+}]_i$ and LTCC current density in active-period myocytes (Collins and Rodrigo 2010). Genes involved in E-C coupling were also assessed with RT-PCR to examine if any diurnal variation in their expression could be observed. It was found there was no difference in the expression of LTCC, SERCA-2A, PLB or RyR2 between the two time points, however expression of NCX and $β_1$-ADR were significantly higher in active-period myocytes and a 5-fold increase in the expression of nNOS in tissue isolated from the LV wall and a more modest 2.65 fold increase in nNOS expression in myocytes isolated in the active-period of the rat. These results lead to the conclusion that the anti-arrhythmic effect of NO signalling protects the heart from Ca^{2+} overload injury in active period myocytes when nNOS expression is at its highest level, preventing arrhythmia generation in response to β-ADR stimulation. The high nNOS expression in active period myocytes corresponds with

the time period where sympathetic activation is also at its greatest level and prone to surges. The protection offered by nNOS could reduce the incidence of arrhythmic activity during periods of high stress.

1.4   Project Aims

In the cardiovascular system, β_3–ADR have been suggested to act as a 'brake' on sympathetic stimulation when catecholamine levels are high, acting to reduce the inotropic response protecting the heart against Ca^{2+} overload injury. The majority of CV events such as myocardial infarction (MI) and sudden cardiac death (SCD) occur in the early hours of the morning, correlating with an increase in sympathetic tone and an increase in a number of CV parameters such as HR, CO and BP.

Previous data from this laboratory has shown that the time-of-day influences Ca^{2+} regulation in cardiomyocytes and their responsiveness to β-ADR stimulation with ISO, which impacts on the arrhythmic activity in response to ISO (Collins and Rodrigo 2010). The data suggest that this variation results from time-of-day changes in NO-signalling, which may be due to differences in β_3–ADR signalling and may be a mechanism to protect the heart against sympathetic stimulation induced arrhythmias. More recently elements of the cardiac AP, such as expression of the ion channels governing repolarisation, have been noted to exhibit time-of-day variations (Jeyaraj, Haldar et al. 2012), which could contribute to in the time-of-day changes in Ca^{2+} regulation that have been observed (Collins and Rodrigo 2010).

The aims and objectives of my PhD were:

1. ***To determine whether the β₃-ADR and its downstream signalling mechanisms are responsible for the time-of-day variation in response to sympathetic stimulation:***

My aim was to investigate whether any time-of-day variation in β_3-ADR signalling exist in the ventricular myocyte, to see whether this affects Ca^{2+} regulation and electrical activity and to determine if this was able to account for the documented time-of-day variation in E-C Coupling and in its response to β-ADR stimulation. Ca^{2+} transients and AP configuration will be assessed to investigate a time-of-day variation in E-C coupling in cardiomyocytes at baseline and in response to β-ADR stimulation with ISO and the β_3-ADR specific agonist BRL_{37344}.

2. ***To develop a cellular model using cultured adult rat ventricular myocytes (ARVM) for investigation of circadian rhythms:***

We set out to determine whether the circadian clock mechanism, when resynchronised using a "serum-shock" protocol in cultured ARVM, behaved in a similar fashion to that identified *in vivo*. The aim of this was to develop a tissue culture based model in order to enable investigation of the impact of the intrinsic circadian clock on ventricular function to provide an animal free model and enable the use of SiRNA gene knockdown in our study.

3. ***To investigate the contribution of the β₁-ADR, β₂-ADR and β₃-ADR to control of Ca^{2+} regulation and to investigate the role each receptor plays in arrhythmogenesis:***

As an increase in sympathetic activity leads to stimulation of all three β-ADR's; β_1-ADR, β_2-ADR and β_3-ADR in the ventricle, the overall inotropic action of sympathetic stimulation is a balance between the positive inotropic action of the β_1-ADR and β_2-ADR stimulation, the negative inotropic action of the β_3-ADR and the restriction of the positive inotropism of β_2-ADRs due to coupling to G_i.

My initial aim was to investigate the inotropic effect of each receptor and dissect their contribution to the overall positive inotropic effect of β-ADR stimulation. In particular, I investigated the signalling pathway of the inhibitory G_i protein in the β_2-ADR and β_3-ADR, comparing the roles of PDE and NO between the β_2-ADR and β_3-ADR signalling.

I also aimed to investigate the arrhythmogenic properties of the three β-ADR's and to examine the role of time-of-day variations in Ca^{2+} regulation on arrhythmogenesis in the myocyte. In particular, investigating the role of the inhibitory G_i protein in arrhythmogenesis and potential cardio-protective benefits of G_i protein stimulation.

Chapter 2: Methods

2.1 Experimental animals and isolation of ventricular myocytes

2.1.1 Experimental animals

Adult male Wistar rats originally obtained from Charles River laboratories were housed in environmentally controlled rooms (lights on from 06.00 to 18.00) with food and water provided *ad libitum* at the Central Research Facility, University of Leicester. The animals used in the present study were at least 8 weeks old at time of sacrifice (200g – 300g). All animals were sacrificed by cervical dislocation followed by severance of major artery, in accordance with Schedule One of the Animals (Scientific procedures) Act, 1986.

2.1.2 Ventricular myocyte isolation

Single ventricular myocytes were isolated using a method previously described by Lawrence and Rodrigo (Lawrence and Rodrigo 1999). Immediately following sacrifice of the animal, the heart was rapidly removed and placed in ice cold Ca^{2+}-free Tyrode solution. The heart was cannulated via the aorta and perfused using the Langendorff retrograde method, which perfuses the heart against a closed aortic value, forcing solution to perfuse the coronary arteries at a constant rate of 10ml/min. Hearts were perfused with Ca^{2+}-free Tyrode solution for 6 minutes, followed by 6-8 minutes of enzyme solution to digest the heart, containing type I Collagenase (1 mg/ml) and type XIV Protease (0.67 mg/ml) and BSA fraction V (1.67 mg/ml) (Sigma) in Ca^{2+}-free Tyrode. The first 90 seconds of enzyme solution was discarded, the remainder was then recirculated. This was followed by perfusion for 3 minutes with 2mM Ca^{2+} Tyrode solution (normal Tyrode) to washout and inactive the enzyme solution. All solutions were bubbled with 100% oxygen throughout and warmed to 35 ± 1°C. During the final minute of normal Tyrode perfusion, the atria were removed and the heart was cut down, coarsely cut in half and placed in a conical flask containing approximately 10ml normal Tyrode. Single ventricular myocytes were released by gentle shaking of the heart at 35°C in a shaking water bath (Stuart, SBS40) at a speed of 150 strokes/minute. The resulting suspensions of cells were sieved using a 200µm^2 pore stainless steel sieve (Sigma) and washed twice by centrifuging cells at 400r.p.m. in 15ml corning tubes for 1 minute, removing the resulting supernatant and

replacing with fresh normal Tyrode. This method of isolation provided cell suspensions with a viability of 60-80%. Cells were stored in Petri dishes at room temperature and all cells were used on the day of isolation.

2.1.3   Time points to investigate diurnal variation

In order to study the effect of time-of-day on cardiac myocyte E-C coupling suitable time points corresponding to the animals' rest- and active-period were required. These time points were chosen and classified according to zeitgeber times. A zeitgeber, which can be translated to time giver, in mammals is commonly a light stimulus which is known to entrain the central circadian clock (Edery 2000), located in the Suprachiasmatic Nuclei (SCN), which is responsible for co-ordination of the peripheral clocks (Young 2003). In order to obtain animals from two time points separated by twelve hours, representing the animals rest-period and active-period in the nocturnal rat, all animals were randomly allocated to one of two rooms with opposing twelve hour light cycles, with the time of lights on representing zeitgeber time period zero (ZT0) and the time of lights off representing zeitgeber time point twelve (ZT12). Animals were housed in either the Normal Light Cycle (NLC) room, lights on from 06.00 to 18.00, or the Reverse Light Cycle (RLC) room, lights on from 18.00 to 06.00, for at least 3 weeks prior to use at 9.00 on experimental days. (See Figure 2.1).

As the rat is nocturnal, animals housed in the NLC room were sacrificed three hours after lights were switched on with a Zeitgeber time of ZT3, which corresponds to the animals' rest-period. Conversely, animals housed in the RLC room were sacrificed 15 hours after lights were switched on with a zeitgeber time of ZT15, and 3 hours into the animals' active-period. Immediately following sacrifice, ventricular myocytes were isolated as previously described and in this investigation referred to as rest-period myocytes (isolated from ZT3 hearts) and active-period myocytes (isolated from ZT15 hearts). This nomenclature also refers to isolated tissue samples.
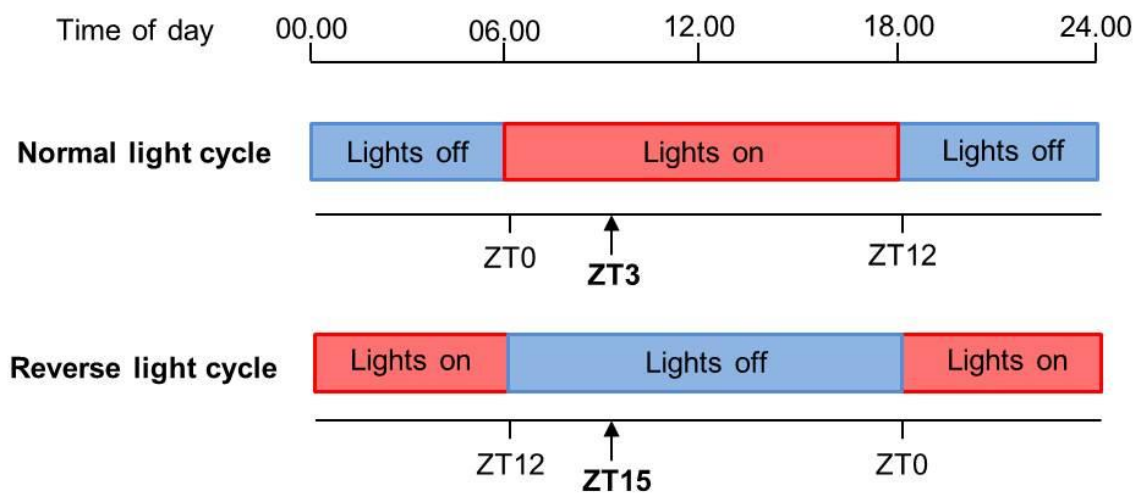
Figure 2.1   A schematic of the light cycle and Zeitgeber Time (ZT).
This figure shows the 12-hour light cycle regime for both the Normal Light Cycle and Reverse Light Cycle rooms in which animals in this investigation were housed. In the normal light cycle room, lights were switched on at 06.00 (corresponding to ZT0) and switched off at 18.00 (corresponding to ZT12). In the reverse light cycle room lights were switched off at 06.00 (corresponding to ZT12) and switched on at 18.00 (corresponding to ZT0). The figure also details the zeitgeber time points investigated; ZT3 (corresponding to three hours after lights were switched off) and ZT15 (corresponding to three hours after lights were switched off).

2.2 Contraction studies and Calcium measurement

2.2.1 Superfusion of cells

Ventricular myocytes used to study contraction and calcium handling were placed into a 500µL diamond-shaped superfusion chamber on the stage of an inverted microscope (Nikon Diaphot) containing normal Tyrode solution and allowed to settle. The myocytes were perfused constantly with Tyrode solution at a rate of 2-4mL/minute via a peristaltic pump. The temperature of the perfusion chamber was maintained at 35 ± 1°C (Single Inline Solution Heater, SH-27B, Warner Instruments). Cells were electrically field stimulated during superfusion using two platinum stimulation electrodes in the bath, connected to a stimulator (Research stimulator, 6002, Harvard). All cells were stimulated at a rate of 1Hz, and any cells not contracting synchronously at the start of superfusion were not used in experimentation. (See Figure 2.2 for a schematic of the superfusion chamber).

2.2.2 Arrhythmia studies

To determine arrhythmic activity, cells were viewed on the stage of an inverted Nikon Diaphot microscope coupled to a charge coupled device camera (WATEC monochrome camera 1/2" Wat-902B) which allowed superfused myocytes to be viewed on a video monitor (Panasonic WV-5340). To determine the development of arrhythmic activity in response to β-ADR stimulation, ventricular myocytes were electrically field stimulated at 1Hz and perfused with normal Tyrode for 5 minutes and a field of 10 to 30 synchronously contracting cells was identified and counted, using a x10 objective. Only cells which were contacting synchronously in response to 1Hz electrical field stimulation were selected for experimentation. To determine the arrhythmic activity of cells in the field of view, the stimulator was switched off for 10 seconds and the number of cells displaying spontaneous extra-contractions were counted. Cells displaying arrhythmic activity at this basal stage were discounted from experimentation. Cells were then superfused with desired agonist for 5 minutes whilst being field stimulated at 1Hz to allow cells to reach a steady state. To determine the arrhythmic activity of cells in the field of view the
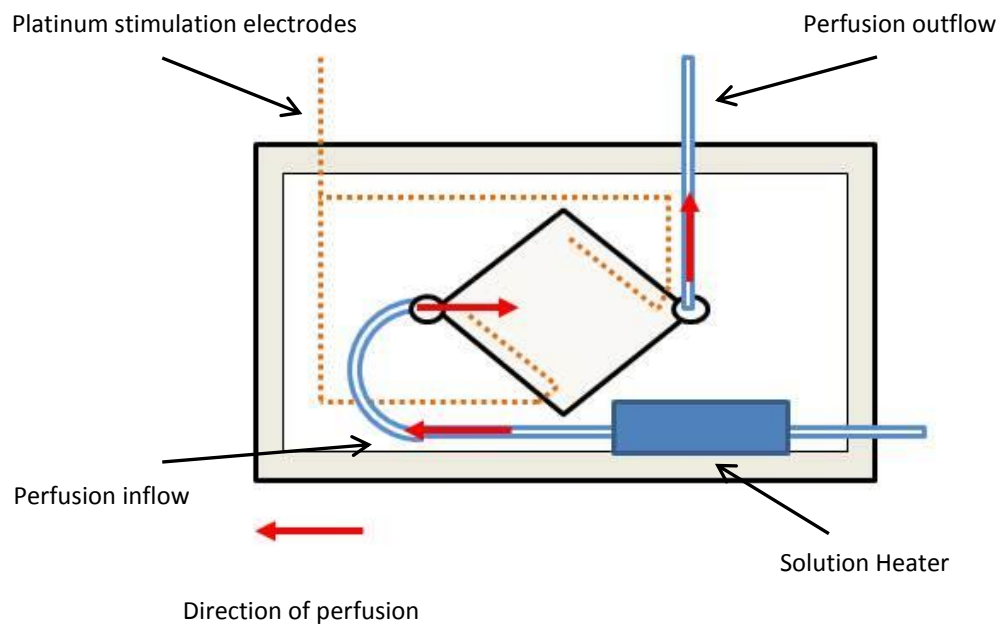
Figure 2.2   A schematic of the Myocyte superfusion chamber.
Figure shows the 500μL diamond-shaped superfusion chamber on the stage of an inverted microscope used in all fluorescence experiments. Cells were perfused constantly with Tyrode solution at a rate of 2-4mL/minute via a peristaltic pump. The temperature of solutions perfusing cells in the chamber was maintained at 35 ± 1°C using the solution heater connected to a temperature controller. Platinum stimulation electrodes enabled electrical field stimulation of cells in the perfusion chamber.

stimulator was again switched off for 10 seconds and the number of cells displaying spontaneous extra-contractions were counted.

To quantify basal arrhythmic activity levels, data was expressed as the percentage of synchronously contracting cells at the start of experimentation in normal Tyrode which displayed spontaneous contractile activity once the stimulator was switched off.

As stated previously, any cells which displayed basal arrhythmic activity in normal Tyrode were discounted from the remainder of the investigation, and so to quantify arrhythmic activity in response to β-agonists, data was expressed as the percentage of quiescent cells in normal Tyrode (with the stimulator off) which developed spontaneous extra-contractions following β-agonist perfusion (with the stimulator off).

2.2.3 Intracellular calcium measurement

Intracellular calcium was measured in single ventricular myocytes using the fluorescent calcium indicator Fura-2, a ratiometric dye whose excitation spectrum changes when bound to calcium. Fura-2 exists in the free and Ca^{2+}-bound forms within the loaded cells, and the ratio of emitted light at 510nm from cells when excited at 340nm and 380nm allows accurate measurement of intracellular Ca^{2+} concentration. The Fura-2 loaded cell is excited alternately at 340nm/380nm and the ratio of fluorescence intensity recorded at 510nm in response to 340nm (Ca^{2+}-bound) to 380nm (Ca^{2+}-free) is proportional to $[Ca^{2+}]_i$ within cells. As such the ratio of fluorescence intensity and therefore Ca^{2+} concentration is independent of dye concentration or cell size and is not affected by photobleaching. (Lambert 2006). This ratio of fluorescence intensity can be calibrated to assess $[Ca^{2+}]_i$.

2.2.3.1   Fura-2 cell loading

Fura-2(AM) (Molecular Probes, Invitrogen) is an acetoxymethyl (AM) ester which is a cell permeable derivative of Fura-2. Fura-2(AM) is able to cross the cell membrane due to ester groups which make Fura-2 lipid soluble, and once inside the esters are cleaved by endogenous intracellular esterases, regenerating the fluorescent Fura-2 salt in a cell impermeable state. Indicative esters such as Fura-2 have a poor solubility in physiological

media; however the addition of pluronic acid, a mild non-ionic detergent, can improve the solubility of indicative esters, emulsifying the lipohpillic Fura-2(AM) into soluble mycelles increasing the likelihood of the Fura-2(AM) ester crossing the cell membrane (Lambert 2006).

Stocks of Fura-2(AM) (2mM) were made by the addition of 25µL of 5% Pluronic acid in DMSO to a 5µg vial, stored at -20°C and protected from the light. Each vial was used within one month.

To load cardiac myocytes with Fura-2, 5µL of 2mM Fura-2 stock solution was added to 2mL of cells suspended in normal Tyrode solution, covered to protect them from the light and left for 20 minutes to allow loading of the Fura-2(AM) into the cell, following which cells were washed twice with normal Tyrode. Cell suspensions were stored at room temperature and protected from light.

2.2.3.2 Fluorescence microscopy

Fluorescence recordings of single Fura-2 loaded myocytes were made using a photomultiplier based system housed in a light proof chamber. Myocytes were viewed using a x40 oil immersion fluorescence objective (fluor 40/1.30 oil) with a Nikon Dipot inverted microscope was housed in the light proof chamber, its output connected to a photomultiplier system (See figure 2.3 for a schematic of the photomultiplier system). A single ventricular myocyte was chosen from the field of electrically stimulated myocytes and screened from all other cells using horizontal and vertical shutters. This cell was excited with light from the monochromator (Delta Ram X, PTI) at 340nm and 380nm alternately at a rate of 60Hz, directed toward the cell of interest using an excitation dichroic mirror. The resulting light emitted from the cell was transmitted to the photomultiplier tube detection system (PTI Felix 32) by an emission dichroic mirror and an emission filter (>510nm).
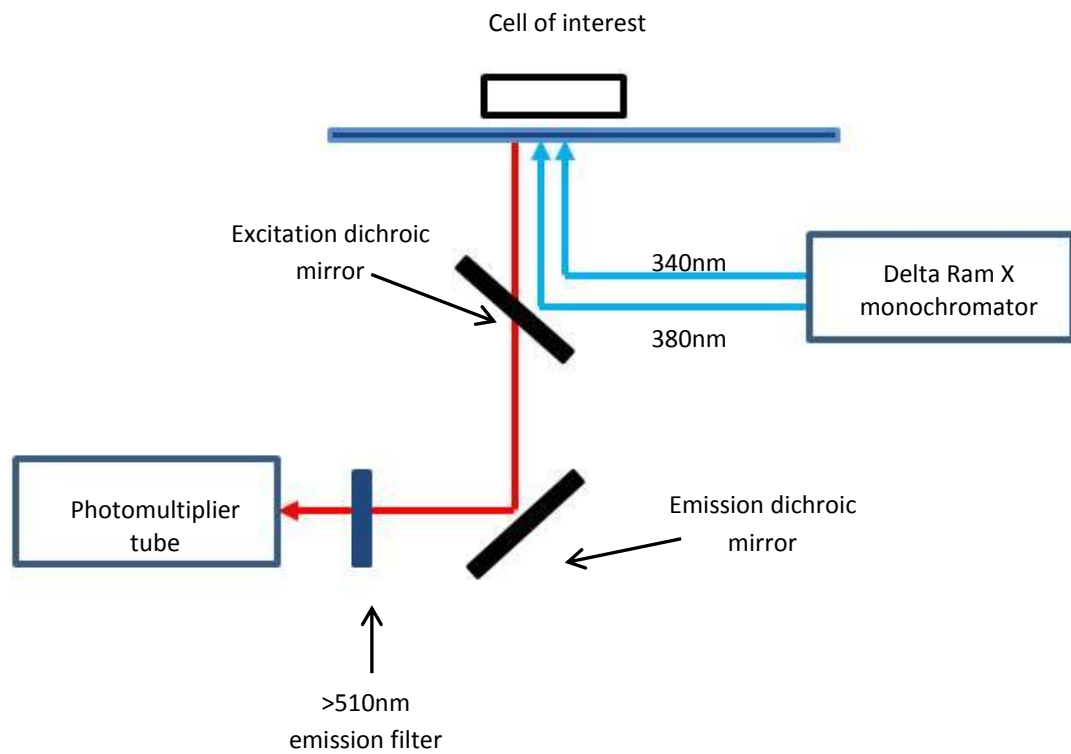
Figure 2.3   A schematic of fluorescence excitation/emission pathway.

Figure shows the light pathway for the dual excitation-single emission fluorescent dye Fura-2. Fura-2 loaded cells were alternately excited at 340/380nm and light emitted collected at 510nm.

2.2.3.3 Measurement of intracellular calcium concentration and sarcoplasmic reticulum calcium stores

Recordings of $[Ca^{2+}]_i$ and SR Ca-stores from single ventricular myocytes were made from cells electrically field stimulated at 1Hz following 5 minutes perfusion with normal Tyrode to ensure recording of a steady state basal transient. To determine $[Ca^{2+}]_i$, 5-10 electrically-induced Ca^{2+} transients were recorded in response to electrical field stimulation at 1Hz, which once calibrated allowed determination of diastolic $[Ca^{2+}]_i$, systolic $[Ca^{2+}]_i$ and the exponential time constant of the calcium transient, which is reflective of SERCA-2A activity (Bers 2001). To allow determination of SR Ca^{2+} loading the electrical stimulator was then switched off and normal Tyrode solution containing 20mM caffeine was rapidly applied to cardiomyocytes for approximately 5 seconds until a caffeine-induced Ca^{2+} transient was visible on the trace, which once calibrated provides an indication of the SR Ca^{2+} loading of the myocyte, and the exponential time constant of the caffeine-induced Ca^{2+} transient, which is reflective of NCX activity (Bers 2001). The electrical stimulator was then switched back on and cells were electrically field stimulated at 1Hz to allow recovery of electrically-induced Ca^{2+} transients. Caffeine solution was applied to cells at 35 ± 1°C (Single Inline Solution Heater, SH-27B, Warner Instruments).
Cells were then superfused with desired agonist/inhibitor for 5 minutes whilst being field stimulated at 1Hz to ensure maximal agonist/inhibitor response and allow cells to reach a steady state before recording of electrically-induced and caffeine-induced Ca^{2+} transients were made, as described above.

2.2.3.4 *In vivo* calibration of $[Ca^{2+}]_i$

In this investigation recorded Fura-2 ratios of Ca^{2+} transients were calibrated to $[Ca^{2+}]_i$ *in vivo* utilising the Grynkiewicz equation;

$$[Ca^{2+}]_i \;=\; K_d \left(\frac{R - R_{min}}{R_{max} - R} \right) \times \left(\frac{F_{380max}}{F_{380min}} \right)$$

The equation requires the use of a number of calibration constants; the Ca^{2+} dissociation constant (K_d), the 340nm/380nm ratio at maximum Ca^{2+} (R_{max}) and Ca^{2+} absence (R_{min}) and the ratio of bound to unbound Ca^{2+} at 380nm (F_{380max}/F_{380min} ratio) (Lambert 2006).

R	=	Measured Fura-2 ratio
K_d	=	285nM
R_{min}	=	0.40
R_{max}	=	4.96
F_{380max}/F_{380min}	=	6.39

In this investigation K_d was obtained from Groden et al. (Groden, Guan et al. 1991), reported to be 285nm at 37°C. The R_{min}, R_{max} and F_{380max}/F_{380min} ratio have previously been calculated by other members of our group in 41 cells from hearts at various time points and no significant difference was found and so the values were used to calibrate the fura-2 ratio in subsequent cells. Determination of R_{min} (the 340nm/380nm ratio in the absence of Ca^{2+}) was achieved by loading of single ventricular myocytes with 2mM BAPTA-AM, fluorescence ratios obtained in these cells were taken as R_{min}. R_{max} (the 340nm/380nm ratio in maximal Ca^{2+}) was determined in Fura-2 myocytes whose membranes had been disrupted with a microelectrode to allow Ca^{2+} absorption to the cell from the surrounding normal Tyrode. The F_{380max}/F_{380min} ratio was determined in R_{min} and R_{max} cells, the ratio of fluorescence emission intensity at 380nm. The experimental data calibrated as $[Ca^{2+}]_i$ of both the electrically-induced and caffeine-induced Ca^{2+} transients were exported from the Felix PTI software and analysed in Graphpad prism 6.

Stimulator on	Stimulator off	Stimulator on
Electrically-evoked	Caffeine-evoked	Electrically-evoked

20mM Caffeine
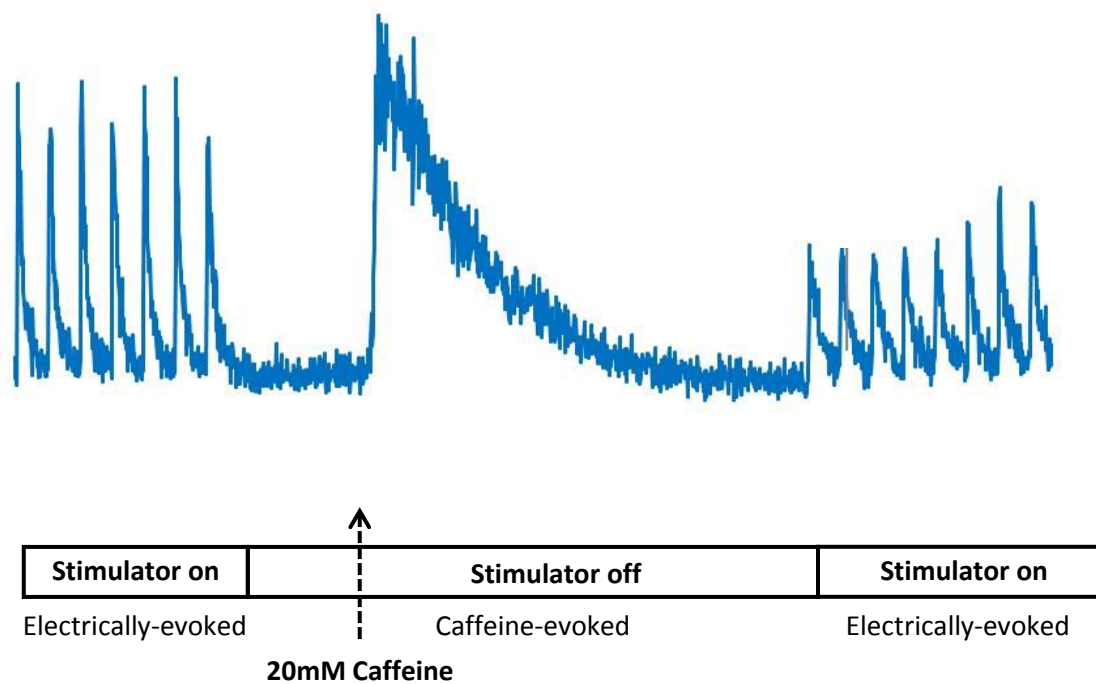
Figure 2.4   **An example** recording of electrically-induced and caffeine-induced calcium transients recorded from a single ventricular myocyte in normal Tyrode solution.
Figure shows 5-10 electrically-induced Ca^{2+} transients were recorded in response to electrical field stimulation (stimulator on). Following which the stimulator was switched off and 20mM Caffeine was rapidly applied to cardiomyocytes for approximately 5 seconds until a caffeine-induced Ca^{2+} transient was visible. The stimulator was then switched on and cells were then electrically field stimulated allow recovery of electrically-induced Ca^{2+} transients.

2.2.3.5   Parameters of $[Ca^{2+}]_i$ measured

Data from 3 of the 5-10 recorded electrically-induced Ca^{2+} transients were averaged and measurements of diastolic $[Ca^{2+}]_i$, systolic $[Ca^{2+}]_i$ and exponential time constant for relaxation of the electrically-induced Ca^{2+} transient were made (See figure 2.5). The exponential time constant was calculated by fitting the relaxation phase of the Ca^{2+} transient with a single exponential decay curve in Graphpad prism 6. The exponential time constant of electrically-induced Ca^{2+} transients are indicative of the function of SERCA-2A in rat cardiomyocytes, as SERCA-2A is the dominant mechanism for removing intracellular Ca^{2+} during relaxation of the electrically-induced Ca^{2+} transient over the NCX in rat cardiomyocytes at a ratio of 10:1 (Bers 2001).

Measurement of peak Ca^{2+} release and exponential time constant of the caffeine-induced Ca^{2+} transient was made for each experimental solution. The exponential time constant was again calculated by fitting the relaxation phase of the Ca^{2+}-transient with a single exponential decay curve in Graphpad prism 6. Peak Ca^{2+} release of caffeine-induced Ca^{2+} transients indicates SR Ca^{2+} loading and was taken as the amount of Ca^{2+} available in the SR for release at that time (Bers 2001). The exponential time constant of decay of the caffeine-induced Ca^{2+} transients are indicative of the function of the NCX in cardiomyocytes, as during a caffeine induced Ca^{2+} transient the decline in $[Ca^{2+}]_i$ is almost entirely due to Ca^{2+} removal by the NCX (Bers 2001).
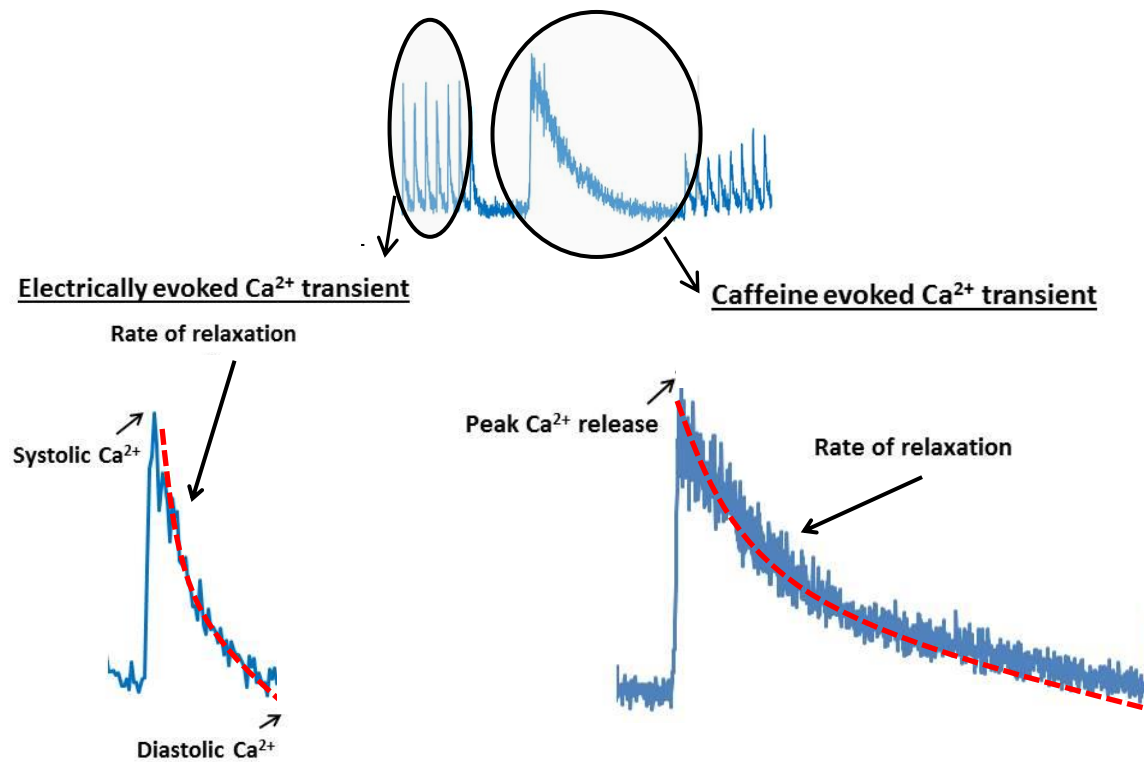
Figure 2.5   An example of analysis of the recorded calcium transients.

Figure shows an example recording of both electrically-induced and caffeine-induced calcium transients recorded from a single ventricular myocyte in normal Tyrode solution. Illustrated are the measurements of systolic and diastolic calcium levels in electrically-induced calcium transients and the peak calcium release in caffeine-induced transients. The rate of relaxation of electrically-induced and caffeine-induced calcium transients was calculated by fitting the relaxation phase of the Ca^{2+}-transient with a single exponential decay curve (red dotted line).

2.3   Electrophysiological recordings

The modern patch-clamp technique, first developed by Neher and Sakmann in 1976, involves the use of a glass microelectrode to record voltage difference across a cell membrane or facilitate voltage-clamp to record ionic membrane currents, allowing the study of a single or multiple ion channel activity. There are a number of patch-clamp configurations available to investigators including cell attached, excised patch (inside-out and outside-out) and whole-cell. In this investigation whole-cell patch-clamp was used to make recordings of action potentials (AP) and single currents (I_{to}, LTCC) from ventricular myocytes.

2.3.1   Electrophysiology set up

Isolated ventricular myocytes were placed in a 500µl diamond shaped perfusion chamber over the stage of an inverted microscope (Nikon eclipse, TE200) containing normal Tyrode. Cells were constantly perfused throughout experimentation at a rate of 2-4ml/min via gravity fed perfusion system. The temperature of the perfusion chamber was maintained at 35 ± 1°C (Single Inline Solution Heater, SH-27B, Warner Instruments). The microscope was placed on an anti-vibration table surrounded by a Faraday cage to minimise electrical noise. The electrode was held in a headstage (Axon CNS, HS-9A x0.1) and moved around the recording chamber in 3 planes by a micromanipulator (Scientifica, ACCi UI). Contact was made between the electrode filling solution and the pre-amplifier using a silver coated silver electrode wire (Ag/AgCl). The bath electrode, also Ag/AgCl, provided an electrical connection to the solution in the bath, holding the bath at zero potential so that all recordings were made with respect to earth (zero mV).

2.3.2   Glass pipettes

Patch pipettes for electrophysiological measurements were pulled from filamented, thick-walled borosilicate glass capillary tubes (1.5mm O.D., Harvard apparatus) using a two-step microelectrode puller (Narishige PB-7). Thick-walled glass was used due to the lower pipette capacitance. High-resistance patch pipettes were used for action potential

recordings (12-15MΩ), but for ionic current measurements during voltage-clamp low-resistance pipettes were used (2-4MΩ). Low resistance pipettes are essential for rapid clamping of cell membrane voltage, thereby minimising errors in measurement of both voltage and current during voltage-clamp protocols by reducing the size and time constant in any series resistance errors (Ogden 1994).

2.3.3   Whole-cell patch-clamp technique

The whole-cell patch-clamp technique involves isolating a patch of cell membrane by placing a pulled glass patch pipette, backfilled with the appropriate pipette solution, on to the surface of a cell and applying a small amount of suction to form a high resistance seal, termed a gigaseal (1GΩ). The bridge balance must be corrected for prior to the glass pipette being touched onto the cell membrane, this corrects for errors in voltage drop across the electrode when a current is injected, and is dependent upon electrode resistance. Once a gigaseal is formed, visible fast capacity transients due to the pipette capacitance are neutralised. Whole-cell configuration is achieved by rupturing the patch of membrane isolated by the patch pipette by applying further suction in a short, sharp burst to disrupt the membrane and achieve contact with the intracellular solution; whole-cell configuration.

2.3.3.1   Current Clamp; Recording of action potentials

High resistance pipettes were filled with K^+ electrode solution and had a resistance of 12-15MΩ. Electrical recordings of membrane potentials were measured in current clamp mode using an Axon integrated Patch clamp instrument (AXOPATCH 200B) and high-resolution, low-noise data acquisition system (DIGIDATA 1322A) or Axon integrated Patch clamp instrument (AXOCLAMP 900A) and the data acquisition system (Axon DIGIDATA 1550).

Cells were stimulated with an above threshold depolarising pulse (1.5 times threshold) for 5ms in order to initiate consistent firing of action potential from the cardiomyocyte.

75

During experimentation myocytes were stimulated constantly to generate action potentials at 1Hz.

For action potential recordings made using the AXOPATCH 200B, basal action potential values were obtained at the end of 5 minutes of superfusion with normal Tyrode. For action potential recordings made using the AXOCLAMP 900A basal action potential values were obtained at the end of 10 minutes of superfusion with normal Tyrode, during which steady state had been reached. Cells were then superfused with desired agonist/inhibitor for 5 minutes ensure maximal agonist/inhibitor response and allow cells to reach a steady state. Action potentials were monitored at all times during experimentation however action potentials were only recorded for analysis during the final 10-15 seconds of perfusion for each solution.

10 action potential traces were averaged and analysed in Clampfit 10.4. Measurement of resting membrane potential (RMP) and calculation of repolarisation to 30% (APD30), 50% (APD50) and 90% (APD90) were made. Repolarisation was calculated as a 30%, 50% or 90% recovery of the amplitude of the action potential (see Figure 2.6).
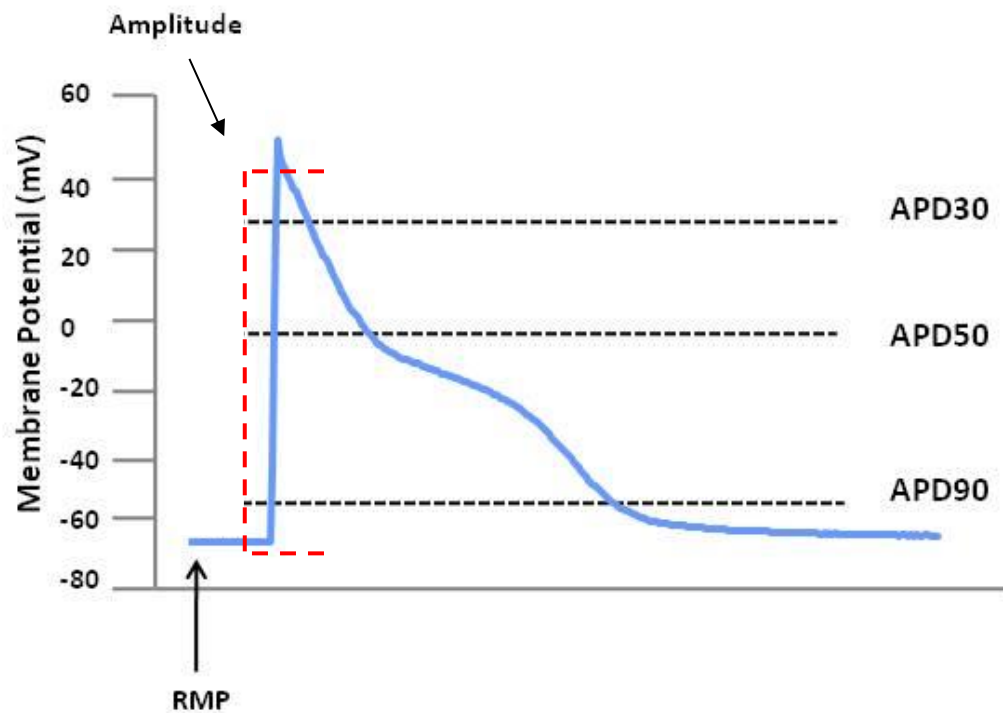
Figure 2.6 **An example recording of an action potential.**
A schematic of an example recording of an action potential showing measurement of resting membrane potential (RMP), the amplitude of the action potential and calculation of repolarisation to 30% (APD30), 50% (APD50) and 90% (APD90).

Figure 2.6 **An example recording of an action potential.**
A schematic of an example recording of an action potential showing measurement of resting membrane potential (RMP), the amplitude of the action potential and calculation of repolarisation to 30% (APD30), 50% (APD50) and 90% (APD90).

2.3.3.2   Voltage-clamp; Recording of ionic currents

Voltage-clamp protocols were used to record I_{to} and LTCC in single isolated cardiomyocytes in discontinuous single-electrode voltage-clamp (dSEVC) mode using an Axon Axoclamp Microelectrode Amplifier (AXOCLAMP 900A) and data acquisition system (DIGIDATA 1550) using the electrophysiology software pClamp10.4. In the dSEVC technique a single electrode is required to penetrate the cell which shares the task of voltage recording and current injection, and is therefore useful in situations where small cells cannot be impaled by two electrodes. The technique involves switching between the voltage recording and current injection modes, effectively providing two micropipettes: a voltage-recording micropipette and a current-passing micropipette. As current does not flow when membrane potential is measured in dSEVC, this provides a more stable and faster clamp than standard whole-cell patch-clamp techniques, in which same electrode is used to simultaneously record voltage and for current passing. The simultaneous recording of voltage and current causes a voltage error due to the voltage drop caused by current flowing across the series resistance of the electrode (Ogden 1994). Standard whole-cell patch-clamp techniques require correction of this series resistance, however this is not required in dSEVC as membrane potential is measured when current does not flow, eliminating any errors in voltage (Ogden 1994).

Low resistance pipettes were filled with the appropriate electrode solution and had a resistance of 2-4mΩ. Prior to voltage-clamp protocols the cell capacitance was calculated. Capacitance of a cell membrane can be determined from the rate and amplitude of a change in voltage across the cell membrane in response to an injection of current when in current-clamp mode (Golowasch, Thomas et al. 2009). A 1nA current injection step (100ms) was applied to the cell once whole-cell configuration was achieved and the resulting change in membrane potential recorded. (see figure 2.7 for a schematic of the recording). Three recordings were averaged and measurement of electrode resistance (R_e), cell membrane resistance (R_m) and the exponential time constant, calculated by fitting the relaxation phase with a single exponential decay curve in Clampfit 10.4. Cell capacitance was then calculated using the following equation: $C_m = \tau_m / R_m$
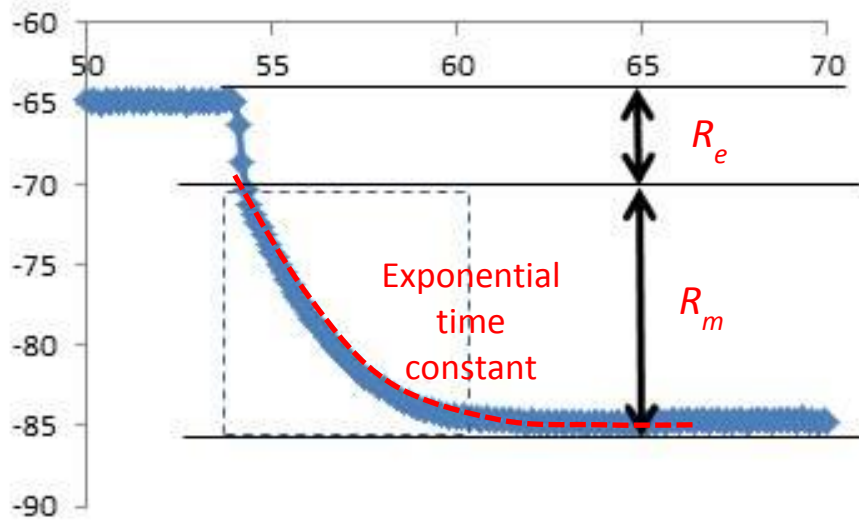
Figure 2.7   An example of cell capacitance determination

A schematic of the cell capacitance protocol displaying the change in membrane potential in response to a 1nA current injection step, showing measurement of electrode resistance (R_e), cell membrane resistance (R_m) and the exponential time constant (red dotted line). The exponential time constant was calculated by fitting the relaxation phase with a single exponential decay curve.
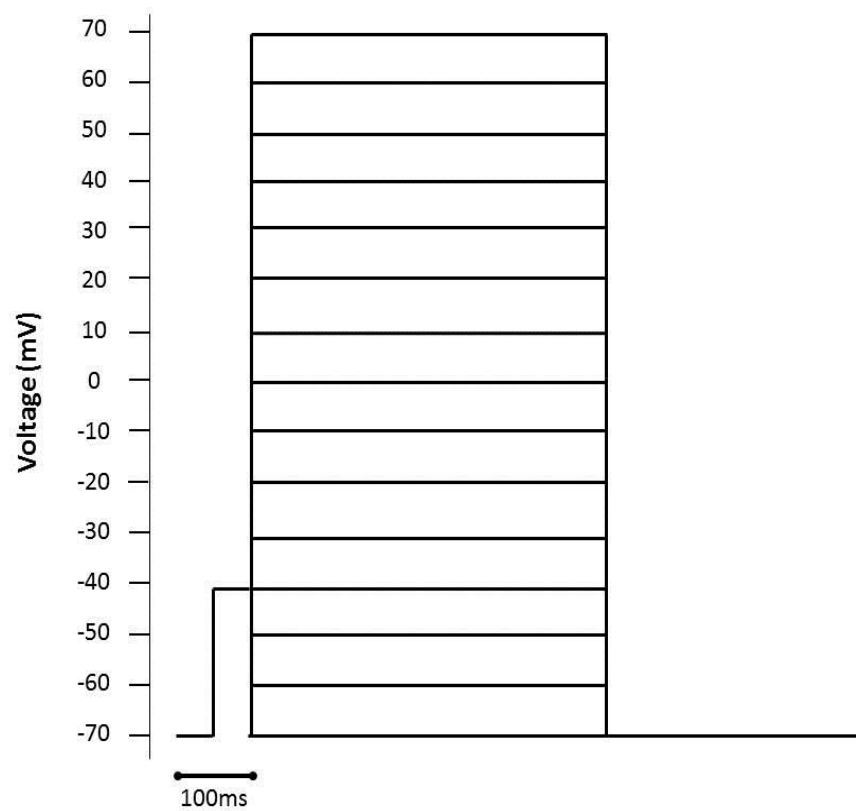
Figure 2.8   **An example of the voltage-clamp protocol applied to ventricular myocytes to measure I_{to} and I_{LTCC}.**

A schematic of the voltage-clamp protocol, showing a holding potential of -70mV and a 50ms depolarising step to -40mV, followed by 500ms 10mV incremental steps from -70mV to either +50mV in recordings of I_{to} or +70mV in recordings of LTCC.

A combination of voltage-clamp protocols and selective current inhibitors were used to isolate the currents of interest for recording. For transient outward current (I_{to}) recordings K$^+$ electrode solution was used to backfill patch pipettes and the calcium channel blocker cadmium chloride ($CdCl_2$) (200nM) was present in all experimental solutions to inhibit the LTCC. For LTCC recordings Cs$^+$ electrode solution was used to backfill patch pipettes, cesium ions block potassium channels in biological membranes thereby blocking I_{to} and all other potassium currents. The voltage protocol clamped cells at a holding potential of -70mV followed by a 50ms depolarising step to -40mV to inactivate fast activating sodium channels. Membrane potential was then stepped from -70mV to either +50mV in I_{to} protocols or +70mV in LTCC protocols, in 10mV incremental steps for 500ms duration to measure individual currents (see figure 2.8). Data was sampled at 5kHz, using a low pass Bessel 10kHz filter and analysed in pClamp 10.4. Cell currents were normalised to cell capacitance (pA/pF) to allow for variation in cell size.

For ionic current recordings baseline values were obtained at the end of 10 minutes of superfusion with normal Tyrode, during which steady state had been reached. The effect of β-ADR modulation on ionic current was obtained following 5 minutes of agonist superfusion. Voltage-step protocols were recorded for analysis during the final minute of each solution perfusion. 3 ionic current traces were averaged and analysed in Clampfit 10.4.

2.4 Investigation of the involvement of the inhibitory G-protein (G_i) in the effect of β-ADR stimulation on isolated cardiomyocytes

In order to investigate the involvement of the inhibitory G-protein (G_i) in the β-ADR effect on E-C coupling, electrophysiology and arrhythmia generation in isolated ventricular cardiomyocytes Pertussis toxin (PTx) (Tocris Bioscience) was used to permanently uncouple the G_i, from the $β_2$-ADR and $β_3$-ADR, so that the effect of β-ADR stimulation and signalling could be studied exclusive of the G_i inhibitory pathway.

PTx is a protein-based exotoxin produced by the bacteria *Bordetella pertussis*. PTx catalyses ADP-ribosylation of the G-proteins G_i/G_o impairing the G proteins heterodimer interaction with receptors, blocking receptor coupling with the G_i/G_o protein. PTx was

supplied as a 50μg vial and reconstituted upon arrival to 50μg/ml by the addition of 1ml MilliQ. 1ml of isolated cardiomyocytes in suspension in normal Tyrode were incubated for 3 hours with PTx (1.5μg/ml) and 2% Penicillin/Streptomycin (Sigma), plated in 6-well tissue culture plates, incubated in a water bath at 37 ± 1°C to inactivate G_i receptor.

In untreated cells adenosine negatively modulates β-ADR stimulation by inhibiting AC and reducing cAMP levels, via a PTx-sensitive G protein pathway (Xiao, Ji et al. 1995). Successful inactivation of the G_i receptor was determined in PTx-treated cells by the loss of the ability of adenosine to reduce the positive inotropic effect of $β_1$-ADR stimulation with dobutamine, measured by recording of Ca^{2+} transients as described previously (see section 2.2.3 Intracellular Calcium measurement) (see Appendix 1).

PTx-treated cells were compared to control cardiomyocytes which had been incubated in suspension in normal Tyrode with 2% Penicillin/Streptomycin in the absence of PTx also for 3 hours.

Comparison of basal parameters of Ca^{2+} handling (systolic $[Ca^{2+}]$, SR Ca^{2+} load, SERCA and NCX activity) and cardiac electrophysiology (APD, I_{to} and LTCC) measured showed relaxation of the Ca^{2+} transient to be slower (p<0.0001) in control cells as compared to freshly isolated cells. No significant difference in all other basal parameters measured was found (data shown in Appendix 2). In all cases, control cells incubated for 3 hours at 37°C responded to $β_2$–ADR stimulation with salbutamol in a similar fashion to freshly isolated myocytes (data not shown).
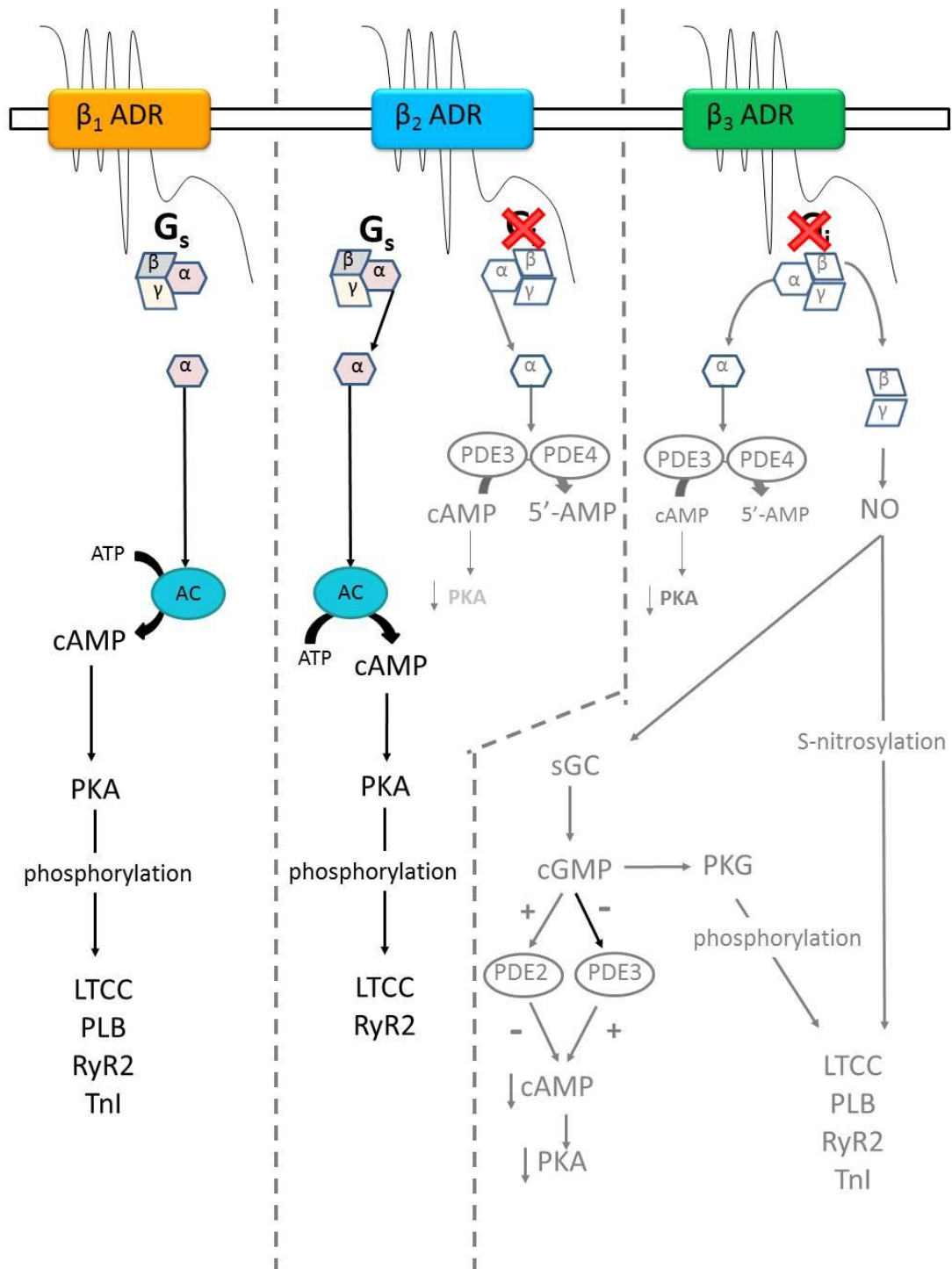
Figure 2.9 **A schematic of the β-adrenergic receptors in the ventricular myocardium and the effect of Gi uncoupling on the signalling pathways**

The figure shows the coupling of β_1, β_2 and β_3 isoforms of the β-adrenergic receptors (ADR) in the ventricular myocardium. Following PTx treatment Gi is uncoupled from the β_2-ADR and β_3-ADR and the signalling pathways taken out of use are coloured greyscale.

2.5 The Circadian Clock in cultured adult rat ventricular myocytes

In order to study diurnal variation of circadian clock and β-ADR genes in isolated Adult Rat Ventricular Myocytes (ARVM), cells placed into tissue culture underwent a serum-shock protocol, which has previously been shown to reactivate circadian clock genes in cultured cells (Balsalobre, Damiola et al. 1998). In summary, cells are 'serum-starved' (0% Fetal Bovine Serum (FBS) (Life Technologies) prior to treatment, following which cells undergo a 'serum-shock' (50% FBS). Cells were then sampled at 3 hour intervals and processed for PCR. By placing cells into tissue culture any neurohumoral influence is removed, leaving only the intrinsic circadian clock to drive oscillation in gene expression (Durgan, Hotze et al. 2005).

2.5.1 Cell culture of adult rat ventricular myocytes

Adult rat ventricular myocytes (ARVM) isolated from adult Wistar rats as previously described were placed into tissue culture and maintained in Media 199 (Sigma) with the addition of a number of supplements due to the lack of serum in culture media; 1% ITS, a mixture of recombinant human insulin (1.0mg/ml), human transferrin (0.55mg/ml) and sodium selenite (0.5μg/ml) (Life Technologies), 2% Penicillin/Streptomycin (Sigma), 0.4mg/ml Carnitine (Sigma), 0.65mg/ml Creatine (Sigma), 0.62mg/ml Taurine (Sigma) and 1.1mg/ml Sodium pyruvate (Sigma). In this investigation serum-free supplemented Media 199 is referred to as Media 199+.

Two or three fractions of isolated ZT3 cardiomyocytes with good yield and viability were washed twice with pre-warmed Media 199+ by centrifuging cells in 15ml tubes at 400r.p.m. for one minute, removing the supernatant and re-suspending the pellet in pre-warmed Media 199+. For cells to adhere to 6-well plates, 1ml of pre-warmed laminin (Sigma) was added to each well in a sterile fume hood and allowed to incubate at room temperature for 1 hour. Laminin was then removed and 2ml of ARVM cell suspension in Media 199+ was added to each well. Plates were shaken gently to distribute cells and incubated (37°C/CO_2) for 2 hours to allow adherence of cardiomyocytes to the laminin coated 6-well plates. Cells were washed twice with 5ml Media 199+ to remove dead,

floating and unattached cells, plates were returned to incubators and allowed to incubate for a further 16 to 18 hours prior to serum shock.

2.5.2 Serum shock Protocol

1. Prior to undergoing the serum-shock protocol cells were subject to serum starvation. ARVM were allowed to equilibrate in serum-free supplemented media 199 for 16-18 hours.

2. Challenge wash (07.00). Control and Serum shock cells were washed twice and media was replaced :

    • Control ARVM's were washed with serum-free media 199 and incubated (37°C/CO2) for 2 hours.

    • Serum-shock ARVM's were washed with 50% FBS supplemented media 199 and incubated (37°C/CO2) for 2 hours.

3. Post-challenge wash. (09.00). Control and Serum shock cells were washed twice and media was replaced with post-challenge serum-free supplemented Media 199 and placed back into the incubator (37°C/CO_2).

4. Control and Serum-shock cells were sampled in 3 hour increments post-challenge in order to assess the circadian rhythm of these cells for a 12 hour period.

2.5.3 Sampling of cell culture cells

ARVM were sampled every 3 hours post-challenge wash and lysed prior to storage for molecular biology.

Cells were washed twice with pre-warmed supplemented Media 199. To detach cells, 1ml 0.25% trypsin/EDTA solution was added to each well incubated (37°C/CO_2) for 5 minutes. Once cells had detached, trypsin was inactivated in ARVM cell suspensions by the addition of 1ml pre-warmed defined trypsin inactivator (Life Technologies) to each well. Cell suspensions were aspirated and placed into 15ml corning tubes, centrifuged at 300r.p.m. and washed twice with normal Tyrode to remove all traces of media which has been shown to inhibit efficient RNA extraction. Tubes were then spun at 2,000r.p.m. for 2 minutes to form dense cell pellets and the resulting supernatant was removed prior
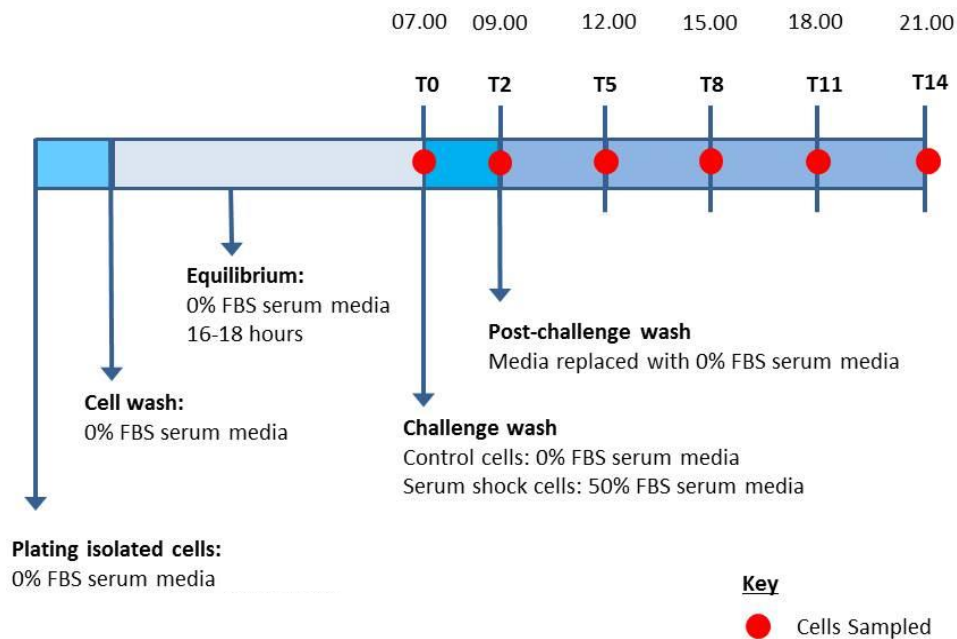
Figure 2.9   A schematic of the serum-shock protocols for adult rat ventricular myocytes.

Cultured ARVM were subject to a serum-shock protocol in order to assess oscillation of circadian rhythms. Prior to undergoing the serum-shock protocol cells were subject to serum starvation; ARVM were allowed to equilibrate in serum-free supplemented media 199 for 16-18 hours. At 07.00 Serum shock cells were washed twice and media was replaced 50% FBS supplemented media. At 09.00 Control and Serum shock cells were washed twice and media was replaced with post-challenge serum-free supplemented Media 199 and placed back into the incubator (37°C/CO2). Samples were collected in 3 hour increments post-challenge in order to assess the circadian rhythm of these cells for a 12 hour period.

to cell lysis. To lyse ARVM cells a mix of QIAzol lysis reagent and buffer RLT (Quigen) was made (5:1) and 600μL added to each cell pellet and triturated to ensure cell pellets were dislodged and lysed. The sample was then homogenized using a 125 Power Gen homogenizer (Fisher Scientific) for 30 seconds.

2.6   Molecular Biology

2.6.1   Sample retrieval, lysis and storage

2.6.1.1   Freshly isolated myocytes

Freshly isolated myocytes (see section 2.1.myocyte isolation), stored at room temperature in normal Tyrode were sampled every 3 hours post-isolation and lysed prior to storage for molecular biology.

Cells were washed twice with warmed normal Tyrode (35 $\pm$ 1°C) in a 15mL tube, following which tubes were span at 2,000r.p.m. for 2 minutes to pellet cells and the supernatant was removed. To lyse cells a mix of Buffer RLT (Quigen) and β-Mercaptoethanol (β-ME) (Sigma) was made (5:1) and 600μL RLT buffer plus β-ME was added and pipette mixed to ensure the pellet was dislodged and lysed. The sample was then homogenized using a 125 Power Gen homogenizer (Fisher Scientific) for 30 seconds and stored at -80°C until required.

2.6.1.2   Cell culture adult rat ventricular myocytes

ARVM cell culture cells were lysed prior to storage for molecular biology and stored at -80°C until required for RNA extraction (see section 2.5.4 Sampling of cell culture cells).

2.6.2   RNA extraction protocols

2.6.2.1   RNeasy mini kit; freshly isolated myocytes

The RNeasy mini kit offered by Qiagen was chosen as the method for RNA extraction in this investigation for isolated cardiomyocyte samples which had not under gone cell culture as it is suitable for the purification of total RNA from both animal cells and tissues. The high salt buffer system of the RNeasy mini kit allows up to 100μg of RNA of up to 200

bases to be extracted as they bind to the silica-based membrane of the RNeasy column from which the bound RNA can then be purified.

In brief, biological samples are first lysed and homogenised in the presence of a denaturing guanidine-thiocyante buffer to inactivate all RNases. Ethanol is added to provide appropriate binding conditions before being added to an RNeasy spin column where total RNA binds to its membrane and contaminants are washed away. High quality RNA is then eluted in RNase-free water. The protocol provided by Qiagen with the RNeasy mini kit was followed throughout the investigation; however some changes were made, such as extending spin times or adding incubation periods to improve RNA quality and quantity.

All work stations and pipettes were decontaminated and cleaned prior to use with Biocleanse (Teknon) and an aseptic technique was used throughout.

RNeasy mini kit protocol:

1. Sample preparation. All myocyte samples previously lysed and stored at -80°C were thawed on ice to prevent RNA degradation.
2. Add 600μL 70% ethanol to each sample and mix well by trituration.
3. Transfer up to 700μL of each sample to individual RNeasy spin columns placed in 2mL collection tubes and centrifuge at 10,000 rpm for 4 minutes. Transfer the remainder of the sample to the same RNeasy spin column and centrifuged again at 10,000 rpm for 4 minutes.
4. Add 700μL of RW1 buffer to each RNeasy spin column and centrifuge at 10,000 rpm for 4 minutes.
5. Add 500μL of RPE buffer to each of the RNeasy spin columns and centrifuge at 10,000 rpm for 4 minutes.
6. Add 500μL of RPE buffer to each of the RNeasy spin columns, incubate in the column for 5 minutes before centrifuging the column at 10,000 rpm for 4 minutes.
7. Spin the RNeasy spin columns at 10,000 rpm for 5 minutes to dry the columns.
8. Add 25μL RNase-free water to each of the RNeasy spin columns placed in 1.5mL RNase-free eppendorf tube, incubate for 5 minutes before centrifuging at 10,000 rpm for 4 minutes to elute the RNA bound to the silica membrane of the RNeasy spin column.

9. As the expected yield of RNA was >30ng it is recommended that this step is repeated. Add 25µL RNase-free water to each RNeasy spin column, incubate for 5 minutes and centrifuge at 10,000 rpm for 4 minutes.

10. Place eluted RNA on ice to prevent RNA degradation until spectrophotometric analysis of RNA yield and quality was assessed.

2.6.2.2 miRNeasy Serum/Plasma kit; adult rat ventricular myocytes

Extraction of RNA from cells cultured in Media 199+ using the RNeasy mini kit proved difficult, providing samples of low yield and poor quality, which were not able to be successfully 'cleaned up'. Following a number of trials with other available RNA extraction kits and methods the miRNeasy Serum/Plasma kit was chosen for RNA extraction from cultured ARVM. The miRNeasy Serum/Plasma kit (Quiagen) makes use of traditional phenol/chloroform based RNA extraction methods, usually used for the purification of cell-free RNA from small volumes of serum and plasma, however this kit provided the most efficient and reliable method of RNA extraction with high yield and quality from our lysed cultured cells.

All work stations and pipettes were decontaminated and cleaned prior to use with Biocleanse (Teknon) and an aseptic technique was used throughout.

miRNeasy Serum/Plasma kit protocol:

1. AVRM cell samples previously lysed and stored at -20°C were thawed on ice to prevent RNA degradation.

2. Add 100µL chloroform to each sample, vortex for 1 minute, incubate for 3 minutes at 20°C and vortex again for 1 minute.

3. Centrifuge samples at 14,000r.p.m. at 4°C for 15 minutes to separate the aqueous phase containing RNA from the interphase and organic phase of the sample.

4. Remove approximately 400µL of the upper aqueous phase and place in RNAase free eppendorf tubes.

5. Add 600µL 100% ethanol to each sample and mix well by trituration.

6. Transfer up to 700µL of each sample to individual miRNeasy spin columns placed in 2mL collection tubes and centrifuge at 10,000r.p.m. for 1 minute. Transfer the remainder of

the sample to the same miRNeasy spin column and centrifuged again at 10,000r.p.m. for 1 minute.

7. Add 700μL of RWT buffer to each miRNeasy spin column and centrifuge at 10,000 rpm for 1 minute.

8. Add 500μL of RPE buffer to each of the miRNeasy spin columns and centrifuge at 10,000r.p.m. for 1 minute.

9. Add 500μL of 80% ethanol to each of the miRNeasy spin columns and centrifuge at 10,000 rpm for 2 minutes.

10. Spin the miRNeasy spin columns at 10,000r.p.m. for 5 minutes to dry the columns.

11. Add 25μL RNase-free water to each of the RNeasy spin columns placed in 1.5mL RNase-free eppendorf tube, incubate for 5 minutes before centrifuging at 10,000r.p.m. for 4 minutes to elute the RNA bound to the silica membrane of the RNeasy spin column.

12. As the expected yield of RNA was >30ng it is recommended that this step is repeated. Add 25μL RNase-free water to each RNeasy spin column, incubate for 5 minutes and centrifuge at 10,000r.p.m. for 4 minutes.

13. Place eluted RNA on ice to prevent RNA degradation until spectrophotometric analysis of RNA yield and quality was assessed.

2.6.3   Spectrophotometric analysis of RNA yield and quality

It is important the yield of RNA is measured in extracted RNA samples to allow for normalisation between samples. In addition, reverse transcription (RT) and its downstream applications, such as real-time PCR, is dependent upon a precise enzyme:primer:RNA ratio and so accuracy of RNA starting quantity is important (Farrell 2005). The quality of the sample should also be assessed as contamination of samples is known to inhibit the PCR reaction (Bustin and Nolan 2004).

To assess RNA yield and quality of extracted RNA samples each sample was analysed using an 8 sample Nanodrop ND-8000 spectrophotometer and ND-8000 VI 0.3 software. The spectrophotometer is able to directly measure both the RNA yield (ng/μL) and the purity of the sample ($A_{260/280}$ and $A_{260/230}$ ratios) by making use of the distinct absorbance profile of nucleic acids between 230nm and 320nm, producing a skewed bell curve with a maximum absorbance at 260nm; any deviation from the absorbance profile is indicative of

sample contamination. The ratio of $A_{260/280}$ is indicative of the purity of RNA with contaminants which absorb light in the UV spectrum, such as protein or phenol. The ratio of $A_{260/230}$ is a secondary measure of the purity of RNA, indicative of contamination of RNA with contaminants which absorb light in the at 230nm such as carbohydrates, salts and solvent carry over from the extraction protocol, such as β-ME. (Farrell 2005).

Assessment of RNA samples was performed immediately following RNA extraction and to minimize degradation all samples were stored on ice whilst the Nanodrop and its software were set up. Nanodrop wells were cleaned and blanked with Milli-Q water following which 1.5μL of sample was pipetted into the centre of a well and a Nanodrop reading was recorded for each sample. RNA yield (ng/μL), $A_{260/280}$ ratio (nm) and $A_{260/230}$ ratio (nm) were recorded.

Following assessment, if a samples RNA yield and quality were acceptable, RNA samples were stored at -80°C prior to reverse transcription. For the purpose of this investigation samples with a $A_{280/260}$ ratio below 1.7 were not reverse transcribed and were therefore excluded from the remainder of the investigation. For samples with an acceptable $A_{280/260}$ ratio (>1.7) but displayed a $A_{260/230}$ ratio below 1.7, indicating salt and solvent carry over from the extraction protocol, a clean-up step was performed.
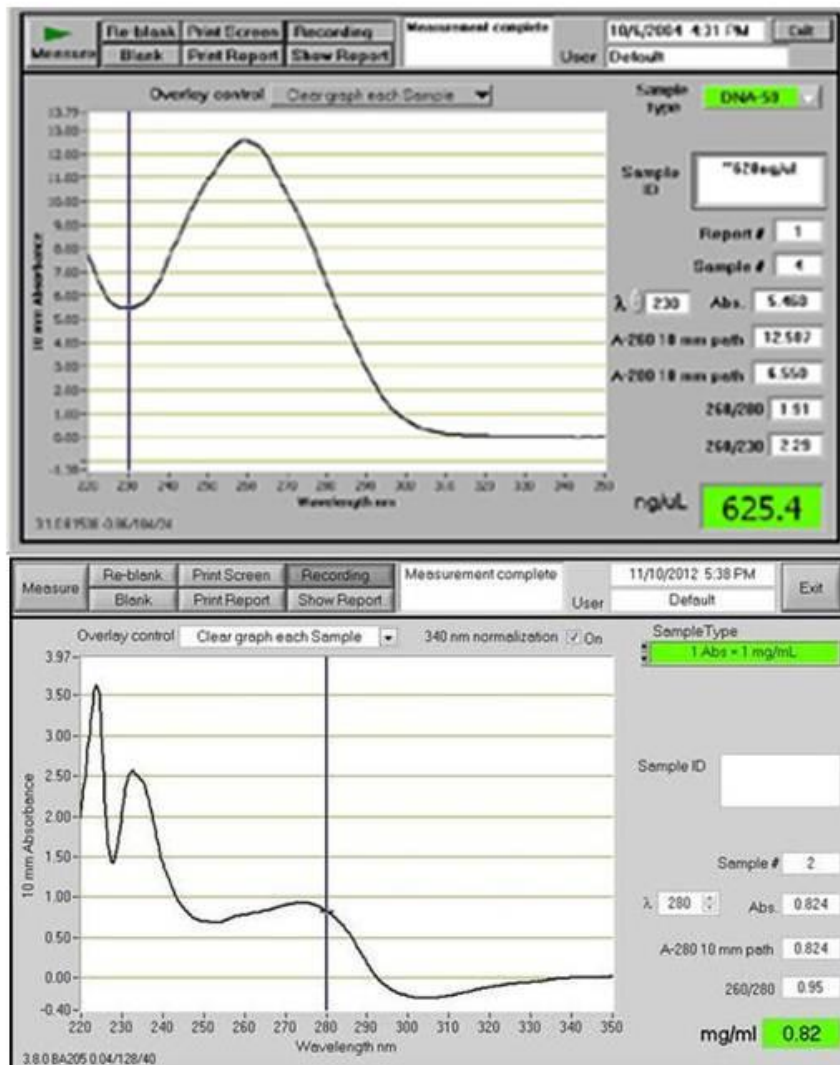
Figure 2.10   Spectrophotometric analysis of RNA yield and quantity
   A.   Nanodrop read out taken from a high quality RNA sample following RNA extraction.
   The RNA yield, A260/280 and A260/230 are all within the acceptable ranges (<1.7).
   B.   Nanodrop read out taken from a low quality RNA sample following RNA extraction. The
   RNA yield was poor and A260/280 and A260/230 are both below the acceptable range (<1.7)
   indicating protein or phenol contamination and salts and solvent carry over from the
   extraction protocol respectively.

2.6.4 RNA "clean-up" step

For samples displaying an acceptable RNA yield and a $A_{280/260}$ ratio above 1.7, but displayed a $A_{260/230}$ ratio below 1.7, indicating salt and solvent carry over from the extraction protocol, a clean-up step was performed. There are a number of clean-up methods available to improve the purity of extracted RNA, however the method chosen here due to its reliability (Farrell 2005) was to re-precipitate the extracted RNA with sodium acetate and ethanol. All samples for RNA clean-up were kept on ice following spectrophotometry to prevent RNA degradation. One tenth of the sample volume of 3M sodium acetate (5µL in a typical 50µL sample) and twice the sample volume of 100% molecular grade ethanol (100µL in a typical 50µL sample) were added to each RNA sample. The re-precipitated samples were then vortexed and stored at -80°C for 2 hours. A vial of 70% ethanol was also stored in the freezer for 2 hours at -80°C. After this time all samples were centrifuged at 13,400 rpm for 30 minutes at 4°C to pellet the RNA contained in the sample. Following centrifugation, all samples were placed on ice, the supernatant was removed and the pellet was then washed twice with 400µL 70% ethanol and centrifuged at 13,400r.p.m. for 3 minutes at 4°C. Following centrifugation the supernatant was removed and pellet samples were allowed to air dry for 15 minutes at room temperature to allow any remaining ethanol to evaporate. Once the sample pellet was dry, 50µL RNase-free water was added to the sample and vortexed to re-suspend the pellet.

Samples were stored on ice before being assessed spectrometerically as previously described. If the $A_{260/230}$ ratio had improved (>1.7), RNA samples were stored at -80°C prior to reverse transcription. If the $A_{260/230}$ ratio had not improved the sample was excluded from the remainder of the investigation.

2.6.5 Reverse Transcription of mRNA samples

As RNA is not suitable product to preform PCR, complementary DNA (cDNA) must first be produced from extracted RNA using specific primers/polymerases by Reverse Transcription (RT). A TaqMan Reverse transcription reagent kit (Invitrogen) was used to generate cDNA, which includes a Multiscribe reverse transcriptase (Moloney Murine leukemia virus (MMLV) enzyme) and random hexamers and oligo dT_{16} reverse primers. oligo dT_{16} enables the transcription of all short mRNAs containing a poly A tails, however if the poly A tail

becomes degraded the reverse transcription my not occur efficiently. The dual use of oligo dT_{16} and random hexamers ensures the transcription of longer mRNAs which have degradation at the poly A tail (Nolan, Hands et al. 2006). 0.1M Dithiotheitol (DTT) (Invitrogen) was also used alongside the TaqMan RT kit, to stabilize enzymes containing free sulfhydryl groups and to facilitate protein denaturation.

RT can be performed in either a one tube step, which incorporates RT and PCR in a single tube, or in a two tube step, which separates the RT and PCR reactions. Separation of the RT and PCR steps allows cDNA generated to be stored for future use and also allows a number of genes to be studied from a stable cDNA pool (Bustin 2000), and for this reason the two-step method was selected for this investigation. To produce cDNA all components of the TaqMan Reverse Transcription kit and previously extracted RNA are combined in a 20μL reaction. A master mix of all kit components was made on ice which contained:

Kit component	Volume per reaction tube (μL)
Buffer	4
MgCl2	2
dNTPs	2
DTT (0.1M) 2	2
Oligo dT16	0.3
Random hexamers	0.3
RNase inhibitor	0.5
Multiscribe RTase	0.3

Once kit components were combined and mixed via trituration, 11.4uL master mix was added to each reaction tube on a 384-well PCR plate. Samples previously which had previously been analysed by the spectrometer showing a high yield and a $A_{260/280}$ and $A_{260/230}$ of >1.7nm were defrosted on ice, alongside the components of the TaqMan Reverse transcription reagent kit. To ensure normalisation among samples, 200ng RNA was reverse transcribed per 20μL reaction, and so samples were diluted with Milli-Q water to give a total of 200ng RNA in 8.6uL for each reaction (8.6-((1/ng/μl)x200) and placed in

labelled reaction tubes and triturated with the master mix. A number of internal non-template controls were also set up containing only Milli-Q water and master mix with no RNA sample. This was to ensure there was no contamination of Milli-Q water or kit components (Dorak 2006).

Once all samples were prepared in PCR plates they were sealed with an optical seal, pulse centrifuged at 10,000r.p.m. and placed in a G-storm thermal cycler (Gene Technologies) and reverse transcribed using the following protocol; 25°C for 10 minutes, 42°C for 12 minutes, 85°C for 5 minutes and then held at 4°C. The cDNA produced was pulse spun and stored at -20°C until required for PCR. All samples within an experiment were reverse transcribed on the same day using the same master mix and placed in the thermal cycler together to maintain conditions.

2.6.6 Quantitative real-time reverse transcription PCR

Quantitative real-time reverse transcription PCR (qRT-PCR) is the most common method for the detection and quantification of RNA from experimental samples (Bustin and Mueller 2005). qRT-PCR differs from conventional PCR in that it allows the continuous detection of a fluorescent signal from the PCR reaction over the cycle range, converting the fluorescent signal from each reaction into a numerical value – the C_T value (Dorak 2006). The C_t value represents the number of cycles of PCR required for the fluorescence to reach the threshold for detection (Bustin and Nolan 2004), which allows quantitative reporting of the starting copy number, the higher the original starting copy number, the sooner fluorescence will be detected (Bustin and Mueller 2005).

The two most widely used detection methods used in qRT-PCR are the non-probe SYBR Green method, which detects binding of SYBR Green to double stranded DNA, and the Taqman fluorescent probe method, which detects fluorescent signal only once the probe binds with its specific target (Bustin and Mueller 2005). Due to its increased specificity the Taqman fluorescent probe method was chosen for the purpose of this investigation.

2.6.6.1   Choice of TaqMan Real-Time PCR gene expression assays

All TaqMan probes used in this investigation were purchased from Applied Biosystems as standard inventoried Real-Time PCR gene expression assays. The TaqMan probes chosen

for this investigation provided the best coverage of the gene of interest, enabling detection of the maximum number of gene transcripts. All probes were species specific to *Rattus norvgicus*. Where possible probes with an amplicon length of less than 100 were chosen, the optimal amplicon length for efficient PCR reaction (Bustin 2000). Probes which span only one exon are capable of amplifying any contaminating genomic DNA (gDNA) contained within samples (Bustin 2000) and so, to avoid false positive results arising from amplification of any contaminating gDNA within samples, where possible probes spanning an exon-exon junction were chosen for use in this investigation.

2.6.6.1.1 Endogenous control gene

An endogenous control gene allows for control of inter-sample variation and pipetting errors, as well as allowing for normalization of cDNA during qRT-PCR. An endogenous control gene or a "housekeeping gene" as it is sometimes referred to, is a gene which is essential for normal cell metabolism or a structural gene, and so its expression is constant and unaffected by experimental conditions, thereby allowing comparison of mRNA levels between a number of experimental conditions (Bustin and Mueller 2005).

As our investigation is looking at the diurnal variation of genes associated with the circadian clock, E-C coupling and β-ADR stimulation, it was important to use a control gene which did not exhibit patterns of circadian rhythm as this would lead to unreliable data. Young *et al.* have previously shown that the levels of expression of β-actin (ACTB), a major constituent of contractile apparatus, remains constant over the course of a day (Young, Razeghi et al. 2001; Young, Razeghi et al. 2001; Young 2003) which was confirmed by the presence of constant expression level in all time points studied in this investigation (see Appendix 3 and 4).

2.6.6.1.2 Standard curves

To ensure efficient replication of each gene of interest during qRT-PCR the efficiency of each TaqMan probe was determined. For efficiency to be calculated a standard curve of known concentration of cDNA is produced by serial dilution. A two-fold dilution was completed using the following concentrations of cDNA; 80ng, 40ng, 20ng, 10ng, 5ng, 2.5ng and 1.25ng. qRT-PCR was then performed on two-fold serial dilution of cDNA with all TaqMan probes in duplicate. All standard curve cDNA samples were run at a volume of

Gene type	Gene name	Gene symbol	Applied biosystems assay I.D.	Amplicon length
Endogenous control gene	Beta-actin (**β-actin**)	Actb	Rn00667869_m1	91
Circadian clock genes	Circadian locomotor output cycles kaput (**CLOCK**)	CLOCK	Rn00573120_m1	112
	Period homolog 2 (**PER2**)	Per2	Rn01427704_m1	100
	Aryl hydrocarbon receptor nuclear translocator-like (**BMAL1**)	Arntl	Rn00577590_m1	137
	Nuclear receptor subfamily 1, group D, member 1 (Rev-ErbA alpha / **Nr1d1**)	Nr1d1	Rn01460662_m1	64
β-adrenergic genes	β_1 adrenergic receptor (**β_1-ADR**)	Adrb1	Rn00824536_s1	65
	β_3 adrenergic receptor (**β_3-ADR**)	Adrb3	Rn00565393_m1	58
Nitric oxide synthase genes	Neuronal nitric oxide synthase 1 (**nNOS**)	NOS1	Rn00583793_m1	65
	Endothelial nitric oxide synthase 3 (**nNOS**)	NOS3	Rn02132634_s1	117

Figure 2.11   TaqMan gene expression probe based assays used in this investigation.
Table shows the TaqMan gene expression probe based assays used in this investigation to assess the mRNA levels of various circadian clock, EC-coupling and NOS signalling genes. The applied biosystems assay I.D. refers to details about each probe. "Rn" refers to the assays compatibility with the species *Rattus norvgicus*. The notation "m1" or "s1" located at the end of the end of the assay I.D. denotes the way in which the assay binds to cDNA; "m1" denotes the probe spans an exon-exon junction, "s1" denotes the probe spans a single exon.
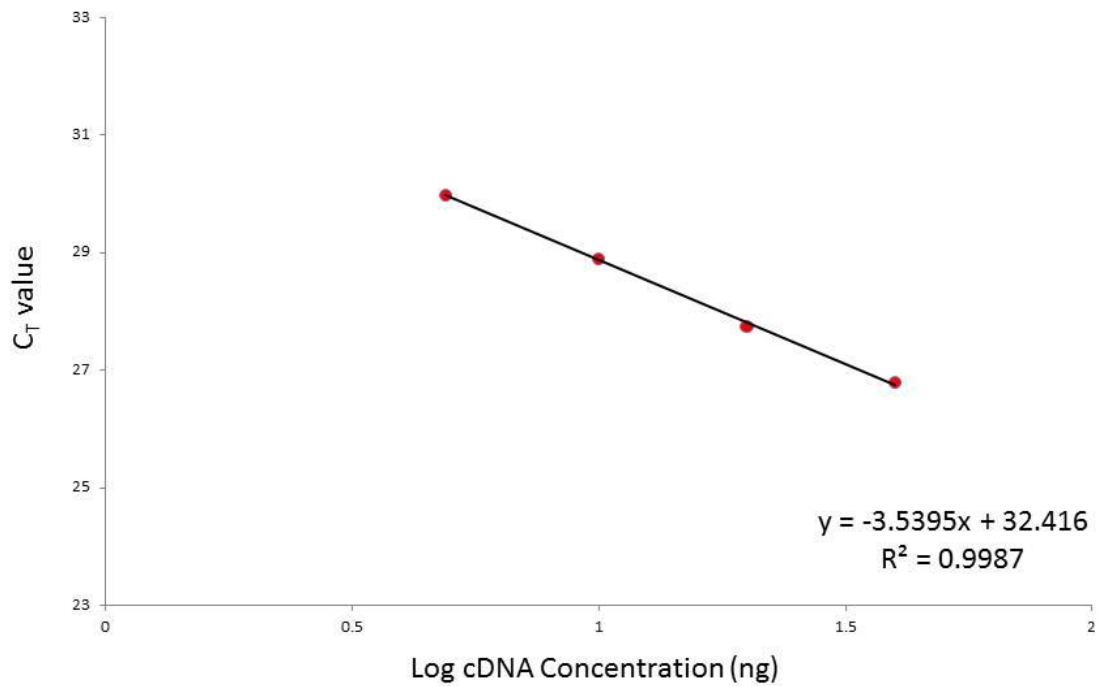
Figure 2.12   Example of a 2-fold standard curve plot.
This figure shows the plot of cycle threshold (C_T) value and Log cDNA concentration of the Beta actin (β-actin) gene used in this investigation, where the slope of the plot is -3.54 and the calculated efficiency of the probe is 91.99%. In cases where efficiency of the probe is 100%, the slope of the plot would show 3.32.

20µl in a 96-well optical PCR plate sealed with optical film (Applied Biosystems), using a Applied Biosystems ViiA 7 Real-Time PCR System. Data was collected using ViiA7 software (Applied Biosystems) and the slope of a plot of Log cDNA versus the cycle threshold (C_T) value was constructed (see figure 2.12), which was used to determine the efficiency of the probe using the following equation: **Efficiency = $10^{(-1/slope)}$ - 1 x 100**.

According to Applied Biosystems, all TaqMan gene expression probes are efficient to 100% + 10% and so do not require a standard curve to be determined. However, standard curves of all Taqman probes used in this investigation were produced in ZT3 isolated adult male wistar cardiomyocytes (shown in Appendix 5) and were efficient to 80 – 110%.

2.6.7 Quantitative real-time RT-PCR protocol

Following determination of the efficiency of TaqMan probes, Quantitative real-time reverse transcription PCR was performed.

All pipettes and workstations were decontaminated with Biocleanse (Teknon) and an aseptic technique was used throughout. Previously reverse transcribed cDNA samples, TaqMan universal PCR master mix and TaqMan gene expression probes which were stored at -20°C were thawed on ice and protected from the light. All cDNA samples and gene expression probes were suspended once defrosted by briefly vortexing samples and centrifuging for 30 seconds. To reduce the possibility of pipetting errors a 'cDNA mastermix' was produced for each cDNA sample, diluted with RNase free water to 50ng/µl cDNA. A 'PCR mastermix' was also produced for each probe investigated, containing the TaqMan universal PCR master mix and TaqMan gene expression probe of interest. qRT-PCR was run on fast 384-well optical PCR plates and 50ng of cDNA for each sample were run in duplicate for both the control gene (β-actin) and the gene of interest within the same plate. The total volume of 5µl per well was contained 1µl cDNA and 4µl TaqMan universal PCR master mix. The PCR plate was sealed with an optical film (Applied Biosystems), pulse spun to ensure efficient mixing of all components before being ran on an Applied Biosystems ViiA 7 Real-Time PCR System in accordance with the manufactures protocol; 50°C or 2 minutes, 95°C for 10 minutes followed by 40 cycles of 95°C for 15 seconds and 60°C for 1 minute. At the end of each amplification cycle fluorescence was detected and C_T value was calculated. The C_T value is defined as the number of PCR cycles required for the specific fluorescent signal, in this investigation the TaqMan probe, to cross

the threshold for detection(exceeds background level) and is inversely proportional to the amount of target cDNA in the sample (Bustin and Nolan 2004).

For analysis, collected C_T values were exported into excel and the comparative CT method ($2^{-\Delta\Delta CT}$) of mRNA expression was used. The comparative C_T method allows for the comparison of two samples, for example a ZT3 sample and a ZT15 sample, and expresses the data as a fold change in expression ($2^{-\Delta\Delta CT}$) from the calibrator sample (Schmittgen and Livak 2008) and is Applied Biosystems suggested method of analysis for TaqMan gene expression assays .

The collected C_T values for each sample in duplicate were averaged and then normalised to their corresponding β-actin C_T value – the delta CT value (ΔC_T).

mean C_T $^{\text{(gene of interest)}}$ - mean C_T $^{\text{(endogenous β-actin)}}$ = ΔC_T

The ΔC_T of the sample is then compared to the ΔC_T of calibrator sample and is expressed as a fold change.

ΔC_T $^{\text{(sample)}}$ - ΔC_T $^{\text{(calibrator sample)}}$ = $\Delta\Delta C_T$

$2^{-\Delta\Delta CT}$ = Fold change

Unless otherwise stated, the calibrator sample was the T0 sample, taken immediately post-isolation, or in the serum-shock experiments taken prior to challenge wash.

2.7 Experimental drugs and solutions

2.7.1 Experimental solutions

2.7.1.1 Extracellular solutions

Normal Tyrode solution contained the following (in mM): NaCl 135, KCl 6, NaH_2PO_4 0.33, Na pyruvate 5, Glucose 10, HEPES 10, $MgCl_2$ 1, $CaCl_2$ 2. The pH of the solution was titrated to 7.4 by the addition of 1M NaOH or 1M HCl.

Calcium free Tyrode solution used in the isolation of myocytes was normal Tyrode solution however 2mM CaCl2 was excluded.

Enzyme-containing Tyrode solution used during myocyte isolation process contained type I collagenase (1mg.ml), Type XIV protease (0.67mg/ml) and bovine serum albumin (1.67mg/ml) in calcium free Tyrode solution.

2.7.1.2 Intracellular solutions

K$^+$ electrode solution (normal potassium electrode solution) contained the following (in mM) KCl 130, MgCl$_2$ 5, Na-ATP 3, HEPES 10. The pH of the solution was titrated to 7.2 with 1M KOH.

Cs-electrode solution (caesium electrode solution) contained the following (in mM) CsCl 130, MgCl$_2$ 5, Na-ATP 3, CaCl$_2$ 0.4, EGTA 10, HEPES 10. The pH of the solution was titrated to 7.2 with 1M CsOH.

All electrode solutions were filtered through a 5µm Minisart Syringe Filter (Sartorious) prior to storage at -20°C.

2.7.1.3 Experimental drugs

N-ώ-nitro-L-arginine (L-NNA) (Caymen Biochemicals) is a competitive inhibitor of nitric oxide synthase (NOS) with selectivity for endothelial NOS (eNOS) and neuronal NOS (nNOS).

3-isobutyl-1-methylxanthine (IBMX) (Sigma) is a competitive non-specific inhibitor of cAMP and cGMP phosphodiesterase (PDE), inhibiting the action of PDE 1-5, 7 and 9.

Adenosine (Sigma) is an endogenous neurotransmitter at adenosine receptors which works through a G$_i$ receptor protein. A 10mM stock solution was made in MilliQ and stored at -20°C.

Caffeine (VWR) has been used previously to assess Ca^{2+} release from intracellular Ca^{2+} stores of the sarcoplasmic reticulum as caffeine is a RyR2 agonist, increasing RyR2 open probability and liberating SR stores at high concentrations.

Cadmium chloride (CdCl$_2$) (Sigma) A 1M stock solution was made in MilliQ, stored at 4°C and protected from the light.

Pertussis Toxin (PTx) (Tocris Bioscience) is a protein-based exotoxin produced by the bacteria *Bordetella pertussis* which block receptor coupling of the G$_i$, G$_o$ and G$_t$ G proteins.

Stocks of PTx were made by the addition of 1ml MilliQ to a 50μg vial, stored at 4°C. Each vial was used within six months of reconstitution with MilliQ, as per manufactures instruction.

(-)-Isoproterenol hydrochloride (ISO) (Sigma) is a non-selective β-ADR agonist. ISO was made as a stock solution of 10mM in ethanol, stored at 4°C, protected from the light and kept for up to 1 month.

Dobutamine hydrochloride (Sigma) is a selective β_1 agonist. A 10mM stock solution was made in ethanol and stored at -20°C.

Salbutamol (Sigma) is a selective β_2 agonist. A 10mM stock solution was made in methanol and stored at -20°C.

BRL37344 (Sigma) is a selective β_3 agonist. A 100μM stock solution was made in MilliQ and stored at -20°C.

2.7.1.4 Fluorescent dyes

Fura-2 (Life Technologies)

Fura-2 is a ratiometric calcium indicator. Stocks of Fura-2(AM) (2mM) were made by the addition of 25μL of 5% Pluronic acid in DMSO to a 5μg vial, stored at -20°C and protected from the light. Each vial was used within one month.

Chapter 3: Time-of-day variation in excitation-contraction coupling in ventricular myocytes

3.1   Introduction

Within the heart, 10-15% of genes involved in transcription, translation, protein turnover, ion homeostasis and metabolism have been shown to exhibit diurnal cycling (Durgan, Hotze et al. 2005). The existence of a peripheral circadian clock within myocytes is well documented (Young, Razeghi et al. 2001) and is potentially able to affect the electrical properties of the heart, Ca^{2+} homeostasis, contractile function, responsiveness to sympathetic stimulation and metabolism, substrate availability or the energy supply:demand ratio (Young 2006).

Previous work by our group highlighted for the first time a time-of-day variation in E-C coupling in isolated myocytes and in its control by sympathetic simulation (Collins and Rodrigo 2010). Basal systolic $[Ca^{2+}]_i$, $[Ca^{2+}]_{SR}$, cell shortening and the rate of relaxation were all found to be greater in myocytes isolated during the rest-period (ZT3) of the rat. They also showed a time-of-day variation in the responsiveness of ventricular myocytes to sympathetic stimulation, with rest-period (ZT3) myocytes responding more strongly to ISO, displaying a greater systolic $[Ca^{2+}]_i$ and $[Ca^{2+}]_{SR}$. As ISO is a non-specific β-ADR agonist, they hypothesised that ISO was also stimulating the $β_3$-ADR, which is known to have a negative inotropic effect on contractility through the production of NO, and that a variation in $β_3$-ADR signalling or expression may exist, causing of the time-of-day variation they observed, however this was not investigated. This study was completed in isolated ventricular myocytes under electrical-field stimulation and the impact of a time-of-day variation in APD and the response of the action potential to ISO was also not investigated and may have been in part responsible for this variation.

Yamashita *et al.* have shown that a significant time-of-day variation in the mRNA levels of the Kv4.2 channel, which partially encodes the I_{to}, with mRNA expression exhibiting a two-fold increase from a the trough at ZT18 (the midpoint of the active-phase) to the peak at ZT6 (the midpoint of the resting-phase), which appeared to have some functional effect on electrical activity (Yamashita, Sekiguchi et al. 2003). More recently, Jeyaraj *et al.* examined the true circadian rhythmicity of these fluctuations in cardiac K^+ channel expression by

placing male rats in constant darkness, and it was found that expression of the α (Kcnd2) and β (KChIP2) subunits of Kv4.2 displayed circadian rhythm (Jeyaraj, Haldar et al. 2012).

Therefore, the initial objective of my research project was to expand on the previous work of our group, to examine if any time-of-day variation exists in the electrical components of E-C coupling (configuration of the cardiac action potential) and its response to β-adrenergic stimulation, to determine if the time-of-day variations observed could be explained by variation in action potential configuration. I also set out to examine signalling pathways potentially responsible for the time-of-day variation, specifically NOS signalling and its relationship to a time-of-day variation in β_3-ADR signalling.

3.2   Results

3.2.1   Time-of-day variation in basal excitation-contraction coupling

E-C coupling is the cellular process which links electrical excitation to contraction through controlled changes in $[Ca^{2+}]_i$. Previous members of our group have reported a time-of-day variation in basal Ca^{2+} handling, with rest-period (ZT3) myocytes displaying a greater systolic $[Ca^{2+}]_i$, diastolic $[Ca^{2+}]_i$ and SR Ca^{2+} content, and a faster rate of relaxation of the Ca^{2+} transient, reflecting an increased activity of SERCA (Collins and Rodrigo 2010).

The cardiac action potential and calcium homeostasis are linked, as the action potential is the activator of E-C coupling, the trigger for which is the influx of Ca^{2+} during the plateau phase of the action potential, either via the LTCC or NCX. Repolarisation of the action potential by K^+ currents is important both for the increase in driving force for Ca^{2+} entry (phase 1, early repolarisation phase; I_{to}) and determining APD (phase 3, late/rapid repolarisation phase; I_{K1}, I_{Kr}, I_{Ks}). APD determines the duration of the plateau phase, which ultimately affects Ca^{2+} entry, either by voltage-dependant inactivation of the LTCC or determining the direction of I_{NCX} (See Introduction 1.1).

I hypothesised that a time-of-day variation may exist in the cardiac action potential (configuration and/or APD) which may account for the time-of-day variation in Ca^{2+} handling previously found by our lab.

3.2.1.1 Time-of-day variation in basal calcium handling

To investigate the time-of-day variation in the basal Ca^{2+} transient, measurement of $[Ca^{2+}]_i$ was made in rest-period (ZT3) and active-period (ZT15) myocytes in normal Tyrode. Measurement of systolic $[Ca^{2+}]_i$, diastolic $[Ca^{2+}]_i$ and the rate of relaxation of the electrically-induced Ca^{2+} transient were made as previously described (See Methods 2.2.3).

Figure 3.1A is a record of a basal Ca^{2+} transient in normal Tyrode recorded from a rest-period (ZT3) (red) and an active-period (ZT15) (blue) myocyte.

Mean systolic $[Ca^{2+}]_i$ and diastolic $[Ca^{2+}]_i$ of rest-period (ZT3) and active-period (ZT15) myocytes are shown in Figures 3.1B and 3.1C and shows a time-of-day variation in systolic

$[Ca^{2+}]_i$. The data shows significantly higher systolic $[Ca^{2+}]_i$ levels in rest-period (ZT3) myocytes at 370.0 ± 20.7nM (n=5(53)) versus active-period (ZT15) myocytes at 311.3 ± 7.5nM (n=6(39);p<0.05). There was no difference in diastolic $[Ca^{2+}]_i$ levels between rest-period (ZT3) and active-period (ZT15) myocytes, at 82.9 ± 3.9nM (n=5(53)) and 79.1 ± 3.5nM (n=6(39);p=0.49) respectively.

Figure 3.1D shows the mean exponential time constant of the decay of the electrically-induced Ca^{2+} transient. The data shows a time-of-day variation in the rate of relaxation of electrically-induced Ca^{2+} transient, with a significantly faster rate of relaxation in rest-period (ZT3) myocytes at 191.2 ± 10.9ms (n=5(52)) versus 231.9 ± 12.4ms in active-period (ZT15) myocytes (n=6(37);p<0.05), indicating increased basal SERCA activity in rest-period (ZT3) myocytes.

I have shown systolic $[Ca^{2+}]_i$ to be greatest in rest-period (ZT3) myocytes and an increased activity of SERCA is suggested by the faster rate of relaxation of the electrically-induced Ca^{2+} transient. An increase in SERCA activity may lead to an increase in SR Ca^{2+} content, as SERCA is the predominant mechanism whereby Ca is re-sequestered to the SR during the relaxation phase of E-C coupling in the rat (Bers 2001). As 90% of the increase in $[Ca^{2+}]_i$ during systole is due to the release of Ca^{2+} from stores in the SR during CICR (Wier, Egan et al. 1994) and the amount of Ca^{2+} released is dependent upon SR Ca^{2+} stores (Bers 2002), I wanted to investigate if an increased SR Ca^{2+} content is responsible for the increased systolic $[Ca^{2+}]_i$ in rest-period (ZT3) myocytes.

To investigate a time-of-day variation in basal SR Ca^{2+} content, cells were perfused with normal Tyrode containing caffeine (20mM for 5 seconds) and the resulting caffeine-induced Ca^{2+} transient was recorded. Measurement of peak caffeine-induced Ca^{2+} release, indicating SR Ca^{2+} content, and the rate of relaxation of the caffeine-induced transient, reflecting the activity of NCX, was made as previously described (See Methods 2.2.3).

Figure 3.2A is a record of basal peak caffeine-induced Ca^{2+} release recorded in normal Tyrode from a rest-period (ZT3) (red) and an active-period (ZT15) (blue) myocyte.
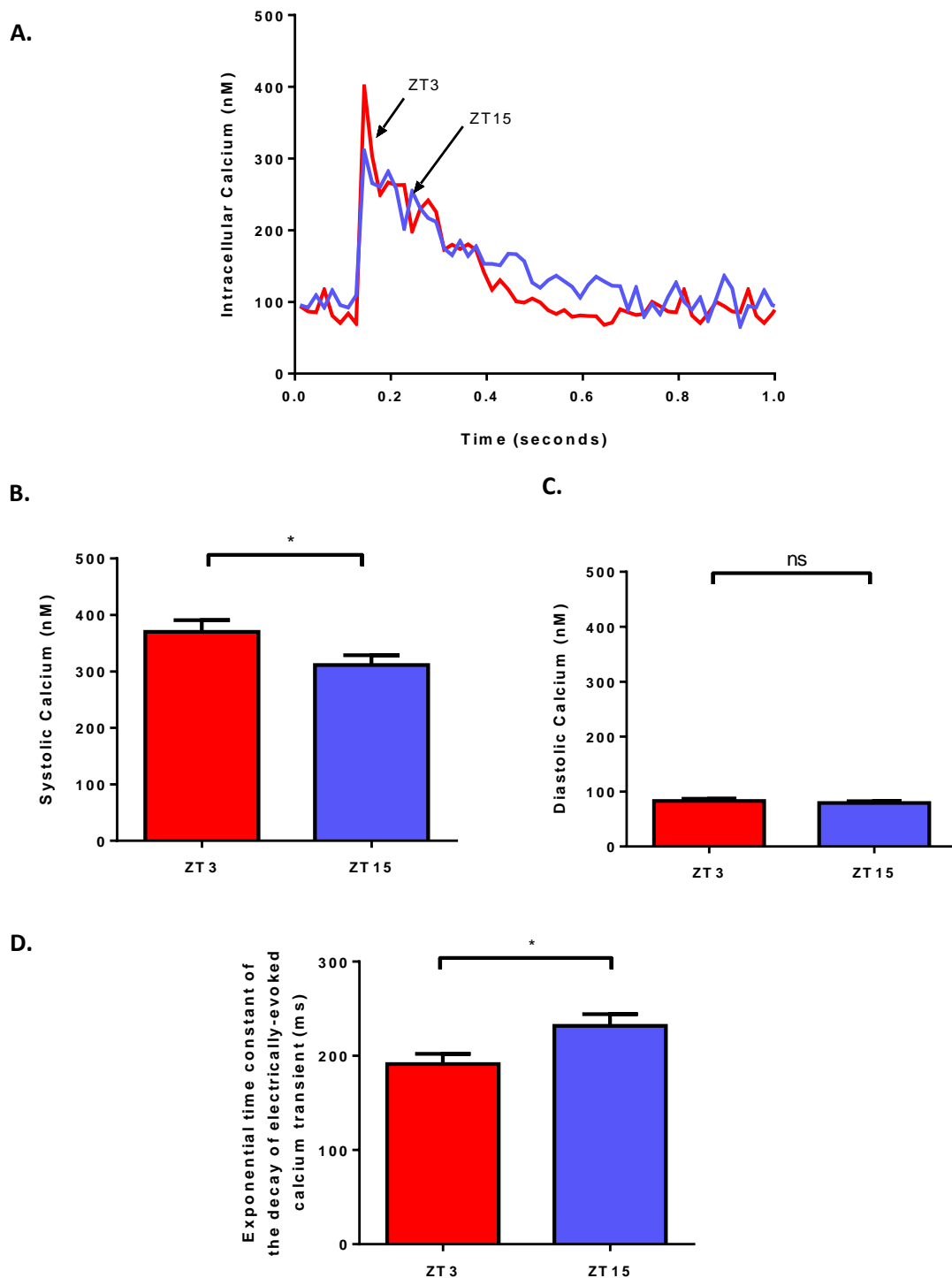
Figure 3.1 **Systolic and diastolic calcium, and rate of relaxation of the electrically-induced Ca^{2+} transient of rest-period (ZT3) and active-period (ZT15) myocytes in normal Tyrode.**

A. Representative electrically-induced Ca^{2+} transient from rest-period (ZT3) (red) and active-period (ZT15) (blue) myocytes in normal Tyrode.

Bar charts showing mean; **B.** systolic [Ca^{2+}]$_i$, **C.** diastolic [Ca^{2+}]$_i$ and **D.** exponential time constant of the decay of the electrically-induced Ca^{2+} transient recorded from rest period (ZT3) myocytes (red, n=5(52-53)) and active-period (ZT15) myocytes (blue, n=6(37-39)) in normal Tyrode.

Values are mean ± S.E.M. Number of hearts (number of experiments); *p<0.05, unpaired t-test.
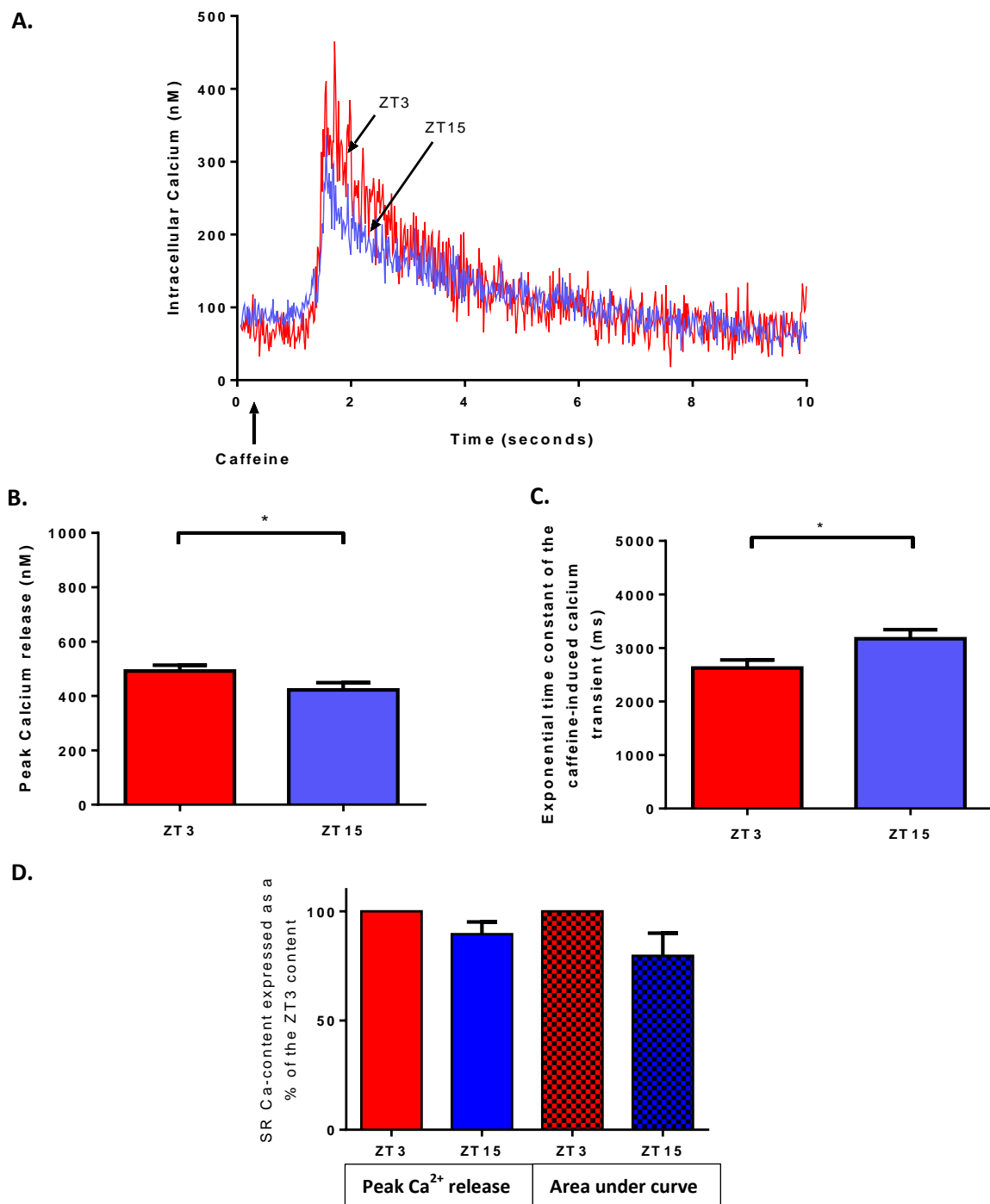
Figure 3.2 **The sarcoplasmic reticulum Ca²⁺ content and the rate of relaxation of the caffeine-induced Ca²⁺ transient of rest-period (ZT3) and active-period (ZT15) myocytes in normal Tyrode.**

A. Representative record of caffeine-induced Ca²⁺ transient recorded from a single rest-period (ZT3) (red) and active-period (ZT15) (blue) myocytes in normal Tyrode.

Bar charts showing mean; **B.** peak caffeine-induced Ca²⁺ release and **C.** exponential time constant of the decay of the caffeine-induced Ca²⁺ transient of rest-period (ZT3) (red, n=5(50-52)) and active-period (ZT15) (blue, n=6(34-35)) myocytes in normal Tyrode; **D.** active-period (ZT15) (blue) sarcoplasmic reticulum Ca²⁺-content expressed as a percentage of rest-period (ZT3) (red) measured by peak caffeine-induced Ca²⁺ release (open bars) and area under curve (hatched bars).

Values are mean ± S.E.M. Number of hearts (number of experiments); *p<0.05, unpaired t-test.

The mean peak caffeine-induced Ca^{2+} release values and exponential decay of the caffeine-induced Ca^{2+} transient are shown in Figure 3.2B and 3.2C and show a time-of-day variation in both parameters. The data shows a significantly greater peak caffeine-induced Ca^{2+} release in rest-period (ZT3) myocytes at 491.5 ± 22.0nM (n=5(52)) as compared to active period (ZT15) myocytes at 422.3 ± 26.4nM (n=6(35);$p<0.05$). The data also shows a significantly shorter relaxation time of caffeine-induced Ca^{2+} transients in rest-period (ZT3) myocytes, at 2626.3 ± 152.1ms (n=5(50)), compared to active-period (ZT15) myocytes, at 3172.2 ± 169.9ms (n=6(34);$p<0.05$), indicating increased basal activity of the NCX in rest-period (ZT3) myocytes.

SR Ca^{2+} content was also measured as the area under the curve. The area under the curve was measured as an alternative to measurement of peak Ca^{2+} release and the data for both conditions are shown as the active-period (ZT15) data expressed a percentage of the mean rest-period (ZT3), shown in Figure 3.2D. Mean active-period (ZT15) peak Ca^{2+} release was 89.53 ± 3.06% (n=6(35)) of the mean peak Ca^{2+} release of rest-period (ZT3) myocytes (n=5(52)). Similarly, mean active-period (ZT15) area under the curve was 79.63 ± 5.60% (n=6(35)) of the area under the curve of rest-period (ZT3) myocytes (n=5(52)). In both cases indicating active-period (ZT15) SR Ca^{2+} content to be reduced, and no statistical significance between estimated SR Ca^{2+} content was found between the two methods (p=0.16).

3.2.1.2 Time-of-day variation in the basal configuration of the cardiac action potential

My data confirms that previously shown by our lab (Collins and Rodrigo 2010), that basal systolic $[Ca^{2+}]_i$, SR Ca^{2+} content, SERCA activity (rate of relaxation of electrically-induced Ca^{2+} transient) recorded in normal Tyrode are significantly higher in rest-period (ZT3) myocytes. However, in a novel finding I have also shown a greater activity of NCX (rate of relaxation of caffeine-induced Ca^{2+} transient) in rest-period (ZT3) myocytes, which was not previously shown by our lab.

The amount of Ca^{2+} released via the RyR2 during CICR is determined by the size of SR Ca^{2+} stores, which I have shown to be greater in rest-period (ZT3) myocytes, but is also

dependent upon on the amount of Ca^{2+} entering the cell via I_{Ca} (Bassani, Yuan et al. 1995), which is indirectly linked to the amplitude and kinetics of the action potential. It has been shown that K^+ channel and repolarisation is time-of-day dependant (Yamashita, Sekiguchi et al. 2003; Jeyaraj, Haldar et al. 2012) and so it is possible that the time-of-day variation displayed in basal systolic $[Ca^{2+}]_i$ and SR Ca^{2+} content is reflective of a variation in the configuration of the cardiac action potential.

To investigate whether a time-of-day variation exists in the configuration of the action potential, action potentials were recorded in rest-period (ZT3) and active-period (ZT15) myocytes in normal Tyrode and measurement of APD_{30}, ADP_{50}, APD90 and RMP were made as previously described (See Methods 2.3.3.1).

Figure 3.3A shows a record of a basal action potential recorded from a rest-period (ZT3) (red) and an active-period (ZT15) (blue) myocyte, in normal Tyrode, showing a shorter APD in active-period (ZT15) myocytes.

Mean APD_{30}, APD_{50} and APD_{90} recorded from rest-period (ZT3) and active-period (ZT15) myocytes are shown in Figure 3.3B and shows a time-of-day variation in basal ADP. The data shows a significantly shorter APD_{50} in active-period (ZT15) myocytes of 16.6 ± 1.5ms (n=3(21)) compared to rest-period (ZT3) myocytes of 30.5 ± 2.9ms (n=3(29);p<0.05). APD_{30} was also shorter in active-period (ZT15) myocytes at 9.8 ± 0.9ms (n=3(21)) than rest-period (ZT3) myocytes at 18.1 ± 1.6ms (n=3(29)), however this was not significant (p=0.07). APD_{90} did not significantly differ between rest-period (ZT3) and active-period (ZT15) myocytes, 84.5 ± 5.1ms (n=3(21)) versus 71.7 ± 4.7ms (n=3(29);p=0.77) respectively.

Figure 3.3C shows the RMP of rest-period (ZT3) and active-period (ZT15) myocytes showing a time-of-day variation. The data shows a hyperpolarised basal RMP in rest-period (ZT3) myocytes at -69.1 ± 0.4mV (n=3(29)) compared to active-period (ZT15) myocytes at -66.22 ± 0.80mV (n=3(21);p<0.001). A time-of-day variation in RMP may indicate a variation in the size of I_{K1}, the driver of RMP.
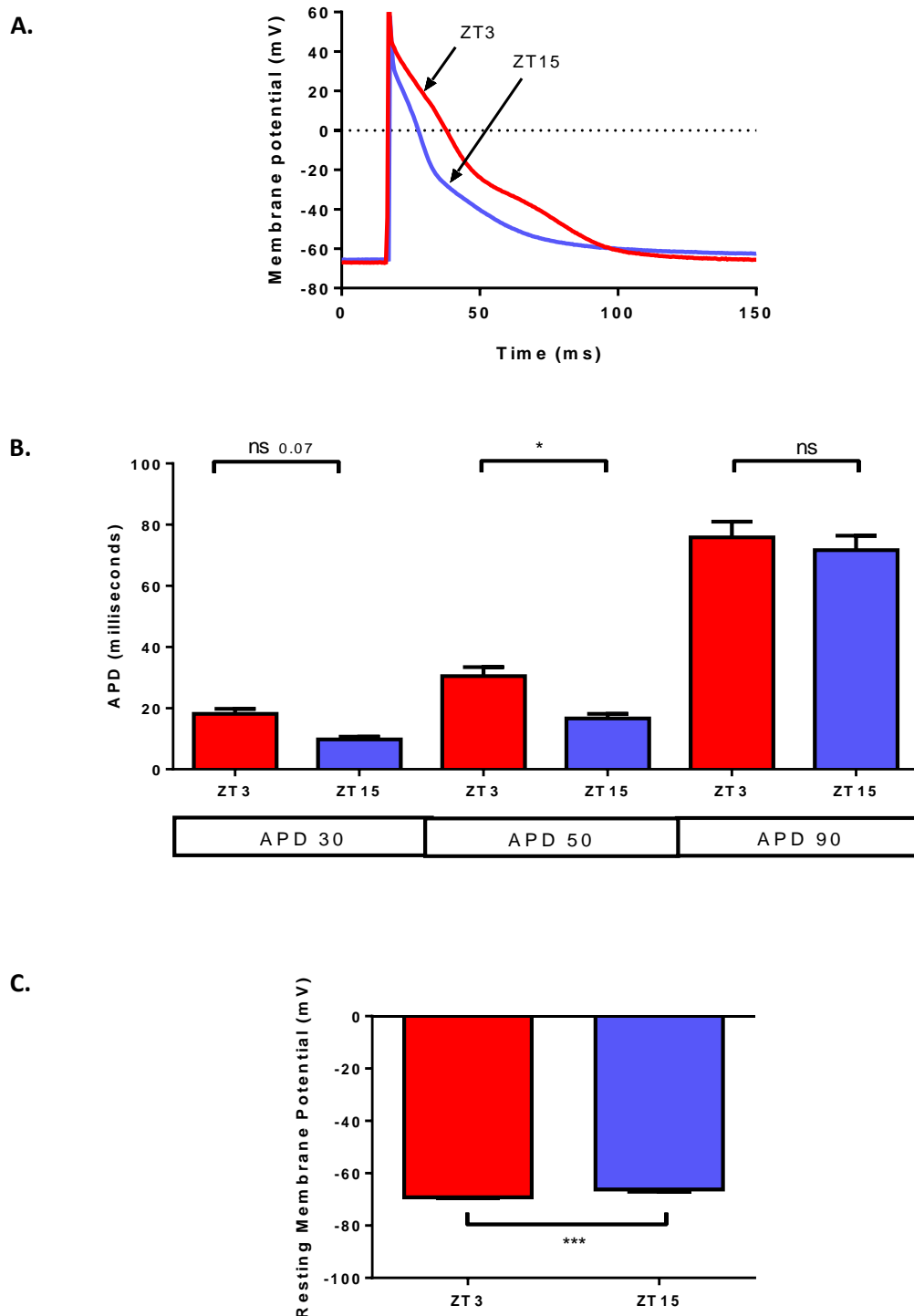
Figure 3.3   The configuration of the action potential of rest-period (ZT3) and active-period (ZT15) myocytes in normal Tyrode.

A.   Representative action potential recorded from a rest-period (ZT3) (red) and active-period (ZT15) (blue) myocytes.

Bar charts showing mean; **B.** APD_{30}, APD_{50} and APD_{90}, and **C.** resting membrane potential, recorded from rest-period (ZT3) (red, n=3(29)) and active-period (ZT15) (blue, n=3(21)) myocytes in normal Tyrode.

Values are mean ± S.E.M. Number of hearts (number of experiments); *p<0.05, ***p<0.001, APD analysed by one-way ANOVA, RMP by unpaired t-test.

In summary:

These data show a time-of-day variation in basal Ca^{2+} handling and configuration of the action potential. During the rest-period (ZT3), systolic $[Ca^{2+}]_i$ and SR Ca^{2+} content (peak caffeine-induced Ca^{2+} release) are significantly higher than during the active-period (ZT15) and the activity of SERCA (relaxation of electrically-induced Ca^{2+} transient) and NCX (relaxation of caffeine-induced Ca^{2+} transient) are also significantly greater. This was associated with a longer APD_{30} and APD_{50} during the rest-period (ZT3) and a hyperpolarised RMP. A longer APD_{30} and APD_{50} indicate a slower repolarisation of the cardiac action potential in rest-period (ZT3) myocytes, and may indicate changes in the ionic currents underlying the action potential. Variations in RMP may indicate a variation in the size of I_{K1} currents, the drivers of RMP.

3.2.2 Time-of-day variation in the response of ventricular myocytes to β-ADR stimulation with isoproterenol

A significant time-of-day variation in the incidence of SCD has been found, with highest incidence between 6am and 12 noon (Maron et al., 1994, Muller et al., 1987, Willich et al., 1987) which has been linked to an increased incidence of arrhythmia during this time. During this time of transition from resting to active state the heart may be more vulnerable to fatal arrhythmia as the increased sympathetic tone upon waking may lead to electrical instability and arrhythmia generation. It is possible therefore, that the time-of-day variation in SCD incidence is reflective of a variation in the sensitivity of the myocardium to sympathetic stimulation, a finding which was previously been observed in our lab. Previous members of our group have reported a time-of-day variation in the responsiveness of Ca^{2+} handling to β-adrenergic stimulation, with rest-period (ZT3) myocytes displaying a greater increase in systolic $[Ca^{2+}]_i$, diastolic $[Ca^{2+}]_i$, SR Ca^{2+} content and SERCA activity in response to ISO (Collins and Rodrigo 2010). As I have shown a time-of-day variation in basal Ca^{2+} handling and configuration of the action potential recorded in normal Tyrode, I hypothesised that a time-of-day variation may exist in the response of the action potential to ISO (change in configuration and APD) which may account for the time-of-day variation in Ca^{2+} handling to β-adrenergic stimulation found previously.

3.2.2.1 Time-of-day variation in calcium handling in response to β-ADR stimulation with isoproterenol

To investigate the time-of-day variation in the Ca^{2+} transient in response to β-adrenergic stimulation, $[Ca^{2+}]_i$ was measured in rest-period (ZT3) and active-period (ZT15) myocytes in normal Tyrode and 10nM ISO. Measurement of systolic $[Ca^{2+}]_i$, diastolic $[Ca^{2+}]_i$ and the rate of relaxation of the electrically-induced Ca^{2+} transient were made as previously described (See Methods 2.2.3).

Figure 3.4 shows example records of Ca^{2+} transients recorded in normal Tyrode and 10nM ISO from A. rest-period (ZT3) myocytes and B. active-period (ZT15) myocytes. The records show clearly a greater increase in $[Ca^{2+}]_i$ in response to ISO in rest-period (ZT3) myocytes compared to active-period (ZT15) myocytes.

Mean systolic $[Ca^{2+}]_i$ and diastolic $[Ca^{2+}]_i$ in rest-period (ZT3) and active-period (ZT15) myocytes are shown in Figure 3.4C and 3.4D, which shows a significant time-of-day variation in the response of myocytes to ISO. Systolic $[Ca^{2+}]_i$ increased significantly in rest-period (ZT3) myocytes in response to ISO, from 319.60 ± 18.46nM to 1040.0 ± 116.9nM (n=5(32);p<0.0001), however the increase in systolic $[Ca^{2+}]_i$ was not significant in active-period (ZT15) myocytes, from 282.3 ± 22.1nM to 428.0 ± 63.1nM (n=3(19);p=0.41). Diastolic $[Ca^{2+}]_i$ increased significantly in rest-period (ZT3) myocytes in response to ISO, from 79.9 ± 3.8nM to 120.1 ± 6.4nM (n=5(32); p<0.0001), however the increase in diastolic $[Ca^{2+}]_i$ was not significant in active-period (ZT15) myocytes, from 77.6 ± 4.4nM to 86.1 ± 4.8nM (n=3(19);p=0.94). Following ISO superfusion, systolic $[Ca^{2+}]_i$ and diastolic $[Ca^{2+}]_i$ was significantly greater in rest-period (ZT3) than active-period (ZT15) myocytes (p<0.001).

The mean exponential time constant of the decay of the electrically-induced Ca^{2+} transient recorded in rest-period (ZT3) and active-period (ZT15) myocytes is shown in Figure 3.4E. The data shows a reduction in relaxation time following ISO stimulation in both rest-period (ZT3) myocytes, from 213.7 ± 15.2ms to 98.9 ± 9.1ms (n=5(32);p<0.0001), and active-period (ZT15) myocytes, from 230.0 ± 17.9ms to 180.0 ± 18.6ms (n=3(16);p<0.05). However, the data shows the reduction in relaxation time following ISO to be greater in rest-period (ZT3) myocytes as compared to active-period (ZT15) myocytes (p<0.0001), indicating a greater increase in SERCA activity in rest-period (ZT3) myocytes in response to β-adrenergic stimulation with ISO.

The positive inotropic effect of the β-ADR agonist ISO is reported to result mainly from its effect on phosphorylation of PLB (Li, Desantiago et al. 2000). Phosphorylation of PLB removes its inhibitory effect on the activity of SERCA, which results in greater amounts of Ca^{2+} being sequestered back to the SR through SERCA during the relaxation of E-C coupling, increasing SR Ca^{2+} content (Bers 2001). As systolic $[Ca^{2+}]_i$ was found to be greatest in rest-period (ZT3) myocytes following ISO-stimulation, I hypothesised that the time-of-day variation in systolic $[Ca^{2+}]_i$ may be reflective of an increased SR Ca^{2+} store.

To investigate a time-of-day variation in the SR Ca^{2+} content in response to β-adrenergic stimulation, SR Ca^{2+} content was measured in rest-period (ZT3) and active-period (ZT15) myocytes, recorded in normal Tyrode and 10nM ISO by rapidly perfusing cells with Tyrode containing caffeine (20mM for 5 seconds) as previously described (See Methods 2.2.3).
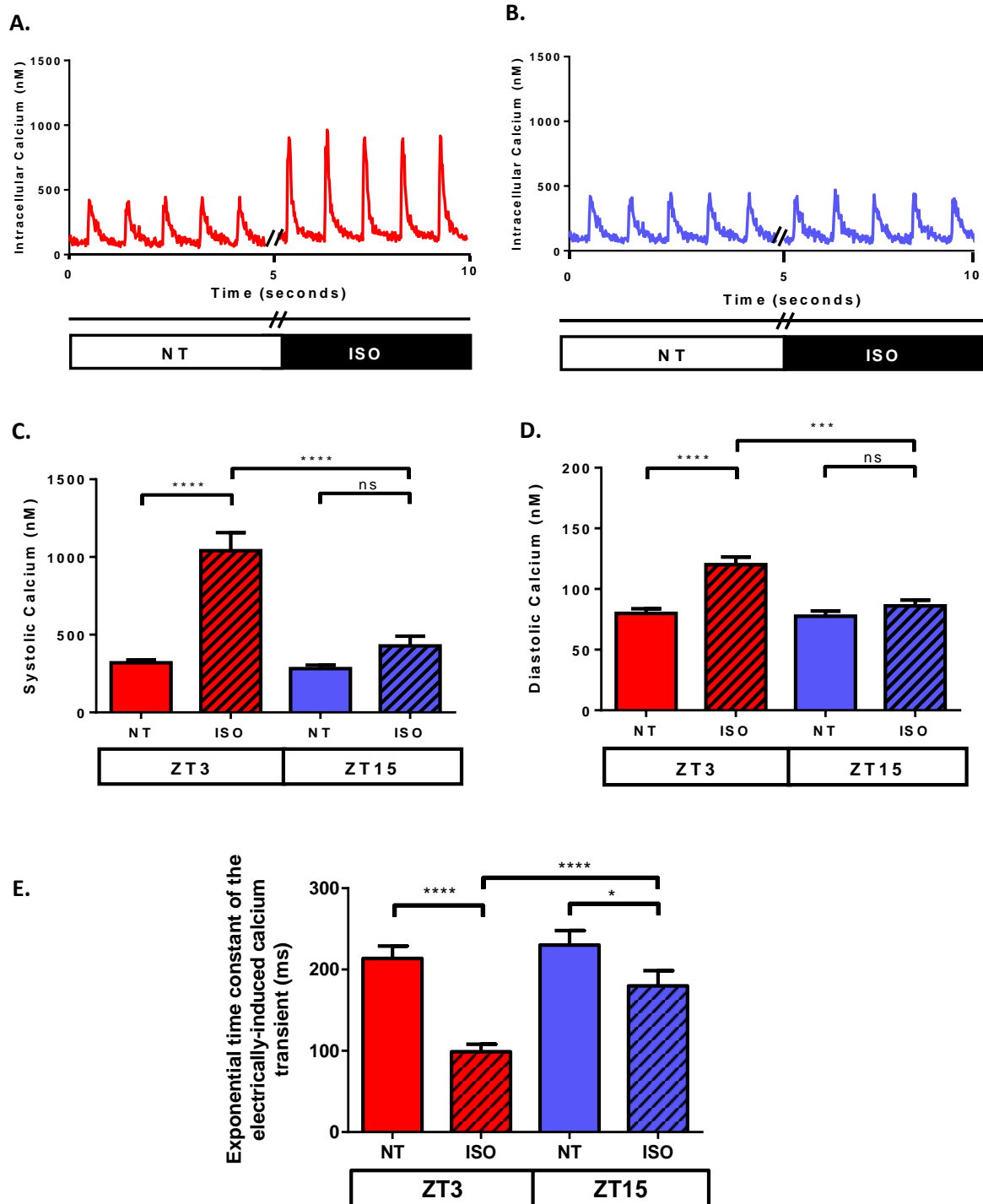
Figure 3.4 **The effect of β-adrenergic stimulation with isoproterenol on systolic and diastolic calcium and rate of relaxation of the electrically-induced Ca^{2+} transient in rest-period (ZT3) and active-period (ZT15) myocytes.**

Example Ca^{2+} transient recording from **A.** rest-period (ZT3) (red) and **B.** active-period (ZT15) (blue) myocytes superfused with normal Tyrode and 10nM isoproterenol (ISO).

Bar charts showing mean; **C.** systolic [Ca^{2+}]$_i$, **D.** diastolic [Ca^{2+}]$_i$ and **E.** exponential time constant of the decay of the electrically-induced Ca^{2+} transient, recorded from rest-period (ZT3) (red, n=5(32)) and active-period (ZT15) (blue, n=3(16-19)) myocytes in normal Tyrode (open bars) and 10nM ISO (striped bars).

Values are mean ± S.E.M. Number of hearts (number of experiments); *p<0.05, ***p<0.001, ****p<0.0001, two-way ANOVA, Bonferroni's *post-hoc* test.
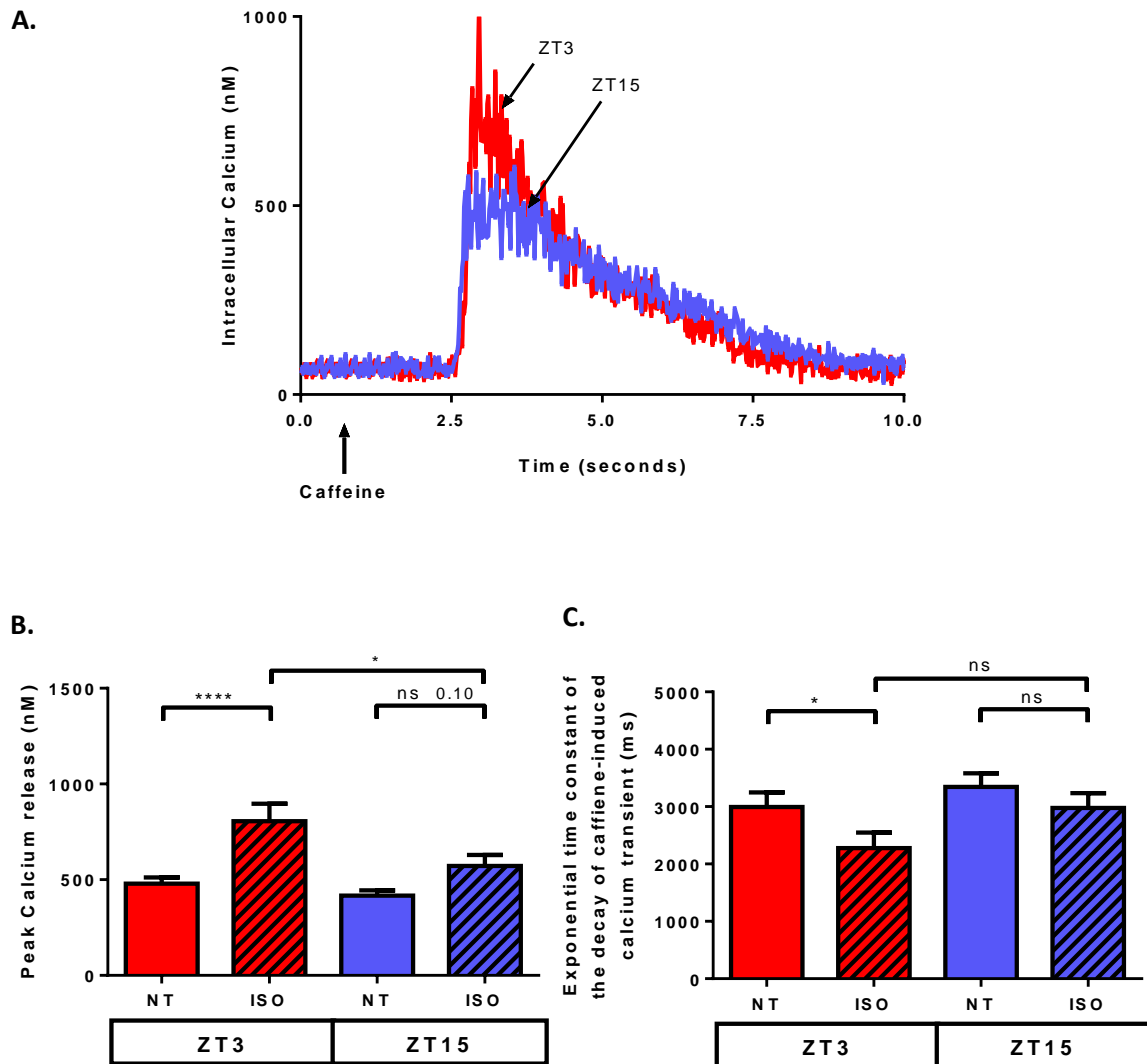
Figure 3.5 **The effect of β-adrenergic stimulation with isoproterenol on sarcoplasmic reticulum Ca²⁺ content and rate of relaxation of the caffeine-induced Ca²⁺ transient in rest-period (ZT3) and active-period (ZT15) myocytes.**

A. Example caffeine evoked Ca^{2+} transient recorded from rest-period (ZT3) (red) and active-period (ZT15) (blue) myocytes superfused with normal Tyrode and 10nM isoproterenol (ISO).

Bar charts showing mean; **B.** peak caffeine-induced Ca^{2+} release and **C.** exponential time constant of the decay of the caffeine-induced Ca^{2+} transient of rest-period (ZT3) (red, n=5(22-27)) and active-period (ZT15) (blue, n=3(16-18)) myocytes in normal Tyrode (open bars) and 10nM ISO (striped bars).

Values are mean ± S.E.M. Number of hearts (number of experiments);*p<0.05, **p<0.01, ****p<0.0001, two-way ANOVA, Bonferroni's *post-hoc* test.

116

Figure 3.5A shows example records of a caffeine-induced Ca^{2+} transient recorded in 10nM ISO from rest-period (ZT3) myocytes (red) and active-period (ZT15) myocytes. (blue). The records show clearly a greater peak caffeine-induced Ca^{2+} release in response to ISO in rest-period (ZT3) myocytes compared to active-period (ZT15) myocytes.

Figure 3.5B shows peak Ca^{2+} release from rest-period (ZT3) and active-period (ZT15) myocytes and shows a time-of-day variation in SR Ca^{2+} content in response to ISO. The data shows a significant increase in peak caffeine-induced Ca^{2+} release in rest-period (ZT3) myocytes in response to ISO, from 479.8 ± 32.8nM to 827.6 ± 96.3nM (n=5(27);p<0.0001). Peak caffeine-induced Ca^{2+} release also increased in active-period (ZT15) myocytes, from 417.3 ± 26.9nM to 572.0 ± 57.3nM (n=3(18)), however this was not significant (p=0.10). As a result, there was a difference in SR Ca^{2+} content between rest-period (ZT3) and active-period (ZT15) myocytes following ISO superfusion (p<0.05).

The mean exponential time constant of the decay of the caffeine-induced Ca^{2+} transient recorded in rest-period (ZT3) and active-period (ZT15) myocytes is shown in Figure 3.5C, and shows a significant time-of-day variation in relaxation time in response to ISO. The data shows a reduction in relaxation time following ISO stimulation in rest-period (ZT3) myocytes, from 2992.1 ± 253.9ms to 2275.1 ± 271.3ms (n=5(22);p<0.05). Relaxation time of caffeine-induced Ca^{2+} transient also reduced in active-period (ZT15) myocytes, from 230.0 ± 17.9ms to 180.0 ± 18.6ms (n=3(16)), however this was not significant (p=0.99). The data suggests a greater increase in NCX activity in rest-period (ZT3) myocytes in response to β-adrenergic stimulation with ISO.

3.2.2.2   Time-of-day variation in the response of the action potential to β-adrenergic stimulation with isoproterenol

My data confirms that previously shown by our lab (Collins and Rodrigo 2010), that systolic $[Ca^{2+}]_i$, SR Ca^{2+} content, SERCA activity (rate of relaxation of electrically-induced Ca^{2+} transient) and NCX activity (rate of relaxation of caffeine-induced Ca^{2+} transient) are significantly higher in rest-period (ZT3) myocytes following ISO (Collins and Rodrigo 2010). As I have shown a time-of-day variation in the configuration of the basal cardiac action potential, I hypothesised that the time-of-day variation in Ca^{2+} handling in response to ISO

may also be due to underlying variation in the action potential in response to β-adrenergic stimulation.

To investigate whether a time-of-day variation exists in the action potential configuration and/or APD in response to ISO, action potentials were recorded in rest-period (ZT3) and active-period (ZT15) myocytes, in normal Tyrode and 10nM ISO and measurement of APD_{30}, ADP_{50} and APD_{90} were made as previously described (See Methods 2.3.3.1).

Figure 3.6 shows a record of an action potential recorded from A. rest-period (ZT3) (red) and B. active-period (ZT15) (blue) myocytes in normal Tyrode and ISO, showing a lengthening of APD in response to ISO.

Mean APD_{30}, APD_{50} and APD_{90} recorded from rest-period (ZT3) and active-period (ZT15) myocytes are shown in Table 3.6C and shows ISO prolonged the APD in both rest-period (ZT3) and active-period (ZT15) myocytes.

Following ISO superfusion there were no differences in APD between rest-period (ZT3) (n=3(14)) and active-period (ZT15) (n=3(9)) myocytes; APD_{30} 17.99 $\pm$ 2.09ms versus 20.58 $\pm$ 2.43ms (p=0.93); APD_{50} 29.47 $\pm$ 3.10ms versus 33.03 $\pm$ 3.35ms (p=0.84); APD_{90} 71.49 $\pm$ 3.87ms versus 74.03 $\pm$ 4.46ms (p=0.94).

As APD was significantly shorter in active-period (ZT15) basal action potentials (see section 3.1), mean percentage change in APD_{30}, APD_{50} and APD_{90} in response to ISO was calculated and is shown in Figure 3.6D, showing a time-of-day variation in the response of the action potential to ISO. The data shows a significantly greater percentage increase in APD_{30} and APD_{50} in active-period (ZT15) myocytes (n=3(14)), APD_{30} of +120.3 $\pm$ 14.9% and ADP_{50} of +95.9 $\pm$ 13.2%, as compared to rest-period (ZT3) myocytes (n=3(9)); APD_{30} of +10.6 $\pm$ 8.2% (p<0.0001) and ADP_{50} of +11.6 $\pm$ 7.4% (p<0.0001). The increase in ADP_{90} in rest-period (ZT3) of 8.9 $\pm$ 8.5% (n=3(14)) and active-period (ZT15) myocytes of 14.1 $\pm$ 12.9% (n=3(9)) was not significantly different (p=0.99).

A.

B.

C.

	APD$_{30}$ (ms)		APD$_{50}$ (ms)		APD$_{90}$ (ms)	
	Normal Tyrode	ISO	Normal Tyrode	ISO	Normal Tyrode	ISO
Rest-period (ZT3) myocytes	17.98 ± 2.50	17.99 ± 2.09	28.66 ± 4.02	29.47 ± 3.10	71.96 ± 7.59	71.49 ± 3.87
Active-period (ZT15) myocytes	9.54 ± 1.09	20.58 ± 2.43	18.11 ± 2.70	33.03 ± 3.35	71.63 ± 8.06	74.03 ± 4.46

D.
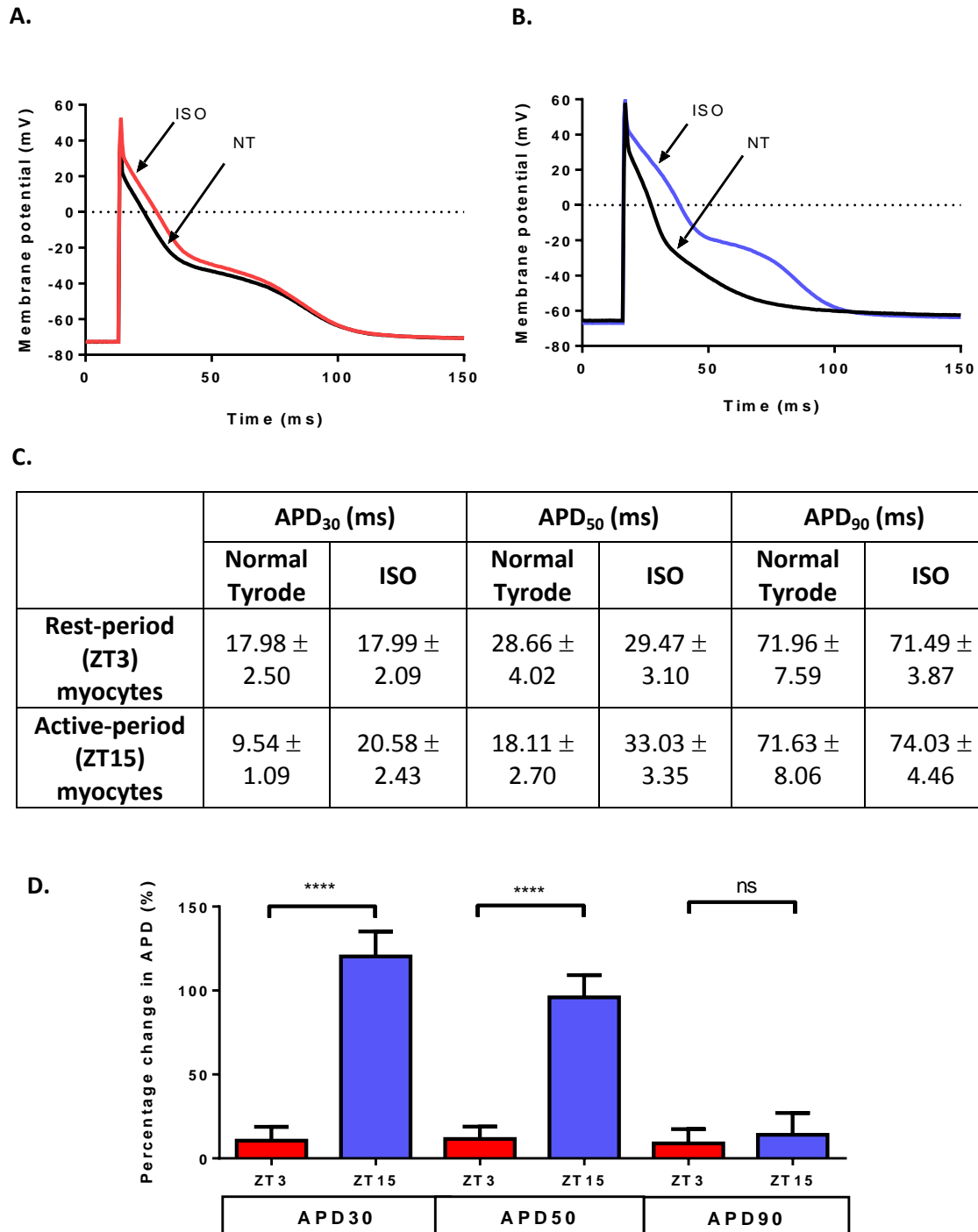
Figure 3.6   The effect of β-adrenergic stimulation with isoproterenol on the configuration of the cardiac action potential in rest-period (ZT3) and active-period (ZT15) myocytes.

Example action potentials recorded from **A.** rest-period (ZT3) and **B.** active-period (ZT15) myocytes in normal Tyrode and 10nM isoproterenol (ISO).

C.   Mean APD$_{30}$, APD$_{50}$ and APD$_{90}$ recorded from rest-period (ZT3, n=3(14)) and active-period (ZT15, n=3(9)) myocytes in normal Tyrode and 10nM ISO.

C.   Bar chart showing the percentage increase in APD$_{30}$, APD$_{50}$ and APD$_{90}$ following superfusion with 10nM ISO, recorded from rest-period (ZT3) (red, n=3(14)) and active-period (ZT15) (blue, n=3(9)) myocytes. Values are mean ± S.E.M. Number of hearts (number of experiments); ****p<0.0001, two-way ANOVA, Sidak's *post-hoc* test.

In summary;

These data show a depressed response to β-ADR stimulation with ISO of systolic $[Ca^{2+}]_i$ and SR Ca^{2+} content in active-period (ZT15) myocytes. The depressed increase in systolic $[Ca^{2+}]_i$ and SR Ca^{2+} content was reflected by a blunted increase in SERCA activity (rate of relaxation of electrically-induced Ca^{2+} transient). I also found a depressed increase in NCX activity (rate of relaxation of caffeine-induced Ca^{2+} transient) in active-period (ZT15) myocytes.

The data also shows a greater percentage prolongation in $APD_{30/50}$ in active-period (ZT15) myocytes following stimulation with ISO, however there was no difference in absolute ADP values (ms) following stimulation with ISO. Together this data suggests that the increase in APD in response to ISO is unlikely to be responsible for time-of-day variation in Ca^{2+} handling in response to ISO that I have shown here.

3.2.3   The role of nitric oxide synthase and the β₃-ADR in the observed time-of-day variation in response to isoproterenol

As a non-specific β-ADR, ISO binds to and activates all isoforms of β-ADR expressed on the myocardium and therefore, the overall inotropic response of the myocardium to ISO will reflect the balance between $β_1$-ADR, $β_2$-ADR and $β_3$-ADR receptor signalling. The $β_1$-ADR and $β_2$ ADR are coupled to G_s proteins and mediate their effects via the classical β-ADR/cAMP/PKA pathway (Lohse et al., 2003), leading to a positive inotropic and lusitropic response. In contrast, the $β_3$-ADR are coupled to the inhibitory G_i protein, and stimulation of the $β_3$-ADR lead to increases in NO production by NOS enzymes and the activation of PDE associated with the breakdown of cAMP leading to reduced contractility (Gauthier et al., 2011). (See Introduction 1.2).

The $β_3$-ADR have a lower affinity for the circulating endogenous catecholamines than the $β_1$-ADR and $β_2$-ADR (Adrenaline; (nM) $β_1$ -5.4, $β_2$ -6.1, $β_3$ -3.9) (Nor-adrenaline; (nM) $β_1$ -5.5, $β_2$ -4.9, $β_3$ -5.8), and similarly the exogenous β-ADR agonist ISO ((nM) $β_1$ -6.6, $β_2$ -6.3, $β_3$ -5.8) (Alexander, Benson et al. 2013). I have shown that the increase in systolic $[Ca^{2+}]_i$ and SR Ca^{2+} content in response to ISO is depressed in active-period (ZT15) myocytes and as ISO stimulates all three β-ADR, I hypothesised that this difference may be due to variation in the activation of $β_3$-ADR and downstream NOS signalling, antagonising the

positive inotropic action of β_1-ADR and β_2-ADR receptor stimulation. I therefore set out to investigate the role of NOS in the time-of-day variation to ISO in active-period (ZT15) myocytes and to investigate any time-of-day variation in β_3-ADR signalling which may be responsible for a time-of-day variation in NOS signalling.

3.2.3.1 The role of nitric oxide synthase in the time-of-day variation in calcium handling in response to isoproterenol

To investigate the effect of NOS inhibition on time-of-day variation in the Ca^{2+} transient in response to β-adrenergic stimulation, $[Ca^{2+}]_i$ was measured in rest-period (ZT3) and active-period (ZT15) myocytes in normal Tyrode, 10nM ISO and 10nM ISO plus 500μM N-$\acute{\omega}$-nitro-L-arginine (L-NNA), a non-specific NOS inhibitor. Measurement of systolic $[Ca^{2+}]_i$, diastolic $[Ca^{2+}]_i$ and rate of relaxation of the electrically-induced Ca^{2+} transient were made as previously described (See Methods 2.2.3).

Figure 3.7 shows example records of Ca^{2+} transients recorded in normal Tyrode, 10nM ISO and 10nM ISO plus 500μM L-NNA from A. rest-period (ZT3) myocytes and B. active-period (ZT15) myocytes. The records show a greater increase in systolic $[Ca^{2+}]_i$ in response to simultaneous β-ADR stimulation and NOS inhibition in active-period (ZT15) myocytes as compared to rest-period (ZT3) myocytes, suggesting that NOS signalling is responsible for the reduced response of active-period (ZT15) myocytes to the non-specific agonist ISO.

Mean systolic $[Ca^{2+}]_i$ and diastolic $[Ca^{2+}]_i$ recorded from these experiments is shown in Figure 3.7C and 3.7D. The data shows a significant increase in systolic $[Ca^{2+}]_i$ in active-period (ZT15) myocytes following NOS inhibition, from 410.8 ± 64.2nM to 1070.0 ± 107.6nM (n=3(19);p<0.0001). The increase in systolic $[Ca^{2+}]_i$ was not significant in rest-period (ZT3) myocytes, from 1040.9 ± 116.9nM to 1185.0 ± 105.6nM (n=5(32);p=0.74). Diastolic $[Ca^{2+}]_i$ also increased significantly in active-period (ZT15) myocytes following NOS inhibition, from 86.1 ± 4.8nM to 140.7 ± 9.4nM (n=3(27);p<0.0001), however the increase in diastolic $[Ca^{2+}]_i$ was not significant in rest-period (ZT3) myocytes, from 120.1 ± 6.4nM to 136.8 ± 7.0nM (n=5(32);p=0.06).
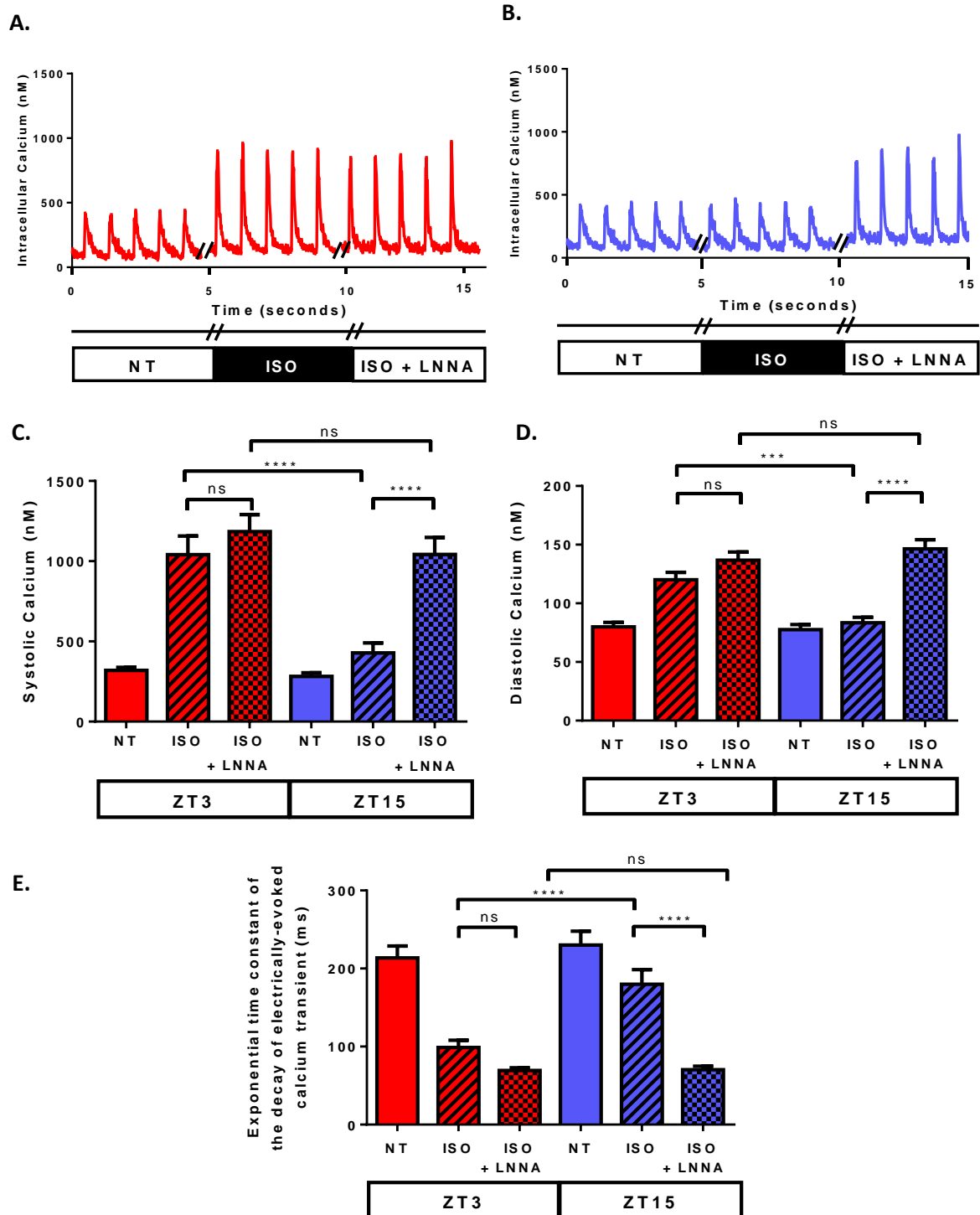
Figure 3.7 **The effect of nitric oxide inhibition on response of systolic and diastolic calcium and rate of relaxation of the electrically-induced Ca^{2+} transient to β-adrenergic stimulation with isoproterenol in rest-period (ZT3) and active-period (ZT15) myocytes**

Example recording of a Ca^{2+} transient from **A.** rest-period (ZT3) (red) and **B.** active-period (ZT15) (blue) myocytes in normal Tyrode, 10nM isoproterenol (ISO) and 10nM ISO plus 500μM N^{G}-nitro-L-Arginine (LNNA).

Bar charts showing mean; **C.** systolic [Ca^{2+}]$_i$, **D.** diastolic [Ca^{2+}]$_i$ and **E.** exponential time constant of the decay of the electrically-induced Ca^{2+} transient, recorded from rest-period (ZT3) (red, n=5(32)) and active-period (ZT15) (blue, n=3(19-27)) myocytes in normal Tyrode (open bars), 10nM ISO (striped bars) and 10nM ISO plus 500μM LNNA (hatched bars). Values are mean ± S.E.M. Number of hearts (number of experiments); ***p<0.001, ****p<0.0001, two-way ANOVA, Bonferroni's *post-hoc* test.

The mean exponential time constant of the decay of the electrically-induced Ca^{2+} transient are shown in Figure 3.7E. The data shows a significant reduction in the time constant following simultaneous β-ADR stimulation and NOS inhibition in active-period (ZT15) myocytes, from 180.0 ± 18.7ms to 70.4 ± 4.4ms (n=3(19);p<0.0001), however the reduction in the time constant was not significant in rest-period (ZT3) myocytes, from 98.9 ± 9.1nM to 69.3 ± 3.6nM (n=5(32);p=0.19). The data indicates a greater increase in SERCA activity in active-period (ZT15) myocytes following NOS inhibition.

Following simultaneous inhibition of NOS and ISO stimulation, the previously reported depressed response of active-period (ZT15) myocytes is abolished, as no difference in systolic $[Ca^{2+}]_i$ (p=0.84), diastolic $[Ca^{2+}]_i$ (p=0.99) or relaxation time of the electrically-induced Ca^{2+} transient (p=0.99) was found between rest-period (ZT3) and active-period (ZT15) myocytes.

I have previously shown the increase in SR Ca^{2+} content and NCX activity (rate of relaxation of caffeine-induced Ca^{2+}-transient) to be significantly higher in rest-period (ZT3) myocytes following ISO, and I postulated that this time-of-day variation in SR Ca^{2+} content and NCX activity would also be abolished via inhibition of NOS during ISO perfusion.

To investigate a time-of-day variation in the SR Ca^{2+} content in response to NOS inhibition during β-adrenergic stimulation, SR Ca^{2+} content was measured in rest-period (ZT3) and active-period (ZT15) myocytes, recorded in normal Tyrode, 10nM ISO and 10nM ISO plus 500μM L-NNA by rapidly perfusing cells with Tyrode containing caffeine (20mM for 5 seconds) as previously described (See Methods 2.2.3).

Figure 3.8 shows example records of a caffeine-induced Ca^{2+} transients recorded in normal Tyrode, 10nM ISO and 10nM ISO plus 500μM L-NNA from A. rest-period (ZT3) myocytes and B. active-period (ZT15) myocytes. The records show an increase in SR Ca^{2+} content following inhibition of NOS with LNNA in active-period (ZT15) myocytes in the presence of ISO.

Figure 3.8C shows the mean peak caffeine-induced Ca^{2+} release values in rest-period (ZT3) and active-period (ZT15) myocytes and shows the increase in SR Ca^{2+} content in response to NOS-inhibition during stimulation with ISO. The increase in SR Ca^{2+} content was only significant in active-period (ZT15) myocytes, from 572.0 ± 57.3nM to 978.0 ± 79.3nM
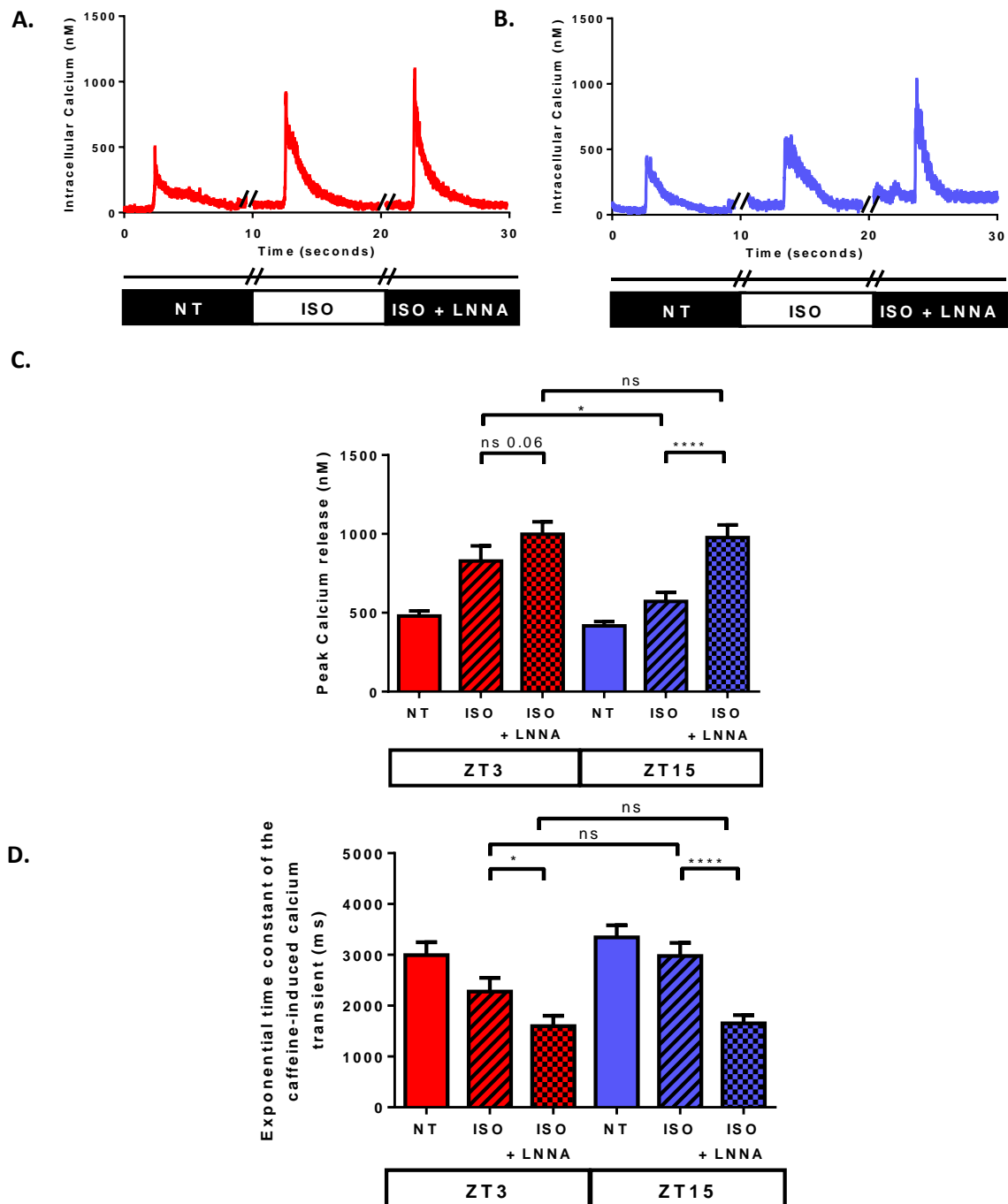
Figure 3.8 **The effect of nitric oxide synthase inhibition on sarcoplasmic reticulum Ca^{2+} content and the relaxation of the caffeine-induced Ca^{2+} transient in response to β-adrenergic stimulation with isoproterenol in rest-period (ZT3) and active-period (ZT15) myocytes.**

Representative caffeine-induced Ca^{2+} transient recordings from **A.** rest-period (ZT3) (red) and **B.** active-period (ZT15) (blue) myocytes in normal Tyrode, 10nM isoproterenol (ISO) and 10nM ISO and 500μM N^G-nitro-L-Arginine (LNNA).

Bar charts showing the **C.** peak caffeine-induced Ca^{2+} release and **D.** exponential time constant of the decay of the caffeine-induced Ca^{2+} transient of rest period (ZT3) (red, n=5(22-25)) and active period (ZT15) (blue, n=3(16-18)) myocytes in normal Tyrode (open bars), 10nM ISO (striped bars) and 10nM ISO plus 500μM LNNA (hatched bars).

Values are mean ± S.E.M. Number of hearts (number of experiments); *p<0.05, ***p<0.001, ****p<0.0001, two-way ANOVA, Bonferroni's *post-hoc* test.

124

(n=3(18);p<0.0001). SR Ca^{2+} content increased in rest-period (ZT3) myocytes, from 827.6 ± 96.3nM to 998.4 ± 78.4nM (n=5(25)), however this was not significant (p=0.06).

Figure 3.8D shows the mean exponential time constant of the decay of the caffeine-induced Ca^{2+} transient in response to NOS inhibition in the presence of stimulation with ISO. The data shows that NOS inhibition results in a decrease the rate of relaxation in both rest-period (ZT3) myocytes, from 2275.0 ± 271.3ms to 1600.0 ± 202.6ms (n=5(22);p < 0.05) and active-period (ZT15) myocytes, from 2976.0 ± 259.0ms to 1651.0 ± 163.7ms (n=3(16);p < 0.0001) myocytes, indicating an increase in NCX activity in both the rest-period (ZT3) and active-period (ZT15).

Following simultaneous inhibition of NOS and ISO stimulation, the previously reported depressed response of active-period (ZT15) myocytes is abolished as no difference in SR Ca^{2+} (p=0.99) or NCX activity (p=0.99) between rest-period (ZT3) and active-period (ZT15) myocytes was found.

In summary;

These data show the reduced response of active-period (ZT15) myocytes to β-ADR stimulation with ISO, observed as a reduced increase in systolic $[Ca^{2+}]_i$ and SR Ca^{2+} content and a blunted increase in SERCA activity and NCX activity can be abolished following NOS inhibition with L-NNA. NOS inhibition with L-NNA during ISO stimulation also induced a further increase in systolic $[Ca^{2+}]_i$, SR Ca^{2+} content and SERCA and NCX activity in rest-period (ZT3) myocytes; however these increases in response to NOS inhibition were not significant (except NCX activity). Following simultaneous inhibition of NOS and ISO stimulation no difference in systolic $[Ca^{2+}]_i$, SR Ca^{2+} content and SERCA and NCX activity existed between rest-period (ZT3) and active-period (ZT15) myocytes. Together this data suggests that NO is responsible for time-of-day variation in Ca^{2+} handling in response to ISO that I have shown.

3.2.3.2 The role of β_3-ADR stimulation in the time-of-day variation in Excitation-Contraction coupling in response to isoproterenol

I have shown inhibition of NOS abolishes the time-of-day variation in systolic $[Ca^{2+}]_i$, SR Ca^{2+} content and SERCA and NCX activity in response to non-specific β-ADR stimulation with ISO, which suggests that NOS-signalling may be responsible for this time-of-day variation the response of in E-C coupling to ISO. β_3-ADR are coupled to the inhibitory G_i protein, and stimulation of the β_3-ADR leads to an increase in NO production by NOS enzymes and activation of PDE3 and PDE4, which facilitate cAMP breakdown, leading to a reduction in contractility (Gauthier et al., 2011). I therefore hypothesised that there may be a time-of-day variation in β_3-ADR signalling which could be causing the time-of-day variation in NOS signalling.

3.2.3.2.1 Time-of-day variation in response of calcium handling to specific β_3-ADR stimulation with BRL$_{37344}$

To investigate a time-of-day variation in the response of Ca^{2+} transient to specific β_3-ADR stimulation, $[Ca^{2+}]_i$ was measured in rest-period (ZT3) and active-period (ZT15) myocytes in normal Tyrode and 200nM BRL$_{37344}$. Measurement of systolic $[Ca^{2+}]_i$, diastolic $[Ca^{2+}]_i$ and rate of relaxation of the electrically-induced Ca^{2+} transient were made as previously described (See Methods 2.2.3).

Figure 3.9 shows example records of electrically-induced Ca^{2+} transients recorded in normal Tyrode and 200nM BRL$_{37344}$ from A. rest-period (ZT3) myocytes and B. active-period (ZT15) myocytes. The records show a reduction in $[Ca^{2+}]_i$ in response to BRL$_{37344}$ in rest-period (ZT3) and active-period (ZT15) myocytes.

The mean systolic $[Ca^{2+}]_i$ and diastolic $[Ca^{2+}]_i$ in rest-period (ZT3) and active-period (ZT15) myocytes from such experiments can be seen in Figure 3.9C and 3.9D.

The data show a significant time-of-day difference in the response of myocytes to BRL$_{37344}$, with a significant decrease in systolic $[Ca^{2+}]_i$ in rest-period (ZT3) myocytes, from 458.5 ± 41.2nM in normal Tyrode to 361.2 ± 18.0nM in BRL$_{37344}$ (n=4(16);p<0.001), however the reduction in systolic $[Ca^{2+}]_i$ was not significant in active-period (ZT15) myocytes, from 311.0 ± 29.0nM to 279.2 ± 18.3nM (n=(18);p=0.32). Diastolic $[Ca^{2+}]_i$

increased in rest-period (ZT3) myocytes in response to BRL$_{37344}$, from 90.9 ± 8.8nM to 107.7 ± 11.9nM (n=4(19); p=0.06) and active-period (ZT15) myocytes, from 80.1 ± 5.6nM to 82.4 ± 5.2nM (n=3(18);p=0.08).

The mean exponential time constant of the decay of the electrically-induced Ca^{2+} transient are shown in Figure 3.9E, and demonstrates a reduction in relaxation time following BRL$_{37344}$ stimulation in rest-period (ZT3) myocytes, from 151.9 ± 9.6ms to 108.2.93 ± 7.9ms (n=4(15);p<0.0001)) indicating an increase in SERCA activity but no change in active-period (ZT15) myocytes, from 228.9 ± 15.7ms to 218.7 ± 23.5ms (n=3(18);p=0.81). Following BRL$_{37344}$ superfusion, the time-of-day variation in relaxation time observed at baseline remained, with relaxation time significantly shorter in rest-period (ZT3) than active-period (ZT15) myocytes (p<0.0001).

BRL$_{37344}$ induced a significant reduction in systolic [Ca^{2+}]$_i$ and an increase in SERCA activity in rest-period (ZT3) myocytes, which would usually increase SR Ca^{2+} stores (Bers 2001). However, it is known that NO is able to increase the P$_o$ of the RyR2 during diastole, causing the RyR2 to become leaky and reducing SR Ca^{2+} stores (Zhang and Casadei 2012) opposing an increase in SR Ca^{2+} content activity.

To investigate a time-of-day variation in the SR Ca^{2+} content in response to β$_3$-ADR stimulation, SR Ca^{2+} content was measured in rest-period (ZT3) and active-period (ZT15) myocytes in normal Tyrode and 200nM BRL$_{37344}$ by rapidly perfusing cells with Tyrode containing caffeine (20mM for 5 seconds) as previously described (See Methods 2.2.3).

Figure 3.10 shows example records of a caffeine-induced Ca^{2+} transient recorded in normal Tyrode and 200nM BRL$_{37344}$ from A. rest-period (ZT3) and B. active-period (ZT15) myocytes. The records show a clear greater reduction in peak caffeine-induced Ca^{2+} release in response to BRL$_{37344}$ in rest-period (ZT3) myocytes compared to active-period (ZT15) myocytes.

The mean peak caffeine-induced Ca^{2+} release and rate of relaxation of the caffeine-induced transient in rest-period (ZT3) and active-period (ZT15) myocytes can be seen in Figures 3.10C and 3.10D.
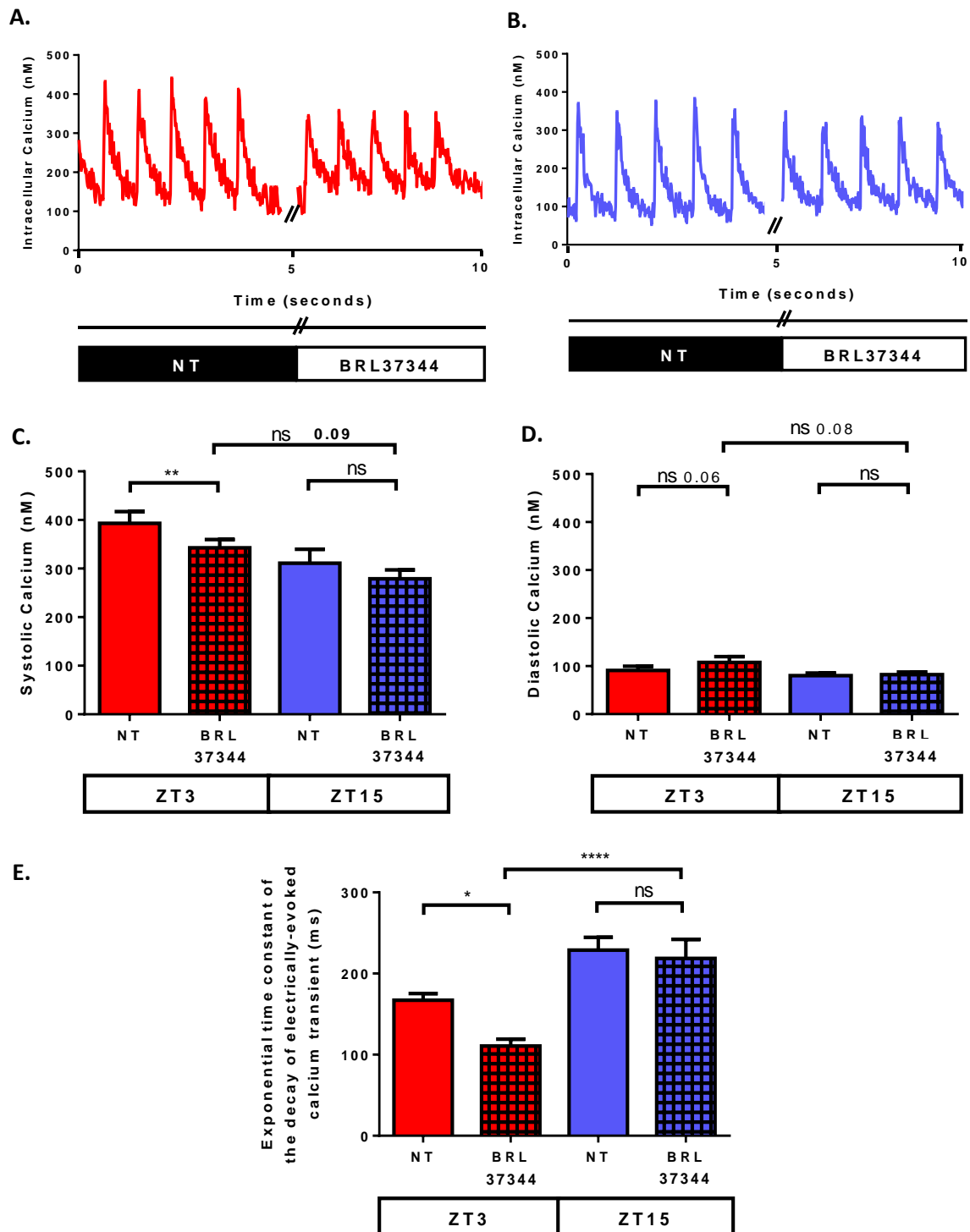
Figure 3.9 **The effect of β₃-adrenergic stimulation on systolic and diastolic calcium, and rate of relaxation of the electrically-induced Ca²⁺ transient in rest-period (ZT3) and active-period (ZT15) myocytes**

Example Ca²⁺ transient recordings from **A.** rest-period (ZT3) (red) and **B.** active-period (ZT15) (blue) myocytes in normal Tyrode and 200nM BRL₃₇₃₄₄.

Bar charts showing mean; **C.** systolic [Ca²⁺], **D.** diastolic [Ca²⁺] and **E.** exponential time constant of the decay of the electrically-induced Ca²⁺ transient, recorded from rest period (ZT3) (red, n=4(15-19)) and active period (ZT15) (blue, n=3(18)) myocytes in normal Tyrode (open bars) and 200nM BRL₃₇₃₄₄ (hatched bars).

Values are mean ± S.E.M. Number of hearts (number of experiments); *p<0.05, **p<0.01, ****p<0.0001, two-way ANOVA, Sidaks's *post-hoc* test.
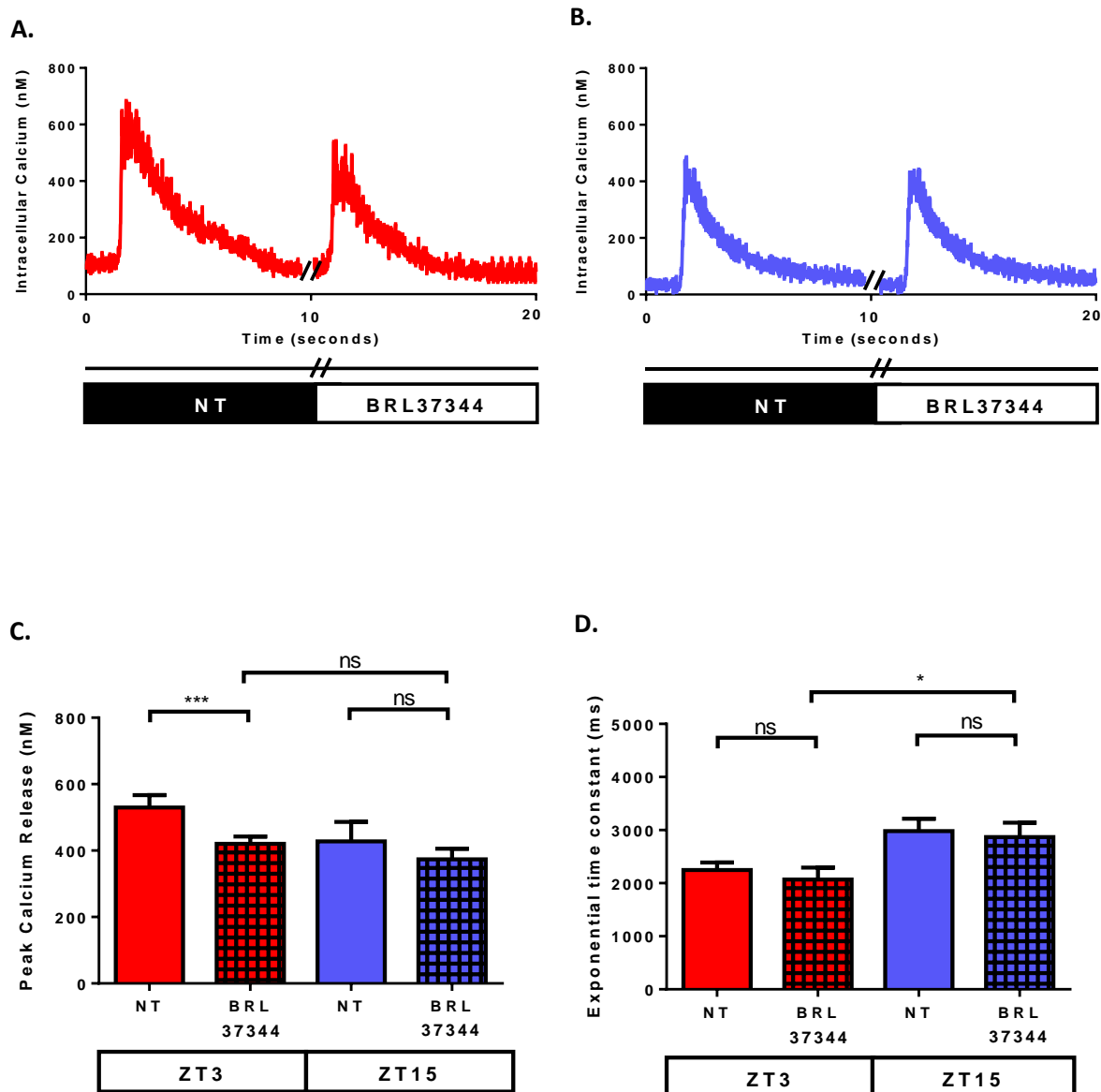
Figure 3.10 **The effect of β₃-adrenergic stimulation on sarcoplasmic reticulum Ca²⁺ content and relaxation of the caffeine-induced Ca²⁺ transient rest-period (ZT3) and active-period (ZT15) myocytes.**

Example caffeine induced Ca²⁺ transient recordings from **A.** rest-period (ZT3) (red) and **B.** active-period (ZT15) (blue) myocytes in normal Tyrode and 200nM BRL₃₇₃₄₄.

Bar charts showing mean; **C.** peak caffeine-induced Ca²⁺ release and **D.** exponential time constant of the decay of the caffeine-induced Ca²⁺ transient in rest-period (ZT3) (red, n=4(19)) and active-period (ZT15) (blue, n=3(13)) myocytes in normal Tyrode (open bars) and 200nM BRL₃₇₃₄₄ (hatched bars).

Values are mean ± S.E.M. Number of hearts (number of experiments); *p<0.05, ***p<0.001, two-way ANOVA, Sidaks's *post-hoc* test.

The data shows a significant reduction in peak caffeine-induced Ca^{2+} release in rest-period (ZT3) myocytes in response to BRL_{37344}, from 529.3 ± 37.7nM to 420.1 ± 22.2nM (n=4(19);p<0.001), however the reduction in active-period (ZT15) myocytes was not significant, from 427.8 ± 58.3nM to 373.4 ± 32.6nM (n=3(13);p=0.13). As a result, there was no difference in SR Ca^{2+} content between rest-period (ZT3) and active-period (ZT15) myocytes following BRL_{37344} (p=0.99).

The mean exponential time constant of the decay of the caffeine-induced Ca^{2+} transient recorded in rest-period (ZT3) and active-period (ZT15) myocytes (Figure 3.10E) shows no change in relaxation time in response to BRL_{37344}, indicating no change in NCX activity in either time-point. Rest-period (ZT3) myocytes, from 2249.0 ± 141.7ms to 2068.0 ± 226.2ms (n=4(19);p=0.99), and active-period (ZT15) myocytes, from 2980.0 ± 233.9ms to 2869.0 ± 269.3ms (n=3(13);p=0.99). As a result, the time-of-day variation in NCX activity observed at baseline remains following BRL_{37344} (p<0.05).

3.2.3.2.2 Time-of-day variation in the response of the action potential to specific β_3-ADR stimulation with BRL_{37344}

In this section I have demonstrated a time-of-day variation in the response of Ca^{2+} transients to specific β_3-ADR stimulation with BRL_{37344}. In previous sections I have shown a time-of-day variation in the configuration of the cardiac action potential recorded in normal Tyrode (Figure 3.3). Perfusion of cells with BRL_{37344} has been associated with an acceleration of the repolarisation phase of ventricular action potential (Gauthier, Langin et al. 2000) and so I hypothesised that the time-of-day variation in Ca^{2+} handling in response to BRL_{37344} may be due to underlying variation in the configuration of the action potential in response to BRL_{37344}.

To investigate whether a time-of-day variation exists in the action potential configuration and/or APD in response to BRL_{37344}, action potentials were recorded in rest-period (ZT3) and active-period (ZT15) myocytes in normal Tyrode and 200nM BRL_{37344} and measurement of APD_{30}, ADP_{50} and APD_{90} were made as previously described (See Methods 2.3.3.1).

Figure 3.11 shows a record of an action potential recorded from A. rest-period (ZT3) (red) and B. active-period (ZT15) (blue) myocytes in normal Tyrode and BRL_{37344}, showing a shortening of APD in response to BRL_{37344}.

Mean APD_{30}, APD_{50} and APD_{90} recorded from rest-period (ZT3) and active-period (ZT15) myocytes are shown in Table 3.11C and the data shows BRL_{37344} shortened the APD in both rest-period (ZT3) and active-period (ZT15) myocytes.

As APD was significantly shorter in active-period (ZT15) basal action potentials (see Figure 3.1), mean percentage change in APD_{30}, APD_{50} and APD_{90} in response to BRL_{37344} was calculated and is shown in Figure 3.11D, which shows no time-of-day variation in the response of the action potential to BRL_{37344}. The data shows no difference in percentage decrease in APD_{30}, APD_{50} and APD_{90} in rest-period (ZT3) myocytes (n=4(15)); APD_{30} of -19.82 ± 1.8%, ADP_{50} of -15.9 ± 2.1% and APD_{90} of -4.6 ± 2.7%, as compared to active-period (ZT15) myocytes (n=4(12)); APD_{30} of -14.9 ± 3.4% (p=0.54), ADP_{50} of -12.4 ± 6.7% (p=0.78) and APD_{90} of 1.1 ± 4.3% (p=0.47).

In summary;

This data shows the "dip" in active-period (ZT15) myocytes in response to β-ADR stimulation with ISO, reflecting a depressed increase in systolic $[Ca^{2+}]_i$, SR Ca^{2+} content, SERCA and NCX activity, was absent following NOS inhibition. NOS inhibition significantly enhanced the positive inotropic effect of ISO in active-period (ZT15) myocytes, the result being that the time-of-day variation between rest-period (ZT3) and active-period (ZT15) myocytes was abolished. This suggests NO availability and/or signalling is responsible for the variation in response to ISO.

The time-of-day variation in NOS signalling could not be explained by either the response of calcium handling or the action potential to $β_3$-ADR activation of NOS as the effect of $β_3$-ADR stimulation was greatest in rest-period (ZT3) myocytes. However, calcium handling in response to $β_3$-ADR adrenergic stimulation displayed a time-of-day variation, with a greater response in rest-period (ZT3) myocytes.

A.

B.

C.

	APD$_{30}$ (ms)		APD$_{50}$ (ms)		APD$_{90}$ (ms)	
	Normal Tyrode	BRL$_{37344}$	Normal Tyrode	BRL$_{37344}$	Normal Tyrode	BRL$_{37344}$
Rest-period (ZT3) myocytes	18.30 ± 2.23	14.43 ± 1.64	32.18 ± 4.27	26.51 ± 3.09	79.42 ± 7.24	74.97 ± 6.29
Active-period (ZT15) myocytes	9.53 ± 1.13	8.19 ± 1.16	15.46 ± 1.70	13.60 ± 1.78	71.67 ± 5.96	76.87 ± 7.11

D.
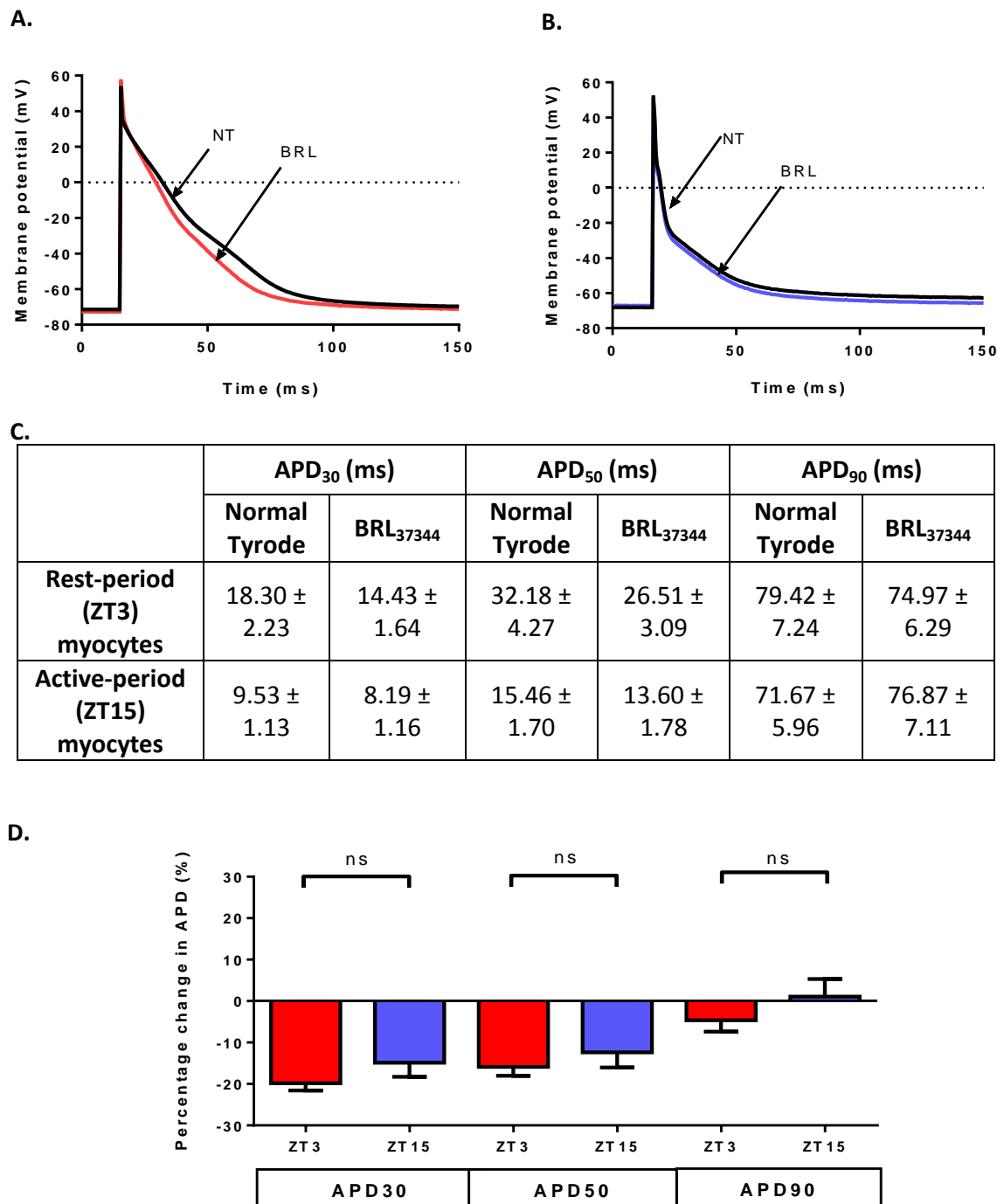
Figure 3.11 **The effect of β$_3$-adrenergic stimulation on action potential configuration in rest-period (ZT3) and active-period (ZT15) myocytes.**

Example action potential recordings from **A.** rest-period (ZT3) and **B.** active-period (ZT15) in normal Tyrode and 200nM BRL$_{37344}$.

C. Mean APD$_{30}$, APD$_{50}$ and APD$_{90}$ recorded from rest-period (ZT3) and active-period (ZT15) myocytes in normal Tyrode and 200nM BRL$_{37344}$.

D. Bar chart showing the percentage change in APD$_{30}$, APD$_{50}$ and APD$_{90}$ following superfusion with 200nM BRL$_{37344}$, recorded from rest-period (ZT3) (red, n=4(15)) and active-period (ZT15) (blue, n=4(12)) myocytes.

Values are mean ± S.E.M. Number of hearts (number of experiments); *p<0.05, **p<0.01, ***p<0.001, one-way ANOVA, Sidak's *post-hoc* test.

3.2.4 Cycling of circadian clocks within myocytes

In the present chapter I have shown here a number of time-of-day variations in calcium handling and action potential configuration in the isolated myocyte. It is known that approximately 10-15% rat cardiac genes display diurnal variation (Martino, Arab et al. 2004) and the existence of an intrinsic circadian clock within myocytes is well documented (Young, Razeghi et al. 2001; Young, Razeghi et al. 2001; Young 2003). It has been proposed that diurnal variation in cardiac function is controlled by a complex interplay of the central and peripheral circadian clock and extracellular neurohumoral influences (Durgan, Hotze et al. 2005) and so it is important to ensure the intrinsic peripheral clock did not continue to cycle post-isolation during the experimental day in order to validate our results. Previous members of the group have shown no difference in the E-C coupling parameters, such as systolic $[Ca^{2+}]_i$ and diastolic $[Ca^{2+}]_i$, in myocytes between 0 to 4 hours or 4 to 8 hours after isolation (Collins and Rodrigo 2010), suggesting that the intrinsic clock did not continue to influence gene transcription post-isolation. However, I set out to examine the expression of circadian clock genes in isolated myocytes sampled throughout the experimental day to rule out the cycling of the clock post-isolation.

In order to rule out the continued cycling of the intrinsic circadian clock in myocytes post-isolation I examined variation in mRNA levels of three key circadian clock genes; *clock*, *per2* and *bmal1*, during the experimental day in myocytes isolated from rest-period (ZT3) hearts.

Cells suspensions were stored at room temperature in normal Tyrode during the experimental day. Samples were taken immediately following isolation and at 3 hour intervals post-isolation and Quantitative real-time TaqMan RT-PCR was then performed on samples, using β-actin as the housekeeping gene. (See appendix). Fold change was calculated using the $2^{-\Delta\Delta CT}$ method. Statistics were performed on ΔCT values.

The data in Table 3.12D shows that cycling of the circadian clock genes *clock*, *per2* and *bmal1* did not occur during the experimental day, with no difference in gene expression at 0, 3 or 6 hours post-isolation.

A.

B.

C.

D.

Gene of interest	ΔCT (normalised to β-actin)			p-value (from ΔCT) (compared to T0)
	T0	**T3**	**T6**	
clock	4.41 ± 0.52	4.23 ± 0.25	3.74 ± 0.22	T0 vs. T3 ns p=0.94 T0 vs.T6 ns p=0.25
per2	7.79 ± 0.18	7.28 ± 0.12	7.67 ± 0.08	T0 vs. T3 *ns* *p*=0.21 T0 vs.T6 *ns* *p*=0.83
bmal1	6.22 ± 0.71	6.59 ± 0.41	5.66 ± 1.02	T0 vs. T3 *ns* *p*=0.65 T0 vs.T6 *ns* *p*=0.57
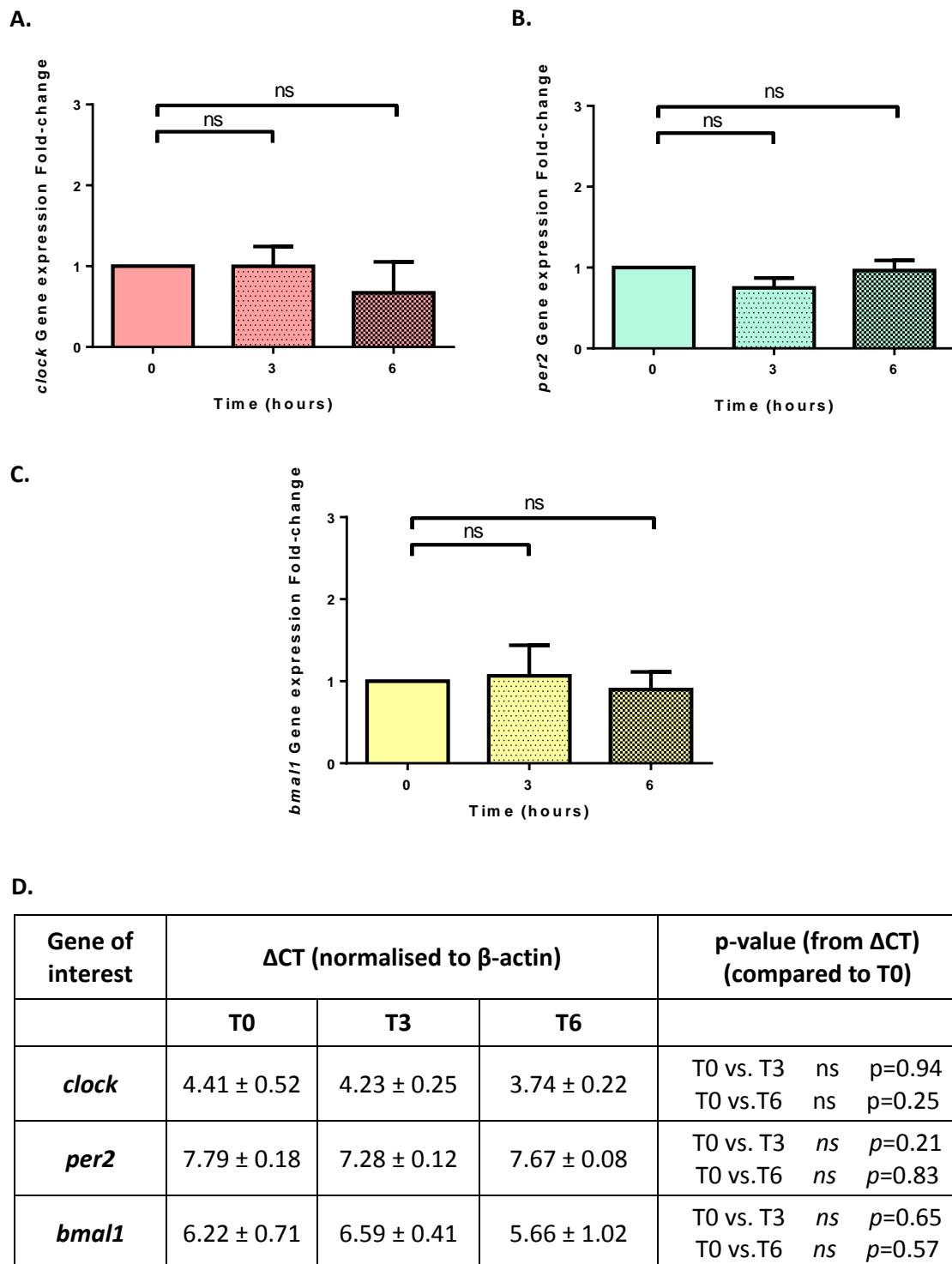
Figure 3.12 **Gene expression levels of circadian clock genes in ZT3 myocytes during the course of an experimental day.**

Bar chart showing quantitative real-time RT-PCR expression as fold change in isolated myocytes of **A.** *clock*, **B.** *per2* and **C.** *bmal1* circadian clock genes. mRNA values were normalised to β-actin. Fold change was calculated 3 hours post isolation (spotted bar) and 6 hours post-isolation (hatched bar) relative to the control (0 hours post isolation).

D. Table showing ΔCT data used to produce the bar chart in figure 3.12A/B/C.

Values are mean ± S.E.M, number of hearts (number of samples) n=3(4-5); one-way ANOVA, Sidak's *post-hoc* test.

3.3 Discussion

In the present chapter, I have shown for the first time that the action potential configuration recorded from ventricular myocytes under basal conditions is subject to a time-of-day variation. The data shows a longer $APD_{30/50}$ in rest-period (ZT3) myocytes, which was associated with a hyperpolarised RMP. This data was accompanied by a time-of-day variation in Ca^{2+} handling, observed as a greater systolic $[Ca^{2+}]_i$, SR Ca^{2+} content and a faster rate of relaxation of electrically-induced and caffeine-induced Ca^{2+} transients, indicating greater SERCA and NCX activity respectively, in rest-period (ZT3) myocytes when compared to active-period (ZT15) myocytes.

On the basis of these findings, I also determined whether the time-of-day variation in Ca^{2+} handling in response to the non-specific β-ADR agonist ISO was due to a variation in the response of the action potential. My data confirms that time-of-day variation in Ca^{2+} handling manifests as a greater increase in systolic $[Ca^{2+}]_i$ and SR Ca^{2+} content in response to ISO in rest-period (ZT3) myocytes. Given that an increase in APD can result in an increase in contraction strength and $[Ca^{2+}]_i$ (Bers 2001) and that β-ADR stimulation with ISO prolongs the APD, I hypothesised that the largest APD lengthening effect of ISO would be observed in rest-period (ZT3) myocytes and may contribute to the observed increase in systolic $[Ca^{2+}]_i$ at this period. However, the increase in APD in response to ISO was greatest in active-period (ZT15) myocytes, which was the reverse to that expected and so it is unlikely the action potential is the cause of the time-of-day variation in Ca^{2+} handling I have observed, and indeed might be expected to reduce the variation. Nevertheless, these findings are novel as a time-of-day variation in APD in response to ISO is yet to be reported in ventricular myocytes isolated at two opposing time points during the rest-period (ZT3) and active-period (ZT15) of adult wistar rats.

I have also shown for the first time a time-of-day variation in the response to specific $β_3$-ADR stimulation. The data shows a greater reduction in systolic $[Ca^{2+}]_i$, SR Ca Ca^{2+} content and relaxation time in rest-period (ZT3) myocytes. This was mirrored by a reduction in APD, however no time-of-day variation in the response of the action potential to BRL_{37344} was found, and so action potential configuration is unlikely to be the cause of a time-of-day variation in Ca^{2+} handling in response to $β_3$-ADR specific stimulation.

These findings are not affected by continued cycling of the intrinsic circadian clock following cell isolation.

3.3.1   Is the isolated ventricular myocyte an appropriate model to investigate time-of-day variations in ventricular function?

To study the influence of the time-of-day on Ca^{2+} handling and action potential configuration of the ventricular myocardium, I have used single isolated ventricular myocytes as an experimental model. The isolation process is a stressful event for the myocardium as the collection of the heart and subsequent isolation of single ventricular myocytes is subject to fluctuations in temperature and $[Ca^{2+}]_i$, brief periods of ischemia and serum starvation, all of which may affect circadian variation in gene expression and function.

In addition, the presence of a peripheral clock within the myocyte is well established (Young, Razeghi et al. 2001; Durgan, Hotze et al. 2005) and may continue to cycle after the isolation process meaning that the ventricular myocytes isolated at any particular time point may continue to drift in time. However, I have shown that following cell isolation no oscillation of clock genes (*clock*, *per2* and *bmal1*) was observed, confirming the intrinsic clock did not continue to influence gene transcription post-isolation. This is consistent with data published by Durgan *et al.* which suggest low levels of FBS (2.5%) during culture are essential for continued cycling of the intrinsic clock once isolated. Our cells were stored in normal Tyrode during the experimental day, this contains 0% FBS and all experimental solutions also contained 0% FBS. FBS is a standard cell culture laboratory reagent containing the growth factors required for cell growth and proliferation, a major component of which is BSA. Although our cells are exposed to <1% BSA during the isolation process (for 6-8 minutes) this does not appear to be sufficient to continue cycling of clock in isolated ventricular myocytes post-isolation. My data did not show any evidence of cycling of the clock genes *clock*, *per2* or *bmal1*, which was as expected as previous members of our group had found no difference in the E-C coupling parameters measured (Ca^{2+} transient, contraction strength and SR Ca^{2+} content) in myocytes 0 - 4 hours or 4 - 8 hours after isolation, suggesting that the intrinsic clock did not continue to influence gene transcription (Collins and Rodrigo 2010).

Studies of circadian rhythms typically investigate a wide range of time-points, usually covering a 24 hour period if not longer. In the present chapter, investigation of Ca^{2+} handling and action potential configuration was only obtained from hearts isolated during the rest-period and active-period myocytes of the nocturnal rat. The time-points chosen for this investigation have been shown by others to display clear differences in circadian clock gene expression profiles (Durgan, Hotze et al. 2005; Young 2006) and in addition, I did not choose time-points on the border of transition from a resting to active state, i.e. ZT0, or from the active to resting state, i.e. ZT12, as these time-points represent a sudden change in activity levels, external cues, such as light, and internal cues, such as sympathetic drive. Instead, I chose time-points that represent approximately 3 hours after the start of the rest and active period and so each animal's diurnal change in gene transcription, protein expression, activity and metabolism will have occurred, and the rat will have definitively entered the rest-period or the active-period of its day.

The expression of a number of frequently used *housekeeping gene* have been shown to be highly variable (Dheda, Huggett et al. 2004) and may be subject to diurnal variations, and so internal validation of the *housekeeping gene* used in this investigation is essential. In this study it was essential that the *housekeeping gene* was not subject to diurnal variation or controlled by the circadian clock, and therefore I compared the expression of the *housekeeping gene* β-actin over the course of the experimental day to ensure no variation. The data showed no variation in β-actin over the experimental day (See Appendix 3). Ideally, I would have compared the expression of β-actin between rest-period (ZT3) and active-period (ZT15) myocytes to ensure no time-of-day variation, however during this period of investigation our animal housing facility moved to a brand new facility and due to disruptions to our reverse light cycle animal room I was unable to complete this comparison. However, the expression of β-actin between rest-period (ZT3) and active-period (ZT15) myocytes had previously been completed by members of our group, and this data demonstrated no variation in β-actin expression. This data taken together with my own, demonstrates that β-actin expression does not cycle and does not vary throughout the experimental day, and so β-actin was taken as a viable *housekeeping gene*.

3.3.2 Time-of-Day variation in Excitation-Contraction coupling

The time-of-day variation in excitation-contraction in basal conditions leads to a greater systolic Ca²⁺ in rest-period (ZT3) ventricular myocytes

Circadian rhythms exist in almost all CV parameters including HR, BP, CO and serum catecholamine levels, which enable an organism to adapt to the higher activity levels during the active period (Guo and Stein 2003). Diurnal variation in Ca^{2+} homeostasis has been well documented in a number of organs, including the brain (Pennartz, de Jeu et al. 2002) and the small intestine (Wrobel and Nagel 1979). In the present chapter, I have shown that basal systolic $[Ca^{2+}]_i$, $[Ca^{2+}]_{SR}$ and SERCA activity were all found to be greater in myocytes isolated during the rest-period (ZT3) of the rat, which confirmed previous findings of our group (Collins and Rodrigo 2010). However, in a novel finding, I have also shown that the activity of the NCX is also greater in the rest-period (ZT3). This effect was revealed by analysing the rate of relaxation of the caffeine-induced Ca^{2+} transient, which results predominantly from Ca^{2+} efflux on the NCX (Bers 2001). I have also shown for the first time that basal action potential configuration is subject to a time-of-day variation. The data shows a longer $APD_{30/50}$ in rest-period (ZT3) myocytes, which was associated with a hyperpolarised RMP.

The greater systolic $[Ca^{2+}]_i$ in the rest-period (ZT3) myocyte could reflect changes in activity/expression of key Ca^{2+} handling proteins (LTCC, NCX, SERCA/PLB, RyR2) and/or in the configuration of the action potential. Each of these possibilities will be discussed in further detail below.

The observed difference in both the systolic $[Ca^{2+}]_i$ and the corresponding time-of-day variation in APD, between rest-period (ZT3) and active-period (ZT15) myocytes under basal conditions (perfused with normal Tyrode and stimulated at 1 Hz) may result from a greater current density of the LTCC during the rest-period (ZT3). An increase in LTCC could lead to an increase systolic $[Ca^{2+}]_i$ directly through the a greater signal for CICR and/or indirectly by prolongation of the APD. Alternatively, the longer APD might result from a reduction in the size of the repolarising currents active during the plateau and repolarising phase of the action potential (I_{K1}, I_{Kr}, I_{Ks}).

An increase in LTCC current can affect $[Ca^{2+}]_i$ independently of APD, triggering Ca^{2+} release from the SR during CICR. An increase in the current density of the LTCC increases the size

of the trigger for CICR from the SR via RyR2, resulting in greater amounts of Ca^{2+} to be released and a greater systolic $[Ca^{2+}]_i$. The LTCC is also able to prolong the plateau phase of the action potential and ultimately APD, which could affect systolic $[Ca^{2+}]_i$. During the rest-period (ZT3) the increased basal systolic $[Ca^{2+}]_i$ is mirrored by a longer basal APD and so it could be proposed that both observations are the result of a greater LTCC during the rest-period (ZT3) of the rat. Instead, data from our laboratory shows basal LTCC density to be greatest in active-period (ZT15) myocytes (Collins and Rodrigo 2010) when systolic $[Ca^{2+}]_i$ and APD are lowest, and so it is therefore unlikely the size of the LTCC is responsible for either the larger systolic $[Ca^{2+}]_i$ or longer APD observed in the rest-period (ZT3) myocytes.

The NCX can also contribute to Ca^{2+} entry early during the plateau phase of the action potential due to the high $[Na^+]_i$ following the upstroke of the action potential and so may be responsible for an increased Ca^{2+} influx independent of the LTCC. The rapid increase in $[Na^+]_i$ in the fuzzy space just beneath the membrane and the more positive membrane potential following the action potential upstroke prompts the NCX to work in "reverse-mode", extruding Na^+ from the cell contributing to the enhanced $[Ca^{2+}]_i$ (Bers 2002). However, the contribution of the NCX to Ca^{2+} influx is minor as compared to the LTCC, as the rapid increase in $[Ca^{2+}]_i$ will cause the NCX to switch to "forward-mode" extruding Ca^{2+} (Bers 2008). Additionally, the ability of the NCX to induce Ca^{2+} release from the SR is controversial with some experimenters finding the NCX is able to induce Ca^{2+} release from the SR (Goldhaber 1999) and others unable to detect Ca^{2+} release from the SR in the absence of an increase in LTCC (Adachi-Akahane, Lu et al. 1997) and so the increased activity of the NCX during the rest-period (ZT3) is unlikely to contribute to the higher systolic $[Ca^{2+}]_i$ observed in rest-period (ZT3) myocyte in the face of a smaller LTCC. However, this is speculative as although we observed an increased activity of the NCX, this was investigated without the influence of SERCA (application of 20mM caffeine causes prolonged RyR2 opening, so that although SERCA activity is unaffected by caffeine application the Ca^{2+} sequestered back to the SR during the caffeine-induced Ca^{2+} release will immediately flow out of the SR through the open RyR2 and so Ca^{2+} is extruded from the cell via NCX). During E-C coupling there is competition between SERCA and "forward-mode" NCX for Ca^{2+} removal during contractile relaxation and it is possible that the increase in NCX activity increases the competition between SERCA and NCX for Ca^{2+} efflux thereby reducing SR Ca^{2+} content. However, this is speculative and further investigation of

139

the NCX current and its influence on basal action potential configuration and Ca^{2+} fluxes during relaxation is required.

The prolonged APD I have observed could equally be caused by a reduction in the size of the repolarising K^+ currents during the rest-period (ZT3). Although I was unable to investigate the currents underpinning the action potential in rest-period (ZT3) and active-period (ZT15) myocytes, evidence in the literature suggests that a time-of-day variation exists in repolarisation of the action potential. Recently Jeyaraj *et al.* examined the circadian rhythmicity of cardiac K^+ channel expression and it was found that expression of the α-subunit (Kcnd2) and the regulatory β-subunit (KChIP2) of I_{to} displayed a circadian rhythm, with expression of both peaking early in the active-phase of the mouse (Jeyaraj, Haldar et al. 2012), indicating a smaller repolarising current during the rest phase, which may explain the prolonged action potential duration in the rest-period (ZT3) of the rat that I have observed.

Unfortunately due to limitations with our animal model I was not able to measure either the LTCC or repolarising K^+ currents (I_{to}, I_{K1}, I_{Kr}, I_{Ks}) in rest-period (ZT3) and active-period (ZT15) myocytes to determine the underlying cause of the time-of-day variation in APD I have observed, and further investigation is needed here. Irrespective of this, it appears unlikely that the observed variation in action potential duration is the cause of the variation in the Ca^{2+} transient I have observed as the hyperpolarised RMP is suggestive of an increase in the size of I_{K1}, but the prolonged APD is reflective of a possible reduction in the size of the repolarising K^+ currents, instead the prolonged APD may instead be reflective of changes in Ca^{2+} handling.

The release of Ca^{2+} from stores in the SR during CICR are responsible for 90% of the $[Ca^{2+}]_i$ in the rat (Wier, Egan et al. 1994) and it is possible the observed greater SR Ca^{2+} stores during the rats rest-period (ZT3) are responsible for the variation in systolic $[Ca^{2+}]_i$ I have observed. SR Ca^{2+} content was determined by measuring peak Ca^{2+} content as well as the area under the curve, the data expressed as a percentage of mean rest-period (ZT3) SR Ca^{2+} content, and the data showed a greater SR Ca^{2+} content in rest-period (ZT3) myocytes than active-period (ZT15) myocytes, with no difference between peak Ca^{2+} content and area under the curve data. In deciding which method of SR Ca^{2+} content determination to use going forward in our investigation I chose to continue with peak Ca^{2+} content, as I

believe that the area under the curve method of estimating Ca^{2+} release is open to error as the area under the curve will directly reflect how quickly it Ca^{2+} is removed from the cytoplasm, therefore for a given release of Ca^{2+}, if the NCX works slower, the area under the curve will be larger even though there may not be any more Ca^{2+} released. The gold standard for measuring SR Ca^{2+} release is to measure the NCX current in response to caffeine in voltage clamped myocytes (Diaz, Trafford et al. 1997). In future experiments measurement of the area under the curve was not completed and only peak Ca^{2+} release data is shown.

The amount of Ca^{2+} released from the SR via the RyR2 is dependent upon a number of factors; the size of the trigger for CICR (LTCC) (Bassani et al., 1995), the size of the store of SR Ca^{2+} (Bers 2002) and on the activity of the RyR2 (Bers, 2008) and its regulatory proteins, such as CASQ and junction, which inhibit P_o of the RyR2 when $[Ca^{2+}]_{SR}$ levels are low but conversely promote P_o of the RyR2 when $[Ca^{2+}]_{SR}$ levels are high (Gyorke and Terentyev 2008).

As mentioned previously, the current density of the LTCC is greatest in active-period (ZT15) and not the rest-period (ZT3) myocyte, and so the size of the LTCC trigger is unlikely to be the cause of a greater SR Ca^{2+} release in the rest-period (ZT3) myocyte.

I have observed the activity of SERCA to be greatest in the rest-period (ZT3) of the rat. An increase in the activity of SERCA results in greater amounts of Ca^{2+} sequestered back to the SR during contractile relaxation, which over a number of cardiac beats increases SR Ca^{2+} stores. It is possible the increased activity of SERCA during the rest-period (ZT3) and the resulting larger SR store of Ca^{2+} has the knock on effect of a larger release of SR Ca^{2+} during the rest-period (ZT3) giving rise to the higher systolic $[Ca^{2+}]_i$ in spite of a smaller LTCC trigger. The increased SERCA activity during the rest-period (ZT3) may be a consequence of increased expression of SERCA, a reduction in PLB expression or an increase in the phosphorylation of PLB. Although the gene expression or protein levels of SERCA and PLB were not determined in this investigation, previous work by our group have observed no difference in the basal gene expression of SERCA and PLB between rest-period (ZT3) and active-period (ZT15) myocytes, suggesting that post-translational changes in PLB phosphorylation are the cause of an increased SERCA activity in the rest-period (ZT3).

Equally, the higher Ca^{2+} transient observed in the rest-period (ZT3) under basal conditions may be due to increased sensitivity of the RyR2 to an incoming trigger for CICR. An increase in sensitivity to Ca^{2+} would cause the RyR2 to open at lower Ca^{2+} levels and so may lead to an increased $[Ca^{2+}]$ released in spite of a smaller trigger for CICR. However, I did not investigate the sensitivity of the RyR2 to Ca^{2+} and so the RyR2 contribution to the time-of-day variation in systolic $[Ca^{2+}]_i$ under basal conditions cannot be determined here.

In conclusion, the observed longer APD observed in rest-period (ZT3) myocytes was not matched by a greater LTCC found by previous members of our group to be greatest during the active-period (ZT15), and so it seems unlikely that the variation in systolic $[Ca^{2+}]_i$ is connected to the LTCC. The observed increased SR Ca^{2+} stores are likely to be the cause of the time-of-day variation in systolic $[Ca^{2+}]_i$, as SERCA activity and SR Ca^{2+} stores are greatest in the rest-period (ZT3), matching the greatest systolic $[Ca^{2+}]_i$.

It is possible that NOS signalling is involved in the time-of-day variation in basal E-C coupling as NO is able to post-transcriptionally modify the activity of the E-C coupling proteins. Indeed endogenous NO-signalling has been implicated in the control of basal contractility in a number of studies (Sears, Bryant et al. 2003; Massion, Pelat et al. 2005; Burkard, Rokita et al. 2007; Seddon, Shah et al. 2007). However due to the spatiotemporal restriction in NO signalling, the isoform of NOS (eNOS/nNOS) associated with the control of contractility has not been fully identified. eNOS is localised to the caveola and is well placed to affect the LTCC, whereas nNOS is localised to RyR2 on the SR and so is placed to affect the SR and sarcolemma. As we have concluded that the SR is central to the time-of-day variation in systolic $[Ca^{2+}]_i$ we observe, nNOS signalling may be involved due to its localisation to the SR. nNOS has been shown by a number of groups to affect basal contractility in nNOS KO mouse models (Sears, Bryant et al. 2003) and mouse over-expression studies (Burkard, Rokita et al. 2007). In a mouse nNOS KO model, nNOS gene disruption increased the LTCC and resulted in a greater amplitude Ca^{2+} transient and SR Ca^{2+} load (Sears, Bryant et al. 2003), whereas over-expression lead to a reduction in the LTCC and Ca^{2+} transient amplitude (Burkard, Rokita et al. 2007), and so it is possible that enhanced nNOS signalling could be the cause of the depressed Ca^{2+} transient observed in active-period (ZT15) myocytes at basal conditions. Unfortunately, the effect of NOS inhibition on the time-of-day variation in the basal Ca^{2+} transient was not able to be completed in this investigation.

The time-of-day variation in E-C coupling in response to sympathetic stimulation with ISO leads to a greater increase in systolic Ca²⁺ in rest-period (ZT3) myocytes:

This seemingly paradoxical reduced Ca^{2+} transient in the active-period (ZT15) of the rat may be reflective of a protective mechanism possibly, in which the myocardium is protected against surges in Ca^{2+} and Ca^{2+} overload during periods of high sympathetic activity occurring during the active-period (ZT15), such as the pronounced morning peak in circulating catecholamines upon waking (Dodt, Breckling et al. 1997) and during stress and exercise (Dimsdale and Moss 1980).

The β-ADRs are G-protein-coupled receptors located on the surface of myocytes which bind the endogenous catecholamines, adrenaline and nor-adrenaline. The actions of adrenaline and nor-adrenaline can be mimicked by the administration of the exogenous non-selective β-ADR agonist ISO. In the rat myocardium, stimulation of the β-ADR with a non-specific agonist such as ISO results in positive inotropic and lusitropic effects, mediated by PKA dependant phosphorylation of the LTCC, PLB, RyR2 and TnI (See introduction 1.2).

The data in the present investigation shows a significant time-of-day variation in the sensitivity of myocytes to the non-specific β-ADR stimulation with ISO, with rest-period (ZT3) myocytes displaying an enhanced systolic $[Ca^{2+}]_i$, SR Ca^{2+} content, SERCA and NCX activity following ISO. This data confers with that previously found by members of our group (Collins and Rodrigo 2010), who in addition to the variation on Ca^{2+} handling also showed a greater increase in the current density of the LTCC to ISO in rest-period (ZT3) myocytes. The larger increase in the current density of the LTCC during the rest-period (ZT3) will have increased the size of the trigger for CICR from the SR, thus contributing to an increasing systolic $[Ca^{2+}]_i$, and this may explain the variation in the increase in systolic $[Ca^{2+}]_i$ in response to ISO that we have both observed.

Following β-ADR stimulation with ISO, the increase in SERCA activity and SR Ca^{2+} content were found to be greatest in rest-period (ZT3) myocytes. ISO stimulation leads to PKA dependant phosphorylation of PLB, relieving SERCA of its inhibitory influence which increases SERCA's affinity for Ca^{2+} 2/3 fold (Bers 2002; Zipes 2012). The greater increase in SERCA activity in the rest-period (ZT3) would lead to the greater increase in the size of SR Ca^{2+} stores I have observed. The greater SR Ca^{2+} content in the rest-period (ZT3) following

ISO will increase the amount of Ca^{2+} available for release from the SR during CICR. As the SR Ca^{2+} release has such a large contribution to increases in $[Ca^{2+}]_i$ during contraction in the rat (~90%; Wier, Egan et al. 1994) this can explain the time-of-day variation in systolic $[Ca^{2+}]_i$ I have observed. Previous work by our group did not measure SERCA activity in response to ISO and so the time-of-day variation in SERCA activity observed in this investigation is novel.

Given that an increase in the LTCC in response to ISO is also able to prolong APD (Nerbonne and Kass 2005) and APD *per se* is able to alter Ca^{2+} regulation in the myocyte and therefore may in part contribute to this variation in response to ISO, I investigated the response of the action potential to ISO. I observed a time-of-day variation in the response of the action potential, finding a greater percentage increase in APD in active-period (ZT15) myocytes as compared to rest-period (ZT3) myocytes. My data shows that the prolongation of the APD in response to ISO stimulation is substantial in active-period (ZT15) myocytes (APD_{30} increase of +120.3 ± 14.9%, APD_{50} increase of +95.9 ± 13.2%) but was not significant in rest-period (ZT3) myocytes in comparison (APD_{30} increase of +10.6 ± 8.2%, APD_{50} increase of +11.6 ± 7.4%). This considerable increase in APD in the active-period (ZT15) is perhaps paradoxical to the modest increase in systolic $[Ca^{2+}]_i$ observed at this time-point.

In active-period (ZT15) myocytes, I observed a modest increase in systolic $[Ca^{2+}]_i$, SR Ca^{2+} content and SERCA activity as compared the increase in these parameters in rest-period (ZT3) myocytes, with no change in diastolic $[Ca^{2+}]_i$ or NCX. Collins and Rodrigo observed a small increase in LTCC current density in response to ISO in active-period (ZT15) myocytes (Collins and Rodrigo 2010) which does not match with the large in APD that I have shown. However, the small increase in LTCC observed by Collins and Rodrigo may explain the modest increase in systolic $[Ca^{2+}]_i$ and SR Ca^{2+} content observed in active-period (ZT15) myocytes.

It should be noted that although the percentage increase in APD was greatest in active-period (ZT15) myocytes, as basal APD was significantly shorter in active-period (ZT15) myocytes as compared to rest-period (ZT15) myocytes, following the increase in APD in response to ISO no difference in APD existed between the two time points. This was similar to the findings of Collins and Rodrigo, who observed that the increase in LTCC

density in response to ISO was greatest in rest-period (ZT3) myocytes, because LTCC was significantly smaller in rest-period (ZT3) myocytes at basal levels, following ISO perfusion there was no difference in the current density of the LTCC (Collins and Rodrigo 2010). These findings imply that the trigger for CICR is in fact the same in rest-period (ZT3) and active-period (ZT15) myocytes, but due to differences in basal parameters the increase in APD or LTCC differs between the two time points.

This finding of a time-of-day variation in APD in response to ISO is novel and has major implications for research into the regulation of E-C coupling. The majority of investigators will have unwittingly investigated E-C coupling in rest-period (ZT3) myocytes, which have a reduced responsiveness to ISO, as almost all animal housing facilities house animals in rooms similar to our normal-light cycle room (lights on 6-7am) and sacrifice animals in the morning (between 7-11am). This may have led to the assumption that the increase in LTCC following ISO is solely responsible for the prolongation of APD.

In addition to an increase in LTCC, SERCA activity and SR Ca^{2+} content, the amount of Ca^{2+} released from the SR giving rise to the increase in systolic $[Ca^{2+}]_i$ can be influenced by the RyR2. PKA mediated phosphorylation of RyR2 increases P_o and the duration time of opening (Marx, Reiken et al. 2000; Bers 2002) contributing to a greater Ca^{2+} release from the SR. It is possible, although speculative, that there is a greater phosphorylation of RyR2 during the rest-period (ZT3), contributing to the greater increase in systolic $[Ca^{2+}]_i$ observed. However, RyR2 contribution to the time-of-day variation in systolic $[Ca^{2+}]_i$ was not investigated here.

In this investigation I have also observed an increase in the activity of the NCX in response to ISO in rest-period (ZT3), but not active-period (ZT15) myocytes. This was an unexpected finding as Bers amongst others have shown ISO does not modulate NCX activity (Ginsburg and Bers 2005; Lin, Jo et al. 2006). An increase in NCX activity in response to ISO will have compensated for the increase LTCC in response to ISO in the rest-period (ZT3), as during steady-state E-C coupling, Ca^{2+} influx via the LTCC must equal Ca^{2+} efflux via the NCX to maintain stable Ca^{2+} homeostasis (Bers 2002; Eisner, Kashimura et al. 2009). An increase in NCX activity would also increase the competition between the NCX and SERCA for Ca^{2+} removal, and so may have impacted upon SR Ca^{2+} stores, limiting the increase in SR Ca^{2+} stores, however this was not investigated and further work is needed.

The time-of-day variation in response to ISO is reflective of NOS-signalling:

 As both eNOS (Umar and van der Laarse 2010; Zhang and Casadei 2012) and nNOS (Danson, Choate et al. 2005; Schulz, Rassaf et al. 2005; Ziolo, Kohr et al. 2008) have been implicated in the control of contractility in response to β-ADR stimulation, it is possible that the observed time-of-day variation in the response to ISO is in part due to NOS signalling. Indeed, my data shows the reduced response of active-period (ZT15) myocytes to β-ADR stimulation with ISO is abolished following NOS inhibition with L-NNA. NOS inhibition during ISO stimulation significantly increased systolic $[Ca^{2+}]_i$, SR Ca^{2+} content, SERCA and NCX activity in active-period (ZT15) myocytes suggesting NOS signalling is the cause of the time-of-day variation in the response of the Ca^{2+} transient to ISO that I have shown. This is in keeping with the findings of Collins and Rodrigo, who have also shown that the depressed Ca^{2+} transient in active-period (ZT15) myocytes to be the result of enhanced NOS signalling during the active-period (ZT15) time-point (Collins and Rodrigo 2010).

Although my data suggests NOS signalling mediates the time-of-day variation in E-C coupling, I was not able to determine which isoform of NOS was responsible. Research into NO signalling in the myocyte has exploded in the last 15 years since the confirmation of nNOS in the myocardium; however the precise NOS isoform involved in control of contraction in response to β-ADR stimulation is still controversial. As I have concluded that the time-of-day variation in basal and β-ADR E-C coupling is heavily reliant on SR Ca^{2+} content, due to the spatiotemporal restriction of NO it would appear that nNOS is the most likely source of NO affecting the time-of-day a variation I have observed. However, it is possible eNOS is also involved as Collins and Rodrigo have observed a time-of-day variation in the response of the LTCC to ISO stimulation, with the increase in current density blunted in the active-period (ZT15), which may reflect eNOS derived NO control of LTCC. Barouch *et al*. have found an enhancement of the response to ISO in eNOS KO mouse models and inhibition in nNOS KO models (Barouch, Harrison et al. 2002), but in contrast Martin *et al.* demonstrate an enhancement of the ISO response in nNOS KO mouse myocytes and little effect of eNOS KO (Martin, Emanuel et al. 2006). Unfortunately, I was unable to investigate the source of NO (eNOS or nNOS), however other members of our lab have concluded nNOS to be the source of NO implicated in the time-of-day variation in E-C coupling. Use of a NOS1 specific inhibitor (4-AAPNT) increased the

responsiveness of the active-period (ZT15) to levels similar to L-NNA perfusion, and so the authors concluded nNOS to be the culprit (Collins and Rodrigo 2010).

As ISO is a non-specific β-ADR agonist and the β_3-ADR mediates a negative inotropic response on the myocyte though NOS signalling pathways, it is possible that any involvement of NOS in the time-of-day variation is due to β_3-ADR expression or signalling.

3.3.3 The role of the β_3-ADR in the observed time-of-day variation in response to isoproterenol

The non-specific β-ADR agonist ISO stimulates all three β-ADR's; β_1-ADR, β_2-ADR and β_3-ADR (Bers 2002) and therefore the overall inotropic action of ISO is a balance between the positive inotropic action of the β_1-ADR and β_2-ADR stimulation and the negative inotropic action of the β_3-ADR. Activation of β_1-ADR (and the β_2-ADR via PKA local phosphorylation of LTCC) results the positive inotropic and lusitropic response similar to that observed in my study in response to ISO. This response is mediated through PKA phosphorylation of LTCC, RyR2, PLB and TnI, which leads to an increase in the Ca^{2+} transient amplitude, SR Ca^{2+} content and contraction strength (Bers 2001). In opposition to β_1-ADR and β_2-ADR signalling, the β_3-ADR has a negative inotropic effect on contractility through the production of NO (Gauthier, Leblais et al. 1998). NO targets the same E-C coupling proteins as PKA (LTCC, RyR2, PLB) through the cGMP-dependant activation of PKG and cGMP-independent S-nitrosylation mediating a negative effect on E-C coupling, reducing the amplitude of the Ca^{2+} transient, SR Ca^{2+} content and contraction strength (Ziolo 2008; Ziolo, Kohr et al. 2008). The β_3-ADR also brings about a negative inotropic effect through the activation of PDE associated with the breakdown of cAMP, limiting the positive inotropism of β_1-ADR activation (Hare 2003) (which I investigate further in Chapter 5 and 6). Any variation in β_3-ADR signalling or expression may be the cause of the time-of-day variation in systolic $[Ca^{2+}]_i$ I observed between rest-period (ZT3) and active-period (ZT15) myocytes in response to ISO, and so I set out to investigate the effect of β_3-ADR pathway stimulation and determine the existence of any time-of-day variations.

I have shown for the first time a time-of-day variation in the response of ventricular myocytes to specific β_3-ADR stimulation with BRL_{37344}. The data shows the reduction in

systolic $[Ca^{2+}]_i$ and SR Ca^{2+} content in response to BRL_{37344} was larger in rest-period (ZT3) myocytes than active-period (ZT15) myocytes.

Following β_3-ADR stimulation with BRL_{37344} APD was reduced in a similar magnitude in both rest-period (ZT3) and active-period (ZT15) myocytes, and so no time-of-day variation in the response of the action potential to BRL_{37344} was found. This reduction in APD following β_3-ADR stimulation is in support of the finding that BRL_{37344} causes an acceleration of the repolarisation phase of ventricular action potential (Gauthier, Langin et al. 2000). As a result, the action potential is unlikely to have driven the time-of-day variation in systolic $[Ca^{2+}]_i$ in response to β_3-ADR specific stimulation we have observed here.

The increase in SERCA activity and the resulting faster uptake of Ca^{2+} to the SR during relaxation is usually associated with an increased SR Ca^{2+} load (Bers 2002), however in this investigation I observed a reduction in SR Ca^{2+} stores, and so it appears that the majority of the time-of-day variation in the response to BRL_{37344} is due to modulation of SR function.

As mentioned previously, nNOS is co-localised to the SR and so is well placed to affect SR proteins (PLB, SERCA, and RyR2). The BRL_{37344} mediated reduction in relaxation time I have observed in rest-period (ZT3) myocytes is due to an increase in SERCA activity, likely due to a post-translational modification of PLB by NO, either by PKG phosphorylation or S-nitrosylation. nNOS genetic knockout or inhibition has been shown to prolong relaxation (Danson 2005) and reduce the phosphorylation levels of PLB (Wang, Kohr et al. 2008; Zhang, Zhang et al. 2008). This indicates that nNOS can impact upon PLB phosphorylation and increase in SERCA activity, which may explain the reduction in relaxation time I have observed in rest-period (ZT3) myocytes following BRL_{37344} stimulation of β_3-ADR. However, the increase in SERCA activity might have been expected to increase SR Ca^{2+} content in rest-period (ZT3) myocytes; whereas I have observed a negative inotropic effect of BRL_{37344} and a reduction in SR Ca^{2+} stores in rest-period (ZT3) myocytes.

nNOS is has been shown to target RyR2, able to reversibly increase RyR2 P_o (Seddon, Shah et al. 2007). The RyR2 have also been shown to be regulated via S-nitrosylation during nNOS signalling, as nNOS genetic deletion results in reduced S-nitrosylation levels and a reduced P_o, preventing Ca^{2+} leak (Ziolo, Kohr et al. 2008). If RyR2 P_o were to be increased, it could lead to a leak of Ca^{2+} from the SR during relaxation, reducing SR Ca^{2+} content in the face of an increase in SERCA activity. In support of this I found that BRL_{37344} caused an increase in diastolic $[Ca^{2+}]_i$ only in rest-period (ZT3) myocytes, which may be indicative of

SR Ca^{2+} leak. Although this hypothesis requires further investigation and could be confirmed by looking at Ca^{2+} sparks in isolated myocytes.

Although I was unable to further investigate the time-of-day variation in β_3-ADR signalling pathway, I have shown for the first time a variation in the response to specific β_3-ADR stimulation, observed as a greater reduction in systolic $[Ca^{2+}]_i$, SR Ca Ca^{2+} content and relaxation time in rest-period (ZT3) myocytes. However, because the response to β_3-ADR activation was only really seen in rest-period (ZT3) myocytes which have the greatest response to ISO-stimulation, I have concluded that the time-of-day variation in response to ISO cannot be explained by a variation in β_3-ADR activation.

However it should be noted, I have only seen a time-of-day variation in β_3-ADR signalling at baseline, the negative inotropic effect induced on the ventricular myocyte by β_3-ADR stimulation may still act as a brake on sympathetic stimulation during periods of excess β_1-ADR/β_2-ADR stimulation. Stimulation of the β_3-ADR activates the $G_{i\alpha}$ and $G_{i\beta}$ subunits. As discussed above, stimulation of the $G_{i\beta}$ subunit sets off NOS signalling pathways which bring about the negative inotropic effect we have observed though PKG mediated phosphorylation and S-nitrosylation. However the $G_{i\alpha}$ subunit, which has not yet been discussed, is responsible for the activation of PDE3 and PDE4 which facilitate cAMP breakdown, opposing the rise in cAMP during β_1-ADR/β_2-ADR stimulation. At basal levels, such as those I have investigated here, due to the affinity of PDE3 (10-100nM) (Conti, Mika et al. 2014) and PDE4 (2-8μM) (Conti, Mika et al. 2014) for cAMP, it is unlikely baseline levels of cAMP will be affected following β_3-ADR stimulation and so the full negative response of β_3-ADR may not have been observed. During global β-ADR stimulation with ISO, cAMP levels will rise due to β_1-ADR and β_2-ADR stimulation, and so the activity of PDE3 and PDE4 will act to oppose this increase in cAMP, limiting the positive inotropic effect of the β_1-ADR and β_2-ADR. However, I was not able to investigate this action of the β_3-ADR in the ventricular myocyte or examine any time-of-day variation in this signalling pathway due to the previously mentioned problems with our reverse-light animals.

3.3.4 Study Limitations

In this chapter I have shown a time-of-day variation in basal E-C coupling, in response to non-specific β-ADR stimulation and to $β_3$-ADR stimulation. My initial aim was to further investigate the time-of-day variation in $β_3$-ADR signalling, by dissecting the signalling pathway using specific agonists and blockers, however this was not possible given the problems with our reverse-light facilities, and so there are a number of experiments I was unable to complete. Following completion of the data set presented in this chapter, our animal housing facility moved to a brand new facility and the room housing our reverse light cycle (ZT15) animals was found to have inadequate lighting and isolation facilities resulting in significant changes to the circadian physiology of these animals. Although attempts to resolve this were made, due to time constraints I was unable to continue with this path of investigation. Due to these issues, I have had to rely on measurement of LTCC made my previous members of my group in rest-period (ZT3) and active-period (ZT15) myocytes as I was unable to complete this myself. In the next chapter I attempt to set up a serum-shock tissue culture protocol with isolated ventricular myocytes, in an effort to enable functional recordings from myocytes during other time points of the circadian cycle of the rat myocyte. An intrinsic limitation of our study is that our model has used isolated ventricular myocytes to infer the action at the whole heart. As mentioned previously, during the isolation process the myocardium is subject to fluctuations in temperature and $[Ca^{2+}]_i$, brief periods of ischemia and serum starvation, all of which may affect E-C coupling, Ca^{2+} handling and AP configuration in the isolated myocyte.

Chapter 4: The intrinsic circadian clock.

4.1   Introduction

In the cardiovascular system there are marked time-of-day variations in a number of cardiovascular parameters, including HR, QT interval and contractility. In mammals, these oscillations are controlled by the circadian clock. The circadian clock is "a transcriptional based molecular system with a free running period of 24 hours" (Bass and Takahashi 2010). The central circadian clock is expressed in the pacemaker neurons of the SCN, which maintain the alignment of peripheral clocks, which are expressed in almost every cell of the body (Dibner, Schibler et al. 2010; Albrecht 2012; Mohawk, Green et al. 2012).

The existence of an intrinsic circadian clock within myocytes is well documented (Young, Razeghi et al. 2001; Young, Razeghi et al. 2001; Young 2003) and investigation of hearts collected from rodents under diurnal (light/dark) and circadian conditions (constant dim light) has led to the suggestion that approximately 10-15% cardiac genes oscillate in a time-of-day manner, encoding for proteins involved in cell signalling, protein synthesis, transcriptional regulation and mitochondrial function (Storch, Lipan et al. 2002; Martino, Arab et al. 2004). The observed time-of-day variation in cardiac gene expression could be mediated by extracellular influences e.g. neurohumoural factors, such as sympathetic stimulation, endocrine factors (e.g. cortisol and insulin) and nutrients (e.g. glucose an lipids), or by intracellular influences e.g. the cycling of the intrinsic clock of the myocytes (Martino and Young 2015). In order to determine the contribution of the intrinsic clock to oscillations in cardiovascular parameters a number of mouse models with disrupted clock components have been developed, for example the myocyte-specific CLOCK mutant (CCM) (Durgan, Trexler et al. 2006) and the myocyte-specific BMAL1 KO (CBK) (Durgan, Tsai et al. 2011). Comparison between WT littermates and these disrupted clock mouse models allows investigation of the influence of the intrinsic clock in the cardiovascular system. An alternative method which has been used previously (Balsalobre, Damiola et al. 1998; Durgan, Hotze et al. 2005) is to place isolated cells into tissue culture, thereby removing all neurohumoural influences from the cell, leaving only the intrinsic circadian clock to drive changes in gene expression and ultimately cardiac function in these cells. Durgan *et al.* have demonstrated the intrinsic clock in myocytes can be 'paused' by cell isolation and can be 'restarted/resynchronised' by both a 'serum shock' and a 'norepinephrine shock' (Durgan, Hotze et al. 2005).

In the previous chapter, I have shown this intrinsic clock within the myocyte is 'paused' following isolation and so I set out to determine whether this was due to irreversible impairment of the circadian clock or if the clock could be 'restarted/resynchronised' in my cells. If the intrinsic clock was functioning in adult rat ventricular myocytes (ARVMs) and I was able to restart/resynchronise the clock, I also determined whether the intrinsic clock would influence functional genes. If the circadian clock were able to be restarted in my cell culture model and effectively impact upon functional gene expression it would be possible to reduce the number of animals used in my investigation, which is in keeping with the principles of the 3R's. To complete a full circadian profile, investigators are required to sample animals in 3 hour intervals over a 24 hour period and so large numbers of animals are required; Young *et al.* required 108 animals in their seminal study (Young, Razeghi et al. 2001). A successful cell culture model of circadian variation would also enable the ability to use siRNA techniques to examine the role of various component output genes (e.g. nNOS, eNOS and β-ADR) in the time-of-day variations I have observed. The model could also be extended to look at other CV tissues, such as vascular smooth muscle, endothelial and cardiac fibroblasts which have been shown to exhibit time-of-day variations in their expression and function.

4.2   Results

4.2.1 The cycling of the intrinsic clock in cultured adult ventricular rat myocytes

It has previously been shown by Durgan *et al.*, and indeed in data presented in Chapter 3, that isolation of single myocytes and the storage/culture of these myocytes in the absence of FBS results in sustained dampening of circadian clock cycling (Durgan, Hotze et al. 2005). In effect, the cycling of the intrinsic clock within the myocyte is stopped. Therefore in order to study circadian cycling of clock and β-ADR genes in ARVM isolated during the rats rest-period (ZT3), myocytes were placed into tissue culture and subject to a serum-shock protocol, which has previously been shown to reactivate circadian clock genes in cultured rat-1 fibroblasts (Balsalobre, Damiola et al. 1998) and isolated myocytes (Durgan, Hotze et al. 2005). In summary, ARVM were 'serum-starved' (0% FBS) prior to treatment, following which ARVM underwent a 'serum-shock' (50% FBS). ARVMs were then sampled at 3 hour intervals and processed for PCR. Control ARVMs were also 'serum-starved' prior to treatment, however these cells did not undergo a serum shock, instead control ARVMs were washed twice and incubated with 0% FBS and again sampled at sampled at 3 hour intervals and processed for PCR (See Methods 2.5 for further details).

To determine the ability of a serum-shock to 'restart' or 'resynchronise' the intrinsic circadian clock in isolated ARVMs I examined variation in mRNA levels of three key circadian clock genes and functional β-adrenergic and NOS genes, following serum-shock in ARVM isolated from rest-period (ZT3) hearts.

Samples of both control and serum-shocked ARVM were taken prior to challenge wash (T0), immediately following the challenge wash (T2), and thereafter at 3 hour intervals post-challenge wash for a 12 hour period (T5, T8, T11 and T14) (See Methods 2.5 for further details). Quantitative real-time TaqMan RT-PCR was then performed on AVM samples, using β-actin as the housekeeping gene, to determine the CT value of samples (See appendix 4 for details of β-actin expression levels).

Gene fold-change was calculated from the CT value of samples, using the $2^{-\Delta\Delta CT}$ method and the sample taken from ARVM at baseline (T0) (prior to challenge wash) was used as the reference sample for control and sample shocked myocytes respectively, the calibrator to which all further control and serum-shocked samples were compared.

Statistics were performed on ΔCT values and the sample taken from ARVM at baseline (T0) (prior to challenge wash) was used as the reference sample for control and sample shocked myocytes respectively, the calibrator to which all further control and serum-shocked samples were compared, to determine the cycling of circadian clock genes in ARVM.

4.2.1.1 Cycling of Circadian clock genes

To determine the ability of a serum-shock to 'restart' or 'resynchronise' the intrinsic circadian clock in isolated ARVMs I examined variation in mRNA levels of four key circadian clock genes; *clock*, *per2*, *bmal1* and *rev-erbα* following serum-shock in ARVM isolated from rest-period (ZT3) hearts. The genes I have investigated here are some of the core components of the circadian clock.

Gene expression fold change of circadian clock genes in control and serum-shocked ARVM are shown in figures 4.1A *clock*, 4.2A *per2*, 4.3A *bmal*1 and 4.4A *rev-erbα*.

The data shows that cycling of *clock* gene (Table 4.1B), *per2* gene (Table 4.2B) or *rev-erbα* was not observed in either control cells or serum-shock cells.

Bmal1 gene expression did not show evidence of cycling in control cells (Table 4.3B), however did exhibit evidence of cycling following serum-shock, increasing in expression. Gene-expression was significantly greater 14 hours post serum shock (4.66 $\pm$ 0.19 ($p<0.05$)) (Table 4.3B), peaking at T14, which corresponded to a 2.84 fold-change as compared to baseline (Figure 4.3A).

A.
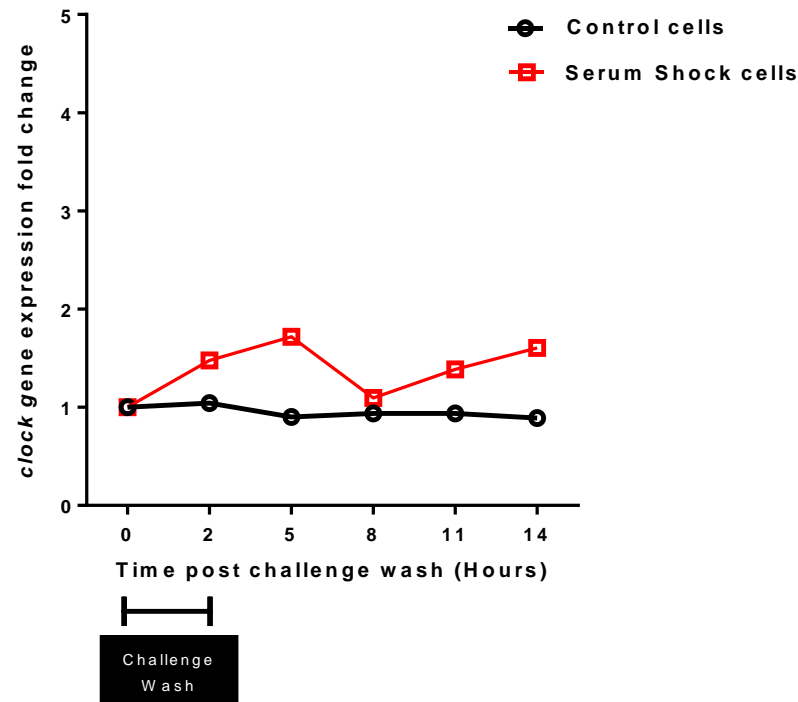
B.

Gene of interest *clock*	ΔCT (normalised to β-actin)					
	T0 hours	**T2 hours**	**T5 hours**	**T8 hours**	**T11 hours**	**T14 hours**
Control AVM	4.63 ± 0.13	4.09 ± 0.35	3.97 ± 0.10	4.60 ± 0.57	4.28 ± 0.62	4.22 ± 0.39
Serum Shock ARVM	3.86 ± 0.14	3.80 ± 0.13	4.01 ± 0.20	3.95 ± 0.13	3.95 ± 0.12	4.02 ± 0.16

Figure 4.1 **Gene expression levels of the circadian *clock* gene clock in control and serum shocked adult rat ventricular myocytes.**

A. Bar chart showing fold-change in the expression of *clock* in control and serum shocked myocytes, post challenge wash (T0) and for 12 hours following, sampled in 3 hour increments (T2, T5, T8, T11, T14). *clock* mRNA values were normalised to β-actin mRNA values. Fold-change was calculated as -2^CT for control ARVM (black) and serum shocked ARVM (red) relative to their respective T0 hour value.

B. Table showing data used to produce the bar chart in figure 4.1A. Number of samples; control ARVM, n=3, serum shock ARVM, n=5; one-way ANOVA, sidak's *post-hoc* test performed on ΔCT values. To determine cycling of Clock expression, statistical difference was calculated for control and serum shocked ARVM relative to their respective T0 hour value.

155

A.
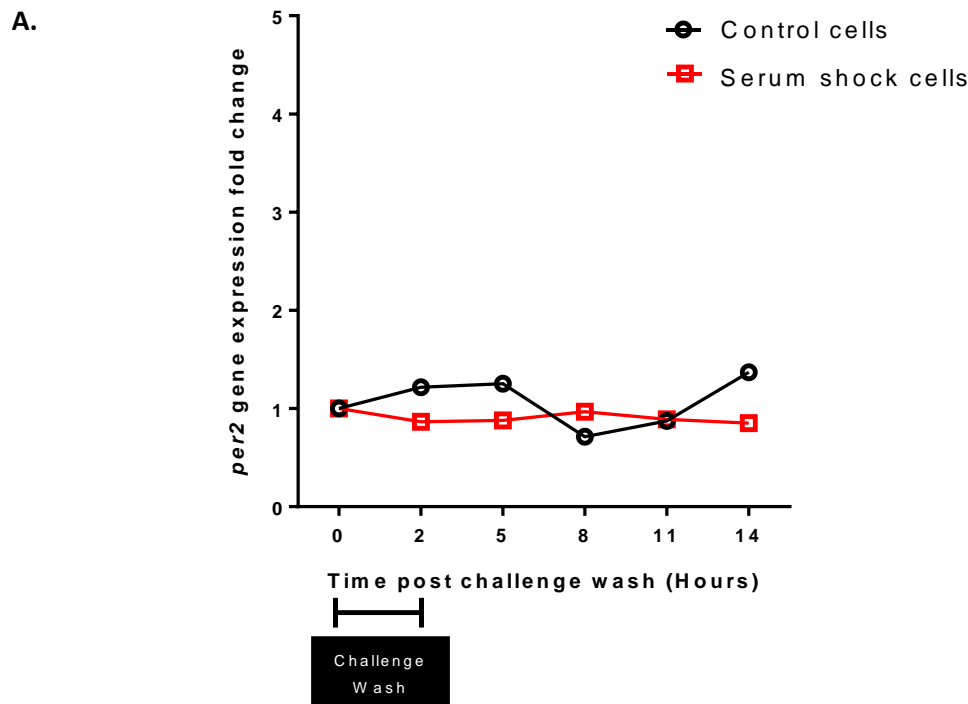
B.

Gene of interest *per2*	ΔCT (normalised to β-actin)					
	T0 hours	**T2 hours**	**T5 hours**	**T8 hours**	**T11 hours**	**T14 hours**
Control AVM	9.20 ± 0.71	9.49 ± 0.27	8.96 ± 0.74	10.56 ± 0.14	9.50 ± 0.51	8.84 ± 0.30
Serum Shock ARVM	8.12 ± 0.20	8.20 ± 0.39	8.45 ± 0.20	8.17 ± 0.37	8.17 ± 0.39	8.23 ± 0.69

Figure 4.2   Gene expression levels of the circadian clock gene *per2* in control and serum shocked adult rat ventricular myocytes.

A.   Bar chart showing fold-change in the expression of *per2* in control and serum shocked myocytes, post challenge wash (T0) and for 12 hours following, sampled in 3 hour increments (T2, T5, T8, T11, T14). *per2* mRNA values were normalised to β-actin mRNA values. Fold-change was calculated as -2^CT for control ARVM (black) and serum shocked ARVM (red) relative to their respective T0 hour value..

B.   Table showing data used to produce the bar chart in figure 4.2A. Number of samples; control ARVM, n=3, serum shock ARVM, n=5; one-way ANOVA, sidak's *post-hoc* test performed on ΔCT values. To determine cycling of Per2 expression, statistical difference was calculated for control and serum shocked ARVM relative to their respective T0 hour value.

A.

B.

Gene of interest *bmal1*	ΔCT (normalised to β-actin)					
	T0 hours	**T2 hours**	**T5 hours**	**T8 hours**	**T11 hours**	**T14 hours**
Control AVM	6.29 ± 0.57	6.01 ± 0.53	5.69 ± 0.45	6.53 ± 0.62	5.80 ± 0.66	5.86 ± 0.40
Serum Shock ARVM	5.96 ± 0.40	5.47 ± 0.15	5.28 ± 0.27	5.25 ± 0.38	5.01 ± 0.25	4.66 ± 0.21 *

Figure 4.3   Gene expression levels of the circadian clock gene *bmal1* in control and serum shocked adult rat ventricular myocytes.

A. Bar chart showing fold-change in the expression of *bmal1* in control and serum shocked myocytes, post challenge wash (T0) and for 12 hours following, sampled in 3 hour increments (T2, T5, T8, T11, T14). *bmal1* mRNA values were normalised to β-actin mRNA values. Fold-change was calculated as -2^CT for control ARVM (black) and serum shocked ARVM (red) relative to their respective T0 hour value..

B. Table showing data used to produce the bar chart in figure 4.3A. Number of samples; control ARVM, n=3, serum shock ARVM, n=5; one-way ANOVA, sidak's *post-hoc* test performed on ΔCT values. To determine cycling of Bmal1 expression, statistical difference was calculated for control and serum shocked ARVM relative to their respective T0 hour value; $*P<0.05$.
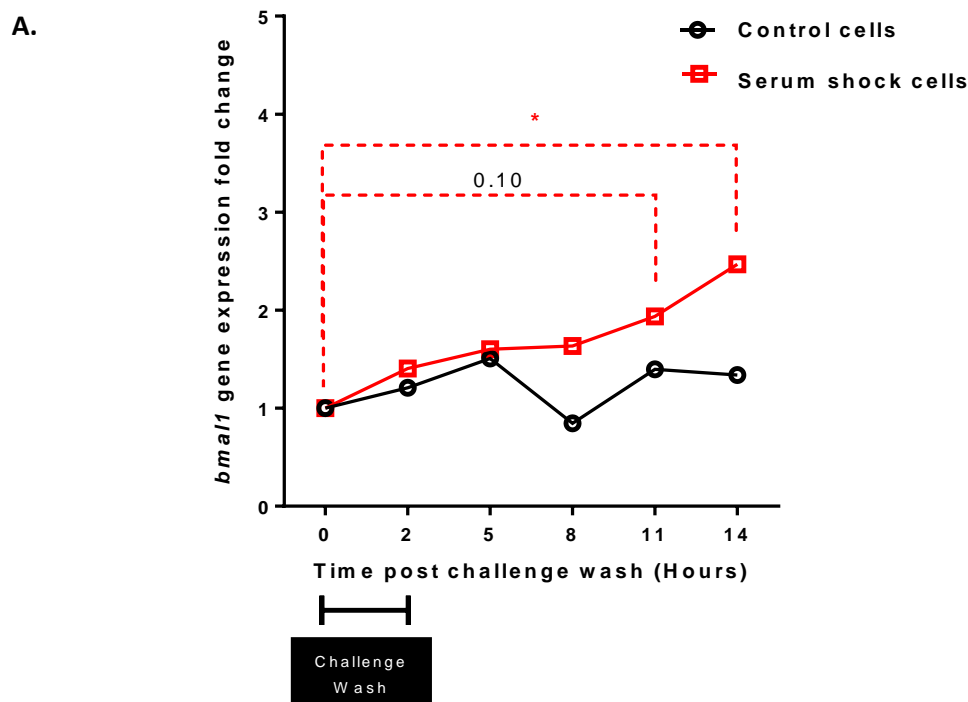
A.
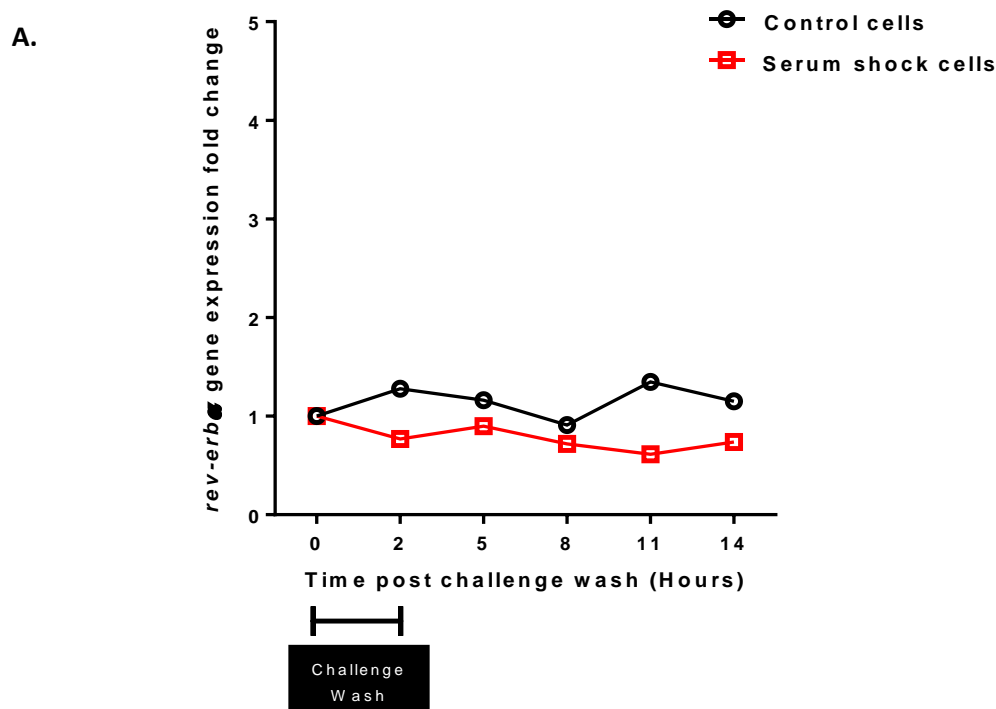
B.

Gene of interest *rev-erbα*	ΔCT (normalised to β-actin)					
	T0 hours	**T2 hours**	**T5 hours**	**T8 hours**	**T11 hours**	**T14 hours**
Control AVM	4.43 ± 0.29	4.74 ± 0.12	5.12 ± 0.10	4.89 ± 0.22	5.22 ± 0.29	5.45 ± 0.34
Serum Shock ARVM	5.31 ± 0.45	4.96 ± 0.61	5.10 ± 0.71	5.45 ± 0.74	4.88 ± 0.95	5.11 ± 0.69

Figure 4.4   Gene expression levels of the gene *rev-erbα* in control and serum shocked adult rat ventricular myocytes.

A.   Bar chart showing fold-change in the expression of *rev-erbα* in control and serum shocked myocytes, post challenge wash (T0) and for 12 hours following, sampled in 3 hour increments (T2, T5, T8, T11, T14). *rev-erbα* mRNA values were normalised to β-actin mRNA values. Fold-change was calculated as $-2^{\wedge}CT$ for control ARVM (black) and serum shocked ARVM (red) relative to their respective T0 hour value..

B.   Table showing data used to produce the bar chart in figure 4.4A. Number of samples; control ARVM, n=3, serum shock ARVM, n=5; one-way ANOVA, sidak's *post-hoc* test performed on ΔCT values. To determine cycling of Rev-erbα expression, statistical difference was calculated for control and serum shocked ARVM relative to their respective T0 hour value.

4.1.1.2 Circadian cycling of functional β-adrenergic and NOS genes

The expression of functional genes associated with control of cardiac cell function in response to sympathetic stimulation; β_1-ADR, β_3-ADR, NOS1 and NOS3, have previously been shown by members of our lab to differ significantly between rest-period and active-period hearts (Collins and Rodrigo 2010) and in vascular tissue (Denniff, Turrell et al. 2014), and so I examined variation in mRNA levels of β_1-ADR, β_3-ADR, NOS1 and NOS3, in the same samples.

Gene expression fold change of β-ADR and NOS genes in control and serum-shocked ARVM are shown in figures 4.5A *Adrb1* (β_1-ADR) and 4.6A *NOS3*.

The data shows that that cycling of *Adrb1* (β_1-ADR) gene expression was not observed in either control cells or serum-shock cells (Table 4.5B).

NOS3 gene expression did not show evidence of cycling in control cells (See Table 4.6B), however *NOS3* gene expression showed evidence of cycling following serum-shock, peaking at T2 (3.30 ± 0.15 (p=0.08)), with a trough at T11 (4.32 ± 0.30 (p=0.11)), which corresponded to a 0.70 fold-change as compared to pre-serum-shock (Figure 4.5A).

NOS1 and *Adrb3* (β_3-ADR) gene expression could not be reliably detected in either control or serum-shocked ARVM.

A.
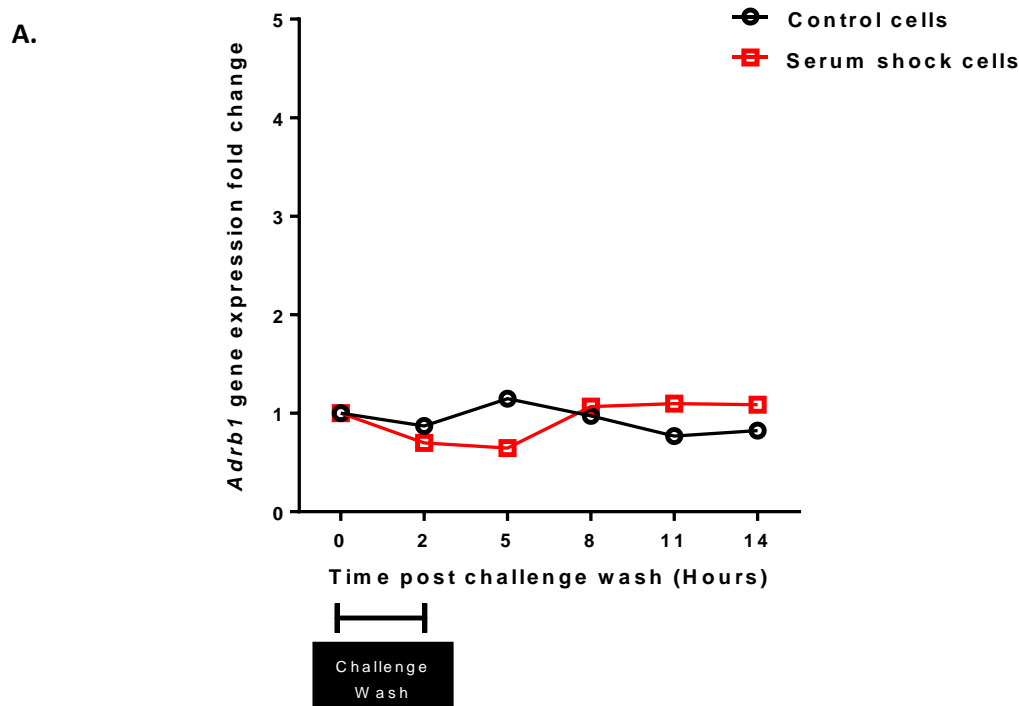
Gene of interest *Adrb1*	ΔCT (normalised to β-actin)					
	T0 hours	**T2 hours**	**T5 hours**	**T8 hours**	**T11 hours**	**T14 hours**
Control AVM	6.12 ± 0.38	6.32 ± 0.26	5.92 ± 0.25	6.16 ± 0.15	6.50 ± 0.02	6.40 ± 0.00
Serum Shock ARVM	6.03 ± 0.18	6.36 ± 0.60	6.54 ± 0.22	5.83 ± 0.46	6.29 ± 0.03	6.38 ± 0.70

Figure 4.5 **Gene expression levels of the gene *Adrb1* in control and serum shocked adult rat ventricular myocytes.**

A. Bar chart showing fold-change in the expression of *Adrb1* in control and serum shocked myocytes, post challenge wash (T0) and for 12 hours following, sampled in 3 hour increments (T2, T5, T8, T11, T14). *Adrb1* mRNA values were normalised to β-actin mRNA values. Fold-change was calculated as -2^CT for control ARVM (black) and serum shocked ARVM (red) relative to their respective T0 hour value..

B. Table showing data used to produce the bar chart in figure 4.5A. Number of samples; control ARVM, n=3, serum shock ARVM, n=5; one-way ANOVA, sidak's *post-hoc* test performed on ΔCT values. To determine cycling of Adrb1 expression, statistical difference was calculated for control and serum shocked ARVM relative to their respective T0 hour value.

A.

B.

Gene of interest *NOS3*	ΔCT (normalised to β-actin)					
	T0 hours	T2 hours	T5 hours	T8 hours	T11 hours	T14 hours
Control AVM	4.43 ± 0.29	3.85 ± 0.14	4.14 ± 0.31	4.50 ± 0.25	4.36 ± 0.17	4.20 ± 0.11
Serum Shock ARVM	3.60 ± 0.15	3.30 ± 0.10	3.35 ± 0.32	4.05 ± 0.27	4.32 ± 0.30	4.17 ± 0.31

Figure 4.6   Gene expression levels of the gene *NOS3* in control and serum shocked adult rat ventricular myocytes.

A.   Bar chart showing fold-change in the expression of *NOS3* in control and serum shocked myocytes, post challenge wash (T0) and for 12 hours following, sampled in 3 hour increments (T2, T5, T8, T11, T14). *NOS3* mRNA values were normalised to β-actin mRNA values. Fold-change was calculated as -2^CT for control ARVM (black) and serum shocked ARVM (red) relative to their respective T0 hour value..

B.   Table showing data used to produce the bar chart in figure 4.6A. Number of samples; control ARVM, n=3, serum shock ARVM, n=5; one-way ANOVA, sidak's *post-hoc* test performed on ΔCT values. To determine cycling of Nos3 expression, statistical difference was calculated for control and serum shocked ARVM relative to their respective T0 hour value.
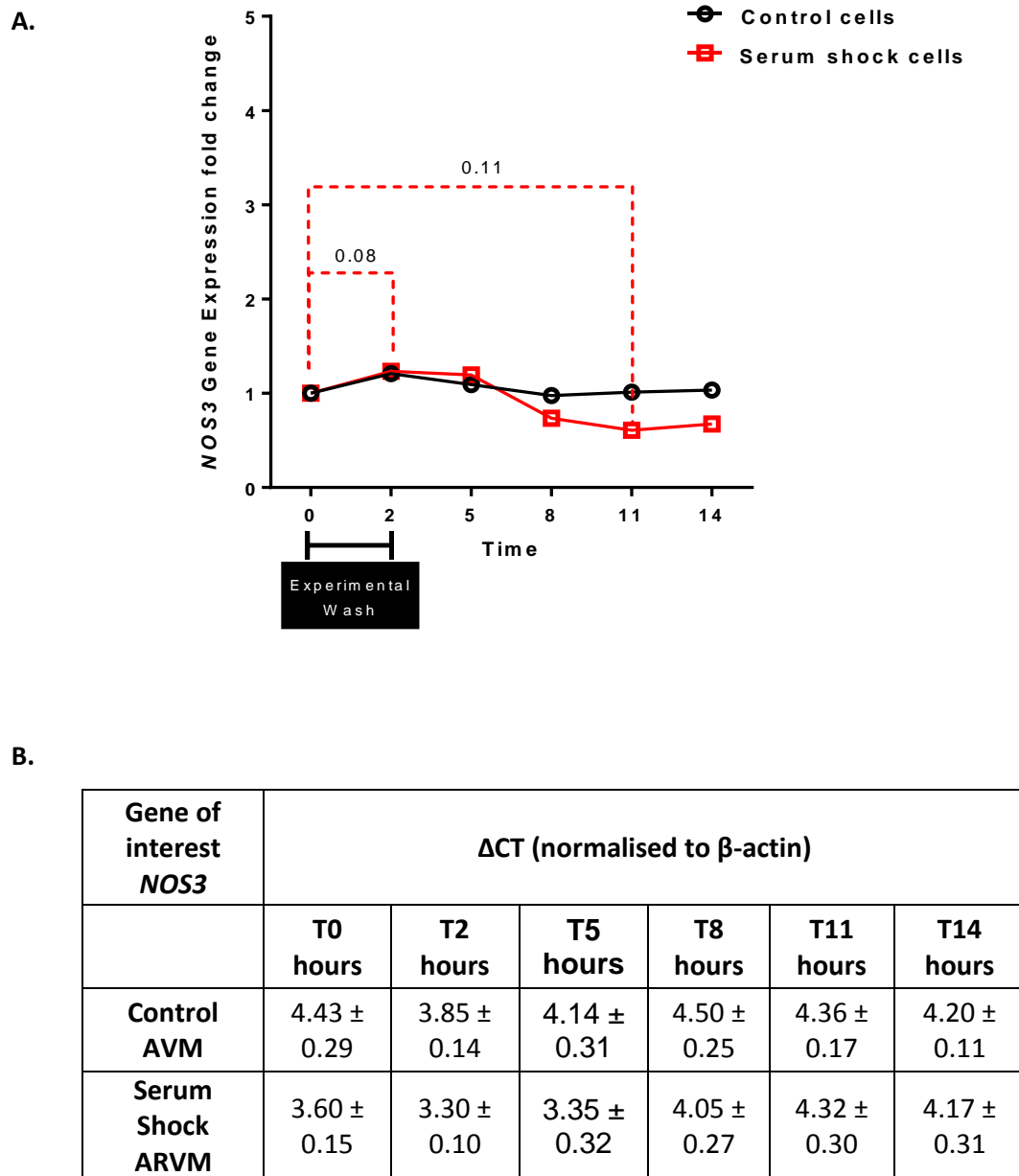
161

4.3   Discussion

In the present chapter I have investigated the intrinsic clock in the isolated ARVM using a 'serum-shock' protocol, with a view of using this as cellular model to study the impact of the circadian clock on E-C coupling in ARVMs. I have shown no evidence of gene expression cycling of circadian clock genes *clock, per2* or *rev-erbα*, but a significant cycling in the gene expression of *bmal1*. Gene expression of *bmal1* increased following serum-shock with a 2.8 fold increase from basal levels.

Investigation of the functional β-ADR and NOS genes showed no evidence of cycling in gene expression of β_1-ADR (*Adrb1*), but a possible cycling of *NOS3* gene expression, however this was not significant. *NOS3* gene expression peaked at 2 hours post serum-shock, with a trough at 11 hours post serum-shock, however this was not significant. Unfortunately *NOS1* and β_3-ADR (*Adrb3*) gene expression in the ARVM could not be determined and so the cycling of these genes could not be assessed.

4.3.1   The Circadian clock genes

Young *et al.* were the first to characterise the existence of circadian clock genes in the intact rat heart, and have since characterised the oscillations in gene expression of the components of the circadian clock in the intact heart (Young, Razeghi et al. 2001) and isolated myocytes (Durgan, Hotze et al. 2005).

The CLOCK:BMAL1 heterodimer induces the expression of a number of target genes, including *per2* and *rev-erbα*. In turn both *per2* and *rev-erbα* output proteins PER2 and REV-ERBα provide feedback loops to the *clock*:*bmal1* heterodimer. PER2 enhances *bmal1* transcription, providing a positive feedback loop for *bmal1* expression, whereas REV-ERBα represses *bmal1* transcription, providing a negative feedback loop for *bmal1* expression. A further feedback loop which I have not examined here are the *per1*, *per3*, *cry1* and *cry2* target genes, the protein products of which repress the CLOCK:BMAL1 heterodimer. The oscillation of the *clock* and *bmal1* gene expression anti-phase to the *per, cry* and *rev-erbα* genes are the drivers of the circadian clock.

In the present investigation I have investigated the cycling of the components of the intrinsic circadian clock in isolated ARVM which have undergone a 'serum-shock' protocol, which has previously been shown to restart/resynchronise the circadian clock in isolated myocytes under tissue culture conditions (Durgan, Hotze et al. 2005) in an attempt to study the impact of the intrinsic clock on the expression of functional genes in the myocyte. My data does not suggest successful restarting/resynchronisation of the intrinsic circadian clock in this ARVM model.

Durgan *et al.* conducted a similar investigation and were able to demonstrate that a serum-shock protocol induced significant oscillations in all of the clock components they investigated; *bmal1*, *per2* and *rev-erbα*. *Bmal1* expression peaked at 8 hours post serum-shock with a trough at 20 hours post serum-shock, and as expected the regulatory transcription factors of *bmal1, per2* and *rev-erbα* cycled anti-phase to *bmal1*, peaking at 16 hours and 12 hours post serum-shock respectively (Durgan, Hotze et al. 2005). Although Durgan *et al.* did not investigate the cycling of *clock* gene expression in serum-shocked myocytes, Young *et al.* have shown previously that in the intact heart the cycling of *clock* follows that of *bmal1* (Young, Razeghi et al. 2001), and so it would have been expected that *clock* gene expression followed a similar cycling pattern to that of *bmal1*, however this was not found in my investigation. My data show that the oscillation of *bmal1* following a serum-shock peaked at 14 hours post serum-shock and follows a similar pattern as that shown by Durgan *et al.* in which *bmal1* expression rose following serum-shock peaking at 8 hours post serum-shock, followed by a decline in expression to its trough at 20 hours post-isolation (Durgan, Hotze et al. 2005). Unfortunately, because I were unable to complete a 24 hour cycle I are unable to determine whether this rise in *bmal1* was the peak of a cycle in a circadian rhythm of expression similar to that found by Durgan *et al.*, or whether this was an exponential rise in *bmal1* gene expression.

Per2 and *rev-erbα* provide a positive and a negative feedback loop for *bmal1* transcription, controlling the expression of *bmal1*. In this investigation I found no cycling of *per2* and *rev-erbα* gene expression following a serum-shock, which was in contrast to the study by Durgan *et al.* in which, *per2* and *rev-erbα* gene expression was found to cycle anti-phase to *bmal1*; *per2* displaying a trough in expression at 8 hours and peaking at 16 hours post serum-shock , *rev-erbα* displaying a trough at 2 hours and a peak at 12 hours post serum-shock (Durgan, Hotze et al. 2005). As I was only able to look at the post serum-shock phase

for 14 hours rather than the 36 Durgan *et al.* completed, it is possible that I missed the timing of the peak gene expression of *per2* and *rev-erbα*. Nonetheless, during the 14 hour post shock period I observed, significant oscillation in the gene expression of these transcription factors should have been seen if the circadian clock were successfully restarted/resynchronised. As the *per2* and *rev-erbα* are part of the transcriptional feedback loops of bmal1 gene expression, the lack of cycling of *per2* and *rev-erbα* gene expression will mean that *bmal1* gene transcription go unregulated, and may account for the apparent exponential rise in *bmal1* gene expression I have observed.

Clock and *bmal1* are the core transcriptional factors of the central and peripheral clocks, their heterodimerisation is the activators of the circadian clock and in the intact heart the cycling of *clock* follows that of *bmal1*. The lack of cycling of *clock* gene expression in sequence with fluctuations in *Bmal1* gene expression implies that the circadian clock within the ARVM has not been successfully resynchronised in this investigation.

4.3.2   The functional β-adrenergic and NOS genes

I had hoped to use the serum-shock protocol to look at the role of the circadian clock in the time-of-day variation in functional genes responsible for the time-of-day variation I and members of the group have previously observed. By placing isolated myocytes into tissue culture and restarting the endogenous clock, the neurohumoural influences which may be regulating gene expression are removed, and so only the intrinsic circadian clock within the myocyte is able to drive changes in gene expression.

The first cardiac myocyte clock controlled genes were identified 10 years ago by Durgan *et al.* who discovered the expression of the fatty acid-responsive genes *pdk4* and *upc3* oscillated in serum shocked myocytes in a similar manner to the cycling of these genes in the intact heart *in vivo* (Durgan, Hotze et al. 2005). The circadian clock is able to influence gene expression in two ways; the clock itself is a transcriptional modulator, which has the potential to modulate the expression of target genes by itself, but the clock also regulates the expression of a number of transcription factors, for example the PAR family of transcription factors, which influence the gene expression of a number of target genes (See Introduction 1.3).

Although I was unable to show that the circadian clock in my serum-shocked ARVM had been resynchronised due to the lack of cycling of the core clock component *clock* and the regulatory transcription factors *per2* and *rev-erbα*, I did observe oscillations in the *NOS3* gene expression during the post serum-shock period, peaking at 2 hours post serum-shock, with a trough at 11 hours post serum-shock. However, there were no fluctuations in $β_1$-*ADR* gene expression during the 12 hour post serum-shock period and *NOS1* and $β_3$-*ADR* gene expression in the ARVM could not be determined.

The lack of $β_1$-*ADR* gene expression cycling was not as expected, as a number of groups have previously described a time-of-day variation $β_1$-*ADR* gene expression and in the sensitivity of the myocardium to β-ADR stimulation. Bray *et al.* have demonstrated a time-of-day variation in the response to β-ADR stimulation, with an enhanced responsiveness to epinephrine in the active-period as compared to the rest-period in WT mice, which was abolished in CCM mice (Bray, Shaw et al. 2008), suggesting co-ordinated circadian clock cycling is responsible for the time-of-day variation in the response to epinephrine, and possibly due to enhanced expression of β-ADR. Witte *et al.* have previously compared $β_1$-ADR gene expression in the rat ventricle and have shown $β_1$-*ADR* gene expression to exhibit a 24 hour rhythm, with a peak at the middle of the rest-period followed by a second peak at the middle of the active-period (Witte, Parsa-Parsi et al. 1995). Indeed, work by previous members of our group has identified a time-of-day variation in $β_1$-ADR gene expression, finding $β_1$-*ADR* gene expression to be 2.4 fold higher in rat left ventricular tissue during the active-period as compared to the rest-period (Collins and Rodrigo 2010). Therefore, my finding of a lack of fluctuation of gene expression over the 12 hours post serum-shock is not what would be expected if the intrinsic circadian clock within my ARVM were functioning and controlling the expression of the β-ADR. However, the data reported above detailing the cycling of expression of the $β_1$-*ADR* gene has been shown in the intact heart or left ventricular tissue, not in isolated myocytes, and it may be that during the isolation process the intrinsic circadian clock control of *β-ADR* gene expression may have been irreversibly impaired.

To date, no investigation of the β-ADR in response to serum-shock in isolated ARVM has been completed. It may be possible that the intrinsic circadian clock is not the driver of reported time-of-day oscillations in the response to β-ADR and $β_1$-*ADR* gene expression, but neurohumoural influences such as sympathetic activity or circulating catecholamines

which drive the changes in β_1-ADR gene expression, which is missing from the serum shock model.

I have observed in this investigation an oscillation in NOS3/eNOS gene expression, peaking at 2 hours post serum-shock with a trough at 11 hours post serum-shock, with p-values approaching significance. To date, eNOS gene expression has not been investigated in serum-shocked ARVM, although members of our group found no time-of-day variation in eNOS gene expression between rest-period and active-period in left ventricular tissue (Collins and Rodrigo 2010). However, in the left ventricular tissue eNOS expression in the endothelium and endocardium may have contributed to total eNOS expression levels, and so may be masking any time-of-day variation in eNOS gene expression. Members of our group have also investigated the cycling of eNOS in mesentery resistance arteries, and have shown a strong time-of-day variation of eNOS gene expression, with a 3.3 fold increased in endothelial eNOS mRNA in the active-period as compared to the rest-period, which translated to a 1.7 fold increase in eNOS protein in the active-period (Denniff, Turrell et al. 2014).

In the present investigation I was unable to successfully determine nNOS and β_3-ADR gene expression in the ARVM in either control or serum-shocked cells. In both cases I had significant technical issues as I was unable to reliably produce standard curves for the probes at standard concentrations of cDNA (See Methods 2.6) and nNOS and β_3-ADR gene expression was undetectable at 80ng cDNA. Problems with the TaqMan probes were ruled out as I was able to successfully complete standard curves with these probes in mesenteric arteries (data not shown). Problems with my cDNA was also ruled out as the *housekeeping gene* β-actin was amplifiable within the normal range (CT value24-25) and also the cDNA obtained from control and serum-shocked ARVM was used to determine the expression of all circadian clock and functional genes. I therefore suggest the low abundance of these genes in my samples were the cause of the failure of the nNOS and β_3-ADR probes to amplify mRNA in these samples.

The failure to detect nNOS and β_3-ADR in my samples was surprising as previous members of our group were able to detect nNOS and β_3-ADR in the intact heart. A significant time-of-day variation in nNOS expression was found in left ventricular tissue samples, all be it at lower levels than eNOS gene expression (nNOS CT values = ~29-30, eNOS CT value ~24-25).

To rule out the contribution of nNOS expressed in fibroblasts or nerve fibres, nNOS gene expression was also determined in isolated myocytes and the time-of-day variation remained (Collins and Rodrigo 2010). In their investigation, Collins and Rodrigo isolated myocytes from rest-period and active-period animals and immediately processed these samples for PCR, however my samples were processed for tissue culture and were processed for PCR ~24-36 hours post isolation and it may be that there was some degradation in my samples during this time which affected expression levels of nNOS and β_3-ADR making them undetectable in my samples. Kits used for RNA extraction were also different from the kit used by Collins and Rodrigo and this may have affected the quantity of RNA in my original samples. Collins and Rodrigo were also able to detect β_3-ADR mRNA and observed no time-of-day variation in β_3-ADR in left ventricular tissue samples. The expression of β_3-ADR is known to be low in the rat heart (Evans, Papaioannou et al. 1996) and in the investigation by Collins and Rodrigo 400ng cDNA per sample was required in order to detect β_3-ADR mRNA in left ventricular tissue, and so it is not surprising I was unable to detect β_3-ADR mRNA in my samples using 80ng cDNA. To overcome this problem I could have begun the experiment with greater numbers of cardiomyocytes for RNA extraction by pooling lysed samples, which may have required greater numbers of hearts for isolation, which may have somewhat defeated the object of this model to investigate circadian variation in gene expression.

Other groups have shown a circadian variation in β_3-ADR gene expression in left ventricular tissue samples of Wistar rats, with peak expression at 12:00 hours (mid-point of the rest-period of the nocturnal rat) and the trough at 24:00 (mid-point of the active-period), which is abolished following an MI injury (Zhou, Zhang et al. 2011). However, in both of these studies the samples were taken from left ventricular wall and not isolated myocytes and so the quantity of the starting mRNA is bound to be greater than that of the ARVM samples I was able to use in my investigation.

4.3.3 Conclusions

My aim was to set up a tissue culture model to investigate time-of-day variation in E-C coupling without the need for rest-period and active-period rat populations, minimising the requirement for animals, which is in keeping with the principles of the 3R's. However, I

was not able to reliably restart/resynchronise the circadian clock within the myocytes which is required to drive time-of-day changes in functional gene expression, and so I conclude that in my hands, the serum-shock protocol used in this investigation is not a reliable model to investigate time-of-day variation in E-C coupling.

4.3.4   Study Limitations

The data presented in the current chapter is from the provisional experiments of serum-shock I have completed. The serum-shock protocol is time-consuming and can be expensive due to the need to maintain ARVM in cell culture and the cost of RNA extraction and subsequent PCR. Initially I followed the post serum-shock period for 12 hours following the 2 hour challenge wash to determine whether the serum-shock protocol was successful, but in hindsight this data does not represent a complete circadian profile, and so it would have been preferable to complete this investigation again, following a 24 hour post serum-shock period. However, due to time and cost constraints I was unable to complete this.

If I were to complete this investigation again, I would also make changes to the post-challenge wash media, changing to 2.5% FBS media instead of 0% FBS media, as Durgan *et al.* have shown that 50% FBS serum shock and 0% FBS post-challenge media induces cycling of the circadian clock which diminishes after one full cycle (20-24 hours post serum-shock), however if the post-challenge wash contained 2.5% FBS, the cycling of the circadian clock components continued for >60 hours, all be it at a dampened magnitude. It is possible that the lack of cycling in this investigation of the *clock*, *per2* and *rev-erbα* circadian clock genes was impaired post-serum shock due to the lack of FBS in the post-challenge media, as this is effectively serum-starving the ARVM for a second time.

Chapter 5: β-adrenergic regulation of Excitation-Contraction coupling in rat ventricular myocytes

5.1   Introduction

The β-ADRs are G-protein-coupled receptors located on the surface of ventricular myocytes which bind the endogenous catecholamines, adrenaline and nor-adrenaline. The mammalian ventricle expresses the β_1-ADR, β_2-ADR and β_3-ADR subtypes, but the relative levels of expression and the functional outcome of each receptor differ. During sympathetic stimulation, binding of adrenaline and nor-adrenaline to the β_1-ADR and β_2-ADR subtypes stimulates the G_s protein, resulting in a positive inotropic, chronotropic and lusitropic effect in myocytes and a positive dromotropic effect at the AV node. The β_2-ADR subtype is dual coupled to both the G_s and G_i proteins, and so the activation of the β_2-ADR subtype results in only a positive inotropic effect in the myocyte. Whereas activation of the G_i protein coupled β_3-ADR subtype induces a negative inotropic effect in myocytes. (See introduction 1.2).

The endogenous catecholamines adrenaline and nor-adrenaline can be mimicked by the administration of the exogenous non-selective β-ADR agonist, isoproterenol (ISO). ISO preferentially activates β-ADR over α-ADR, and is a full agonist at all 3 β-ADR (Alexander, Benson et al. 2013). In fact, all 3 β-ADRs preferentially bind ISO over adrenaline and nor-adrenaline (Vrydag and Michel 2007). The endogenous catecholamines and ISO, bind to all 3 β-ADR and so the effect of adrenaline, nor-adrenaline or ISO are the result of the combined activation of β_1–ADR, β_2–ADR and β_3-ADR–ADR (Bers 2001).

I have previously shown a negative effect of β_3-ADR stimulation on systolic $[Ca^{2+}]_i$, and a time-of-day variation in the outcome of the β_3-ADR, finding a greater reduction in systolic $[Ca^{2+}]$ and SR Ca^{2+} content in rest-period (ZT3) myocytes (See chapter 3.2.3.2.1).

My initial aim was to look at the mechanism for this time-of-day variation in the effects of β_3-ADR activation and to dissect the signalling pathway using specific agonists and blockers, however this was not possible to complete. During this period of investigation our animal housing facility moved to a brand new facility and the reverse light cycle room was found to have inadequate lighting (the red light used for husbandry purposes was visible to the rats) and the room was shared with another group that performed surgical interventions with animals recovering in this room. These disruptions severely impacted

on the animals, and resulted in the absence of the previously identified robust time-of-day variation. My research now concentrates on the potential cardio-protective effects of β_3–ADR and G_i signalling pathway, with regard to sympathetic-driven arrhythmic activity and to compare and contrast these to β_1-ADR and β_2-ADR signalling. These experiments were carried out in normal light cycle (rest-period/ZT3) myocytes, whose sleep pattern and physiology was not altered following the move.

The aim of this chapter was to investigate the contribution of each of the β_1-ADR, β_2-ADR and β_3-ADR to Ca^{2+} regulation and the overall positive inotropic effect of β-ADR stimulation in cardiac myocytes, specifically to investigate the role of the G_i protein and PDE activity in β_2-ADR and β_3-ADR's.

5.2   Results

5.2.1   Effect of isoproterenol on excitation-contraction coupling in rest-period rat ventricular myocytes; calcium handling and electrophysiology

β-ADR activation by adrenaline and nor-adrenaline is the physiological means by which CO is increased in response to an increase in demand, e.g. during exercise. The increase in CO is achieved by altering contractile efficiency (inotropic and lusitropic) and HR (chronotropic). At the cellular level, the increase in contraction strength (positive inotropy) results from an increase in systolic $[Ca^{2+}]_i$, and the increased rate of relaxation (positive lusitropy) result in part from faster decline in $[Ca^{2+}]_i$. This effect can be mimicked by the non-specific β-ADR agonist ISO, which stimulates all β-ADR expressed on the myocardium and therefore the overall inotropic response of ISO will reflect the balance between the activation of the $β_1$–ADR, $β_2$–ADR and $β_3$–ADR and their respective pathways.

I set out to investigate the effect of β-ADR stimulation Ca^{2+} handling (E-C coupling) and determine if the response of the action potential (change in configuration and APD) may account for any changes in Ca^{2+} handling as a result of β-ADR stimulation.

5.2.1.1   The effect of isoproterenol on calcium handling

To investigate the response of the Ca^{2+} transient to non-specific β-ADR stimulation, $[Ca^{2+}]_i$ was measured in myocytes superfused with normal Tyrode to obtain a basal Ca^{2+} transient and in response to 10nM ISO. The resulting Ca^{2+} transients were recorded and measurement of systolic $[Ca^{2+}]$, diastolic $[Ca^{2+}]$ and rate of relaxation of the electrically-induced Ca^{2+} transient were made (See Methods 2.2.3).

Figure 5.1 shows example records of A. electrically-induced and B. caffeine-induced Ca^{2+} transients recorded in normal Tyrode and 10nM ISO. Mean systolic $[Ca^{2+}]_i$ and relaxation time of the electrically-induced Ca^{2+} transient recorded from these experiments are shown in Figure 5.1C and 5.1D. The data shows a significant increase in systolic $[Ca^{2+}]_i$ in response to ISO, from 319.6 ± 18.5nM to 1040.0 ± 116.9nM (n=5(32);p<0.0001) and a significant reduction in relaxation time in response to ISO, from 220.9 ± 11.4ms to 99.3 ± 6.9ms (n=5(32);p<0.0001), suggesting an increase in the activity of SERCA.

The positive inotropic effect of ISO is reported to result mainly from its effect on phosphorylation of PLB (Li, Desantiago et al. 2000), which removes its inhibitory effect on the activity of SERCA, resulting in greater amounts of Ca^{2+} being sequestered back to the SR during the relaxation of E-C coupling. As SERCA is the predominant mechanism whereby Ca^{2+} is removed from the cytosol during the relaxation phase of E-C coupling in the rat this leads to an increased SR Ca^{2+} content (Bers 2001). As I have shown an increase in SERCA activity in response to ISO, I investigated the SR Ca^{2+} content in response to β-adrenergic stimulation with ISO. SR Ca^{2+} content was estimated by rapidly perfusing cells with Tyrode containing caffeine (20mM), recorded in normal Tyrode and 10nM ISO. The resulting caffeine-induced Ca^{2+} transient was recorded and measurements of peak caffeine-induced Ca^{2+} release, indicating SR Ca^{2+} content, and the rate of relaxation of the caffeine-induced transient, which reflects the activity of NCX (Bers 2001), were made as previously described (See Methods 2.2.3).

Figure 5.1 shows mean E. peak caffeine-induced Ca^{2+} release and F. relaxation time of the caffeine-induced Ca^{2+} transient in response to 10nM ISO. The data shows a significant increase in SR Ca^{2+} content in response to ISO, from 538.5 ± 37.1nM to 915.9 ± 102.8nM (n=5(31); p<0.0001) and significant reduction in relaxation time in response to ISO, from 2992.0 ± 253.9ms to 2275.0 ± 271.3ms (n=5(31);p<0.05), indicating an increase in the activity of NCX.
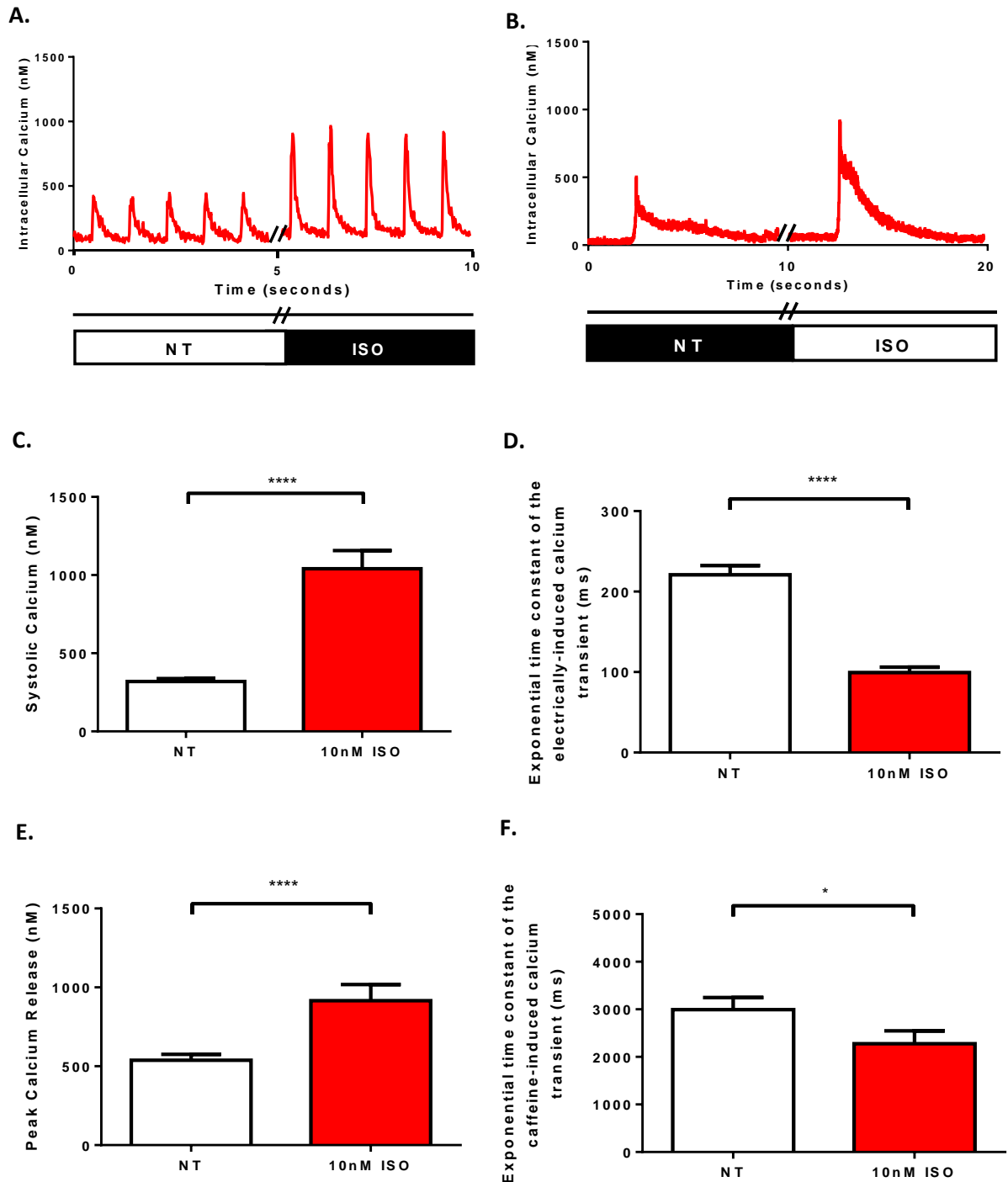
Figure 5.1   The effect of the non-specific β-ADR isoproterenol on the calcium handling of the rat ventricular myocyte.

Example recordings of **A.** electrically-induced and **B.** caffeine-induced Ca^{2+} transients recoreded in normal Tyrode and 10nM Isoproterenol (ISO). Bar charts showing **C.** systolic $[Ca^{2+}]$ and **D.** the exponential time constant of the decay of the electrically-induced calcium transient, stimulated at 1Hz by electrical field stimulation, and **E.** peak caffeine-induced calcium release and **F.** the exponential time constant of the decay of the caffeine-induced calcium transient, recorded from ventricular myocytes after superfusion with normal Tyrode (white bars) followed by 10nM ISO (red bar). Values are mean ± S.E.M. Number of hearts (number of experiments); n=5(31-32). *p<0.05, ****p<0.0001, paired t-test.

5.2.1.2 The effect of isoproterenol on cardiac electrophysiology

The action potential is the initiator of contraction, the trigger for which is an influx of Ca^{2+} during the plateau phase of the action potential either via the LTCC or NCX (see Introduction 1.2.2). The APD can modify net Ca^{2+} influx directly through the LTCC and NCX, and indirectly by modulating Ca^{2+} efflux on the NCX. The amount of Ca^{2+} released via the RyR2 during CICR is determined by the size of SR Ca^{2+} stores, which I have shown to be altered by β-ADR stimulation, but is also dependent upon on the amount of Ca^{2+} entering the cell through the LTCC and reverse-mode NCX (Bassani, Yuan et al. 1995), and may therefore result from changes to APD.

To investigate the response of the action potential (change in configuration and APD) in response to global β-ADR stimulation (β_1-ADR, β_2-ADR, β_3-ADR), action potentials were recorded in normal Tyrode followed by 10nM ISO. The resulting action potentials were recorded and measurement of RMP and APD_{30}, ADP_{50}, APD_{90} were made as previously described (See Methods 2.3.3.1).

Figure 5.2A are records of an action potential from a rat ventricular myocyte recorded in NT (black) and in the presence of 10nM ISO (red) and shows an increase in APD in response to non-specific β- ADR stimulation with ISO.

Figure 5.2B is the analysed data of such experiments, showing the mean APD_{30}, APD_{50} and APD_{90} in normal Tyrode and following ISO. The data shows that ISO increases APD_{30}, from 14.6 ± 1.8ms to 27.1 ± 1.8ms (p<0.001) and APD_{50}, from 22.3 ± 2.8ms to 42.6 ± 2.3ms (p<0.001). There was no significant effect on APD_{90} in response to ISO, from 65.7 ± 6.7ms to 73.1 ± 3.7ms (n=6(9);p=0.32).

Figures 5.2C shows RMP of the action potential in normal Tyrode and following ISO. The data shows the RMP was hyperpolarised by ISO, from -68.3 ± 1.5mV to -71.2 ± 1.8mV (n=6(9);p<0.05).

A. Representative action potential recordings from myocytes superfused with normal Tyrode (black) and 10nM isoproterenol (ISO) (red).
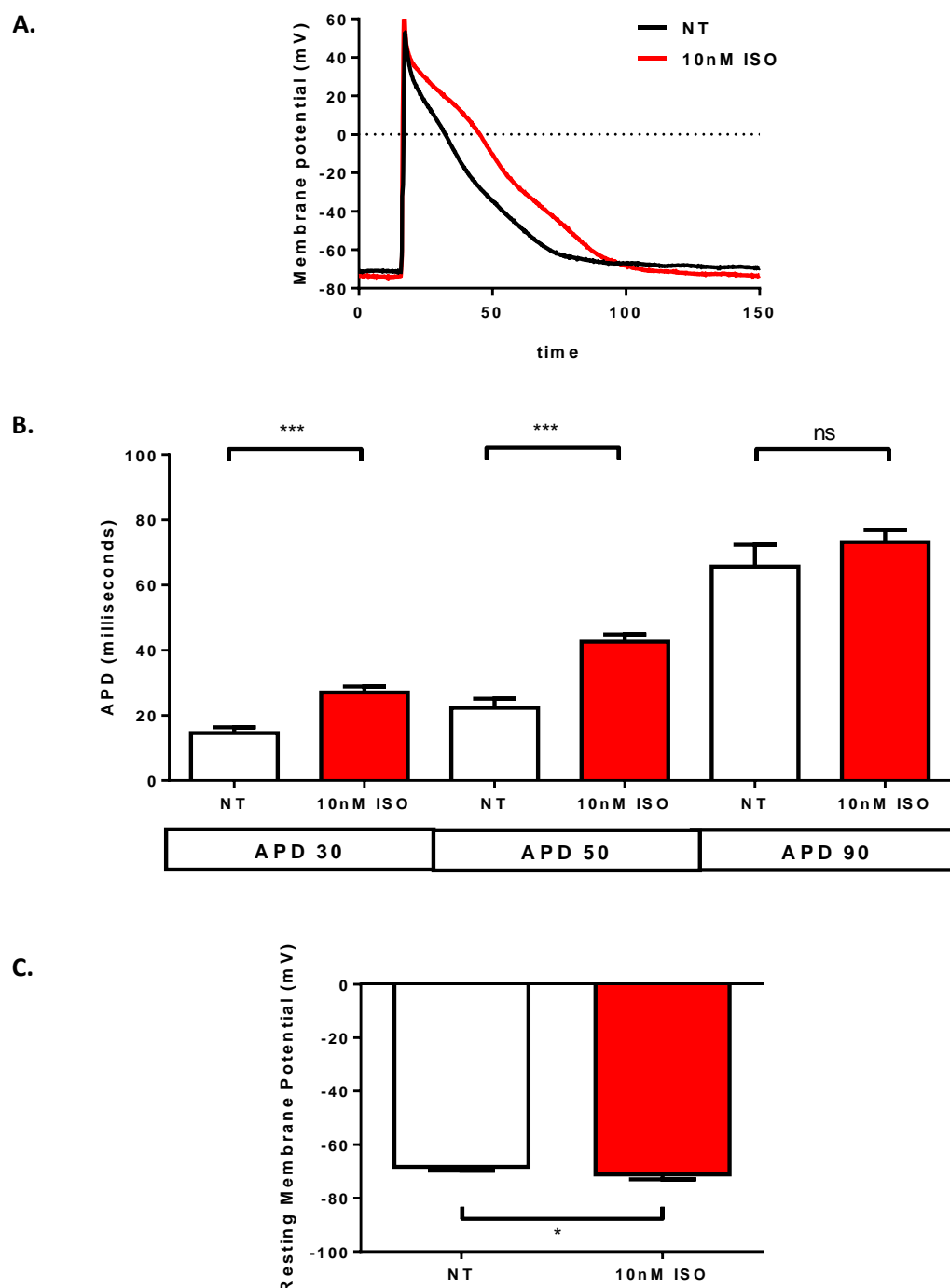
Figure 5.2   The effect of the non-specific β-ADR isoproterenol on the rat ventricular myocyte action potential.

A. Representative action potential recordings from myocytes superfused with normal Tyrode (black) and 10nM isoproterenol (ISO) (red).

Bar charts showing; **B.** APD_{30}, APD_{50} and APD_{90} and **C.** resting membrane potential recorded from myocytes superfused with normal Tyrode (white bars) followed by 10nM ISO (red bars). Values are mean ± S.E.M. Number of hearts (number of experiments) n=6(9); *p<0.05, ***p<0.001, APD analysed by a one-way ANOVA with Sidak's *post-hoc* test and resting membrane potential analysed by a paired t-test.

5.2.2 Effect of specific β-ADR agonist stimulation on Excitation-Coupling coupling in rat ventricular myocytes; calcium handling and cardiac electrophysiology

I have shown stimulation of β-ADR in response to ISO leads to an increase in systolic $[Ca^{2+}]$ and SR Ca^{2+} content, and an increase in the activity of SERCA and NCX. I have also shown a lengthening of $APD_{30/50}$ and a hyperpolarisation of RMP. As ISO is non-specific β-ADR agonist, the overall inotropic response of ISO will reflect the balance between the activation of the β_1–ADR, β_2–ADR and β_3–ADR and their respective pathways. I therefore set out to investigate the effect of specific β_1–ADR, β_2–ADR and β_3-ADR stimulation on E-C coupling and Ca^{2+} handling.

In order to control for any differences in cell isolations, basal parameters of Ca^{2+} handling (systolic $[Ca^{2+}]$, SR Ca^{2+} load, SERCA and NCX activity) and cardiac electrophysiology (APD, I_{to} and LTCC) between data sets (different isolations) were compared, and unless otherwise stated no differences in basal parameters were found.

5.2.2.1 The effect of specific β-ADR agonist stimulation on calcium handling

To investigate the response of the Ca^{2+} transient to β-adrenergic stimulation, $[Ca^{2+}]_i$ was measured in myocytes superfused with normal Tyrode and in response to the β_1-ADR agonist dobutamine, β_2-ADR agonist salbutamol or β_3-ADR agonist BRL_{37344} and measurement of systolic $[Ca^{2+}]$, diastolic $[Ca^{2+}]$ and rate of relaxation of the electrically-induced Ca^{2+} transient were made as previously described (See Methods 2.2.3).

Figure 5.3 shows concentration-response curves of systolic $[Ca^{2+}]$ and diastolic $[Ca^{2+}]$ in response to A. the β_1-ADR agonist dobutamine, B. the β_2-ADR agonist salbutamol and C. the β_3-ADR agonist BRL_{37344}. The records show an increase in systolic $[Ca^{2+}]_i$ and diastolic $[Ca^{2+}]_i$ following dobutamine (n=5(6-53)) and salbutamol (n=7(66)) perfusion, and a reduction in systolic $[Ca^{2+}]_i$ but an increase in diastolic $[Ca^{2+}]_i$ following BRL_{37344} perfusion (n=5(6-53)).

A.

B.

C.
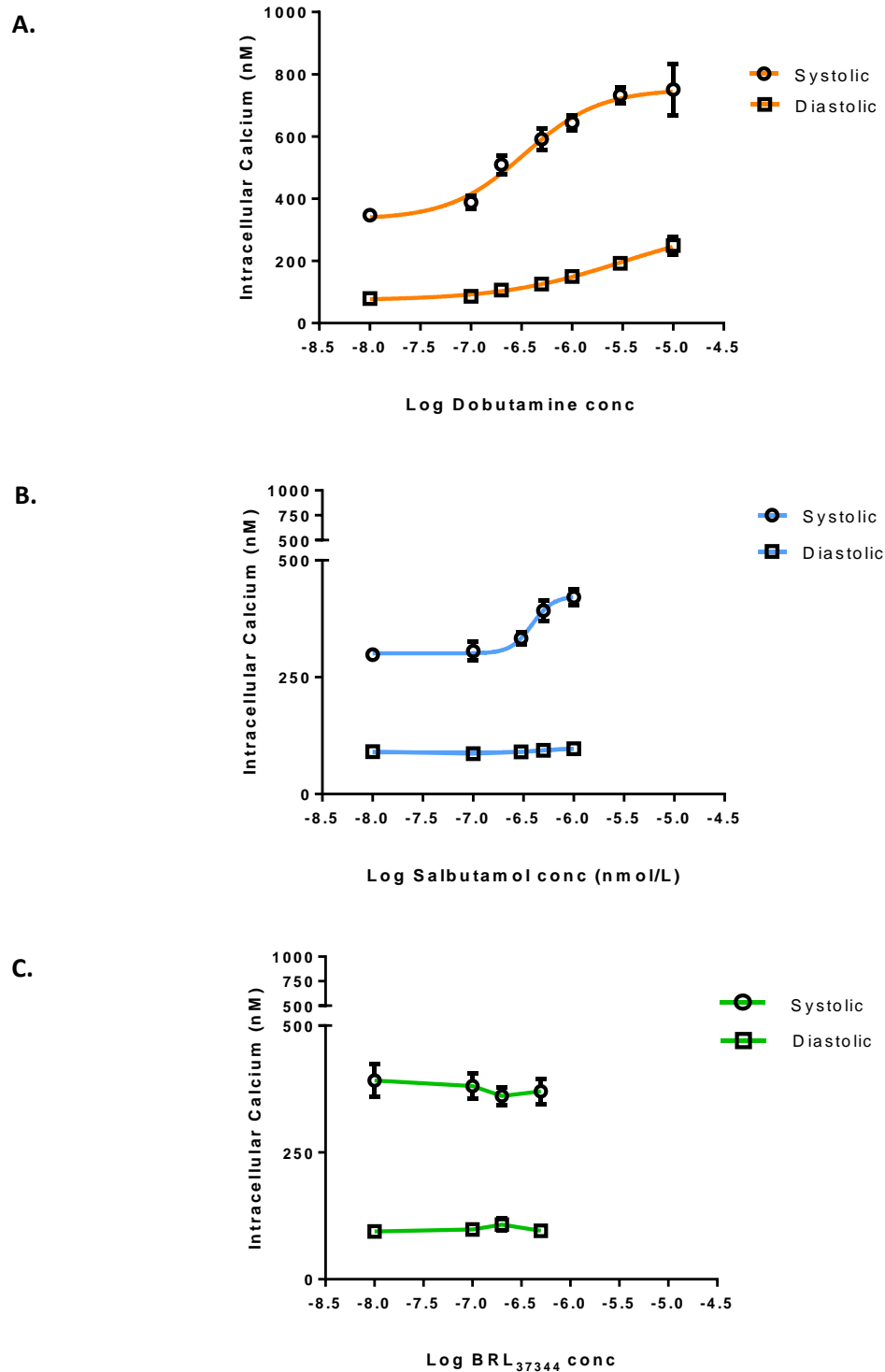
Figure 5.3 **Concentration-response curves of specific β-adrenergic receptor agonists.**
Concentration-response curves of systolic (square) and diastolic (circle) [Ca^{2+}] in response to **A.** β$_1$-ADR agonist dobutamine, **B.** β$_2$-ADR agonist salbutamol and **C.** β$_3$-ADR agonist BRL$_{37344}$, recorded in myocytes stimulated at 1Hz by electrical field stimulation. Values are mean ± S.E.M. Number of hearts (number of experiments); dobutamine, n=5(6-53), salbutamol, n=7(66), BRL$_{37344}$, n=4(19).

A.

B.

C.
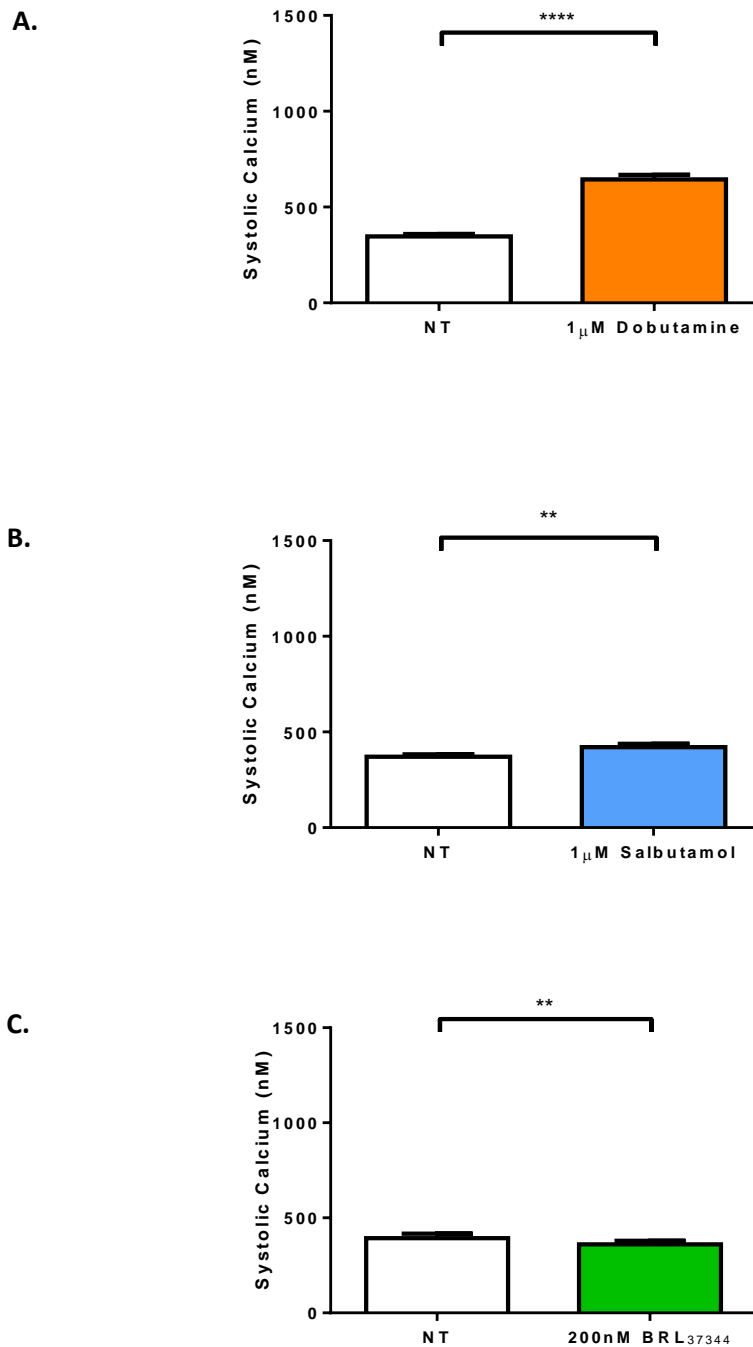
Figure 5.4   The effect of specific β-adrenergic receptor stimulation on systolic [Ca^{2+}]$_i$.
Bar charts showing systolic [Ca^{2+}] recorded from ventricular myocytes, stimulated at 1Hz by electrical field stimulation, after superfusion with normal Tyrode (white bars) followed by; **A.** 1μM Dobutamine   (orange, n=5(46)), **B.** 1μM salbutamol (blue, n=7(66)) and **C.** 200nM BRL$_{37344}$ (green, n=4(19)). Values are mean ± S.E.M. Number of hearts (number of experiments), **p<0.01, ****p<0.0001, paired t-test.

A.

B.

C.
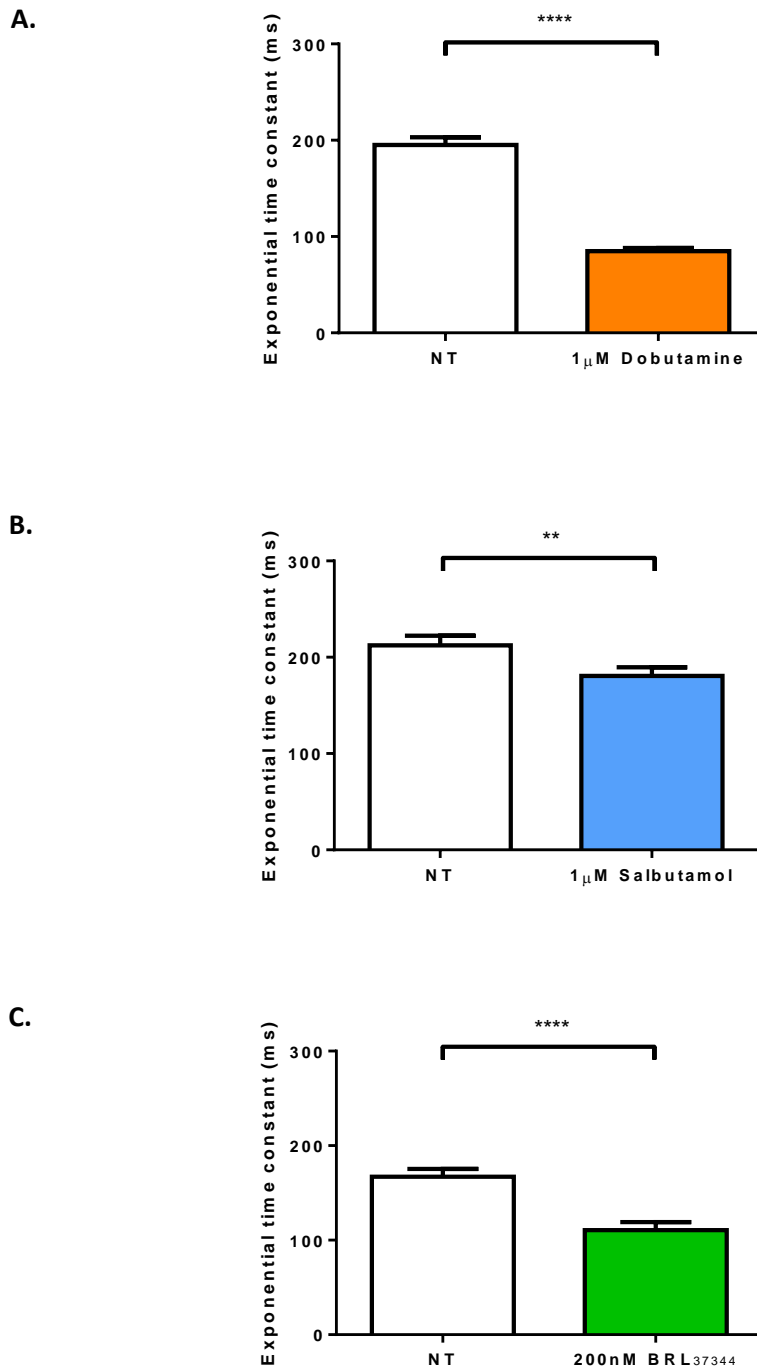
Figure 5.5 **The effect of β-adrenergic stimulation on the rate of relaxation of electrically-induced calcium transients**

Bar charts showing the exponential time constant of the decay of the electrically-induced calcium transient recorded from myocytes, stimulated at 1Hz by electrical field stimulation in normal Tyrode (white bars) and after superfusion with; **A.** 1μM Dobutamine (orange, n=5(46)), **B.** 1μM salbutamol (blue, n=7(66)) and **C.** 200nM BRL_{37344} (green, n=4(19)). Values are mean ± S.E.M. Number of hearts (number of experiments), $**p<0.01$, $****p<0.0001$, paired t-test.

Mean systolic $[Ca^{2+}]_i$ in response to A. 1µM dobutamine, B. 1µM salbutamol and C. 200nM BRL$_{37344}$ are shown in Figure 5.4 (data taken from concentration curves in figure 5.3).

The concentrations of salbutamol and BRL$_{37344}$ were the concentrations chosen for further investigation as they were the concentrations which showed the maximal change (increase/decrease) in systolic $[Ca^{2+}]_i$. The maximal increase in systolic $[Ca^{2+}]_i$ in response to dobutamine was reached at 3-10µM, however these concentrations induced significant arrhythmic activity which impeded investigation, and so 1µM dobutamine was chosen for further investigation.

The data shows a significant increase in systolic $[Ca^{2+}]_i$ in response to dobutamine, from 340.6 ± 14.3nM to 644.0 ± 24.7nM (n=5(46);p<0.0001) and salbutamol, from 370.7 ± 12.5nM to 421.0 ± 17.2nM (n=7(66);p<0.01). The data shows a significant reduction in systolic $[Ca^{2+}]_i$ in response to BRL$_{37344}$, from 393.2 ± 24.0nM to 342.7 ± 17.29nM (n=4(19);p<0.01).

As previously stated, the positive inotropic effect of ISO is reported to result mainly from phosphorylation of PLB and the subsequent increase in SR Ca^{2+} content. As I have shown an increase in SERCA activity in response to ISO I therefore investigated the effect of specific agonist stimulation on SERCA activity.

Figure 5.5 shows mean relaxation time of the electrically-induced Ca^{2+} transient in response to A. 1µM dobutamine, B. 1µM salbutamol and C. 200nM BRL$_{37344}$. The data shows a significant reduction in relaxation time in response to dobutamine, from 195.2 ± 7.9ms to 84.9 ± 3.1ms (n=5(46);p<0.0001), salbutamol, from 212.3 ± 10.0ms to 180.7 ± 9.0ms (n=7(66);p<0.01) and BRL$_{37344}$, from 167.2 ± 8.1ms to 110.6 ± 8.6ms (n=4(19);p<0.0001).

It was noted that both the increase in systolic $[Ca^{2+}]_i$ and reduction in relaxation time of the electrically-induced Ca^{2+} transient was significantly lower in response to maximal concentration of the agonist salbutamol as compared to maximal concentration of the agonist dobutamine.

A.

B.

C.
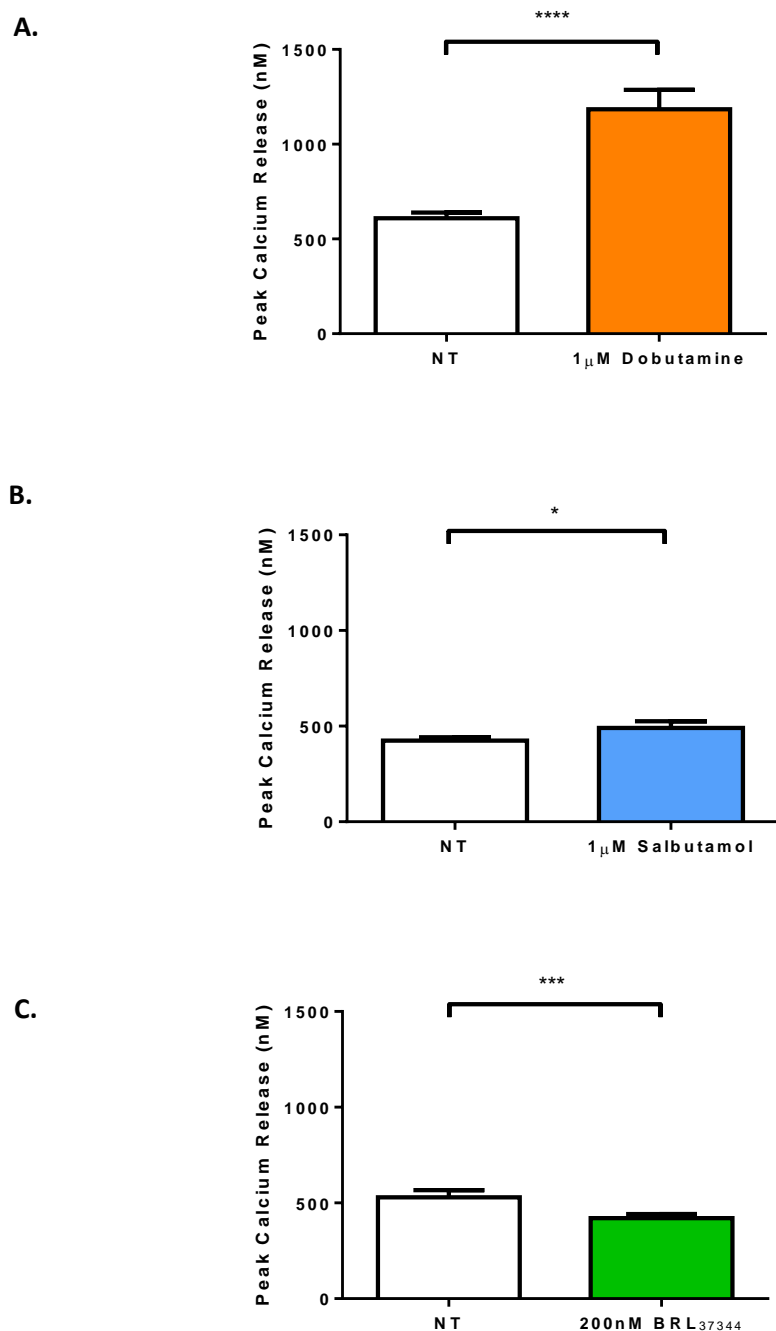
Figure 5.6   The effect of β-adrenergic stimulation on sarcoplasmic reticulum calcium content.

Bar charts showing peak caffeine-induced calcium release recorded from myocytes in normal Tyrode (white bars) and after superfusion with; **A.** 1μM Dobutamine (orange, n=5(37)), **B.** 1μM salbutamol (blue, n=7(26)) and **C.** 200nM BRL$_{37344}$ (green, n=4(19)). Values are mean ± S.E.M. Number of hearts (number of experiments), *p<0.05, ***p<0.001, ****p<0.0001, paired t-test.

A.

B.

C.
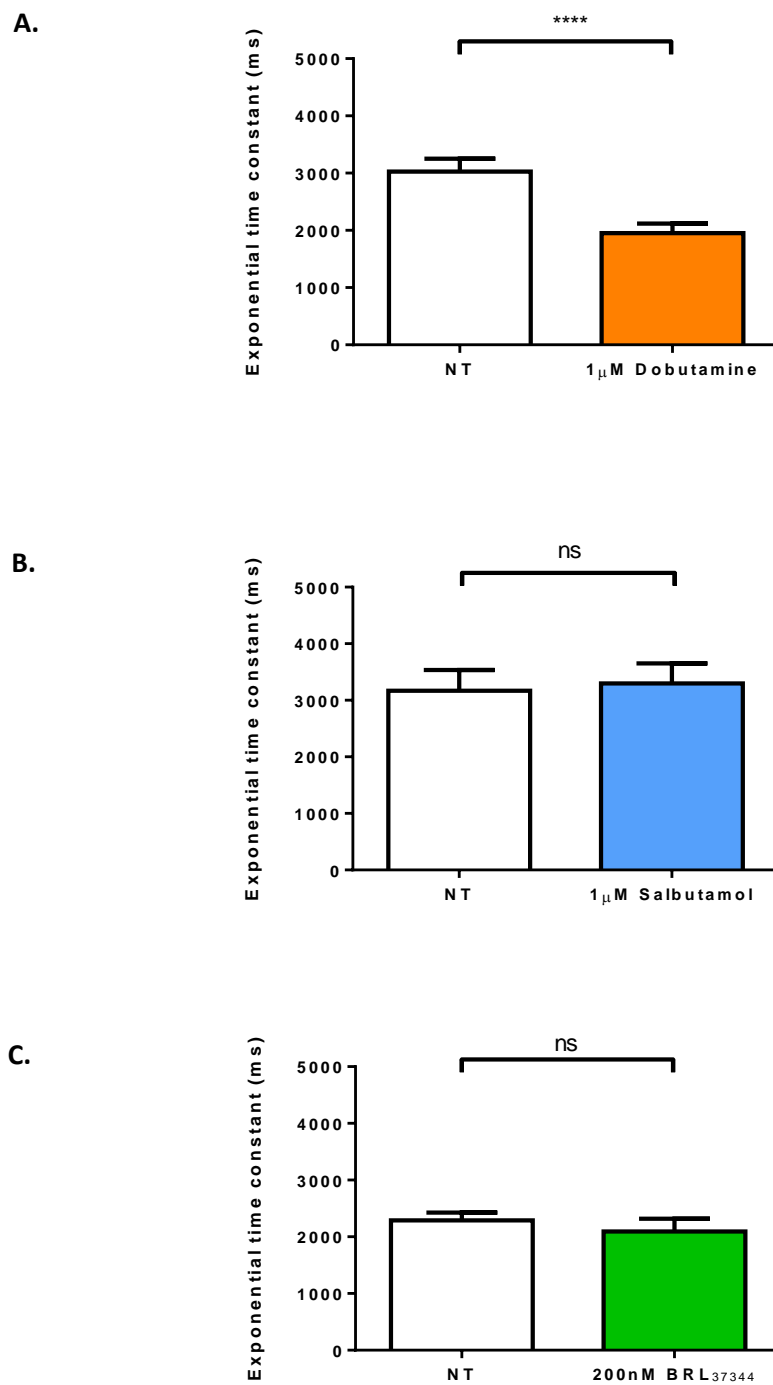
Figure 5.7 **The effect of specific β-adrenergic receptor stimulation on the rate of relaxation of the caffeine-induced calcium transients.**

Bar charts showing the exponential time constant of the decay of the caffeine-induced calcium transient recorded from myocytes in normal Tyrode (white bars) and after superfusion with;

A. 1μM dobutamine (orange, n=5(34)), **B.** 1μM salbutamol (blue, n=7(26)) and **C.** 200nM BRL$_{37344}$ (green, n=4(19)). Values are mean ± S.E.M. Number of hearts (number of experiments), ****p<0.0001, paired t-test.

An increase in the activity of SERCA resulting in greater amounts of Ca^{2+} being sequestered back to the SR during the relaxation of E-C coupling increases SR Ca^{2+}-content (Bers 2001). I have shown an increase in SR Ca^{2+} content in response to ISO and therefore investigated the effect of specific agonist stimulation on SR Ca^{2+} content by determining SR Ca^{2+} content as previously described (see Methods 2.2.3) in normal Tyrode followed by 1μM dobutamine, 1μM salbutamol or 200nM BRL_{37344}.

A significant difference in basal SR Ca^{2+} content were found between dobutamine and salbutamol groups (574.4 ± 23.5nM vs 429.4 ± 16.7nM;p<0.001).

The change in peak caffeine-induced Ca^{2+} release (SR Ca^{2+} content) in response to A. 1μM dobutamine, B. 1μM salbutamol and C. 200nM BRL_{37344} are shown in Figure 5.6. The data shows a significant increase in SR Ca^{2+} content in response to dobutamine, from 609.6 ± 29.3nM to 1184.0 ± 102.3nM (n=5(37); p<0.0001) and salbutamol, from 424.9 ± 16.8nM to 490.7 ± 35.0nM (n=7(26); p<0.05). The data also shows a reduction in SR Ca^{2+} content in response to BRL_{37344}, from 529.3 ± 37.6nM to 420.1 ± 22.2nM (n=4(19);p<0.001).

Figure 5.7 shows mean relaxation time of the caffeine-induced Ca^{2+} transient in response to A. 1μM dobutamine, B. 1μM salbutamol and C. 200nM BRL_{37344}. The data shows a significant reduction in relaxation time in response to dobutamine from 3025.0 ± 226.1ms to 1952.0 ± 167.0ms (n=5(34);p<0.0001), indicating an increase in NCX activity. The data also shows no change in relaxation time in response to salbutamol, from 3170.0 ± 365.3ms to 3300.0 ± 350.3ms (n=7(26);p=0.93) and BRL_{37344}, from 2290.0 ± 138.5ms to 2096.0 ± 225.0ms (n=4(19);p=0.31).

Again it was noted that the increase in SR Ca^{2+} content and reduction in relaxation time of the caffeine-induced Ca^{2+} transient, indicating NCX activity, was reduced in response to the maximal concentration of the β_2-ADR agonist salbutamol as compared to the maximal concentration of the β_1-ADR agonist dobutamine.

In summary;

The data shows that specific agonists of the β_1-ADR and β_2-ADR induce a positive inotropic and lusitropic effect on myocytes, observed as an increase in systolic $[Ca^{2+}]$ and SR Ca^{2+} stores, and a reduction in relaxation time of the electrically-induced Ca^{2+} transient, indicating an increase in SERCA activity.

The positive inotropic effect of maximal β_2-ADR agonist concentration appears to be depressed, as compared to maximal concentrations of β_1-ADR agonist, with β_1-ADR stimulation displaying a positive inotropic effect similar to that of global β-ADR activation with ISO.

In contrast β_3-ADR stimulation induces a negative inotropic effect, reducing systolic $[Ca^{2+}]$ and SR Ca^{2+} stores, whilst supporting relaxation, indicated by an increase in SERCA activity.

5.2.2.2   The effect of specific β-ADR agonist stimulation on cardiac electrophysiology

β-ADR stimulation with ISO increases the I_{Ca}, elevating the plateau phase of the action potential, and is also associated with an increase in the conductance of K^+, hyperpolarising the RMP and shortening APD, increasing refractory time which allows higher heart rates *in vivo* (Bers 2001). I have previously shown an increase in APD_{30} and APD_{50} and a hyperpolarisation of RMP in response to ISO. As ISO is a non-specific β-ADR agonist I set out to investigate the response of the action potential (change in configuration and/or APD) to specific β-ADR agonists and to investigate the response of the ionic currents underpinning the action potential.

5.2.2.2.1   The effect of specific β-ADR agonist stimulation on the cardiac action potential

To investigate the response of the action potential (change in configuration and APD) to specific β-ADR stimulation, action potentials were recorded in normal Tyrode followed by 1μM dobutamine, 1μM salbutamol or 200nM BRL_{37344} and measurement of RMP and APD_{30}, ADP_{50}, APD_{90} were made as previously described (See Methods 2.3.3.1).

Figure 5.8A is an action potential recorded from a rat ventricular myocyte in normal Tyrode (black) and in the presence of 1μM dobutamine (orange) and shows an increase in APD in response to specific β_1-ADR stimulation with dobutamine.

Figure 5.8B is the analysed data of such experiments, showing the mean APD_{30}, APD_{50} and APD_{90} in normal Tyrode and following dobutamine. The data shows that dobutamine

results in an increase in ADP_{30}, from 14.0 ± 1.5ms to 24.0 ± 1.9ms (p<0.0001), APD_{50}, from 22.8 ± 2.3ms to 41.2 ± 2.5ms (p<0.0001) and APD_{90}, from 67.4 ± 5.6ms to 87.3 ± 2.9ms (n=6(16); p<0.05).

Figure 5.8C shows RMP of the action potential in normal Tyrode and following dobutamine. The data shows the RMP was hyperpolarised by ISO, from -73.6 ± 0.5mV to -74.9 ± 0.6mV (n=6(16);p<0.01).

Figure 5.9A is an action potential recorded from a rat ventricular myocyte in normal Tyrode (black) and in the presence of 1µM salbutamol (blue) and shows no change in APD in response to specific β_2-ADR stimulation with salbutamol.

Figure 5.9B is the analysed data of such experiments, showing the mean APD_{30}, APD_{50} and APD_{90} in normal Tyrode and following salbutamol. The data shows that salbutamol has no effect ADP_{30}, from 12.4 ± 1.3ms to 12.6 ± 1.2ms (n=4(13);p=0.99), or APD_{50}, from 20.4 ± 1.9ms to 21.1 ± 1.8ms (n=4(13);p=0.77). However salbutamol lengthened APD_{90}, from 58.3 ± 3.7ms to 66.1 ± 3.3ms (n=4(13);p<0.01).

Figure 5.9C shows RMP of the action potential in normal Tyrode and following salbutamol. The data shows the RMP was hyperpolarised by salbutamol, -74.5 ± 0.9mV to -76.1 ± 1.0mV (n=4(13);p<0.001).

Figure 5.10A is an action potential recorded from a rat ventricular myocyte in normal Tyrode (black) and in the presence of 200nM BRL_{37344} (green) and shows a reduction in APD in response to specific β_3-ADR stimulation with BRL_{37344}.

Figure 5.10B is the analysed data of such experiments, showing the mean APD_{30}, APD_{50} and APD_{90} in normal Tyrode and following BRL_{37344}. The data shows that BRL_{37344} results in a significant reduction in ADP_{30}, 11.4 ± 1.4ms to 10.8 ± 1.4ms (n=5(14);p<0.05). APD_{50} was also shorter following BRL_{37344}, from 18.8 ± 2.2ms to 17.9 ± 2.2ms, however this was not significant (n=5(14);p<0.0001) and there was no effect on APD_{90}, from 63.7 ± 5.4ms to 64.7 ± 64.7ms (n=5(14);p=0.96).

Figure 5.8 **The effect of the β_1-ADR specific agonist dobutamine on the rat ventricular myocyte action potential.**

B. Representative action potential recordings from ventricular myocytes superfused with normal Tyrode (black) and 1µM Dobutamine hydrochloride (orange).

Bar charts showing; **B.** APD_{30}, APD_{50} and APD_{90} and **C.** resting membrane potential from myocytes superfused with normal Tyrode (white bars) followed by 1µM Dobutamine (orange bars). Values are mean ± S.E.M. Number of hearts (number of experiments) n=6(16); *p<0.05, **p<0.01, ****p <0.0001, APD analysed by a one-way ANOVA with Sidak's *post-hoc* test and resting membrane potential analysed by a paired t-test.

186
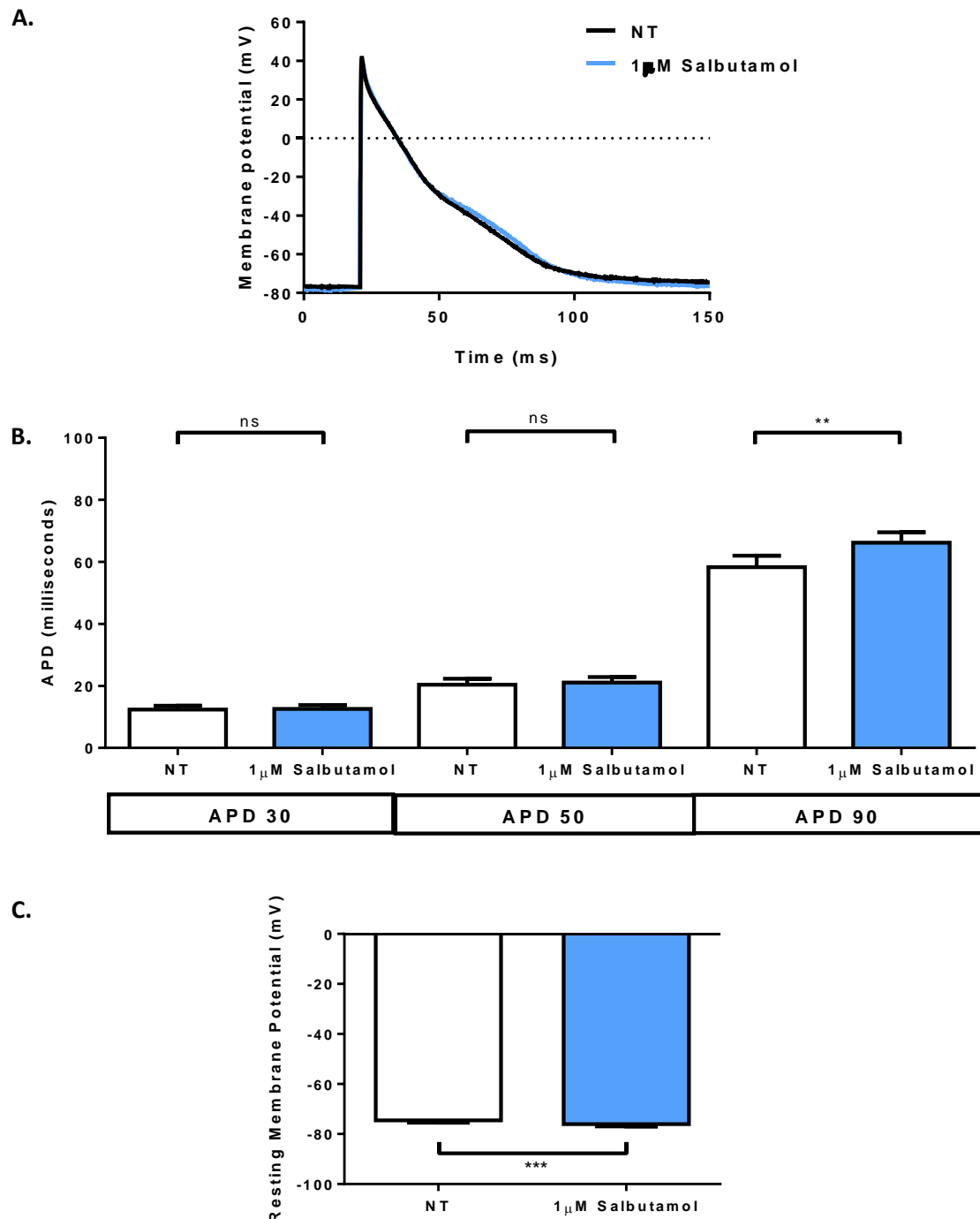
Figure 5.9 **The effect of the β_2-ADR specific agonist salbutamol on the rat ventricular myocyte action potential.**

A. Representative action potential recordings from ventricular myocytes superfused with normal Tyrode (black) and 1µM salbutamol (blue).

Bar charts showing; **B.** APD$_{30}$, APD$_{50}$ and APD$_{90}$ and **C.** resting membrane potential from myocytes superfused with normal Tyrode (white bars) followed by 1µM salbutamol (blue bars).

Values are mean ± S.E.M. Number of hearts (number of experiments) n=4(13); **p<0.01, ***p<0.001, APD analysed by a one-way ANOVA with Sidak's *post-hoc* test and resting membrane potential analysed by a paired t-test.
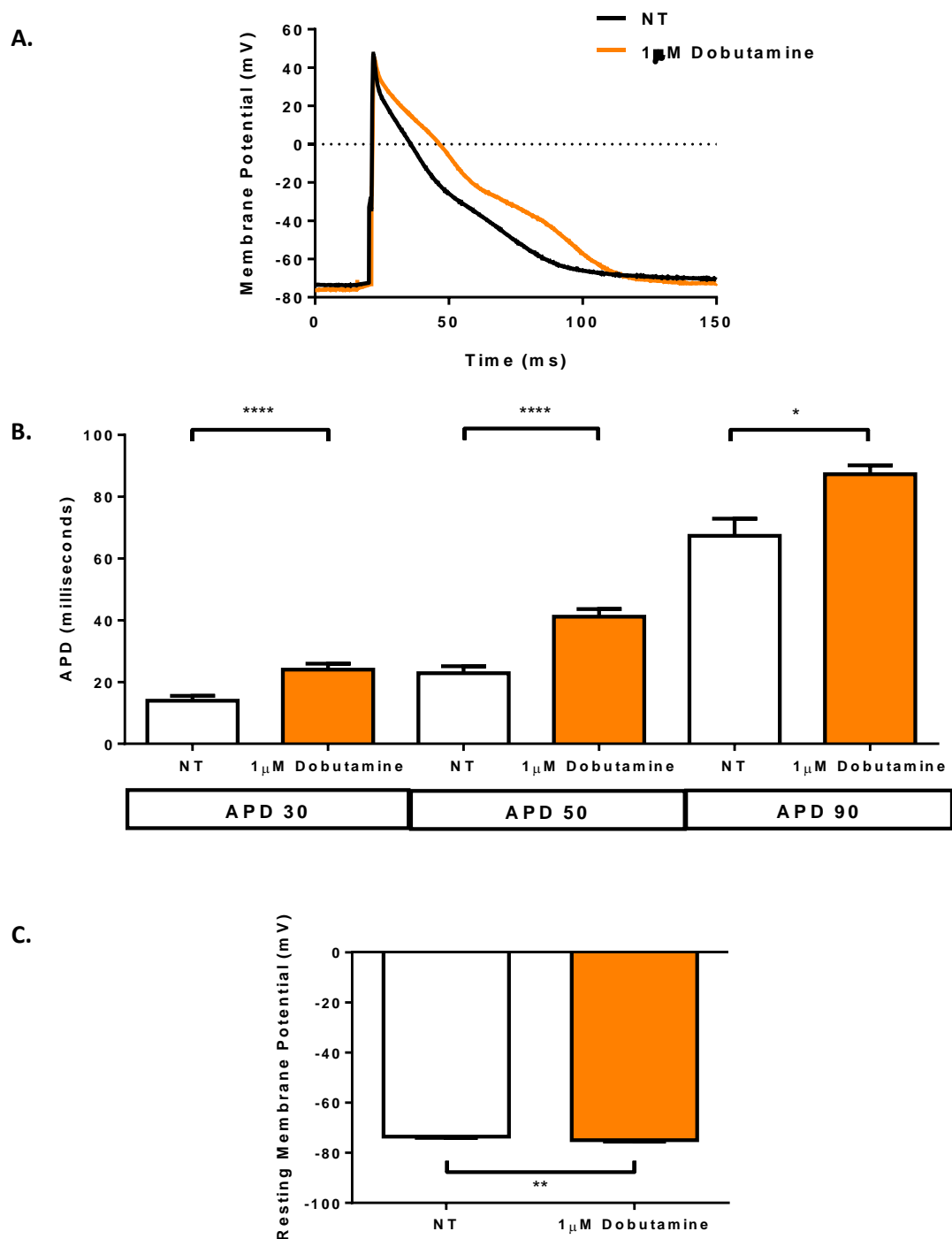
A.

B.

C.
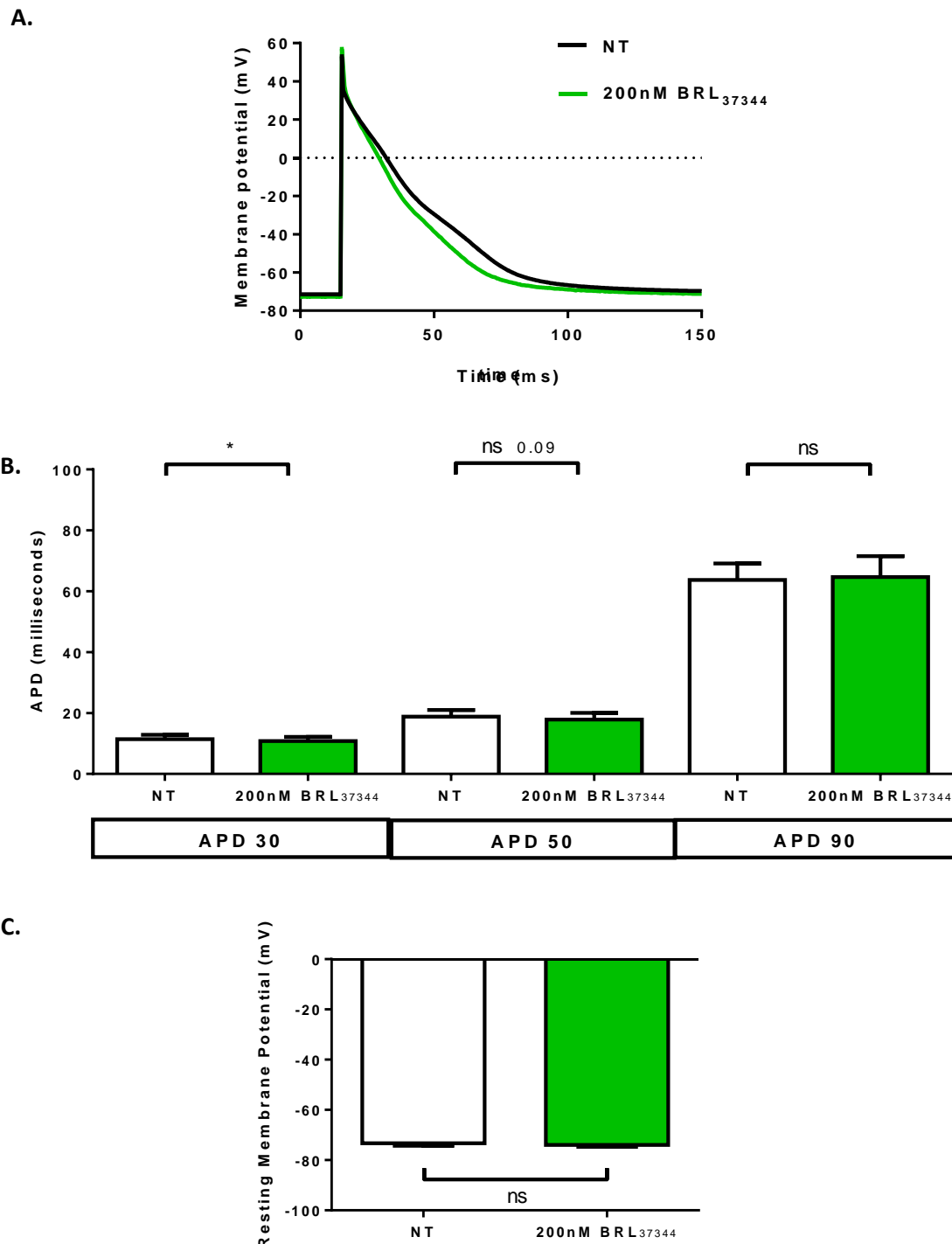
Figure 5.10   The effect of the β_3-ADR specific agonist salbutamol on the rat ventricular myocyte action potential.

Representative action potential recordings from ventricular myocytes superfused with normal Tyrode (black) and 200nM BRL$_{37344}$ (green).

Bar charts showing; **B.** APD$_{30}$, APD$_{50}$ and APD$_{90}$ and **C.** resting membrane potential recorded from myocytes superfused with normal Tyrode (white bars) followed by 200nM BRL$_{37344}$ (green bars). Values are mean ± S.E.M. Number of hearts (number of experiments) n=5(13-14); *p<0.05, APD analysed by a one-way ANOVA with Sidak's *post-hoc* test and resting membrane potential analysed by a paired t-test.

Figure 5.10C shows RMP of the action potential in normal Tyrode and following BRL$_{37344}$. The data shows the BRL$_{37344}$ had no effect on RMP, from -73.56 ± 0.49mV to -74.92 ± 0.64mV (n=5(14);p<0.01).

In summary;

The data shows an increase in APD$_{30/50}$ in response to β$_1$-ADR stimulation with dobutamine. This effect was similar in magnitude to the non-specific β-ADR agonist ISO. RMP was also hyperpolarised following dobutamine.

The data shows stimulation of β$_2$-ADR with salbutamol did not induce any increase in APD$_{30/50}$ and RMP was hyperpolarised following salbutamol.

The data also shows a shortening of the ADP$_{30/50}$ following β$_3$-ADR stimulation with BRL$_{37344}$, with no change in RMP.

5.2.2.2.2   The effect of specific β-ADR agonist stimulation on ionic currents

I have shown that β-ADR agonists had an effect on the APD mainly at APD$_{30/50}$, with little significant effect on the APD$_{90}$. Therefore, in this section I have attempted to look at specific ion channels likely to contribute to these phases of action potential repolarisation. The I_{to} plays a vital role in cardiac repolarisation, activated at approximately -30mV and responsible for the initial repolarisation of the action potential. Although relatively large in amplitude, only partial repolarisation occurs due to the fast activation and deactivation of transient outward channels (Bers 2001).

The LTCC are activated around -40mV and the LTCC is responsible for the plateau phase of the action potential, where there is little change in membrane potential.

To investigate the effect of the specific β-ADR agonists on the transient outward current in voltage-clamped rat ventricular myocytes, the I/V relationship for the I_{to} was obtained in normal Tyrode followed by 1µM dobutamine, 1µM Salbutamol or 200nM BRL$_{37344}$.as previously described (See Methods 2.3.3.2).

Figure 5.11 shows the I-V relationship for the I_{to} recorded in normal Tyrode and in response to A. 1µM dobutamine (n=3(12)), B. 1µM salbutamol (n=2(6)), and C. 200nM BRL$_{37344}$ (n=5(14)). In my investigation 0mV represented the average potential corresponding to APD$_{30}$ and the inserts are I_{to} recorded at this potential are shown. The

figure shows voltage activation of the I_{to} appearing in all groups at around -30mV, increasing in amplitude with the increase in test potentials.

The data shows stimulation of cells with dobutamine and salbutamol had no effect on I_{to}. However the amplitude of the I_{to} was reduced by BRL$_{37344}$ at test potentials more positive than 0mV, although this was not significant (p=0.06 to 0.09).

To investigate the effect of the specific β-ADR agonists on the LTCC in voltage-clamped rat ventricular myocytes, the I/V relationship for the LTCC was obtained in normal Tyrode followed by 1µM dobutamine, 1µM salbutamol or 200nM BRL$_{37344}$.

Figure 5.12 shows the I-V relationship for the LTCC recorded in normal Tyrode and in response to A. 1µM dobutamine (n=3(12)), B. 1µM salbutamol (n=3(11)), and C. 200nM BRL$_{37344}$ (n=3(23)). In my investigation -20mV represented the average potential corresponding to APD$_{50}$ and the inserts are LTCC recorded at this potential are shown. The figure shows voltage activation of the LTCC appearing in all groups at around -30mV, with maximal current density between -20mV and -10mV.

The data shows stimulation of cells with dobutamine lead to a significant increase in the current density of the LTCC between holding potentials -20mV and +20mV representative of APD$_{30/50}$. In addition the maximal current shifted to a more negative potential from -6.06 ± 0.54pA/pF at -10mV to -9.87 ± 1.19pA/pF at -20mV. The data shows stimulation of cells with salbutamol and BRL$_{37344}$ had no effect on LTCC.
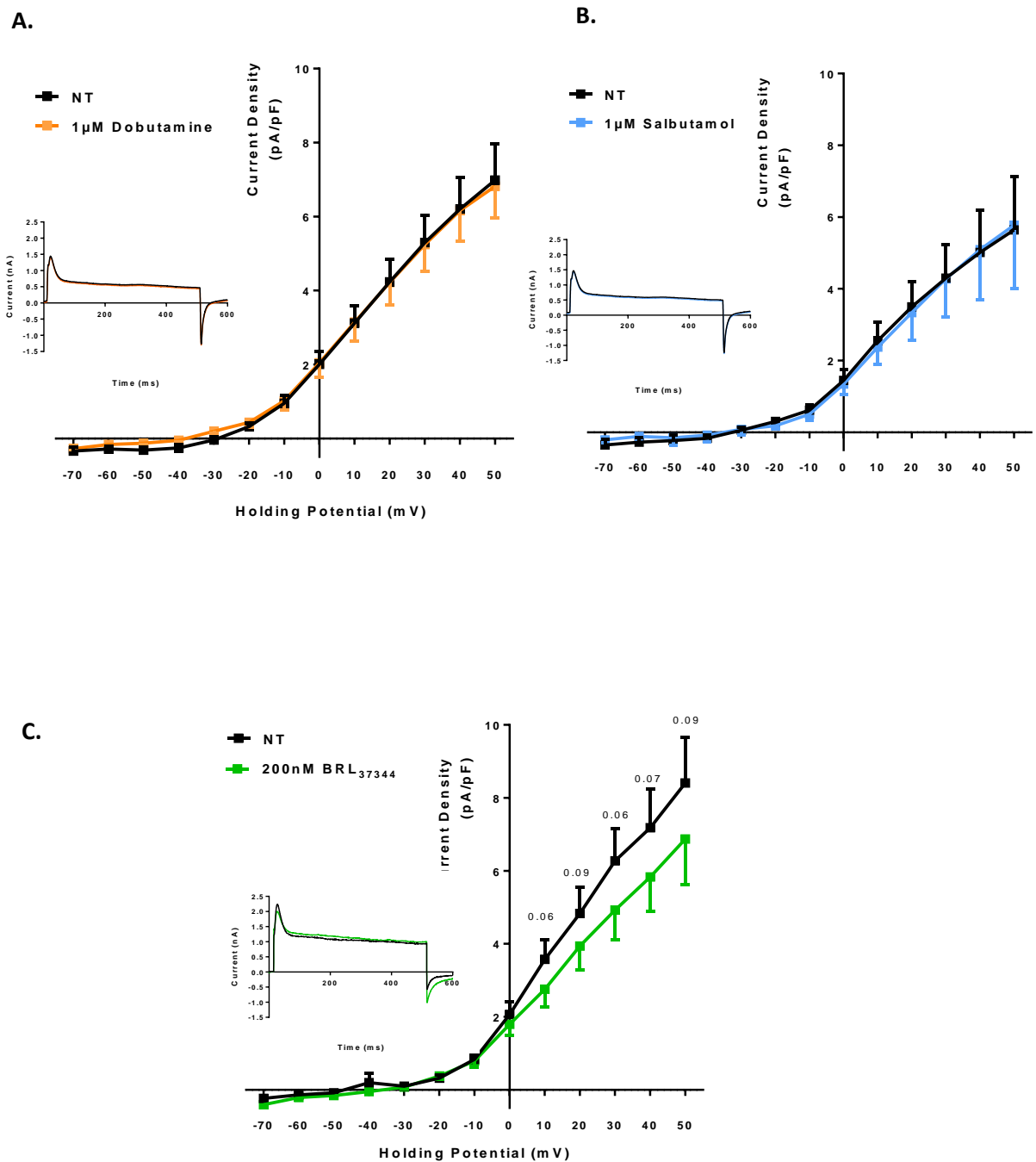
Figure 5.11 **The effect of specific β-adrenergic agonists on the transient outward current (I_{to}).**

Current-voltage relationship of the I_{to} of ventricular myocytes, recorded in normal Tyrode plus 200nM Cadmium Chloride (black) and in response to; **A.** 1μM Dobutamine (orange, n=3(12)), **B.** 1μM salbutamol (blue, n=2(6)) and **C.** 200nM BRL$_{37344}$ (green, n=5(14)). Inserts are representative I_{to} recordings at 0mV, representative of APD$_{30}$. Values are mean ± S.E.M. Number of hearts (number of experiments); two-way repeated measures ANOVA, Sidak's *post-hoc* test.
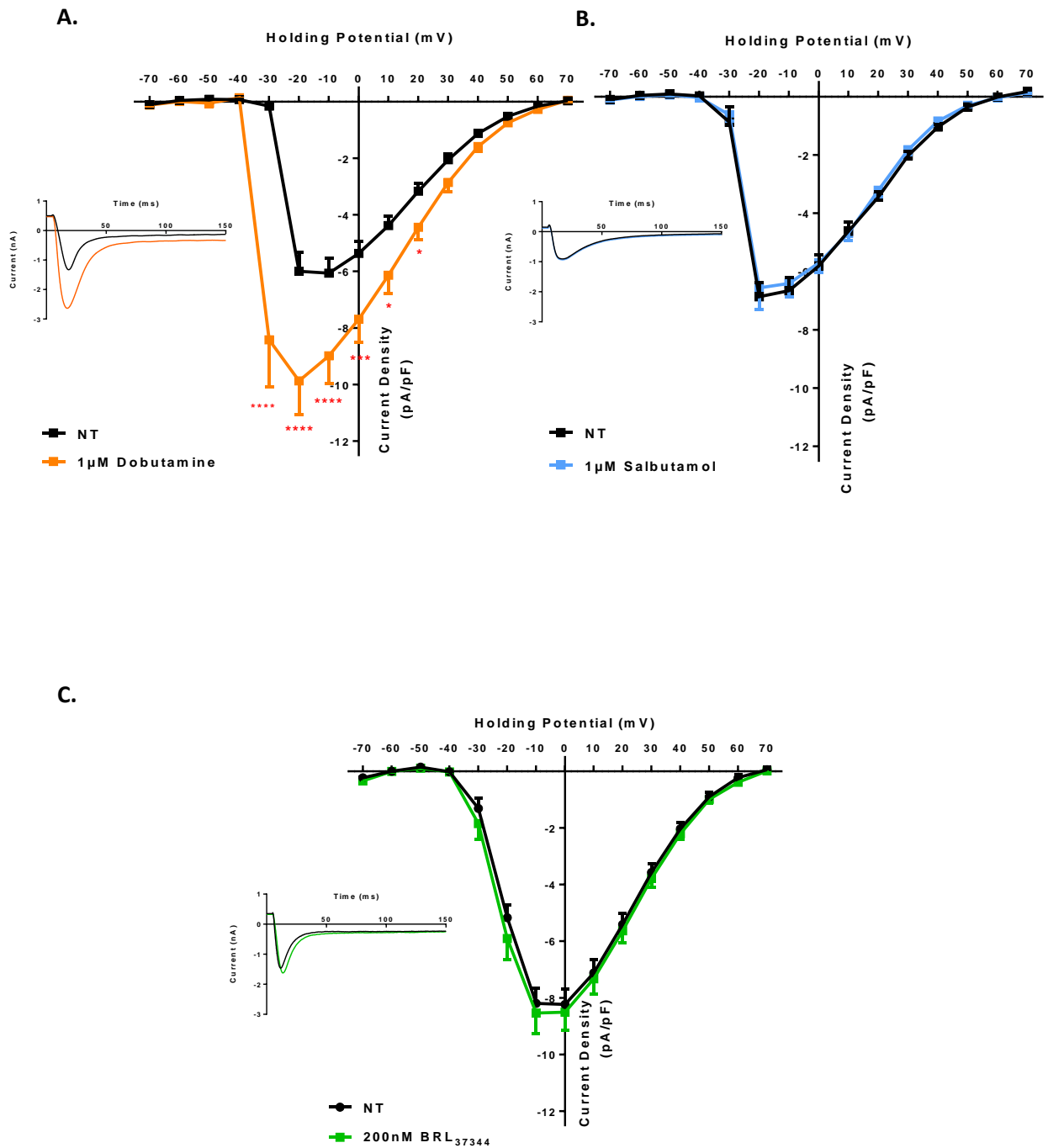
Figure 5.12 **The effect of β-adrenergic stimulation on the L-type calcium current (LTCC).**
Current-voltage relationship of the LTCC of ventricular myocytes, recorded in normal Tyrode (black) and in response to **A.** 1µM Dobutamine (orange, n=3(12)), **B.** 1µM salbutamol (blue, n=3(11)) and **C.** 200nM BRL$_{37344}$ (green, n=3(23)). Inserts are representative LTCC recordings at-20mV, representative of APD$_{50}$. Values are mean ± S.E.M. Number of hearts (number of experiments); *p<0.05, ****p<0.0001, two-way ANOVA, Sidak's *post-hoc* test.

The data shows that the I_{to} is partially inhibited by β_3-ADR specific stimulation with BRL$_{37344}$, however this was not significant and is contrary to the reduction in APD$_{30/50}$ following BRL$_{37344}$ stimulation.

The data also shows an increase in the amplitude of the LTCC in response to dobutamine and that the maximal current passes at a more negative membrane potential.

5.2.3   Investigation of the dual coupling of the β_2-ADR to G_s and G_i proteins

My previous data (Figures 5.4 to 5.7) has shown an increase in systolic [Ca^{2+}]$_i$, SR Ca^{2+} content and rate of relaxation of electrically-induced Ca^{2+} transients (increased SERCA activity) in response to salbutamol. However this was not accompanied by a change in the configuration of the action potential or in the I_{to} or LTCC (Figures 5.9, 5.11 and 5.12). In addition, I have shown that the increase in systolic [Ca^{2+}]$_i$ in response to maximal β_2-ADR stimulation with salbutamol is lower than the maximal increase in systolic [Ca^{2+}]$_i$ in response to β_1-ADR stimulation with dobutamine (Figure 5.3 and 5.4).

It is known that the β_2-ADR is dual coupled to the stimulatory G-protein, G_s, and the inhibitory G-protein, G_i, and that this coupling to G_i prevents a maximal inotropic response (Brodde, Bruck et al. 2006). The dual coupling of β_2-ADR to both the G_s and G_i proteins initiates two opposing pathways, leading to only local increases in cAMP which can result in a null inotropic effect (Xiao, Ji et al. 1995). The G_i protein leads to the activation of PDEs which hydrolyse cAMP, limiting the inotropic effects of β_2-ADR stimulation. (See figure 5.13 and Introduction 1.2 for further detail).

I set out to investigate the dual coupling of the β_2-ADR, to determine if the dual coupling of β_2-ADR to G_i is responsible for the reduced inotropic effect of β_2-ADR stimulation. I examined which aspects of Ca^{2+} handling (systolic [Ca^{2+}]$_i$, SR Ca^{2+} load, SERCA and NCX activity) and cardiac electrophysiology (APD, I_{to} and LTCC) are affected by the local and global increases in cAMP.
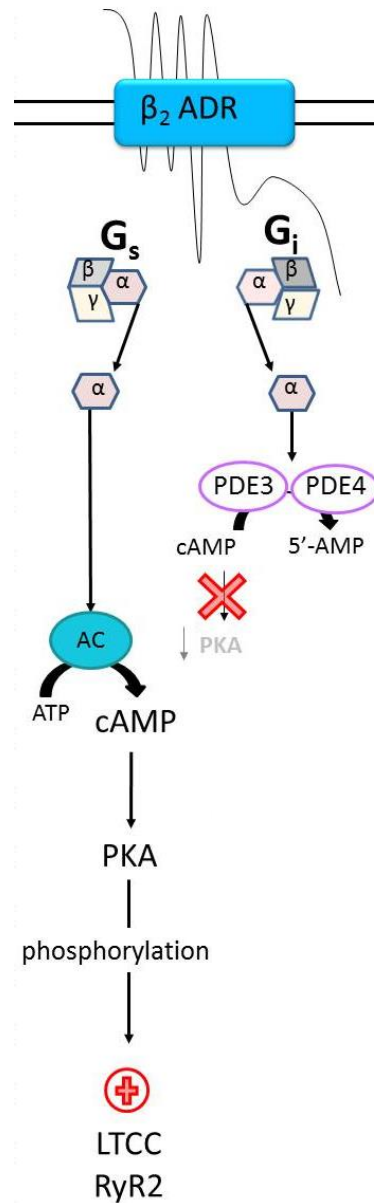
Figure 5.13   A schematic of the β₂-adrenergic receptors in the ventricular myocardium.
The figure shows the dual coupling of β₂-ADR to the stimulatory G-protein, G$_s$, and the inhibitory G-protein, G$_i$. Stimulation of the β₂-Adrenergic receptor leads to the activation of PKA via the G$_s$ pathway which is able to phosphorylate local targets the L-type calcium channels (LTCC) leading to the inotropic effects of β₂-Adrenergic receptor stimulation. Activation of the G$_i$ pathway leads to activation of phosphodiesterase (PDE) PDE3 and PDE4 which hydrolyse cAMP, reducing levels of cAMP and PKA activation.

5.2.3.1 The effect of PDE inhibition on the β_2-adrenergic response to salbutamol

The dual coupling of β_2-ADR is associated with the α-subunit of the G_i-protein and activation of PDE3 and PDE4, which hydrolyse cAMP (Mika, Leroy et al. 2012). A number of studies have shown PDE inhibition, either with IBMX or specific PDE3 and/or PDE4 inhibitors, during β_2-ADR stimulation increased levels of cAMP globally in the myocyte, activating distant LTCC channels and increasing the amplitude of LTCC (Rochais, Abi-Gerges et al. 2006; Gonzalez-Munoz, Fuente et al. 2009; Mika, Leroy et al. 2012). I set out to investigate which aspects of Ca^{2+} handling (systolic $[Ca^{2+}]_i$, SR Ca^{2+} load, SERCA and NCX activity) and cardiac electrophysiology (APD, I_{to} and LTCC) are affected by PDE signalling during β_2-ADR stimulation.

In order to control for any differences in cell isolations, basal parameters of Ca^{2+} handling (systolic $[Ca^{2+}]_i$, SR Ca^{2+} load, SERCA and NCX activity) and cardiac electrophysiology (APD, I_{to} and LTCC) between data sets were compared, and unless otherwise stated no differences in basal parameters were found.

As a control, I also investigated the effect of 30µM IBMX on all parameters and found no effect on basal parameters (data shown in appendix 6).

5.2.3.1.1 The effect of PDE inhibition on the regulation of calcium handling in response to salbutamol

To investigate the effect of PDE inhibition on the β_2-ADR Ca^{2+} transient, $[Ca^{2+}]_i$ was measured in myocytes, recorded in normal Tyrode, followed by salbutamol and salbutamol plus IBMX and measurement of systolic $[Ca^{2+}]_i$, diastolic $[Ca^{2+}]_i$ and rate of relaxation were measured as described previously (See Methods 2.2.3).
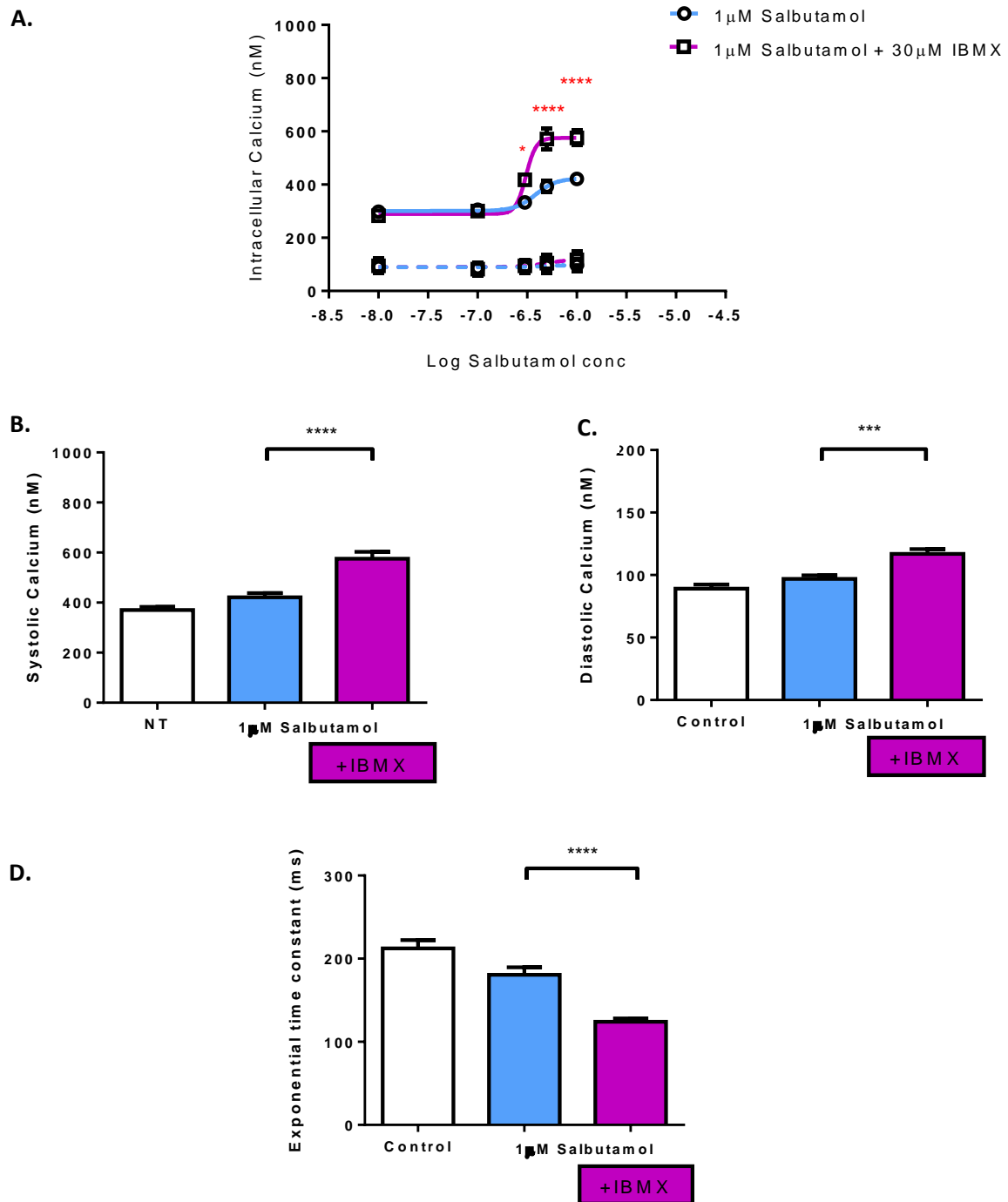
Figure 5.14   The effect of PDE inhibition on the calcium transient in response to β$_2$-ADR stimulation with salbutamol.

A. Concentration-response curves of systolic [Ca^{2+}] (bold line) and diastolic [Ca^{2+}] (dashed line) to β$_2$-adrenergic stimulation with salbutamol (blue) and with salbutamol plus 3-Isobutyl-1-methylxanthine (IBMX) (purple).

Bar charts showing; **B.** systolic [Ca^{2+}], **C.** diastolic [Ca^{2+}] and **D.** exponential time constant of the decay of the electrically-induced calcium transient recorded from myocytes in normal Tyrode (white bars), 1μM salbutamol (blue bars) and 1μM salbutamol and 30μM IBMX (purple bars). Values are mean ± S.E.M. Number of hearts (number of experiments) n=5(22-66); *p<0.05, ***p<0.001, ****p<0.0001, one-way ANOVA, Sidak's *post-hoc* test.

Figure 5.14A shows concentration-response curves of systolic $[Ca^{2+}]_i$ and diastolic $[Ca^{2+}]_i$ in response to varying concentrations (10nM to 1µM) of salbutamol (blue) and salbutamol plus IBMX (purple) (n=5(22-66)).

Mean systolic $[Ca^{2+}]_i$ and diastolic $[Ca^{2+}]_i$ in response in normal Tyrode (white), 1µM salbutamol (blue) and 1µM salbutamol plus 30µM IBMX (purple) are shown in Figures 5.14B and 5.14C (data taken from concentration curves in figure 5.14A). The data shows that β_2-ADR stimulation with salbutamol in the presence of IBMX to inhibit PDE activity, causes an additional increase in systolic $[Ca^{2+}]$ above the increase induced by salbutamol alone, from 421.0 ± 17.2nM to 575.2 ± 27.6nM (n=5(66);p<0.0001). PDE inhibition also caused an additional increase in diastolic $[Ca^{2+}]$, from 96.9 ± 3.0nM to 116.9 ± 3.8nM (n=5(66);p<0.001).

Figure 5.14D shows the effects of PDE inhibition during β_2-ADR stimulation on the mean time constant of the rate of relaxation of electrically-induced Ca^{2+} transient. The data shows that β_2-ADR stimulation with salbutamol in the presence of IBMX to inhibit PDE activity, causes an additional reduction in relaxation time, from 180.7 ± 9.0ms to 124.0 ± 4.1ms (n=5(65);p<0.0001), indicating an additional increase in SERCA activity following PDE inhibition.

SERCA is the predominant mechanism whereby Ca^{2+} is re-sequestered to the SR during the relaxation phase of E-C coupling in the rat (Bers 2001) and an increase in SERCA activity can lead to an increase in SR Ca^{2+} content. As I have shown that inhibition of PDE resulted in an additional increase in SERCA activity, I therefore set out to investigate if an increased SR Ca^{2+} content following PDE inhibition is associated with the additional increase in systolic $[Ca^{2+}]_i$. SR Ca^{2+} content was determined as previously described (See Methods 2.2.3) recorded in normal Tyrode followed 1µM salbutamol and 1µM salbutamol plus 30µM IBMX.

A.

B.

Figure 5.15   The effect of PDE inhibition on the sarcoplasmic reticulum Ca^{2+} content in response to β$_2$-ADR stimulation with salbutamol.

Bar charts showing the **A.** peak caffeine-induced Ca^{2+} release and **B.** exponential time constant of the decay of the caffeine-induced calcium transient recorded from myocytes in normal Tyrode (white bars), 1μM salbutamol (blue bars) and 1μM salbutamol and 30μM IBMX (purple bars). Values are mean ± S.E.M. Number of hearts (number of experiments) n=7(30); ***$p < 0.001$, one-way ANOVA, Sidak's *post-hoc* test.

Figure 5.15A is a bar chart of the mean peak caffeine-induced Ca^{2+} release in normal Tyrode and in response to salbutamol and shows a significant additional increase in SR Ca^{2+} stores following PDE inhibition during salbutamol stimulation, from 490.7 ± 35.0nM in salbutamol alone to 644.4 ± 56.1nM in the presence of IBMX (n=7(30);p<0.001).

Figure 5.15B is a bar chart of the mean relaxation time of the caffeine-induced Ca^{2+} transient in myocytes stimulated with salbutamol and in the presence of IBMX, and shows no effect of PDE inhibition on the relaxation time, from 3415.0 ± 334.2ms in salbutamol and 3075.0 ± 275.1ms in the presence of IBMX (n=7(30);p=0.73), which suggests that there is no additional effect of PDE inhibition on the NCX activity.

5.2.3.1.2 The effect of PDE inhibition on the regulation of cardiac electrophysiology in response to salbutamol

In this study, I have shown that β_2-ADR specific stimulation with salbutamol has no effect on the configuration of the cardiac action potential, the I_{to} or the LTCC. As PDE inhibition resulted in an increase in systolic $[Ca^{2+}]_i$, I postulated that this may have been due in part to a change in the configuration of the action potential, driven by changes in underlying ionic currents underpinning the action potential.

5.2.3.1.2.1 The effect of PDE inhibition on the regulation of the action potential in response to salbutamol

To investigate the effect of PDE inhibition on the response of the action potential to β_2-ADR stimulation, action potentials were recorded as previously described (See Methods 2.3.3) in normal Tyrode followed by 1μM salbutamol or 1μM salbutamol plus 30μM IBMX.

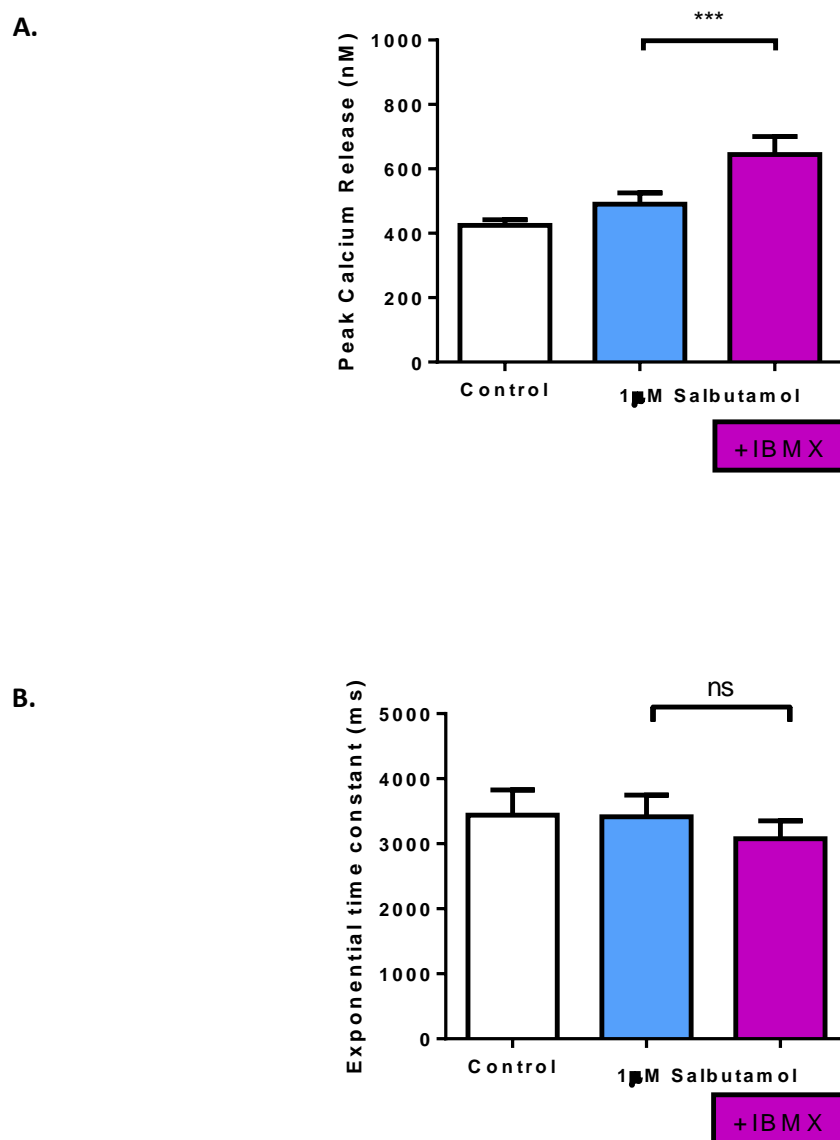Figure 5.16 shows the effect of salbutamol on the action potential, showing a record of a single action potential recorded in normal Tyrode (black) and A. 1μM salbutamol (blue) and B. 1μM salbutamol plus 30μM IBMX (purple), and shows that whilst salbutamol had no effect on the cardiac action potential, PDE inhibition with IBMX caused a prolongation of the action potential.
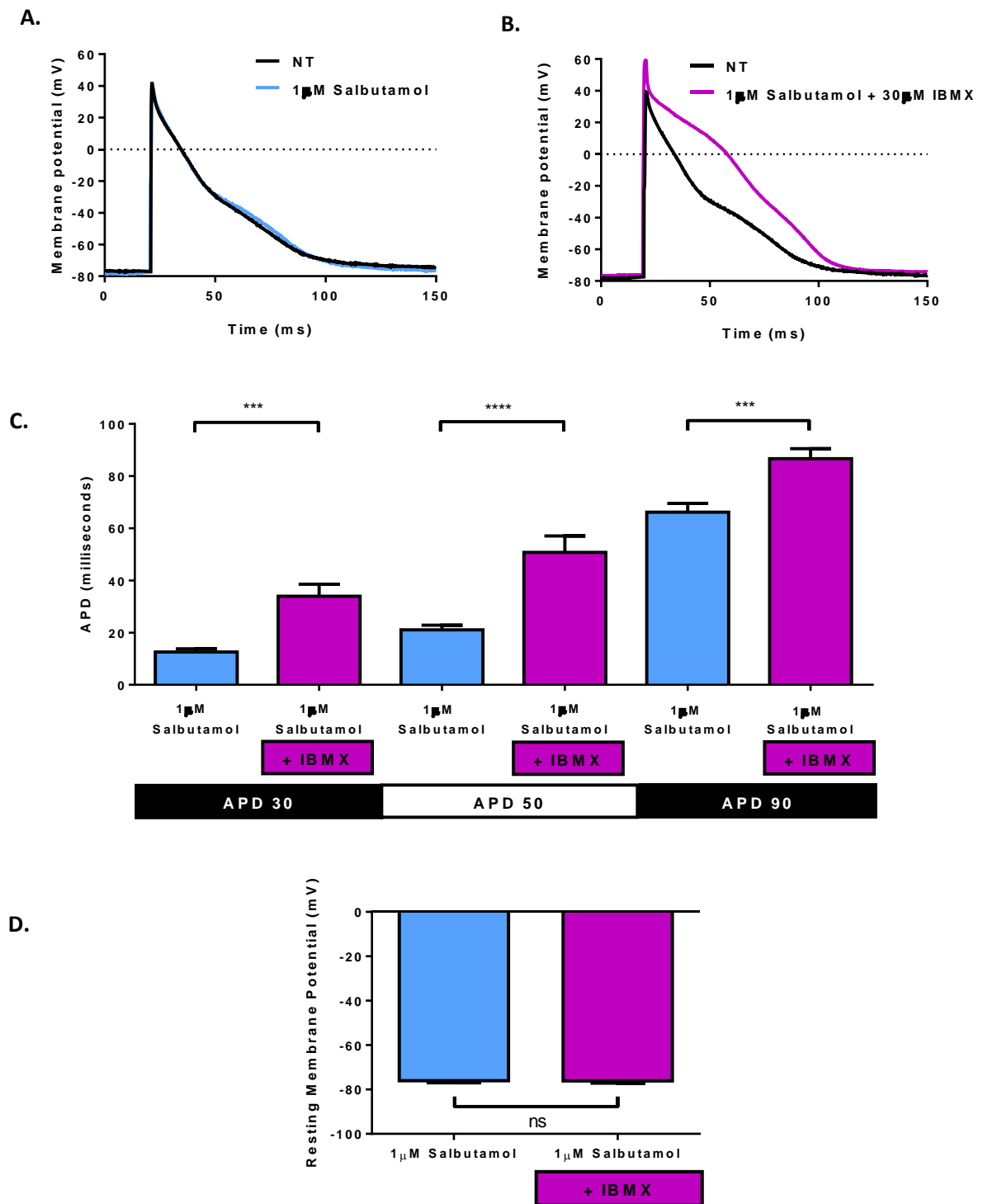
Figure 5.16 **The effect of PDE inhibition on the response of the cardiac action potential in response to β₂-ADR stimulation with salbutamol.**

Representative action potential recordings from myocytes superfused with **A.** normal Tyrode (black) and 1μM salbutamol (blue) and **B.** normal Tyrode (black) and 1μM salbutamol and 30μM 3-Isobutyl-1-methylxanthine (IBMX) (purple).

Bar charts showing; **C.** APD$_{30}$, APD$_{50}$ and APD$_{90}$ and **D.** resting membrane potential recorded from myocytes superfused with 1μM salbutamol (blue bars, n=4(13)) and 1μM salbutamol plus 30μM IBMX (purple bars, n=3(10)). Values are mean ± S.E.M. Number of hearts (number of experiments; ***p<0.001, ****p<0.0001, APD analysed by a one-way ANOVA with Sidak's *post-hoc* test and resting membrane potential analysed by a paired t-test.

Figure 5.16C shows the mean APD_{30}, APD_{50} and APD_{90} in salbutamol and salbutamol plus IBMX, and shows significant lengthening effect of PDE inhibition on all three metrics of APD in response to salbutamol; with APD_{30} increasing from 13.2 ± 1.4ms to 34.0 ± 4.6ms (p<0.001), APD_{50} from 22.5 ± 2.24ms to 50. 8 ± 6.3ms (p<0.001), and APD_{90} from 66.2 ± 3.3ms (n=4(13)) to 89.7 ± 3.9ms (n=4(10);p<0.001).

Figures 5.16D shows RMP of the action potential in salbutamol and salbutamol plus IBMX. The data shows RMP was not affected by PDE inhibition, -75.5 ± 0.7mV (n=4(13)) compared to -79.2 ± 0.9mV (n=4(10);p=0.58).

5.2.3.1.2.2   The effect of PDE inhibition on the regulation of ionic currents in response to salbutamol

I have previously shown that β_2-specific stimulation with salbutamol had no effect on the configuration of the action potential which correlated with no change in the I_{to} or the LTCC. However, I have shown that PDE inhibition using IBMX resulted in a significant increase in $APD_{30/50}$ in response to β_2-ADR specific stimulation and so I set out to investigate the effect of PDE inhibition on the effects of salbutamol on I_{to} and the LTCC.

To investigate the effect of PDE inhibition on response of the I_{to} and LTCC to β_2-ADR stimulation, the I/V relationship for the I_{to} and LTCC was obtained in 1µM salbutamol or 1µM salbutamol plus 30µM IBMX.

Figure 5.17 shows the mean I-V relationship of I_{to} recorded in normal Tyrode and in response to A. 1µM salbutamol (n=2(6)) and B. 1µM salbutamol plus 30µM IBMX (n=4(12)). The data shows stimulation of cells with salbutamol alone had no effect on I_{to}, and this was not affected by the presence of IBMX during β2-ADR stimulation with salbutamol.
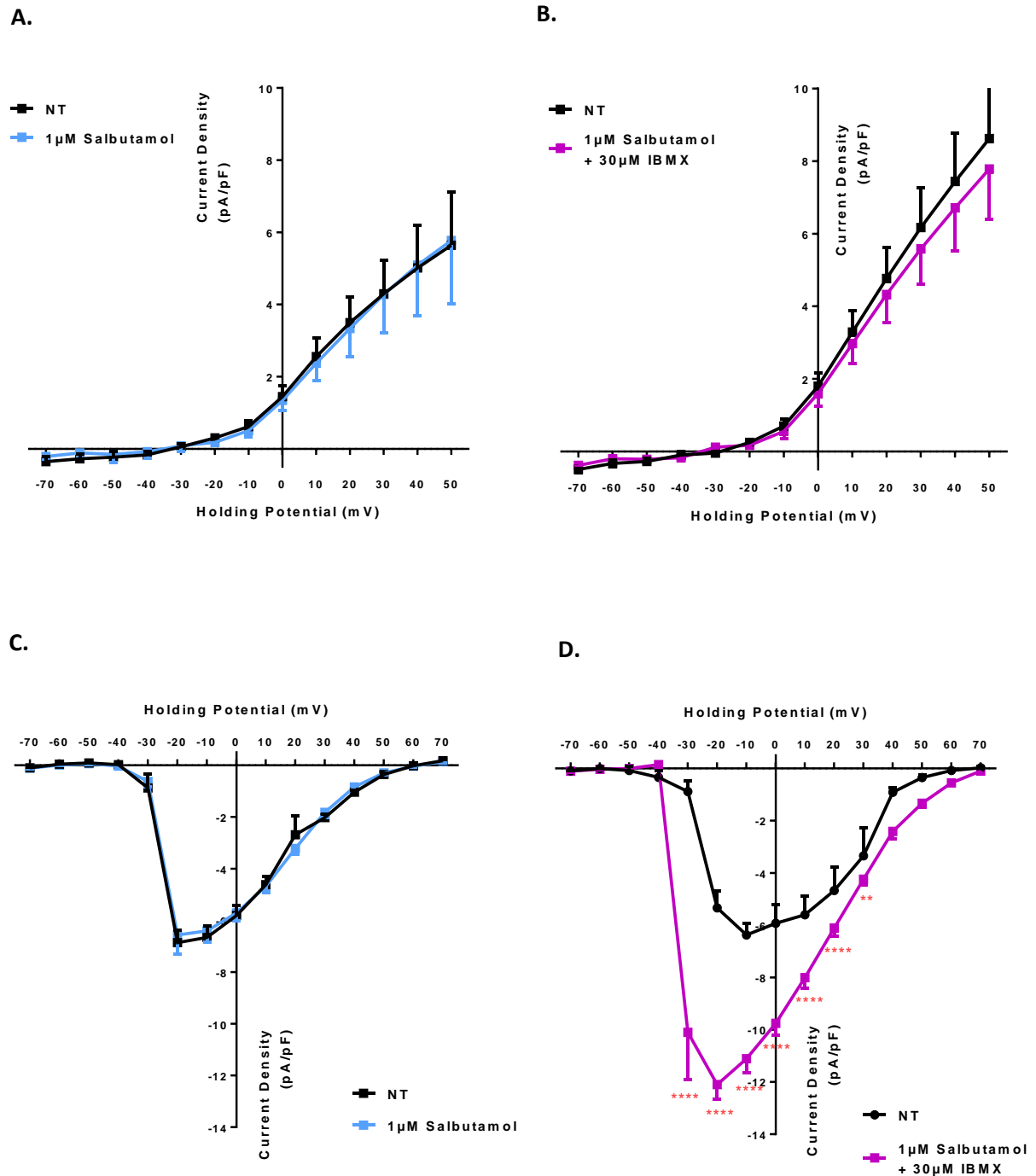
Figure 5.17 **The effect of PDE inhibition on the response of the transient outward current and L-type calcium current in response to β₂-ADR stimulation with salbutamol.**

Current-voltage relationship of the I_{to} current recorded in **A.** normal Tyrode (black) and 1μM salbutamol (blue, n=2(6)) and **B.** normal Tyrode (black) and 1μM salbutamol and 30μM 3-Isobutyl-1-methylxanthine (IBMX) (purple, n=4(12)).

Current-voltage relationship of the LTCC recorded in **C.** normal Tyrode (black) and 1μM salbutamol (blue, n=3(11)) and **D.** normal Tyrode (black) and 1μM salbutamol and 30μM IBMX (purple, n=4(11)).

Values are mean ± S.E.M. Number of hearts (number of experiments); *p<0.05, **p<0.01, ***p<0.001, ****p<0.0001, two-way ANOVA, Sidak's *post-hoc* test

202

Figure 5.17 shows the mean I-V relationship of LTCC recorded in normal Tyrode and in response to C. 1µM salbutamol (n=3(11)) and D. 1µM salbutamol plus 30µM IBMX (n=4(11)).

The data shows that whilst salbutamol had no effect on LTCC, PDE inhibition with IBMX caused a significant increase in the density of the LTCC between holding potentials -30mV and +30mV, representative of $APD_{30/50}$. PDE inhibition with IBMX during β_2-ADR stimulation with salbutamol caused the maximal current to shift to a more negative holding potential, from -6.38 ± 0.44pA/pF at -10mV to -12.10 ± 0.55pA/pF at -20mV.

In summary;

The data shows that β_2-ADR stimulation with salbutamol in the presence of IBMX to inhibit PDE activity causes an additional increase in systolic $[Ca^{2+}]$ and SERCA activity, above the increase induced by salbutamol alone. This was accompanied by an additional increase in SR Ca^{2+} stores above the increase induced by salbutamol alone; however there was no change in the activity of the NCX following PDE inhibition.

Moreover, PDE inhibition during β_2-ADR stimulation induces an increase in $APD_{30/50}$ and the current density of LTCC which is not seen in the presence of β_2-ADR stimulation alone. The result of PDE inhibition is an enhanced Ca^{2+} handling response to salbutamol, so that the response is no longer depressed as compared to β_1-ADR stimulation, suggesting the dual coupling of β_2-ADR to G_i and the resulting activation of PDE is involved in the depressed inotropic response to β_2-ADR activation.

5.2.3.2 The effect of PTx treatment on the β_2-adrenergic response to salbutamol

I have shown that PDE inhibition increases the inotropic response of β_2-ADR stimulation with salbutamol. However, as IBMX is a non-specific PDE inhibitor all PDE will be inhibited, not only the PDE activated by the G_i. The G_i protein can be permanently uncoupled from the β-ADR by the incubation of cells with the endotoxin Pertussis Toxin (PTx) (See Methods 2.4). I hypothesised that inhibition of the G_i protein would cause an increase in the inotropic effect of β_2-ADR stimulation, similar to the effect seen by PDE inhibition.

In order to control for any differences in cell isolations, basal parameters of Ca^{2+} handling (systolic $[Ca^{2+}]_i$, SR Ca^{2+} load, SERCA and NCX activity) and cardiac electrophysiology (APD, I_{to} and LTCC) between control and PTx-treated cells were compared, and unless otherwise stated no differences in basal parameters were found.

5.2.3.2.1 The effect of PTx treatment on the response of calcium handling to salbutamol

To investigate the effect of G_i inhibition with PTx on Ca^{2+} transients were recorded from Fura-2 loaded Control and PTx-treated myocytes in normal Tyrode and 1µM salbutamol and measurement of systolic $[Ca^{2+}]_i$, diastolic $[Ca^{2+}]_i$ and rate of relaxation of the electrically-induced Ca^{2+} transient were made as previously described (See Methods 2.2.3).

Figure 5.18 shows bar charts of the mean A. systolic $[Ca^{2+}]_i$, B. diastolic $[Ca^{2+}]_i$ and C. exponential time constant for the decay of the electrically-induced Ca^{2+} transient in control and PTx-treated cells .

The data shows salbutamol perfusion increased systolic $[Ca^{2+}]_i$ in control cells, from 293.3 ± 19.6nM to 363.2 ± 26.3nM (n=5(19);p=0.10), and PTx-treated cells, from 273.0 ± 12.2nM to 524.2 ± 30.3nM (n=5(18);p<0.0001). However, the increase in systolic $[Ca^{2+}]_i$ in response to salbutamol was significantly larger in PTx-treated cells compared to control cells (p<0.001).

The data shows that diastolic $[Ca^{2+}]_i$ did not change in response to salbutamol in control cells, from 115.6 ± 8.2nM to 117.4 ± 8.9nM (n=5(19);p=0.99), however diastolic $[Ca^{2+}]_i$

A.
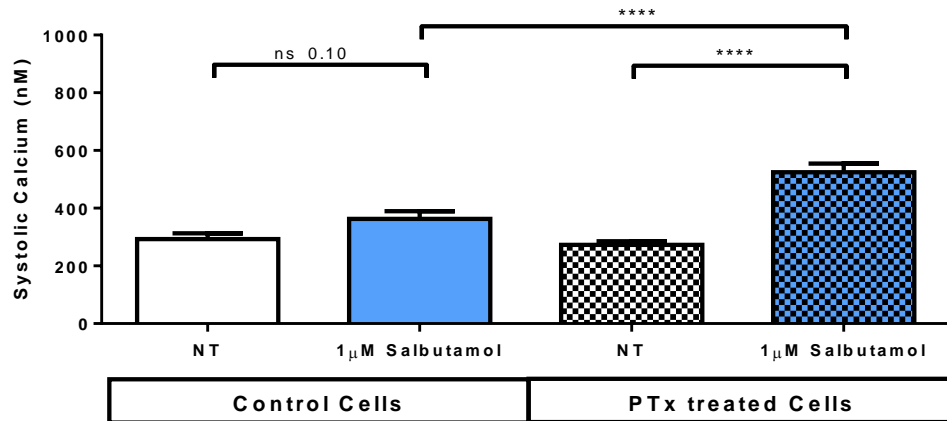
B.
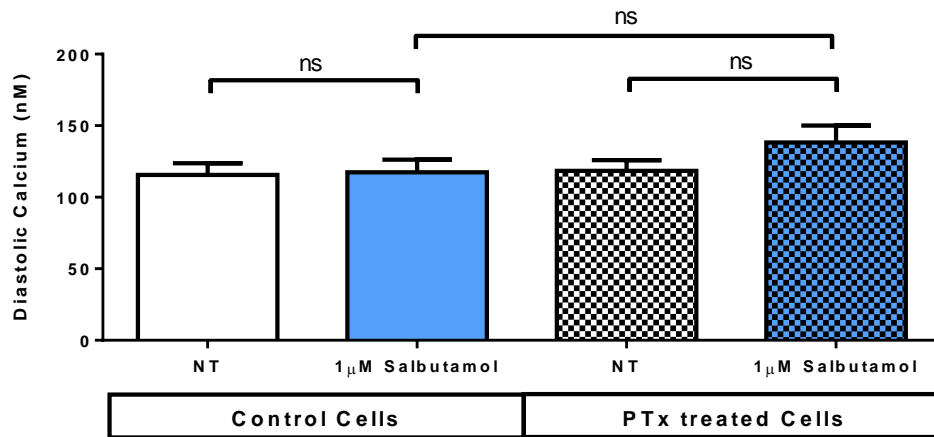
C.
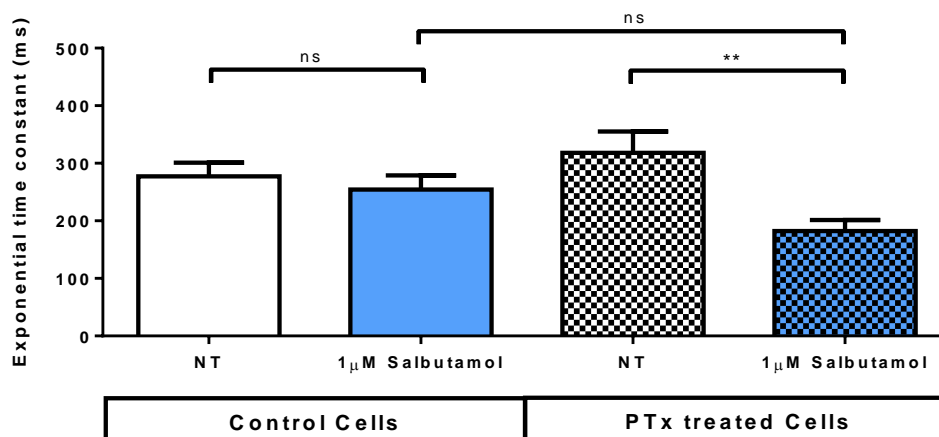
Figure 5.16 **The effect of G$_i$ inhibition on the response of Ca^{2+} transient to salbutamol.**
Bar charts showing **A.** systolic [Ca^{2+}], **B.** diastolic [Ca^{2+}] and **C.** exponential time constant
of the decay of the electrically-induced Ca^{2+} transient recorded from Control cells (open
bars) and PTx treated cells (hatched bars), after superfusion with 1μM salbutamol.
Values are mean ± S.E.M. Number of hearts (number of experiments); salbutamol
control cells, n=5(10-19), salbutamol PTx treated cells, n=5(17-18), unpaired t-test, * p <
0.05, *** p < 0.001.

increased in PTx-treated cells in response to salbutamol, from 118.4 ± 7.5nM to 138.3 ± 11.8nM (n=5(18)), although this was not significant (p=0.36). Despite an increase in diastolic $[Ca^{2+}]_i$ in PTx-treated cells in response to salbutamol, no difference between control and PTx-treated cells were found (p=0.30).

The data shows salbutamol had no effect on relaxation time in control cells, at 277.4 ± 23.5ms to 264.5 ± 23.8ms (n=5(18);p=0.88), however relaxation time was significantly shortened in PTx-treated cells in response to salbutamol, at 318.1 ± 37.1ms to 182.5 ± 19.0ms (n=5(13);p<0.01). Despite the reduction in relaxation time in PTx-treated cells in response to salbutamol, no difference between control and PTx-treated cells were found (p=0.17).

5.2.3.2.2 The effect of PTx treatment on the response of the action potential to salbutamol

I have previously shown that β_2-ADR stimulation with salbutamol has no effect on the cardiac action potential and that PDE inhibition during salbutamol perfusion increased APD (See Figure 5.16). As G_i uncoupling from the β_2-ADR augmented the increase in systolic $[Ca^{2+}]_i$ in response to β_2-ADR stimulation, I hypothesised this was due to a change in the action potential in response to salbutamol following G_i uncoupling.

To investigate the effect of G_i uncoupling on the response of the cardiac action potential to β_2-ADR stimulation, action potentials were recorded as previously described (See Methods 2.3.3.1) in control and PTx-treated cells in normal Tyrode and 1μM salbutamol.

Figure 5.19 shows the effect of salbutamol on the action potential, displaying a record of a single action potential recorded in normal Tyrode (black) and 1μM salbutamol (blue) recorded in A. Control cells and B. PTx-treated cells, and shows that whilst salbutamol had no effect on the cardiac action potential in control cells, PTx treatment caused a lengthening of action potential in response to salbutamol.

Figure 5.16C shows the mean APD_{30}, APD_{50} and APD_{90} in control and PTx-treated cells in response to salbutamol. The data shows no effect of salbutamol on the metrics of the action potential recorded from control cells; APD_{30}, from 15.7 ± 2.0ms to 17.5 ± 2.1ms (n=6(12);p=0.99), at APD_{50}, from 22.8 ± 4.0ms to 26.6 ± 4.1ms (n=6(10);p=0.93) and at APD_{90}, from 77.8 ± 7.8ms to 87.3 ± 6.7ms (n=6(10);p=0.43). However APD increased
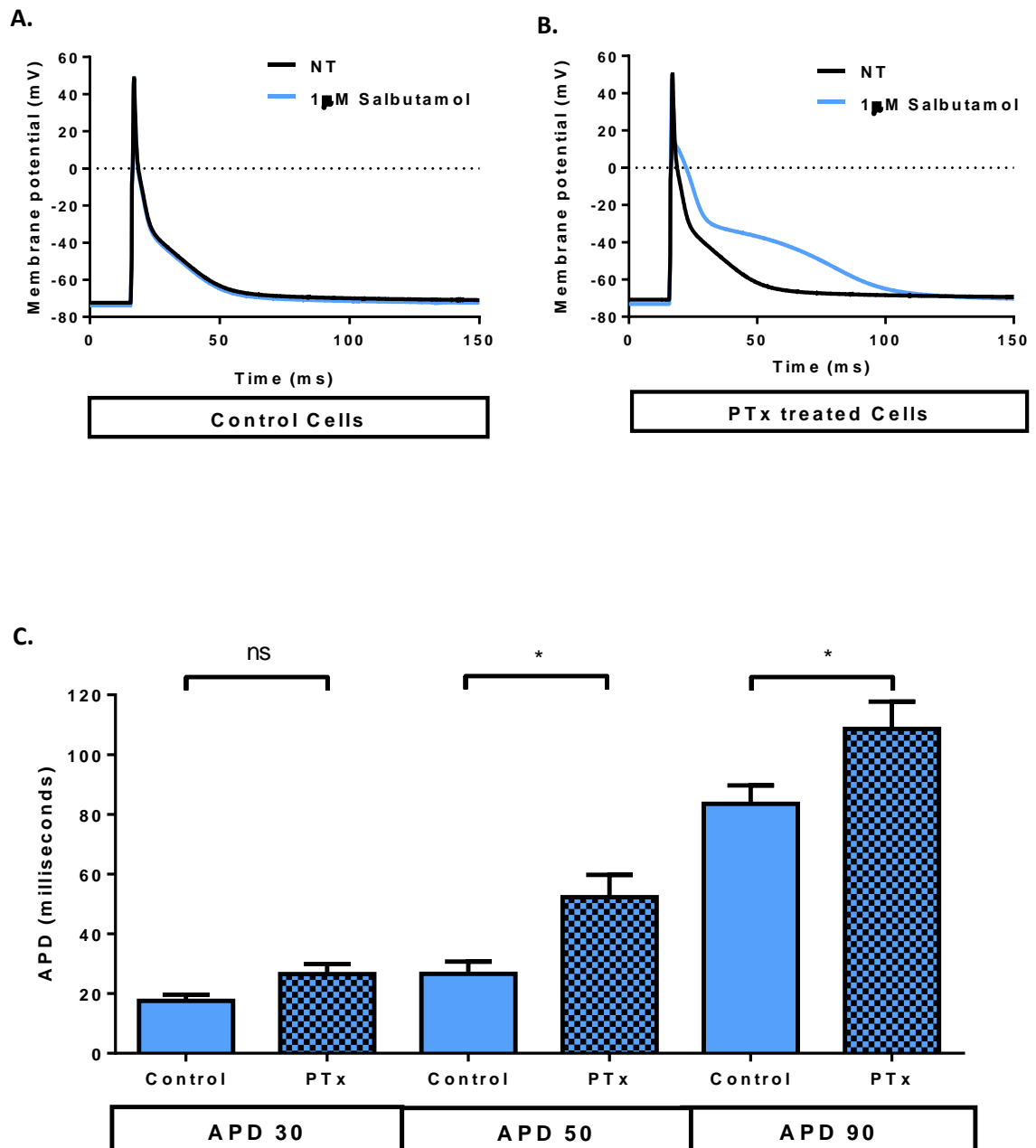
Figure 5.19   The effect of PTx treatment on the response of cardiac action potential to salbutamol.

Representative action potential recordings from **A.** Control myocytes and **B.** PTx-treated myocytes, superfused with normal Tyrode (black) and 1μM salbutamol (blue).

C. Bar chart showing APD_{30}, APD_{50} and APD_{90} recorded in Control (open bars, n=6(10-12)) and PTx-treated myocytes (hatched bars, n=7(12-14)) after superfusion with 1μM salbutamol. Values are mean ± S.E.M. Number of hearts (number of experiments); *p<0.05, one-way ANOVA, Sidak's *post-hoc* test.

significantly following salbutamol in PTx-treated cells, at APD_{30}, from 16.1 ± 2.0ms to 26.6 ± 3.3ms (n=7(12);p<0.01) and at APD_{50}, from 32.5 ± 5.1ms to 52.2 ± 7.5ms (n=7(13);p<0.05), but not at APD_{90}, from 93.8 ± 9.6ms to 108.6 ± 9.2ms (n=7(14);p=0.13).

As a result, APD in the presence of salbutamol was greater in PTX-treated cells than control cells at APD_{50}, 52.2 ± 7.5ms versus 26.6 ± 4.2ms (p<0.05), and APD_{90}, 108.6 ± 9.2ms versus 83.5 ± 6.7ms (p<0.05) as shown in Figure 5.17. APD_{30} was greater in PTx-treated cells, at 26.6 ± 3.3ms, as compared to control cells at 17.5 ± 2.1ms, although this was not significant (p=0.69).

5.2.2.2.3 The effect of PTx treatment on the response of L-type calcium current to salbutamol

I have just shown that G_i uncoupling from β_2-ADR increased $APD_{50/90}$ during salbutamol stimulation and so I set out to investigate the effect on the LTCC to see if an increase in LTCC can account for the increase in $APD_{30/50}$ following β_2-ADR stimulation in PTx treated cells.

To investigate the effect of G_i inhibition on response of the LTCC to β_2-ADR stimulation, the I/V relationship for the LTCC was obtained as previously described (See Methods 2.3.3.2) in normal Tyrode followed by 1µM salbutamol in control and PTx-treated cells.

Figure 5.20 shows the mean I-V relationship of LTCC recorded in normal Tyrode and in response to 1µM salbutamol in A. Control cells (n=4(9)) and B. PTx-treated cells (n=5(11)). The figure shows activation threshold and peak current/voltage was unaffected by PTx treatment.

The data shows that whilst salbutamol had little effect on LTCC in control cells, PTx-treatment caused a significant increase in the density of the LTCC in response to salbutamol between holding potentials -20mV and +20mV, representative of $APD_{50/50}$. PTx-treatment during β_2-ADR stimulation with salbutamol caused the maximal current to shift to a more negative potential, from -7.90 ± 0.70pA/pF at -10mV to -10.21 ± 1.01pA/pF at -20mV.
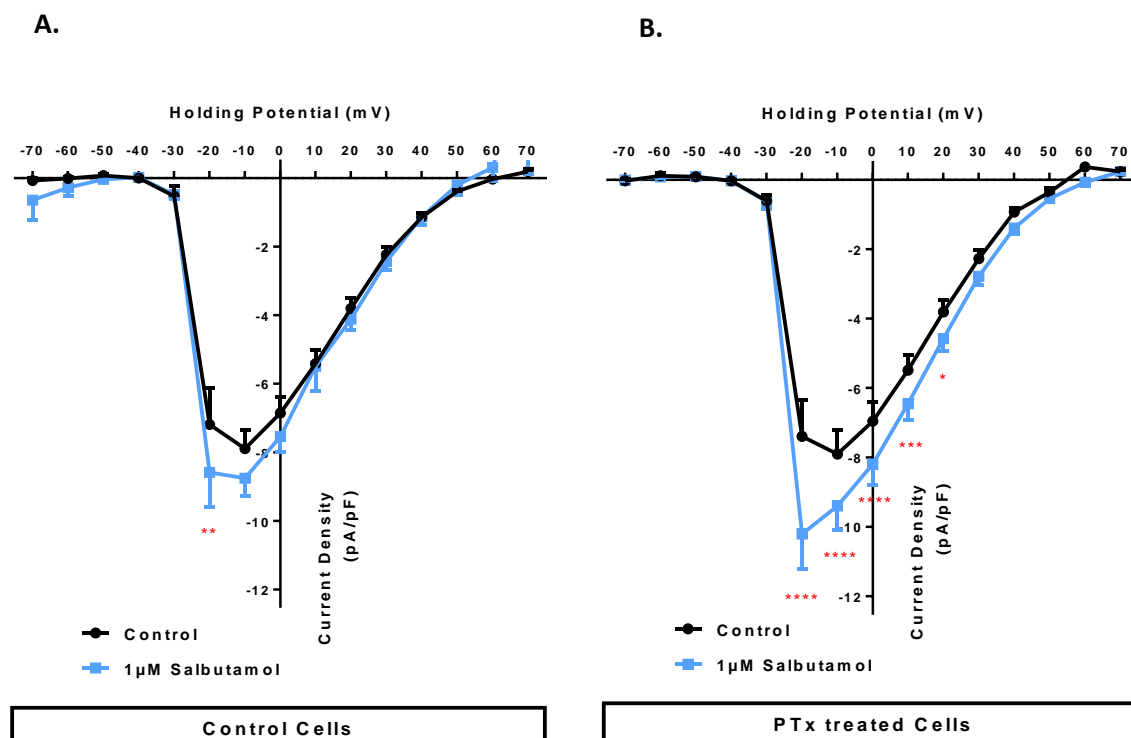
Figure 5.20   The effect of PTx treatment on the response of the L-type calcium current in response to salbutamol.

Current-voltage relationship of the LTCC recorded in normal Tyrode (black) and 1μM salbutamol (blue) from A. Control myocytes (n=4(9))   and B. PTx-treated myocytes (n=5(11)).

Values are mean ± S.E.M. Number of hearts (number of experiments); two-way ANOVA, Sidak's *post-hoc* test.

In summary;

These data shows disruption of the G_i protein by treatment of cells with PTx significantly increases the inotropic effect of β_2-ADR stimulation with salbutamol, observed as an augmented increase in systolic $[Ca^{2+}]$, SR Ca^{2+} content and the activity of SERCA. In addition, disruption of the G_i protein induced an increase in APD and the current density of LTCC in response to salbutamol. These data confirms the dual coupling of β_2-ADR to both G_s and G_i, the coupling to G_i dampening the full inotropic effect of β_2-ADR stimulation.

5.3   Discussion

In the present chapter I have investigated the roles of the β_1–ADR, β_2–ADR and β_3–ADR in sympathetic control of E-C coupling in rat ventricular myocytes. I have also investigated the role of phosphodiesterase activity and G_i protein coupling on E-C coupling in the β_2–ADR signalling pathway in the ventricular myocyte.

I have shown a positive effect of β_1-ADR stimulation with dobutamine on Ca^{2+} handling, observed as an increase in systolic $[Ca^{2+}]_i$, SR Ca^{2+} content, and an increase in the density of the LTCC current. A reduction in relaxation time of both the electrically-induced Ca^{2+} transient and the caffeine-induced Ca^{2+} release in response to dobutamine were also observed, indicating an increase in the activity of SERCA and NCX respectively. This positive effect on Ca^{2+} handling was similar to the positive inotropic effect of ISO stimulation.

Specific β_2-ADR activation with salbutamol caused an increase in systolic $[Ca^{2+}]_i$ and SR Ca^{2+} content but at maximal activation this was significantly lower compared to β_1-ADR activation. My data suggests that this is due to the coupling of the β_2-ADR to the G_i protein and subsequent activation of PDE responsible for the breakdown of cAMP as inhibition of PDE with IBMX resulted in an additional increase in systolic $[Ca^{2+}]_i$, SR Ca^{2+} stores and SERCA activity above the increase induced by salbutamol alone. There was also an increase in $APD_{30/50}$ which was reflected by changes in the LTCC but no effect on I_{to}.

Uncoupling of G_i with PTX resulted in an augmented increase in systolic $[Ca^{2+}]$, SR Ca^{2+} content and the activity of SERCA, with no change in NCX activity. There was also an increase in $APD_{30/50/90}$ which was reflected by changes in the LTCC, suggesting a coupling of G_i to the β_2-ADR which is responsible for the activation of PDE which lead to the compartmentalised cAMP signalling of the β_2-ADR

I have also shown, in contrast to β_1–ADR and β_2–ADR stimulation, specific β_3-ADR stimulation with BRL_{37344} induces a negative effect on Ca^{2+} handling, reducing systolic $[Ca^{2+}]_i$ and SR Ca^{2+} stores, whilst supporting relaxation, indicated by an increase in SERCA activity, which is somewhat paradoxical, as this might be expected to increase rather than reduce the SR Ca^{2+} stores as I showed. Stimulation of β_3-ADR with BRL_{37344} also induced a reduction in $APD_{30/50}$, with no accompanying change in I_{to} or LTCC current densities.

5.3.1 Sympathetic control of Excitation-Contraction coupling in rat ventricular myocytes

Sympathetic stimulation induces a positive inotropic and lusitropic effect on the ventricular myocardium, resulting mainly from an increase in systolic $[Ca^{2+}]_i$ and an increase in the rate of Ca^{2+} sequestration, which both increases the rate of relaxation and SR Ca^{2+} stores. These changes in myocardial function are elicited by the binding of adrenaline and nor-adrenaline to β-ADR. The endogenous catecholamines bind to all 3 β-ADR and so the effect of adrenaline and nor-adrenaline are the result of the combined activation of $β_1$-ADR, $β_2$-ADR and $β_3$-ADR (Bers 2001). Adrenaline preferentially binds $β_2$ > $β_1$ > $β_3$, nor-adrenaline $β_1 = β_3 > β_2$ (Vrydag and Michel 2007).

70% of the β-ADR in the ventricle are $β_1$-ADR, with the remaining 20-30% $β_2$-ADR and $β_3$-ADR (Wallukat 2002; Brodde, Bruck et al. 2006). Physiological levels of adrenaline and nor-adrenaline in the plasma, 0.1-0.3nM and 0.5-3.0nM, rise to ~5nM and ~10nM during exercise (Levick 2013). At these physiological levels, adrenaline and nor-adrenaline bind to $β_1$-ADR and $β_2$-ADR and induce a positive inotropic and lusitropic effect in myocytes via the classical β-ADR/cAMP/PKA pathway. PKA phosphorylation of LTCC, RyR2, PLB and TnI lead to increases in LTCC, Ca^{2+} release from the SR during CICR, a faster uptake of Ca^{2+} to the SR during relaxation and a faster off rate of Ca^{2+} from TnC respectively (Bers 2002). (See introduction 1.2).

At higher levels of sympathetic stimulation, adrenaline and nor-adrenaline will also bind to $β_3$-ADR, which induce a negative inotropic effect. The $β_3$-ADR has a lower affinity for catecholamines and so a greater concentration is required for $β_3$-ADR stimulation. The $β_3$-ADR mediated negative inotropic effects have been shown to be elicited at near pathophysiological levels of nor-adrenaline, however this was under $β_1$-ADR and $β_2$-ADR blockade (Gauthier, Tavernier et al. 1996). The negative inotropic effect of $β_3$-ADR is mediated by NO that involves both cGMP-dependant (PKG phosphorylation) and cGMP-independent (S-nitrosylation) pathways, which are able to directly affect components of E-C coupling including the LTCC, RyR2, PLB and TnI (Gauthier, Leblais et al. 1998; Layland, Li et al. 2002; Rozec and Gauthier 2006; Yang, Liu et al. 2007).

ISO is a synthetic agonist which mimics the effect of the endogenous catecholamines adrenaline and nor-adrenaline (Alexander, Benson et al. 2013). ISO is a full agonist at all 3

β-ADR, preferentially binding $\beta_1 > \beta_2 > \beta_3$, and so like the endogenous catecholamines adrenaline and nor-adrenaline, the response of the myocyte to ISO stimulation is the result of the combined activation of β_1-ADR, β_2-ADR and β_3-ADR (Bers 2001). ISO preferentially activates β-ADR over α-ADR, therefore allows the β-ADR pathways to be studied in isolation (Alexander, Benson et al. 2013).

In this investigation, ISO induced a positive effect on Ca^{2+} handling, observed as an increase in systolic $[Ca^{2+}]_i$, SR Ca^{2+} content, SERCA and NCX activity. ISO, through PKA phosphorylation of LTCC increases LTCC. Although I did not measure LTCC, I measured APD, and ISO increased APD_{30} and APD_{50} which is indicative of an increase in LTCC and there are numerous accounts in the literature of an increase in LTCC by ISO, including from our group (Collins and Rodrigo 2010). The observed increase in SR Ca^{2+} content is the result of an increased activity of SERCA I observed, due to PKA phosphorylation of PLB, but also due to the increase in LTCC. This is important as LTCC only contributes to approximately 10% of the increase in systolic $[Ca^{2+}]_i$, the remaining 90% of the increase in systolic is due to the Ca^{2+} release from the SR (Wier, Egan et al. 1994; Bassani, Yuan et al. 1995; Bers 2001). The increase in the activity of the NCX as observed is compensatory of the increase in LTCC, as Ca^{2+} in through the LTCC must equal Ca^{2+} extrusion by the NCX over a number of beats to maintain steady state E-C coupling (Bers 2002; Eisner, Kashimura et al. 2009).

5.3.1.1 β_1-ADR control of Excitation-Contraction coupling in rat ventricular myocytes

The β_1-ADR is the most abundant in the ventricle, distributed across the entire cell and functionally present at surface sarcolemma and t-tubules in rat ventricle. During physiological levels of β-ADR stimulation the β_1-ADR and β_2-ADR preferentially activated due to their higher affinity for circulating catecholamines than the β_3-ADR (Alexander, Benson et al. 2013). The positive inotropic effect of β_1-ADR stimulation is mediated by the classical β-ADR/cAMP/PKA pathway. Unlike the β_2-ADR, β_1-ADR signalling is diffusive within the myocyte and leading to a global rise in cAMP (Chen-Izu, Xiao et al. 2000). β_1-ADR stimulation is able to induce an increase in the Ca^{2+} transient in both the intact myocyte and in detubulated cells, indicting the presence of β_1-ADR at the sarcolemma and

the T-tubules, however quantitative analysis of the data has shown β_1-ADR stimulation to be three times more effective at inducing an increase in Ca^{2+} transient at the sarcolemma than the T-tubules (Cros and Brette 2013), suggesting that the dominant effect of the β_1-ADR signalling comes from receptors on the sarcolemma rather than in the T-tubules.

To examine the role of β_1-ADR signalling in the rat myocyte, I investigated the response of Ca^{2+} handling and cardiac electrophysiology to the specific β_1-ADR agonist dobutamine. dobutamine is a selective β_1-ADR agonist used clinically to treat cardiogenic shock (Alexander, Benson et al. 2013).

In this investigation I have shown an effect of dobutamine on both Ca^{2+} handling and electrophysiological parameters which correlates closely with the data collected following ISO administration.

Perfusion of cells with dobutamine lead to an increase in systolic $[Ca^{2+}]_i$ and diastolic $[Ca^{2+}]_i$, an increase in SR Ca^{2+} content and a reduction time of the electrically-induced Ca^{2+} transient (increase in SERCA activity) caffeine-induced Ca^{2+} transient (increase in NCX activity). Although there is limited data available which discusses the action of dobutamine on isolated ventricular myocytes, investigation of the action of dobutamine in the intact rat heart has shown an increase in contractility which was accompanied by an increase in the amplitude of the Ca^{2+} transient (Auffermann, Stefenelli et al. 1989; Stefenelli, Wikman-Coffelt et al. 1990) and systolic $[Ca^{2+}]_i$ (Stefenelli, Wikman-Coffelt et al. 1990). Investigations into the effect of β_1-ADR stimulation in the isolated myocyte has mainly focused on the use of ISO with a β_2-ADR blocker, which have also shown an increase in increase in the amplitude of the Ca^{2+} transient and systolic $[Ca^{2+}]_i$ (Xiao and Lakatta 1993; Chen-Izu, Xiao et al. 2000). Chen-Izu *et al.* also demonstrated an increased phosphorylation of PLB following perfusion of cells with ISO under β_2-ADR blockade (Chen-Izu, Xiao et al. 2000). An increase in PLB phosphorylation removes its inhibitory effect from SERCA, increasing SERCA activity and the rate of Ca^{2+} extrusion from the cytoplasm during relaxation but also increasing SR Ca^{2+} stores. These finding support my own of an inotropic response to β_1-ADR stimulation with dobutamine. The increase in the activity of the NCX I have observed will increase the competition for available Ca^{2+} indicating a greater extrusion of Ca^{2+} from the myocyte via the NCX during relaxation, helping to maintain steady-state E-C coupling. However, recently Yan *et al.* have shown that dobutamine increases NCX activity as a consequence of an up regulation of voltage gated Na^+ channel

214

function, promoting "reverse-mode" and Na^+ extrusion rather than Ca^{2+} extrusion (Yan, Ban et al. 2015), which would contribute to lengthening APD and may go some of the way to increasing SR Ca^{2+} content we have observed, as more Ca^{2+} is sequestered back to the SR as NCX Ca^{2+} extrusion is inhibited. Although I did not measure the phosphorylation of TnI, other groups have shown dobutamine can increase TnI phosphorylation by 10 fold (Chou, Lo et al. 2012), increasing the off rate of Ca^{2+} from TnC allowing Ca^{2+} to be removed from the cytosol at a faster rate by SERCA and the NCX.

Dobutamine increased APD at all parameters (ADP$_{30/50/90}$), which confers with data from Yan et al. who observed an increased APD in mouse isolated ventricular myocytes (Yan, Ban et al. 2015). As I observed no effect on I_{to} in response to dobutamine, the increase in ADP$_{30/50}$ was assumed to be due to the increase in the LTCC that I have observed. The increase in the current density is due to a phosphorylation of the LTCC, increasing the P_o by shifting the voltage-dependant activation to a more negative E_m (Bers 2001), indeed the peak current increased 1.5 fold in response to dobutamine and that activation shifted to a more negative potential, which confers with the current literature showing an increase in LTCC in response to dobutamine in the intact mouse heart (Vandsburger, French et al. 2012) and isolated mouse myocytes (Yan, Ban et al. 2015), with no effect on I_{to} (Yan, Ban et al. 2015).

In my hands dobutamine hyperpolarised RMP, suggesting an increased K^+ conductance and therefore a stronger repolarising current, which might be expected to speed up late phase repolarisation, however APD$_{90}$ paradoxically increased during dobutamine superfusion and measurement of the K^+ steady state current, an indication of I_{K1}, indicated no change in the current density in response to dobutamine.

5.3.1.2 β_2-ADR control of Excitation-Contraction coupling and the dual coupling to the G_i inhibitory protein in rat ventricular myocytes

During physiological levels of β-ADR stimulation the β_2-ADR are activated due to their high affinity for circulating catecholamines (Alexander, Benson et al. 2013) and may have a modifying effect on the response to β_1-ADR activation. β_2-ADR signalling is highly compartmentalised, due to activation of PDE3 and PDE4 which hydrolyse cAMP, limiting cAMP diffusion in the cytosol to only local targets of E-C coupling (LTCC and NCX), with a failure to phosphorylate distal E-C coupling protein targets (PLB, RyR2 and TnI), and this limits the inotropic effect of β_2-ADR stimulation (Xiao, Ji et al. 1995; Xiao, Avdonin et al. 1999; Xiao 2001; Heijman, Volders et al. 2011; Cros and Brette 2013).

In this investigation salbutamol was used to selectively simulate β_2-ADR, which is used clinically as a short term bronchodilator (Alexander, Benson et al. 2013).

I have shown that stimulation of the β_2-ADR lead to an increase in systolic $[Ca^{2+}]$, SR Ca^{2+} content and an increase in SERCA activity. I have also shown that unlike stimulation with ISO or the β_1-ADR specific agonist dobutamine, bath application of the β_2-ADR agonist salbutamol failed to induce an increase in the LTCC, which correlated with no change in $APD_{30/50}$.

The inability of β_2-ADR to phosphorylate distal targets of E-C coupling due to compartmentalisation of β_2-ADR derived cAMP was first identified in the frog ventricular myocyte, in which the β_2-ADR subtype dominates over the β_1-ADR subtype. Local β_2-ADR stimulation with ISO at one end of the cell increased LTCC current density at the local LTCC, however there was little stimulatory effect on remote LTCC at the opposite end of the myocyte, measured by whole-cell recording of I_{Ca} using two-patch clamp electrodes and two amplifiers (Jurevicius and Fischmeister 1996). This has also been shown in rat ventricular myocytes, with β_2-ADR stimulation only able to increase LTCC when the agonist was applied to the myocyte in the recording pipette during patch-clamp recordings (local stimulation), and not when the agonist was applied in the perfusion solution (diffuse stimulation) (Chen-Izu, Xiao et al. 2000). However, from this evidence I would have expected salbutamol to have a greater effect on LTCC than SERCA/PLB function. This lack of an increase in LTCC is perhaps paradoxical as the LTCC are local targets of phosphorylation by β_2-ADR mediated increase in local cAMP levels. Moreover, my data shows an increase in systolic $[Ca^{2+}]_i$ in spite of a lack of increase in LTCC. However, due to the proximity of the RyR2 to β_2-ADR, the RyR2 could perhaps be a local target for

phosphorylation and this may explain the increase in $[Ca^{2+}]_i$ as ~90% of the increase in systolic $[Ca^{2+}]_i$ during contraction is due to Ca^{2+} release from the SR during CICR (Wier, Egan et al. 1994). PKA mediated phosphorylation of RyR2 increases the sensitivity to an incoming LTCC increasing the P_o of the receptor, enhancing CICR, and so despite no increase in LTCC the increase in systolic $[Ca^{2+}]_i$ may be due to a greater Ca^{2+} release from the SR during CICR. However, a number of splice variants of PDE3 and PDE4 are known to localise to the SR, PDE3A-135 (Movsesian 2002) and the RyR2, PDE4D3 (Kass 2008), which may prevent phosphorylation of RyR2 and PLB during β_2-ADR stimulation, preventing increases in PKA around the SR.

My data also shows an increase in the SR Ca^{2+} content, likely to be caused by the increase in SERCA activity I observed. An increase in the size of the SR Ca^{2+} store could also be responsible, at least in part, for the increase in systolic $[Ca^{2+}]_i$. CASQ has been proposed to act as a luminal Ca^{2+} sensor, inhibiting RyR2 P_o at low luminal concentrations of Ca^{2+}, but increasing RyR2 P_o at high luminal concentrations of Ca^{2+} (Gyorke and Terentyev 2008). It is possible the increase in SR Ca^{2+} stores due to SERCA activity may promote RyR2 P_o. However, at any one time the P_o of the RyR2 is determined by luminal and cytoplasmic concentrations of Ca^{2+} and the lack of an increase in LTCC in response to β_2-ADR stimulation will impact upon this, and may in part be responsible for the apparent reduced response as compared to β_1-ADR stimulation.

The increase in SERCA activity in response to β_2-ADR stimulation was surprising, as PLB is considered a distal target for the β_2-ADR derived cAMP and PKA phosphorylation (Xiao, Ji et al. 1995; Xiao, Avdonin et al. 1999; Xiao 2001). It is possible that the increase in SR Ca^{2+} stores was not caused by PKA phosphorylation and instead may have been caused by CaMKII. CaMKII targets the same E-C coupling proteins as PKA, including RyR2 (Ferrero, Said et al. 2007) and PLB (Said, Mundina-Weilenmann et al. 2002) mediating Ca^{2+} release from the SR (Curran, Hinton et al. 2007; Ferrero, Said et al. 2007) and increasing contractility (Wang, Zhu et al. 2004). Baltas *et al.* have shown global β-ADR activation can activate CaMKII in the intact beating heart (Baltas, Karczewski et al. 1997). CaMKII activation is induced by an increase in local Ca^{2+} and so a global increase in cytoplasmic Ca^{2+} is not required for activation, meaning that slight increases in Ca^{2+} in the dyadic cleft would activate CaMKII (Grimm and Brown 2010) and may lead to the CaMKII phosphorylation of PLB at Thr17 (Said, Mundina-Weilenmann et al. 2002) (the same phosphorylation site as PKA) lead to the increase in SERCA activity I have shown here. My

findings would suggest the β_2-ADR specific agonist may be able to activate CaMKII, which has not been shown before and needs further investigation. If PKA phosphorylation of RyR2 had occurred as I have suggested, this increased P_o and greater release of Ca^{2+} from the SR could activate CaMKII and lead to phosphorylation of PLB increasing SERCA activity, and over a number of beats increase SR Ca^{2+} content.

It is proposed that the NCX can act as a trigger for CICR and the location of the NCX at the sarcolemma makes the NCX a potential local target for β_2-ADR mediated PKA phosphorylation. Although it is widely accepted that PKA can phosphorylate the NCX (Barman, Choisy et al. 2011), the results of investigation into the ability of PKA to increase NCX activity remains controversial with reports of no change (Fan, Shuba et al. 1996; Main, Grantham et al. 1997) or an increased activity of the NCX (Pabbathi, Zhang et al. 2002). In my investigation I did not detect any change in the activity of the NCX, and so it is unlikely the NCX is responsible for the increased systolic $[Ca^{2+}]_i$.

Electrically there was no change in $APD_{30/50}$, which was not surprising as there were no observable changes in the I_{to} or the LTCC, however perfusion of cells with salbutamol induced a small, but significant lengthening of APD_{90}, indicating a reduction in the current density of repolarising currents, which was contrary to the observed hyperpolarisation of RMP in response to salbutamol. Measurement of the K^+ steady state current, an indication of I_{K1}, indicated no change in the I_{K1} current density in response to β_2-ADR stimulation.

The positive inotropic effect of PDE inhibition and G_i uncoupling on β_2-ADR signalling:

The overall effect of β_2-ADR stimulation in this investigation is a modest inotropic effect, which was less that that observed by a maximal concentration of the β_1-ADR agonist dobutamine. This reduced effect is likely to be due to compartmentalised cAMP signalling in the myocyte, as described earlier. A more pronounced inotropic effect of salbutamol was observed in the presence of the global PDE inhibitor IBMX and following uncoupling of the G_i protein from the β_2-ADR by PTx treatment. This resulted from a classic "β_1-ADR style action", where LTCC and SR function (SERCA activity, SR Ca^{2+} content) were enhanced.

In the rat heart, 60% of cAMP degradation is mediated by PDE4, 20-30% by PDE3 and the remaining 10-20% is mediated by PDE1 and PDE2. However, this is species dependant and in humans PDE4 only accounts for 10% cAMP degradation (Mika, Leroy et al. 2012). Removing the action of PDE3 and PDE4, either by inhibition with IBMX or preventing their activation by G_i uncoupling, prevents to break down of cAMP allowing diffusion away from the β_2-ADR and to impact on distal targets to the β_2-ADR (Gonzalez-Munoz, Fuente et al. 2009).

My data shows an augmented increase in the size of SR Ca^{2+} stores by salbutamol in the presence of PDE inhibition, likely to be caused by an increase in SERCA activity, which was detected as a reduction in relaxation time of the electrically-induced Ca^{2+} transient, which would drive the increase in SR Ca^{2+} content that I observed. Coupled with the increase in LTCC, this SR Ca^{2+} load and possible increase in RyR2 activity (not determined in my study) is probably responsible for the enhanced Ca^{2+} transient observed. PDE inhibition in ventricular myocytes during β_2-ADR stimulation has been documented to lead to an increased cardiac contractility mediated by increase in global cAMP levels (Gonzalez-Munoz, Fuente et al. 2009), the amplitude of the Ca^{2+} transient (Beca, Aschars-Sobbi et al. 2011), PLB phosphorylation (Kerfant, Zhao et al. 2007; Beca, Aschars-Sobbi et al. 2011) and an increased SR Ca^{2+} load (Kerfant, Zhao et al. 2007; Beca, Aschars-Sobbi et al. 2011), although no change in RyR2 phosphorylation (Beca, Aschars-Sobbi et al. 2011). However, the effects on the LTCC are mixed with reports of either an increase in LTCC (Matsui, Kiyosue et al. 1999) or no change in the LTCC (Kerfant, Zhao et al. 2007; Beca, Aschars-Sobbi et al. 2011). In line with current literature, during β_2-ADR stimulation in the presence of PDE inhibition $APD_{30/50/90}$ were all significantly prolonged and this possibly reflected the increased the current density of the LTCC as the I_{to} current density was not affected by PDE inhibition. Matsui *et al.* investigated PDE inhibition with a number of clinically used PDE inhibitors, and have shown that the additional positive inotropic effect of PDE inhibition is roughly proportional to the drugs ability to increase the LTCC (Matsui, Kiyosue et al. 1999) and showed that a maximal increase in LTCC , of around 2-fold was seen during β_2-ADR stimulation with IBMX following PDE inhibition.

PTx treatment of cells to uncouple G_i from the β_2-ADR, has also been shown to augment contractility on response to β_2-ADR stimulation. As G_i no longer activates the PDE responsible for the compartmentalised cAMP signalling, cAMP signalling becomes diffuse

in the cell. My findings of an augmented increase in systolic $[Ca^{2+}]_i$, an increase in SERCA activity and a greater current density of the LTCC following PTx treatment, correlates with the current literature in which PTx treatment of myocytes lead to increases in the amplitude of the Ca^{2+} transient (Xiao, Ji et al. 1995), the LTCC (Xiao, Ji et al. 1995; Xiao, Avdonin et al. 1999; Xiao 2001) and phosphorylation of PLB (Xiao 2001) and greater contractility of the myocyte. The use of PTx treatment to uncouple G_i from the β_2-ADR shows that the increase in PDE activity is likely to be due to G_i coupled signalling.

5.3.1.3 β₃-ADR control of Excitation-Contraction coupling in rat ventricular myocytes

The gene encoding the β_3-ADR were first identified in humans in 1989 (Emorine, Marullo et al. 1989) and has since been identified in numerous species including the rat in 1991 (Granneman and Whitty 1991). The β_3-ADR has been found to be functionally present in rat ventricle (Gauthier, Tavernier et al. 1999) eliciting a negatively inotropic effect, reducing contractility in the myocyte, mediated by a β-ADR/NO/PKG pathway (See Introduction 1.2.4).

It is thought that the β_3-ADR pathway may act as a negative feedback mechanism in the heart, preventing damage from excessive $\beta_{1/2}$-ADR stimulation during periods of high levels of circulating catecholamines. This came from the observation that a negatively inotropic effect was seen at near pathophysiological levels of nor-adrenaline (0.7μM), under $\beta_{1/2}$-ADR blockade (Gauthier, Tavernier et al. 1996). Indeed, β_3-ADR and NO have recently been identified in cardio-protective mechanisms against ischemia-reperfusion injury (Aragon, Condit et al. 2011; Calvert, Condit et al. 2011; Heusch 2011) and hypertrophy induced by excessive β-ADR stimulation (Belge, Hammond et al. 2014) and pressure overload hypertrophy (Niu, Watts et al. 2012).

To examine the role of β_3-ADR signalling in the rat myocyte, I investigated the response of Ca^{2+} handling and cardiac electrophysiology to the specific β_3-ADR agonist BRL$_{37344}$. BRL$_{37344}$ is a "rodent specific" selective β_3-ADR agonist (Alexander, Benson et al. 2013), as several agonists of the β_3-ADR which are functional in humans, such as CL$_{316243}$ or CGP$_{12177}$, have no effect in the rat. BRL$_{37344}$ was the only β_3-ADR agonist eliciting a significant negative

inotropic effect in the rat, and interestingly BRL_{37344} proved the most potent β_3-ADR agonist in the human heart (Gauthier, Tavernier et al. 1999).

Use of the agonist BRL_{37344} has been questioned in the past, as some studies have found that at μM concentrations it can act as a weak agonist at the β_1-ADR and β_2-ADR. BRL_{37344} has a rank order of potency of $\beta_3 > \beta_2 > \beta_1$, Ki values (nM) β_3; 287, β_2; 1120, β_1; 1750, and so the concentration of 200nM selected for my investigation would not have acted as an agonist at β_1-ADR and β_2-ADR at this concentration

The effect of BRL_{37344} on Ca^{2+} regulation:

I observed a dose dependant negative effect on Ca^{2+} handling in response to β_3-ADR stimulation with BRL_{37344}, determined as a reduction in systolic $[Ca^{2+}]_i$ and SR Ca^{2+} content. The reduction in systolic $[Ca^{2+}]_i$ has been reported before in the human and rat ventricle in response to BRL_{37344} (Gauthier, Leblais et al. 1998; Deng, Wu et al. 2009). I have also observed a reduction in relaxation time of the Ca^{2+} transient (indicative of SERCA activity) which is a novel finding in the isolated rat ventricular myocyte.

BRL_{37344} stimulation of β_3-ADR leads to the production of NO which elicits its effects via cGMP-dependant PKA phosphorylation of E-C coupling proteins or by cGMP-independent mechanisms, e.g. S-nitrosylation. As mentioned in the previous chapter (Chapter 3), there is currently a great deal of interest in determining which isoform of NOS (eNOS/nNOS) are responsible for the increase in NO and resulting reduction in contractility following β_3-ADR stimulation and the precise isoform involved is still controversial.

The BRL_{37344} mediated increase in SERCA activity is likely to be brought about via phosphorylation of PLB. PLB is localized to the SR and so is situated close to nNOS which co-immunoprecipitates with RyR2 on the SR (Massion, Pelat et al. 2005) and so nNOS is well placed to affect the phosphorylation state of PLB. Zhang *et al.* and others have reported nNOS inhibition or gene deletion in the mouse myocyte slows the rate of relaxation by decreasing the phosphorylation of PLB at Ser16, both implicating cGMP-independent mechanisms (Wang, Kohr et al. 2008; Zhang, Zhang et al. 2008). This indicates that nNOS can impact upon PLB phosphorylation and so may increase in SERCA activity, which may explain the reduction in relaxation time we have observed following BRL_{37344} stimulation of β_3-ADR.

The increase in SERCA activity I have observed might have been expected to increase SR Ca^{2+} content, however I have observed a paradoxical decline in SR Ca^{2+} content. An increase in SERCA activity and the resulting enhanced sequestration of Ca^{2+} to the SR during relaxation is usually associated with an increased SR Ca^{2+} load and an increase in contraction strength (Bers 2002). However, in my investigation the increase in SERCA activity was associated with a negative inotropic effect of BRL_{37344} and a reduction in SR Ca^{2+} stores. As mentioned in Chapter 3, a possible explanation for this may be the effects of NO produced by nNOS. NO has been shown to increase the P_o of the RyR2, leading to an increase in diastolic leak (Ziolo, Kohr et al. 2008), thereby reducing SR Ca^{2+} content (Barouch, Harrison et al. 2002). Any Ca^{2+} leak from the SR would be expected to increase diastolic $[Ca^{2+}]_i$, and indeed I did observe this, and so it is possible a RyR2 leak is responsible for the reduction in SR Ca^{2+} content in the face of an increase in SERCA activity. Again, due to the co-localisation of the RyR2 to nNOS I believe nNOS is likely to be the isoform responsible for any increase in RyR2 leak. Indeed, Lim $et\ al.$ have shown nNOS derived NO increases RyR2 leak, particularly at high SR Ca^{2+} loads, and propose this is due to an increased RyR2 channel phosphorylation by PKG (Lim, Venetucci et al. 2008). RyR2 P_o can also be increased by S-nitrosylation as the RyR2 have a number of thiol residues which when S-nitrosylated increase the P_o of the RyR2 (Stoyanovsky, Murphy et al. 1997; Xu, Eu et al. 1998). Any increase in RyR2 P_o, which could also have contributed to a diastolic leak from the SR, leading to the reduction in SR Ca^{2+} content we have observed.

The effect of BRL$_{37344}$ on electrical activity:

I found a reduction in $APD_{30/50}$ but no effect of $β_3$-ADR stimulation with BRL_{37344} on the current density of the I_{to}, LTCC or I_{K1}. This was surprising, as others have shown a reduction in LTCC in response to BRL_{37344} in both rat (Zhang, Cheng et al. 2005) and rabbit ventricular myocytes (Bundgaard, Liu et al. 2010). A reduction in LTCC will reduce the trigger for CICR from the SR during contraction, thereby reducing systolic $[Ca^{2+}]_i$. Any reduction in LTCC is likely to be mediated via eNOS derived NO deactivating the LTCC via PKA phosphorylation at Ser533 (van der Heyden, Wijnhoven et al. 2005), however, in our hands no reduction in LTCC was found following BRL_{37344}. It is possible that the reduction in $APD_{30/50}$ is the consequence, rather than the cause, of a reduced systolic $[Ca^{2+}]_i$ we have observed. The

combination of reduced systolic $[Ca^{2+}]_i$ and SR Ca^{2+} content and the increase in SERCA activity we have observed will mean that a lower $[Ca^{2+}]$ is released into the cytoplasm during contraction and that $[Ca^{2+}]$ released is sequestered back to the SR at a faster rate, allowing for a faster decline in $[Ca^{2+}]$ during relaxation, which may impact on the plateau and repolarising phases of the action potential, shortening APD as the balance between the opposing LTCC and I_{Kr}/I_{Ks} currents is altered (Bers 2001), allowing the I_{Kr}/I_{Ks} repolarising currents to dominate earlier. It is also possible that β_3-ADR stimulation with BRL$_{37344}$ may have impacted upon the repolarising currents which are able to influence APD. Although we observed no change in I_{K1} in response to BRL$_{37344}$, others have found an acceleration of repolarisation due to an increased I_{Ks} current density following BRL$_{37344}$ in guinea pig (Bosch, Schneck et al. 2002) and rabbit (Audigane, Kerfant et al. 2009) ventricular myocytes. During the plateau phase of the action potential, the repolarising currents I_{Kr} and I_{Ks} oppose the depolarising LTCC, and so any increase in the current density of I_{Kr} and I_{Ks} will upset the balance between inward depolarising and outward repolarising currents and accelerate repolarisation, which may account for the reduction in APD$_{30/50}$ that we have observed. However, we did not measure the I_{Ks} current and so cannot determine if BRL$_{37344}$ had any effect on this repolarising current, however, it should be noted that the guinea pig and rabbit have stronger repolarising I_{Kr} and I_{Ks} currents, and so any effect seen on these currents due to BRL$_{37344}$, may be less prominent in the rat.

In this investigation BRL$_{37344}$ stimulation of the β_3-ADR lead to a reduction in systolic $[Ca^{2+}]_i$, SR Ca^{2+} content and a corresponding reduction in APD$_{30/50}$. As I found no effect of β_3-ADR stimulation with BRL$_{37344}$ on the current density of the LTCC, the reduction in SR Ca^{2+} content is mostly the cause of the reduction in systolic $[Ca^{2+}]_i$ and the resulting decline in contractility and shortening of APD$_{30/50}$, as ~90% of the increase in systolic $[Ca^{2+}]_i$ during contraction is due to Ca^{2+} release from the SR during CICR (Wier, Egan et al. 1994). The reduction in SR Ca^{2+} content means a lower concentration of Ca^{2+} can be released via the RyR2 during CICR, reducing systolic $[Ca^{2+}]_i$.

5.3.2 Conclusions

Majority of the response to ISO is mediated by the β_1-ADR, due to compartmentalisation of β_2-ADR derived cAMP, limiting the ability of the β_2-ADR to elicit a strong inotropic effect.

In the healthy myocyte, dual coupling of the β_2-ADR to G_i provides a 'break' against excessive sympathetic activity by limiting the drivers of arrhythmia. β_2-ADR in the myocardium may be a mechanism to focus the β-ADR signal to the LTCC, enhancing the trigger for CICR increasing contractility, whilst limiting the adverse effects of β-ADR stimulation at the SR, such as SR Ca^{2+} overload and arrhythmia generation, however paradoxically I did not observe this.

However, in pathophysiological states, such as HF, the sustained elevated SNS activity is accompanied by a down-regulation of the β_1-ADR inotropic response (Osadchii 2007). The down regulation of β-ADR is selective for β_1-ADR, as levels of mRNA of the β_1 ADR can be reduced by $\approx$50% where as β_2 levels appear unchanged (Lohse, Engelhardt et al. 2003). This causes a reduction in the β_1-ADR density in the failing heart, altering the β_1:β_2 ratio, becoming more equal ($\approx$50:50) (Port and Bristow 2001). This alteration in the ratio of β_1:β_2 is likely to mean that the β_2-ADR will have a greater impact during sympathetic stimulation and the G_i mediated activation of PDE3 and PDE4 may reduce the impact of β_1-ADR stimulation further. Together with the loss of β_1-ADR receptor numbers, this may contribute to the loss of sensitivity of the failing heart to sympathetic stimulation. Although β_2-ADR expression remains unchanged, as with the β_1-ADR, their function is altered as they become significantly desensitised to the high circulating levels of catecholamine's, thought to be due to the increased activity of β-agonist receptor kinase (β-ARK) or GRK2, a G-protein coupled kinase (Lohse, Engelhardt et al. 2003; Brodde, Bruck et al. 2006; El-Armouche and Eschenhagen 2009), this depresses the action of G_s signalling and as the G_i signalling pathway beings to dominate, there is a further loss of sensitivity to sympathetic stimulation in the failing heart.

The β_3-ADR induced a negative inotropic effect on the ventricular myocyte and may well act as a brake on sympathetic stimulation. In addition β_3-ADR have been shown to be upregulated in human HF patients (Napp, Brixius et al. 2009) and an increase in G_i mRNA in canine models of HF (Lohse, Engelhardt et al. 2003) and ISO-treated rats (Osadchii 2007), possibly providing protection against sustained and excessive sympathetic stimulation. This up-regulation of β_3-ADR and G_i in diseased states and their resistance to desensitization suggest they may be a possible therapeutic target against the adverse consequences of excessive or prolonged β_1/β_2-ADR stimulation.

5.3.3 Study Limitations

In the present study the concentrations of the specific β-agonists used were not physiological levels, rather I attempted to use maximal agonist concentrations in order to observe the full positive inotropic response of the β_1-ADR and β_2-ADR and the full proposed protective negative inotropic effect of the β_3-ADR. Unfortunately I was unable to use the maximal concentration of the β_1-ADR agonist dobutamine (3-10μM), as these concentrations induced significant arrhythmic activity which impeded investigation. The β_3-ADR agonist BRL_{37344} has a high affinity for β_3-ADR, however at high concentrations is able to act as a weak agonist at β_1-ADR and β_2-ADR, and so a concentration which induced a maximal negative inotropic response without stimulation of β_1 and β_2-ADR was required. The concentration of BRL_{37344} used in this investigation, 200nM, elicited a maximal reduction in systolic Ca^{2+}. This concentration of BRL_{37344} should not have elicited an agonist response at β_1 and β_2-ADR, and this is supported by the observations of Gauthier *et al.* who observed a reduction in peak tension in response to BRL_{37344} at 1μM which was not modified by β_1 and β_2-ADR blockade with nanadol (Gauthier, Tavernier et al. 1996). Therefore, the concentration used in this investigation of 200nM should not elicit a response at β_1 and β_2-ADR. In hindsight it would have been useful to complete recordings of Ca^{2+} parameters in response to 200nM BRL_{37344} in the presence of nanadol to ensure this concentration had no agonist activity at β_1-ADR and β_2-ADR.

It should also be noted that basal I_{to} and LTCC were approximately 20% greater in the β_3-ADR data set as compared to the β_1 and β_2-ADR data sets. The measurements of I_{to} and LTCC in response to BRL_{37344} were made as some of the first electrophysiological recordings I had made and it is possible that a poor giga-seal of the myocytes (due to inexperience) lead to an overestimation of membrane resistance (R_m) which would have led to an underestimation of membrane capacitance (C_m). However, as all currents measured are normalised to C_m, if an underestimation of C_m had occurred this would have led to an overestimation of the current density in the BRL_{37344} data set. However, as the data within this section was performed at the same time and comparisons made to controls taken from the same cells, so I assume that any errors would have been constant within this study on the electrophysiological effects of BRL_{37344}.

The dual coupling of β_2–ADR to both G_s and G_i proteins and activation of PDE3 and PDE4 by the $G_{i\alpha}$ subunit leading to compartmentalised cAMP signalling is well established (Xiao, Avdonin et al. 1999; Xiao 2001; Wallukat 2002; Rochais, Abi-Gerges et al. 2006; Gonzalez-Munoz, Fuente et al. 2009; Nikolaev, Moshkov et al. 2010; Heijman, Volders et al. 2011; Cros and Brette 2013). However, what is less known is the role of the $G_{i\beta}$ subunit in the β_2–ADR signalling cascade. Following β_3–ADR stimulation, downstream signalling of the $G_{i\alpha}$ and $G_{i\beta}$ subunits, leads to activation of PDE3/4 and an increase in NO. An extensive literature search for β_2–ADR and NO in myocytes provided no results which conclusively rule in or out the involvement of the $G_{i\beta}$ subunit or NO in β_2–ADR signalling. Some groups have attempted to examine the role of NO in β_2–ADR signalling in atrial myocytes in looking at the increase in LTCC and cardiac alternans in response to β_2–ADR stimulation (Dedkova, Wang et al. 2002; Florea and Blatter 2012), however they have failed to account for the β_3–ADR, using ISO with a β_1–ADR blocker to stimulate β_2–ADR. Therefore, it would be interesting to examine the role of NO in the β_2–ADR downstream signalling pathway, using a β_2–ADR specific agonist and NOS inhibitor.

Chapter 6: The anti-arrhythmic effect of β₃-adreoceptors

6.1 Introduction

In the previous chapter, I have shown the effects of specific β-ADR agonists on Ca^{2+} regulation in rat ventricular myocytes. Sympathetic activation of β-ADR induces both positive inotropic and chronotropic effects, leading to increases in SV and HR, during the "fight or flight" response to stressful stimuli, which increase CO from the heart. However, excessive or prolonged sympathetic activation of β-ADR is known to result in the generation of spontaneous arrhythmic activity *in vitro* in isolated myocytes and *in vivo* in hearts in many animal species, including Wistar rats (Collins and Rodrigo 2010; Penna and Bassani 2010) and guinea pigs (Song, Shryock et al. 2001), but also in humans (Coumel, Escoubet et al. 1984; Meredith, Broughton et al. 1991).

The generation of arrhythmic activity in response to β-adrenergic stimulation is known to result from the induction of both early and delayed after-depolarisations (See Introdution 1.1.5). EAD are triggered in the plateau phase of an action potential (phase 2), and arise due to reactivation of LTCC, which are able to recover from voltage- and Ca^{2+}-dependant inactivation during long APDs whereas DAD are triggered under conditions of increased $[Ca^{2+}]_{SR}$, such as elevated/prolonged sympathetic activity due to increase levels of circulating catecholamine. During β-adrenergic stimulation, due to PKA mediated phosphorylation of the LTCC and PLB, there is an increase in LTCC and in the activity of SERCA, which together over a number of cardiac beats increase the SR Ca^{2+} content, (Bers 2001). When $[Ca^{2+}]_{SR}$ is high, the likelihood of spontaneous Ca^{2+} release from the SR is increased. If $[Ca^{2+}]_{SR}$ is sufficiently high, Ca^{2+} sparks can initiate Ca^{2+} waves which can propagate in myocytes, initiating a Ca^{2+} activated transient inward depolarising current, (I_{NCX}, $I_{Cl(Ca)}$ or $I_{NS(Ca)}$) depolarising the membrane (Venetucci, Trafford et al. 2008; Eisner, Kashimura et al. 2009). Any pharmacological agent which inhibits SR Ca^{2+} storage or RyR2 Ca^{2+} release and/or modify the inward Ca^{2+} current can reduce the occurrence of DAD in myocytes (Podrid and Kowey 2001).

During β-ADR stimulation *in vivo* with endogenous catecholamines and *in vitro* with exogenous ISO, all 3 β-ADR are stimulated by binding of catecholamines or ISO to the β₁-

ADR, β_2-ADR and β_3-ADR, and so the effects of adrenaline, nor-adrenaline or ISO are the result of the combined activation of β_1-ADR, β_2-ADR and β_3-ADR.

In this investigation I have shown specific β_3-ADR stimulation with BRL$_{37344}$ reduces systolic Ca^{2+} and SR Ca^{2+} content of ventricular myocytes (Chapter 5.2.2), which may provide a protective mechanism during prolonged or excessive β-ADR sympathetic stimulation. Indeed, β_3-ADR and NO have recently been identified in cardio-protection mechanisms against ischemia-reperfusion injury (Aragon, Condit et al. 2011; Calvert, Condit et al. 2011; Heusch 2011) and hypertrophy induced by excessive β-ADR stimulation (Belge, Hammond et al. 2014) and pressure overload hypertrophy (Niu, Watts et al. 2012).

I therefore postulated that β_3-ADR stimulation may be protective against sympathetic-induced arrhythmias. In order to dissect out any protective effects of β_3-ADR activation against sympathetic induced arrhythmias I have looked at the anti-arrhythmic actions of the β_3-ADR specific agonist BRL$_{37344}$ on the pro-arrhythmic action of the specific β_1-agonist dobutamine, and to determine the cellular mechanism of protection, examining the involvement of the G$_i$ downstream signalling pathways of PDE and NO.

I also set out to determine the potential role of β_2-ADR coupling to G$_i$ as a protective mechanism against β_2-ADR induced arrhythmia. I have previously shown β_2-ADR stimulation with salbutamol induces a only a modest increase in SR Ca^{2+} content, which can be augmented by PDE inhibition with PTx or G$_i$ uncoupling by PTx treatment, and so postulate that G$_i$ uncoupling may augment β_2-ADR induced arrhythmias in a similar manner, due to the increased SR Ca^{2+} content; a driver of DAD's.

6.2 Results

6.2.1 Development of arrhythmic activity in ventricular myocytes in response to β-ADR stimulation

In order to investigate an anti-arrhythmic action of β_3-ADR stimulation, I first quantified the development of arrhythmic activity in isolated rat ventricular myocytes in response to non-specific β-ADR stimulation with ISO and to the β_1-ADR specific agonist dobutamine. As I have previously shown stimulation of the β_2-ADR induces a reduced positive inotropic effect as compared to β_1-ADR, I also wanted to look at the development of arrhythmic activity in response to maximal activation of β_2-ADR with salbutamol.

The percentage of myocytes exhibiting spontaneous extra-contractions in basal conditions (normal Tyrode) and in response to 10nM ISO, 1µM dobutamine and 1µM salbutamol were measured as previously described (See Methods 2.2.2).
Data sets are expressed as number of hearts (number of experiments/number of cells).
Throughout all experiments, there was no difference in the percentage of myocytes exhibiting spontaneous activity in basal conditions (normal Tyrode) between data sets (data not shown).

Figure 6.1 shows the mean percentage of ventricular myocytes exhibiting spontaneous extra-contractions during the 10 seconds the electrical stimulator was switched off following superfusion with 10nM ISO, 1µM dobutamine and 1µM salbutamol.

A significant percentage of myocytes developed spontaneous extra-contractions following perfusion with ISO, from 0.0 ± 0.0% in normal Tyrode to 38.7 ± 2.7% following ISO perfusion (n=3(23/221);p<0.0001)) and dobutamine, from 0.5 ± 0.3% in normal Tyrode to 50.8 ± 2.2% (n=8(24/386);p<0.0001). However, there was no significant development of spontaneous extra-contractions following perfusion with salbutamol, from 0.8 ± 0.4% in normal Tyrode to 0.9 ± 0.3% following salbutamol perfusion (n=4(30/401);p=0.84).
The data also demonstrates a significant difference in the development of arrhythmic activity between β_1-ADR and β_2-ADR agonist stimulation, with significantly more myocytes exhibiting spontaneous contractile activity following β_1-ADR stimulation with dobutamine perfusion as compared to β_2-ADR stimulation with salbutamol, 50.8 ± 2.2% versus 0.9 ± 0.3% (p<0.0001).
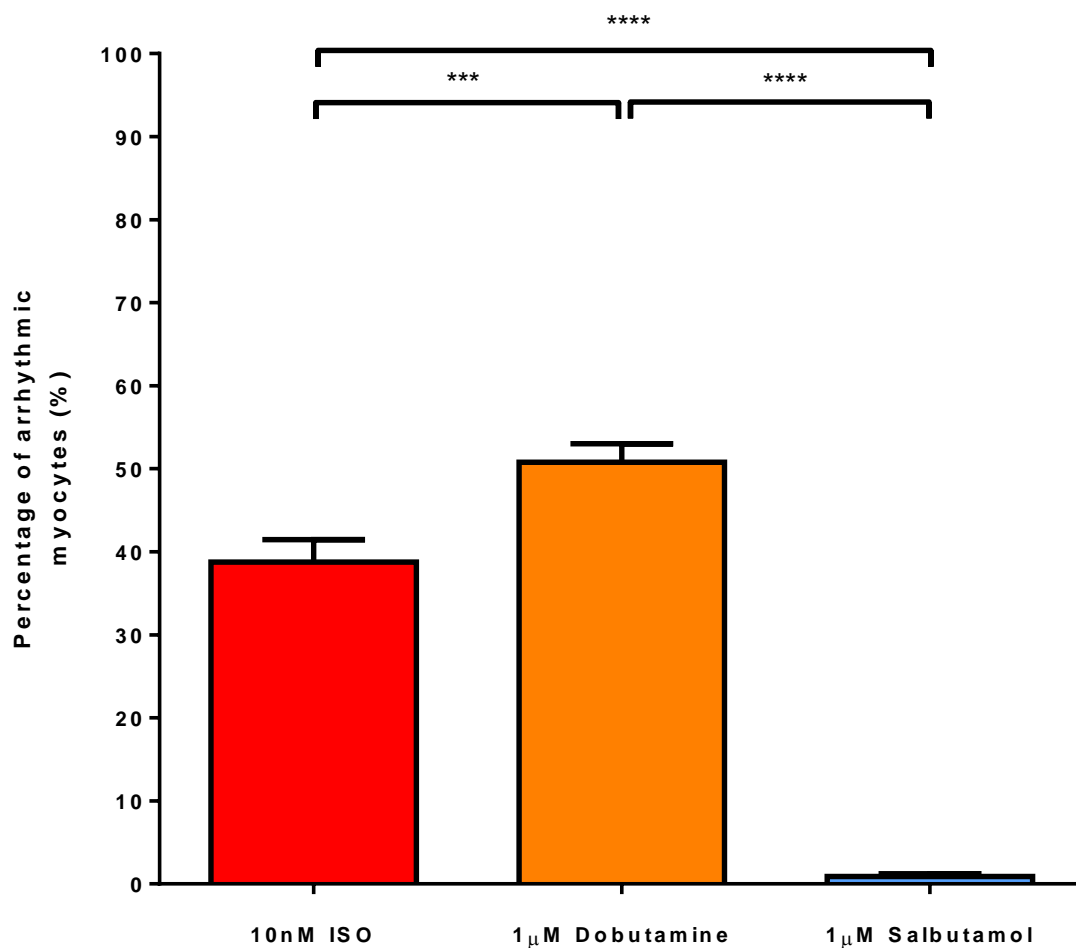
Figure 6.1 **Development of arrhythmic activity in rat ventricular myocytes in response to β-adrenergic stimulation.**

Bar chart showing the mean percentage of myocytes that develop spontaneous extra-contractions in response to 10nM ISO (red bar, n=3(23/221)), 1μM dobutamine (orange bar, n=8(42/656)) and 1μM salbutamol (blue bar, n=4(30/401)). Percentages were calculated from a field of 10-20 cells synchronously contracting cells stimulated at 1Hz by electrical field stimulation. Values are mean ± S.E.M. Number of hearts (number of experiments/number of cells); ***p<0.001, ****p<0.0001, one-way ANOVA, sidak's *post-hoc* test.

6.2.2 The effect of β_3-ADR activation on the development of arrhythmic activity in ventricular myocytes

We have previously shown that stimulation of β_3-ADR with BRL_{37344} induced a reduction in systolic $[Ca^{2+}]_i$ and a reduction in SR Ca^{2+} stores. We proposed that specific stimulation of β_3-ADR would be protective against β_1-ADR agonist induced arrhythmias. We set out to examine the effect of stimulation of β_3-ADR, using the specific agonist BRL_{37344}, on the arrhythmic activity induced by the non-specific β-ADR stimulation with ISO and the β_1-ADR agonist dobutamine, in isolated rat ventricular myocytes.

To determine the effect of β_3-ADR stimulation on the development arrhythmic activity in response to ISO and dobutamine, I looked at the effects of pre-treating myocytes with 200nM of the β_3-ADR specific agonist BRL_{37344} on the subsequent development of arrhythmic activity in response to 10nM ISO and 1µM dobutamine perfusion in the continued presence of BRL_{37344}. Arrhythmic activity was determined as previously described (See Methods 2.2.2).

Figure 6.2 shows the mean percentage of ventricular myocytes exhibiting spontaneous contractile activity in response to A. 10nM ISO and B. 1µM dobutamine in control myocytes and those pre-treated with 200nM BRL_{37344} prior to superfusion with ISO or dobutamine.

The data shows that β_3-ADR stimulation with BRL_{37344} significantly reduced the percentage of myocytes developing arrhythmic activity in response to ISO, from $38.7 \pm 2.7\%$ (n=3(23/221)) in control cells to $23.0 \pm 6.6\%$ (n=3(7/108)) in BRL_{37344} pre-treated myocytes (p<0.05), and in response to dobutamine, from $50.8 \pm 2.2\%$ (n=8(24/386)) in control cells to $31.9 \pm 2.7\%$ (n=4(8/113)) in BRL_{37344} pre-treated myocytes (p<0.01).
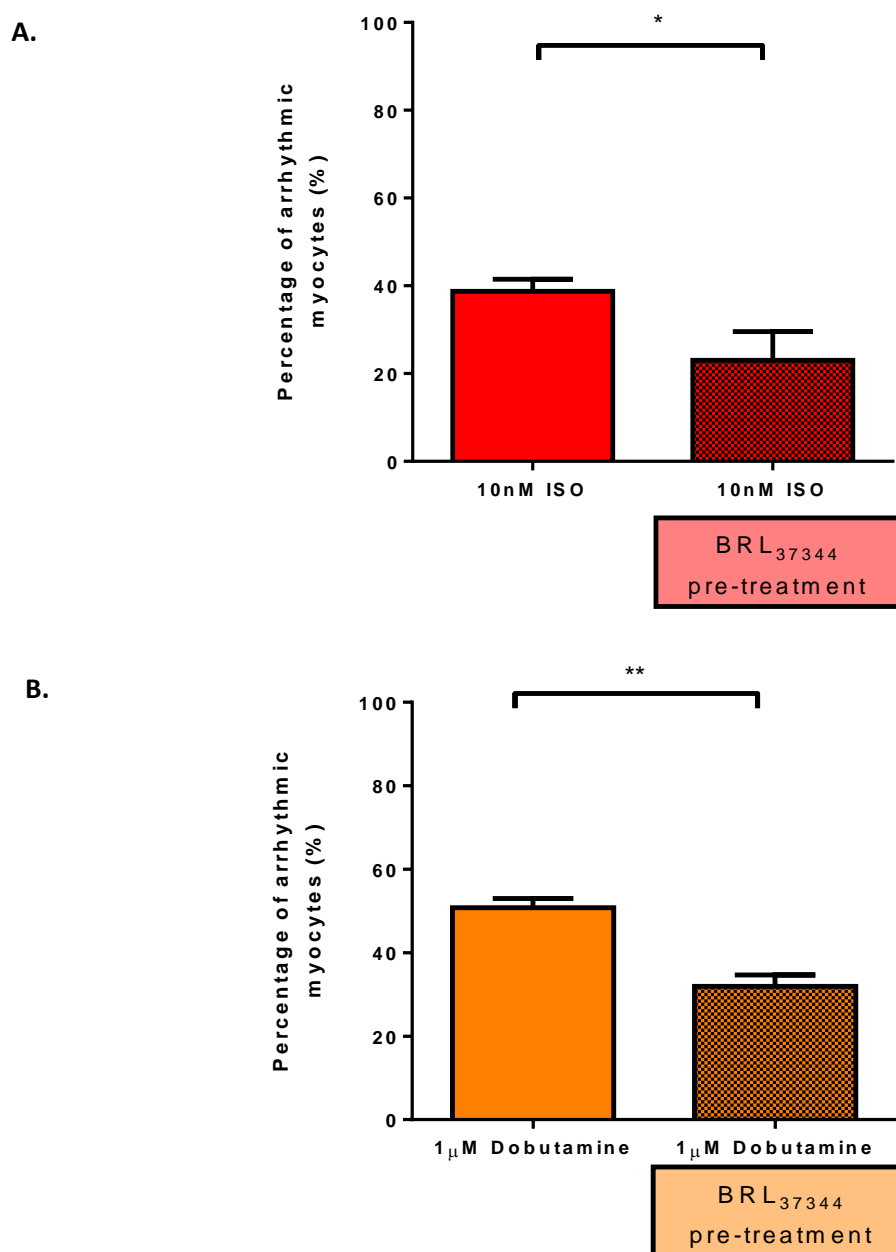
**Figure 6.2** **β_3-ADR activation with BRL$_{37344}$ pre-treatment reduces the development of arrhythmic activity in ventricular myocytes in response to β-adrenergic stimulation.**

Bar charts showing the effect of β_3-ADR stimulation by pre-treatment with BRL$_{37344}$ on the development of spontaneous extra-contractions in response to non-specific β-adrenergic stimulation with isoproterenol and specific β_1-ADR stimulation dobutamine.

A. 10nM ISO (open bar, n=3(23/221)) and in cells pre-treated with 200nM BRL$_{37344}$ prior to 10nM ISO (hatched bar, n=3 (7/108)).

B. 1µM Dobutamine (open bar, n= 8 (24/386)) and in cells pre-treated with 200nM BRL$_{37344}$ prior to 1µM Dobutamine (hatched bar, n = 4 (8/113).

Values are mean ± S.E.M. Number of hearts (number of experiments/number of cells); *p<0.05, **p<0.01, unpaired t-test.

6.2.3 The mechanism of the anti-arrhythmic effect of β_3-ADR stimulation in isolated myocytes

We have shown β_3-ADR stimulation with BRL_{34377} is effective at preventing arrhythmic activity in response to ISO and the β_3-ADR specific agonist dobutamine in isolated myocytes. The β_3-ADR is coupled to the inhibitory G_i protein; the $G_{i\alpha}$ subunit activates PDE3 and PDE4, leading to hydrolysis of cAMP (Berthouze, Laurent et al. 2011), and the $G_{i\beta}$ subunit stimulates NO production by NOS, initiating cGMP-dependent and cGMP-independent pathways, which directly phosphorylate (cGMP-dependent) and S-nitrosylate (cGMP-independent) the components of E-C coupling leading to a negatively inotropic effect (Hare 2003; Gonzalez, Fernandez et al. 2008).

I have shown that specific activation of β_3-ADR receptors has a negative effect on Ca^{2+} handling (Chapter 5.2.2), observed as a reduction in systolic $[Ca^{2+}]$ and SR Ca^{2+} stores, whilst enhancing SERCA activity, leading to faster Ca_{2+} sequester to the SR during relaxation. Together, the faster decline in Ca^{2+} during relaxation and a reduced SR Ca^{2+} content, could impact upon the drivers of triggered arrhythmias, namely DADs. We propose that BRL_{37344} pre-treatment modulates the normal Ca^{2+} handling or action potential response to non-specific β-adrenergic stimulation with ISO and β_1-ADR stimulation with dobutamine, which provides the anti-arrhythmic effect of β_3-ADR stimulation I have observed.

6.2.3.1 The effect of β_3-ADR stimulation on the response of calcium handling to further β-ADR stimulation

To investigate the effect β_3-ADR stimulation on Ca^{2+} handling in response to subsequent stimulation with ISO and dobutamine, $[Ca^{2+}]_i$ was measured in myocytes pre-treated with 200nM BRL_{37344} prior to 10nM ISO or 1µM dobutamine (in the continued presence of 200nM BRL_{37344}) and compared to myocytes in response to 10nM ISO and 1µM dobutamine alone. Systolic $[Ca^{2+}]_i$, diastolic $[Ca^{2+}]_i$ and relaxation time of the electrically-induced Ca^{2+} transient were determined as previously described (See Methods 2.2.3).

Figure 6.3 shows the effect of β_3-ADR stimulation with BRL_{37344} pre-treatment on the response of A. mean systolic $[Ca^{2+}]_i$, B. mean diastolic $[Ca^{2+}]$ and C. mean relaxation time of

the electrically-induced Ca^{2+} transient, to the non-specific β-adrenergic stimulation with ISO.

ISO perfusion significantly increased systolic $[Ca^{2+}]_i$, from 319.6 ± 18.5nM in normal Tyrode to 1040.0 ± 110.6nM (p<0.0001), diastolic $[Ca^{2+}]_i$, from 79.9 ± 3.8nM in normal Tyrode to 141.1 ± 3.9nM (p<0.0001) and significantly reduced relaxation time, from 220.9 ± 11.4ms in normal Tyrode to 99.3 ± 6.9ms following ISO (p<0.0001).

Figure 6.3A shows no effect of BRL_{37344} pre-treatment on this increase in systolic $[Ca^{2+}]_i$ in response to ISO, at 1040.0 ± 116.9nM (n=5(32)) versus 1107.0 ± 54.4nM in BRL_{37344} pre-treated myocytes (n=3(22);p=0.66).

Figure 6.3B shows no effect of BRL_{37344} pre-treatment on this increase in systolic $[Ca^{2+}]_i$ in response to ISO, at 141.1 ± 3.9nM (n=3(11)) versus 161.1 ± 15.2nM in BRL_{37344} pre-treated myocytes (n=5(22);p=0.10).

Figure 6.3C shows the reduction in relaxation time in response to ISO was significantly augmented following BRL_{37344} pre-treatment, at 66.2 ± 5.9ms (n=3(17)) following pre-treatment versus 99.3 ± 6.9ms (n=5(46)) in response to ISO alone (p<0.01), indicating an additional increase in the activity of SERCA in BRL_{37344} pre-treated cells, beyond the increase induced by ISO alone.

Figure 6.4 shows the effect of β3-ADR stimulation with BRL_{37344} pre-treatment on the response of A. mean systolic $[Ca^{2+}]_i$, B. mean diastolic $[Ca^{2+}]$ and C. mean relaxation time of the electrically-induced Ca^{2+} transient, to specific β1-ADR stimulation with dobutamine.

As previously shown, dobutamine perfusion significantly increased systolic $[Ca^{2+}]_i$, from 337.7 ± 19.6nM in normal Tyrode to 872.0 ± 57.6nM (p<0.0001), diastolic $[Ca^{2+}]_i$, from 84.6 ± 5.0nM in normal Tyrode to 129.8 ± 8.1nM (p<0.0001) and significantly reduced relaxation time, from 239.7 ± 19.4ms in normal Tyrode to 121.4 ± 3.6ms following dobutamine (p<0.0001).

Figure 6.4A shows no effect of BRL_{37344} pre-treatment on this increase in systolic $[Ca^{2+}]_i$ in response to dobutamine, at 872.0 ± 57.6nM (n=3(14)) versus 953.7 ± 63.7nM in BRL_{37344} pre-treated myocytes (n=4(22);p=0.38).

Figure 6.3 **The effect of β3-ADR activation with BRL$_{37344}$ pre-treatment on the Ca^{2+} transient in response to non-specific β-adrenergic stimulation with ISO.**

Bar charts showing **A.** systolic [Ca^{2+}], **B.** diastolic [Ca^{2+}] and **C.** exponential time constant of the decay of the electrically evoked Ca^{2+} transient, recorded from ventricular myocytes, stimulated at 1Hz by electrical field stimulation. Data are for cells superfused with 10nM ISO (open bars, n=5(22-46)) and in cells pre-treated with 200nM BRL$_{37344}$ prior to 10nM ISO (hatched bars, n=3(11-22)). Values are mean ± S.E.M. Number of hearts (number of experiments); *p<0.05, unpaired t-test.
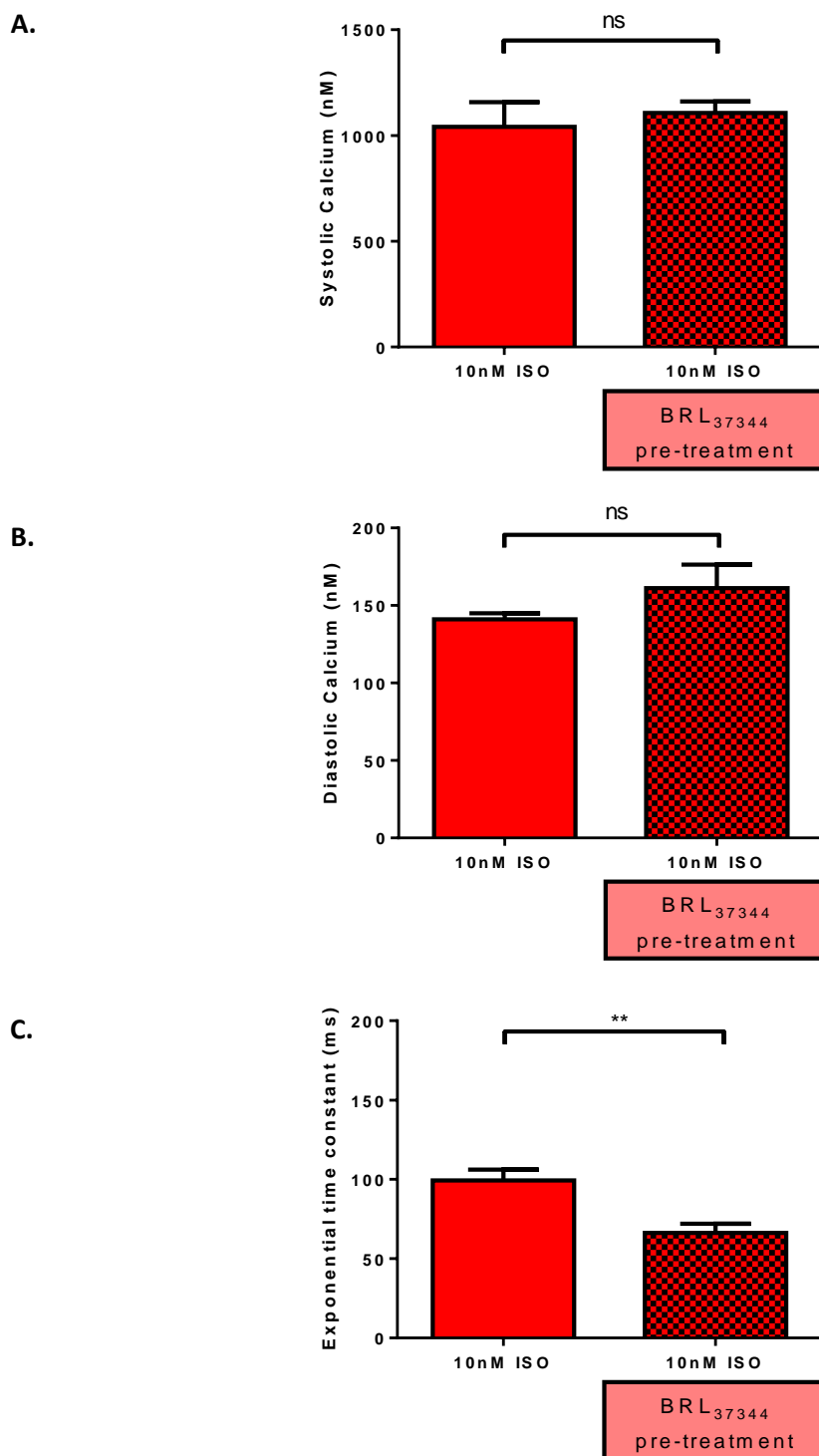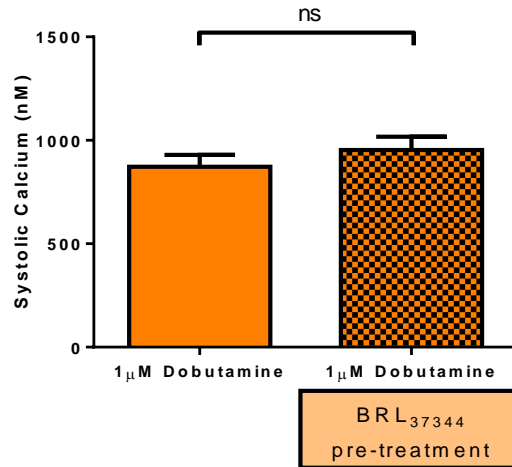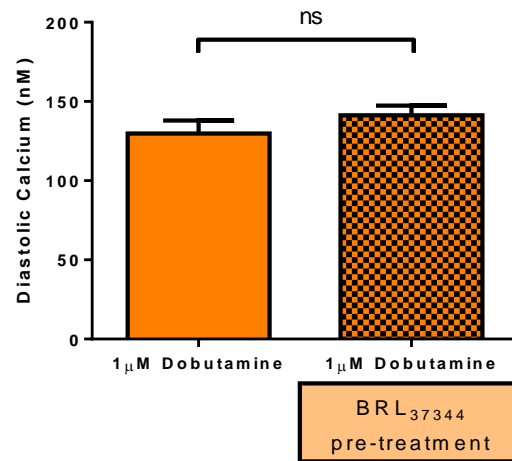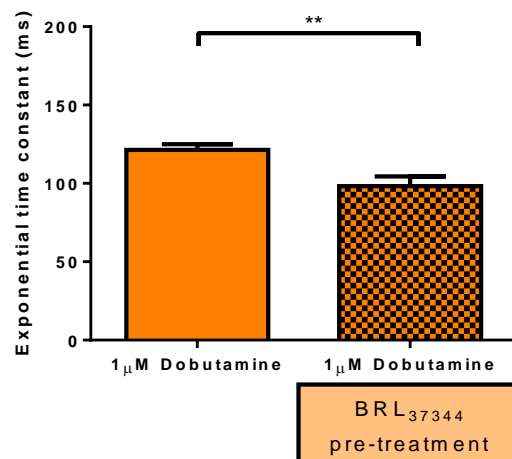
Figure 6.4 The effect of β3-ADR activation with BRL_{37344} pre-treatment on the Ca^{2+} transient in response to non-specific $β_1$-adrenergic stimulation with dobutamine.
Bar charts showing **A.** systolic $[Ca^{2+}]$, **B.** diastolic $[Ca^{2+}]$ and **C.** exponential time constant of the decay of the electrically evoked Ca^{2+} transient recorded from ventricular myocytes, stimulated at 1Hz by electrical field stimulation. Data are for cells superfused with 1μM Dobutamine (open bars, n=3(14)) and in cells pre-treated with 200nM BRL_{37344} prior to 1μM Dobutamine (hatched bars, n=4(20-22)). Values are mean ± S.E.M. Number of hearts (number of experiments); ** p<0.01, unpaired t-test.

236

Figure 6.4B shows no effect of BRL_{37344} pre-treatment on the increase in diastolic $[Ca^{2+}]_i$ in response to dobutamine, at $129.8 \pm 8.1nM$ (n=3(14)) versus $141.2 \pm 6.2nM$ in BRL_{37344} pre-treated myocytes (n=4(22);p=0.26).

Figure 6.4C shows the reduction in relaxation time in response to dobutamine was significantly augmented following BRL_{37344} pre-treatment, at $98.3 \pm 6.2ms$ (n=3(14)) following pre-treatment versus $121.4 \pm 3.6ms$ (n=5(20)) in response to dobutamine alone (p<0.01), indicating an additional increase in the activity of SERCA in BRL_{37344} pre-treated cells, beyond the increase induced by dobutamine alone.

An increase in SERCA activity, indicated by the exponential time constant for decay in $[Ca^{2+}]_i$, might be expected to lead to an increase in SR Ca^{2+} content (Bers 2001), and this was the case for ISO and dobutamine treatment alone (See Chapter 5, Figure 5.1 and Figure 5.6), and this would usually be considered be pro-arrhythmic (See Introduction 1.4). However, the effects of BRL_{37344} pre-treatment are anti-arrhythmic and BRL_{37344} was shown to reduce SR Ca^{2+} content in the face of an increase in SERCA activity (See Chapter 5, Figure 5.6). Therefore I set out to look at the effect β_3-ADR stimulation on the SR Ca^{2+} loading of myocytes in response to ISO and dobutamine. The SR Ca^{2+} content was measured in myocytes by rapidly perfusing cells with normal Tyrode containing caffeine (20mM for 5 seconds), in response to 10nM ISO and 1µM dobutamine and compared to myocytes pre-treated with 200nM BRL_{37344} prior to 10nM ISO or 1µM dobutamine (in the continued presence of 200nM BRL_{37344}). Peak caffeine-induced Ca^{2+} release and relaxation time of the caffeine-induced Ca^{2+} transient were determined as previously described (See Methods 2.2.3).

Figure 6.5 shows the effect of BRL_{37344} pre-treatment on A. mean peak caffeine-induced Ca^{2+} release and B. mean relaxation time of the caffeine-induced Ca^{2+} transient, following non-specific β-adrenergic stimulation with ISO.

ISO perfusion significantly increased SR Ca^{2+} content from $479.8 \pm 32.7nM$ in normal Tyrode to $966.0 \pm 97.39nM$ (n=5(36);p<0.0001) and significantly reduced relaxation time of the caffeine-induced Ca^{2+} transient, from $2992.0 \pm 253.9ms$ in normal Tyrode to $2275.0 \pm 271.3ms$ (n=5(22);p<0.05).

Figure 6.5A shows no effect of BRL_{37344} pre-treatment on this increase in SR Ca^{2+} content in response to ISO, at 966.0 ± 97.39 (n=5(36)) versus 966.7 ± 161.2nM in BRL_{37344} pre-treated myocytes (n=3(5);p=0.91).

Figure 6.5B shows no effect of BRL_{37344} pre-treatment on the reduction in relaxation time of the caffeine-induced Ca^{2+} transient in response to ISO, 2275.0 ± 271.3ms (n=5(22)) versus 2425.0 ± 183.4ms (n=3(4);p=0.82) , indicating no change in the activity the NCX following BRL_{37344} pre-treatment.

Figure 6.6 shows the effect of BRL_{37344} pre-treatment on mean A. peak caffeine-induced Ca^{2+} release and B. relaxation time of the caffeine-induced Ca^{2+} transient, following specific β_1-ADR stimulation with dobutamine.

Dobutamine perfusion significantly increased SR Ca^{2+} content from 563.0 ± 21.2nM in normal Tyrode to 1020.0 ± 67.9nM (n=5(33);p<0.0001) and significantly reduced relaxation time of the caffeine-induced Ca^{2+} transient, from 2992.0 ± 226.4ms in normal Tyrode to 2066.0 ± 169.5ms (n=5(32);p<0.0001).

Figure 6.6A shows no effect of BRL_{37344} pre-treatment on the increase in SR Ca^{2+} content in response to dobutamine, at 1020.0 ± 67.9nM (n=5(33)) versus 996.2 ± 183.0nM in BRL_{37344} pre-treated myocytes (n=3(8);p=0.88).

Figure 6.6B shows no effect of BRL_{37344} pre-treatment on the reduction in relaxation time of the caffeine-induced Ca^{2+} transient in response to dobutamine, 22066.0 ± 169.5ms (n=5(32)) versus 2546.0 ± 293.1ms (n=3(6);p=0.26), indicating no change in the activity the NCX following BRL_{37344} pre-treatment.

The data shows β_3-ADR stimulation augments an increase in SERCA activity additional to the increase in activity induced by ISO and dobutamine alone, meaning faster relaxation of the electrically-induced Ca^{2+} transient, with no change in systolic $[Ca^{2+}]$, diastolic $[Ca^{2+}]$, and the SR Ca^{2+} content or in the activity of NCX.

A.

B.
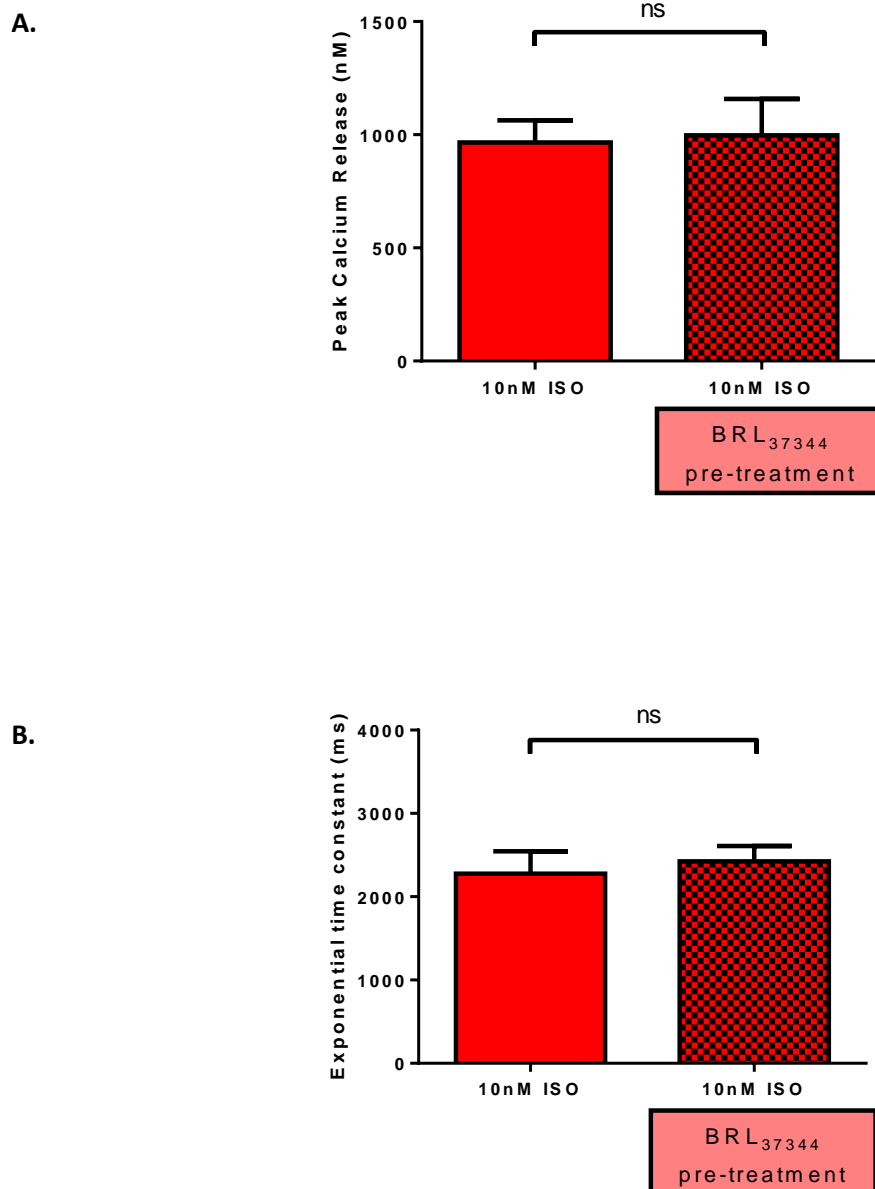
Figure 6.5 **The effect of β_3-ADR activation with BRL$_{37344}$ pre-treatment on the response of SR Ca^{2+}-content and the activity of the NCX to non-specific β-adrenergic stimulation with ISO.**

Bar charts showing the **A.** sarcoplasmic reticulum Ca^{2+} content and **B.** exponential time constant of the decay of the caffeine-induced Ca^{2+} transient of ventricular myocytes after superfusion with 10nM ISO (open bars, n=5(32-36)) and in cells pre-treated with 200nM BRL$_{37344}$ prior to 10nM ISO (hatched bars, n=3(5-8)). Values are mean ± S.E.M. Number of hearts (number of experiments); unpaired t-test.

A.

B.

Figure 6.6   The effect of β₃-ADR activation with BRL₃₇₃₄₄ pre-treatment on the response of SR Ca²⁺-content and the activity of the NCX to β₁-adrenergic stimulation with dobutamine. Bar charts showing the **A.** sarcoplasmic reticulum Ca²⁺ content and **B.** exponential time constant of the decay of the caffeine-induced Ca²⁺ transient of ventricular myocytes after superfusion with 1μM Dobutamine (open bars, n=7(34-37)) and in cells pre-treated with 200nM BRL₃₇₃₄₄ prior to 1μM Dobutamine (hatched bars, n=4(5-8)). Values are mean ± S.E.M. Number of hearts (number of experiments); unpaired t-test.

6.2.3.2 The effect of β_3-ADR stimulation on the response of the action potential to further β-ADR stimulation

In the previous section I investigated the action of BRL_{37344} on Ca^{2+} regulation in the ventricular myocyte. Although I observed an increase in SERCA activity, there did not seem to be an expected change in SR Ca^{2+} content which may have helped to explain any anti-arrhythmic actions of BRL_{37344}, and so next I investigated the electrical properties of E-C coupling to determine if any effects of BRL_{37344} on APD may be anti-arrhythmic.

To investigate the effect β_3-ADR stimulation on the response of the action potential to ISO and dobutamine, action potentials were recorded in myocytes pre-treated with 200nM BRL_{37344} prior to 10nM ISO or 1µM dobutamine (in the continued presence of 200nM BRL_{37344}) and compared to myocytes in response to 10nM ISO and 1µM dobutamine only. Measurement of APD_{30}, APD_{50} and APD_{90} were made as previously described (See Methods 2.3.3.1).

Figure 6.7 are records of a single action potentials recorded in normal Tyrode (black) and A. 10nM ISO (red) and B. 10nM ISO following BRL_{37344} pre-treatment (red), showing the effect of ISO on APD and the modifying effect of BRL_{37344} pre-treatment.

Figure 6.7C shows the mean APD_{30}, APD_{50} and APD_{90} in ISO only and BRL_{37344} pre-treated myocytes, showing no effect of BRL_{37344} pre-treatment on the lengthening of the action potential in response to ISO at APD_{30}, 27.1 ± 1.8ms (n=6(9)) versus 25.3 ± 2.3ms (n=3(11);p=0.96), APD_{50}, 42.6 ± 2.3ms (n=6(9)) versus 39.2 ± 2.8ms (n=3(11);p=0.80) or APD_{90}, 73.1 ± 3.7ms (n=6(9)) versus 80.6 ± 3.7ms (n=3(11);p=0.22).

Figure 6.8 are records of single action potentials recorded in normal Tyrode (black) and A. 1µM dobutamine (orange) and B. 1µM dobutamine following BRL_{37344} pre-treatment (orange), showing the effect of dobutamine on APD and the modifying effect of BRL_{37344} pre-treatment.

Figure 6.8C shows the mean APD_{30}, APD_{50} and APD_{90} in dobutamine only and BRL_{37344} pre-treated cells, showing no effect of BRL_{37344} pre-treatment on the lengthening of the action potential in response to dobutamine at APD_{30}, 24.0 ± 1.9ms (n=6(16)) versus 26.3 ± 3.0ms (n=3(15);p=0.96), APD_{50}, 41.2 ± 2.5ms (n=6(16)) versus 41.5 ± 4.2ms (n=3(15);p=0.99) or APD_{90}, 83.3 ± 2.9ms (n=6(16)) versus 82.5 ± 6.4ms (n=3(15);p=0.74).
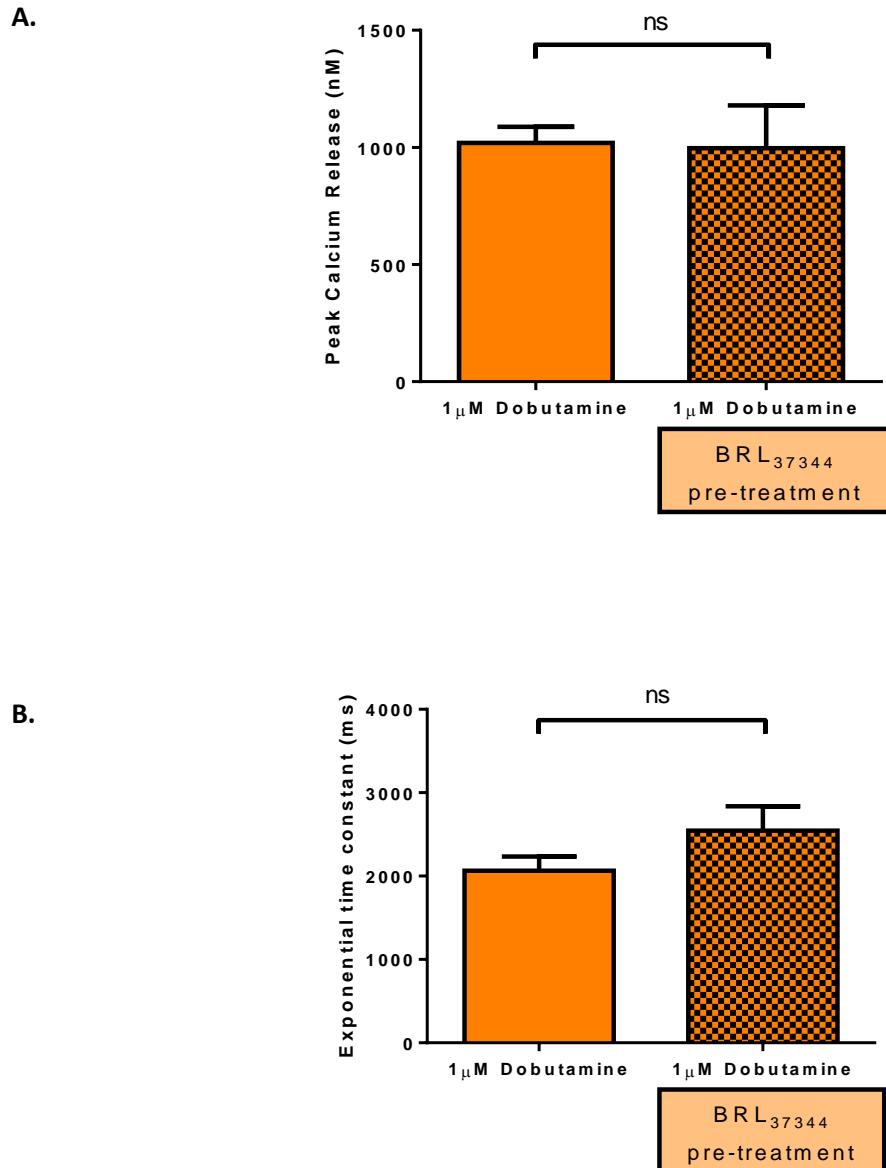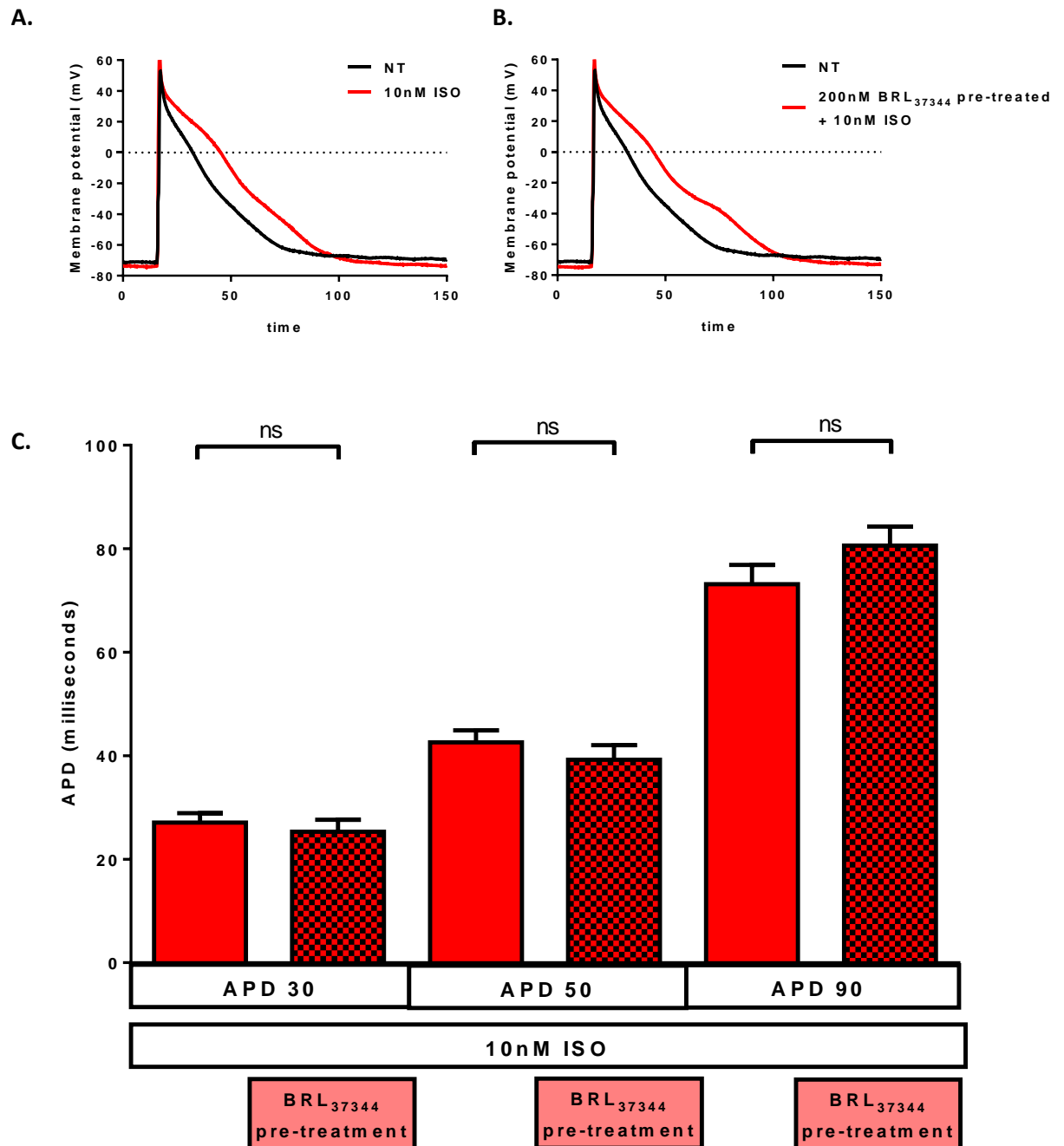
Figure 6.7 **The effect of β₃-ADR activation with BRL₃₇₃₄₄ pre-treatment on the response of the cardiac action potential to non-specific β-adrenergic stimulation with ISO.**

Representative action potential recordings from myocytes superfused with **A.** normal Tyrode (black) and 10nM ISO (red) and **B.** normal Tyrode (black) and pre-treated with 200nM BRL₃₇₃₄₄ prior 10nM ISO (red).

C. Bar chart showing APD_{30}, APD_{50} and APD_{90} recorded from ventricular myocytes superfused with 10nM ISO (open bars, n=3(9)) and in cells pre-treated with 200nM BRL₃₇₃₄₄ prior 10nM ISO (hatched bars, n=4(11)). Values are mean ± S.E.M. Number of hearts (number of experiments); one-way ANOVA, Sidak's *post-hoc* test.
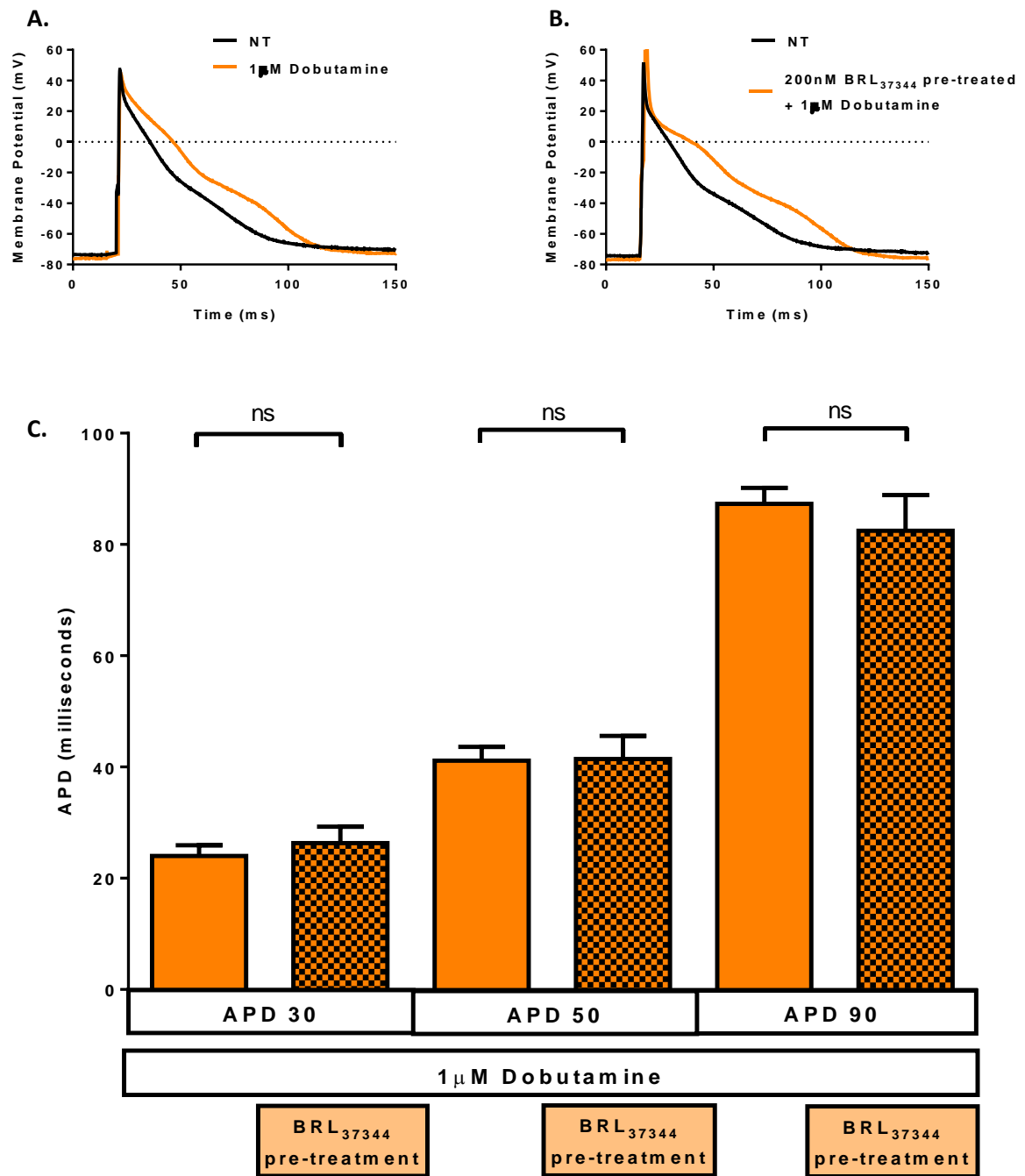
Figure 6.8 **The effect of β_3-ADR activation with BRL$_{37344}$ pre-treatment on the response of the cardiac action potential β_1-adrenergic stimulation with dobutamine.**

Representative action potential recordings from myocytes superfused with **A.** normal Tyrode (black) and 1µM dobutamine (orange) and **B.** normal Tyrode (black) and pre-treated with 200nM BRL$_{37344}$ prior 1µM dobutamine (orange).

C. Bar charts showing APD$_{30}$, APD$_{50}$ and APD$_{90}$ recorded from ventricular myocytes superfused with 1µM Dobutamine (open bars, n=5(16)) and in cells pre-treated with 200nM BRL$_{37344}$ prior 1µM Dobutamine (hatched bars, n=4(15)). Values are mean ± S.E.M. Number of hearts (number of experiments); one-way ANOVA, Sidak's *post-hoc* test.

These data show no effect of BRL$_{37344}$ pre-treatment on the increase in APD following non-specific β-adrenergic agonist ISO or the specific β$_1$-ADR agonist dobutamine.

6.2.4 The anti-arrhythmic effect of β$_3$-ADR stimulation is mediated through G$_i$ and its downstream signalling pathways

BRL$_{37344}$ is reported as a β$_3$-ADR specific agonist, however at high concentrations is suggested to also bind to β$_1$-ADR and β$_2$-ADR. Therefore, in order to exclude any additional stimulation of β$_1$-ADR by BRL$_{37344}$ being responsible for the additional increase in SERCA activity it would be beneficial to complete these experiments using specific β3-ADR antagonists, such as SR$_{59230A}$ (Alexander, Benson et al. 2013). However, β$_3$-ADR antagonists are unreliable, with little specificity for β$_3$-ADR and even exhibiting agonist properties in some tissue types (Vrydag and Michel 2007). I therefore decided to use PTx treatment to functionally uncouple G$_i$ from the β$_3$-ADR receptor, rendering it inactive to investigate the G$_i$ signalling pathway in the BRL$_{37344}$ pre-treatment induced anti-arrhythmic effect and its augmentation of SERCA activity.

Comparison of basal arrhythmic activity between freshly isolated and control cells (incubated in NT for 3 hours at 37°C) showed the no difference in development of arrhythmic activity in response to β–ADR stimulation (See Appendix 2). In order to control for any differences in cell isolations, basal arrhythmic activity between control and PTx-treated cells were compared, and unless otherwise stated no differences in basal parameters were found.

6.2.4.1 PTx treatment removes the anti-arrhythmic effect of β$_3$-ADR stimulation with BRL$_{37344}$

To examine the impact of G$_i$ protein uncoupling by PTx treatment on the development of spontaneous contractile activity following β$_3$-ADR activation with BRL$_{37344}$ pre-treatment, I compared the percentage of control myocytes and PTx-treated myocytes developing displaying spontaneous extra-contractions in response to β$_1$-ADR stimulation with 1µM dobutamine and how the protective effects of BRL$_{37344}$ pre-treatment affected this, by pre-treating cells with 200nM BRL$_{37344}$ prior to 1µM dobutamine perfusion (in the continued

presence of 200nM BRL$_{37344}$). Arrhythmic activity was determined as previously described (See Methods 2.2.2).

Figure 6.9 is a bar chart of mean percentage of control and PTx-treated myocytes exhibiting spontaneous contractile activity in response to 1μM dobutamine alone and following pre-treatment with BRL$_{37344}$, showing the effect of G$_i$ uncoupling with PTx-treatment on the anti-arrhythmic actions of BRL$_{37344}$ pre-treatment.

The data shows no difference in the level of arrhythmic activity in response to β$_1$-ADR activation with dobutamine between control cells at 59.6 + 5.32% (n=3(9/110)) and PTx-treated cells at 70.83 ± 3.20% (n=3(8/85;p=0.22). As previously shown (Figure 6.2B), BRL$_{37344}$ pre-treatment significantly reduced the induction of arrhythmic activity in response to dobutamine in fresh cells. The anti-arrhythmic effect of BRL$_{37344}$ pre-treatment was sustained in control myocytes, from 59.6 ± 5.3% (n=3(9/110) in control cells to 41.3 ± 4.6% (n=3(6/68;p<0.05)) in BRL$_{37344}$ pre-treated myocytes. However BRL$_{37344}$ pre-treatment had no effect on arrhythmia generation response to dobutamine in PTx-treated cells, 70.8 ± 3.2% (n=3(8/85) versus 69.3 ± 3.1% (n=3(7/93);p=0.99)).

These data show G$_i$ inhibition removes the cardio-protective effect of BRL$_{37344}$ pre-treatment on arrhythmia generation, indicating the G$_i$ protein and its downstream pathway is responsible for the protective effect of BRL$_{37344}$ pre-treatment.

6.2.4.2 PTx treatment removes the additional increase in SERCA activity induced by β$_3$-ADR stimulation with BRL$_{37344}$

My data showed that BRL$_{37344}$ pre-treatment enhanced the increase in SERCA activity (rate of relaxation of the electrically-induced Ca^{2+} transient) in response to dobutamine. I have also shown that G$_i$ uncoupling with PTX inhibits the anti-arrhythmic actions of BRL$_{37344}$ pre-treatment. I therefore proposed that this enhanced increase in SERCA activity in response to dobutamine in BRL$_{37344}$ pre-treated myocytes would be lost following PTx treatment.
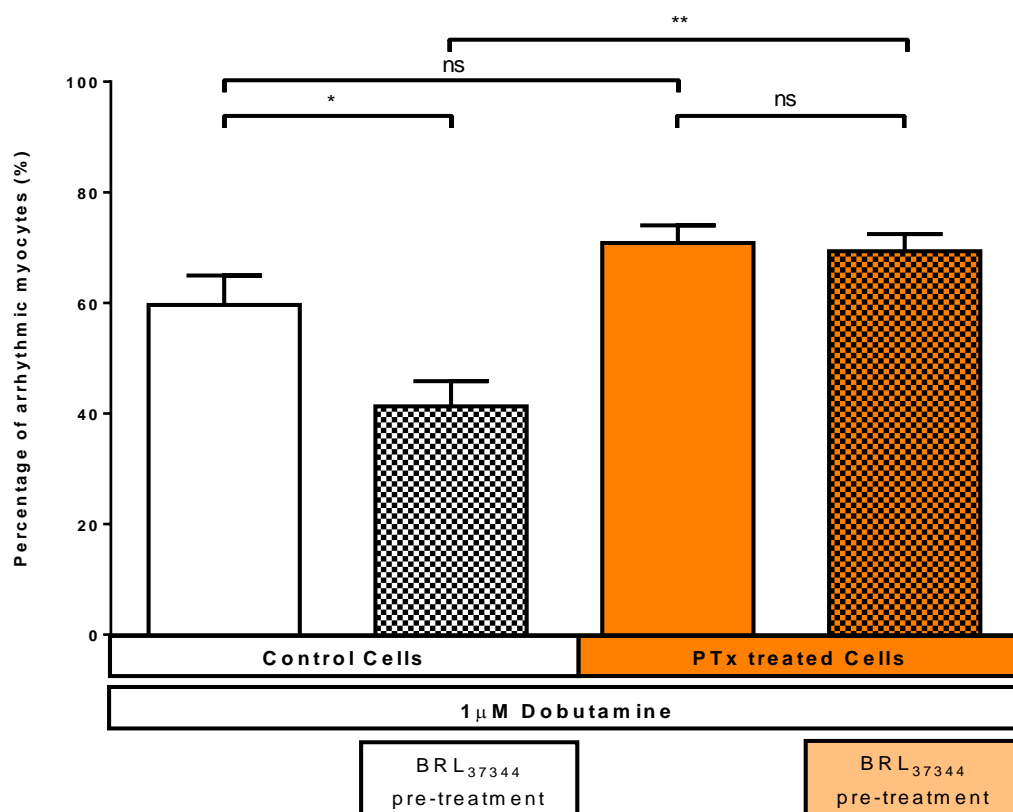
Figure 6.9 **The effect of PTx treatment on the anti-arrhythmic effect of β_3-ADR activation with BRL$_{37344}$ pre-treatment.**

Bar chart showing the percentage of control and PTx-treated myocytes that developed spontaneous extra-contractions, calculated from a field of 10-20.

Control cells; perfused with 1μM dobutamine (open white bar, n=3(9/110)) and pre-treated with 200nM BRL$_{37344}$ prior to dobutamine (hatched white bar; n=3(6/68)). PTx-treated cells; perfused with 1μM dobutamine (open orange bar, n=3(8/95)) and pre-treated with 200nM BRL$_{37344}$ prior to dobutamine (hatched orange bar, n=3(7/93)).

Values are mean ± S.E.M. Number of hearts (number of experiments/number of cells); *p<0.05, **p<0.01, two-way ANOVA, Sidak's *post-hoc* test.

To determine the impact of G_i protein uncoupling by PTx treatment on the ability of β_3-ADR stimulation with BRL_{37344} to enhance the increase in SERCA activity by dobutamine, I compared the activity of SERCA (the exponential time constant of the electrically-induced Ca^{2+} transient) in control and PTX-treated myocytes pre-treated cells with 200nM BRL_{37344} prior to 1µM dobutamine perfusion (in the continued presence of 200nM BRL_{37344}) compared to in response to 1µM dobutamine alone. SERCA activity was determined as previously described (See Methods 2.2.3).

Figure 6.10 is a bar chart showing the effect of BRL_{37344} pre-treatment on the rate of relaxation of the electrically-induced Ca^{2+} transient (SERCA activity) in control and PTx-treated myocytes in response to 1µM dobutamine.

The data shows no difference in the activity of SERCA in response to β_1-ADR activation with dobutamine between control cells at 153.3 ± 9.6ms (n=5(10)) and PTx-treated cells at 136.6 ± 8.0ms (n=4(18);p=0.25).

As previously shown (Figure 6.4CB), BRL_{37344} pre-treatment significantly increased the activity of SERCA (reduced relaxation time) in response to dobutamine in fresh cells. This augmented increase in SERCA activity by BRL_{37344} pre-treatment was sustained in control myocytes, from 153.3 ± 9.6ms (n=-5(10)) to 119.6 ± 6.8ms (n=4(16);p<0.05) in BRL_{37344} pre-treated myocytes. However BRL_{37344} pre-treatment had no effect on the increase in SERCA activity in response to dobutamine in PTx-treated cells, 136.6 ± 8.0ms (n=4(18)) versus 122.6 ± 7.8ms (n=5(20);p=0.99).

These data show G_i inhibition abolishes the augmented reduction in relaxation time of the Ca^{2+} transient, indicating the G_i protein and the downstream pathway is responsible for the protective effect of BRL_{37344} pre-treatment on the increase in SERCA activity beyond the level of dobutamine alone.

However, it is possible that this result could be misleading due to the shorter relaxation time in PTx cells following dobutamine. Although this was not significantly different to relaxation time in control cells following PTx treatment (p=0.25), relaxation time in both control and PTx treated cells was shortened further by BRL37344 pre-treatment to approximately the same level, control cells at 119.6 ± 6.8ms (n=4(16)) versus PTx treated cells at 122.6 ± 7.8ms (n=5(20)), and no significant difference in relaxation time with BRL_{37344} pre-treatment existed between control and PTx treated cells (p=0.99).
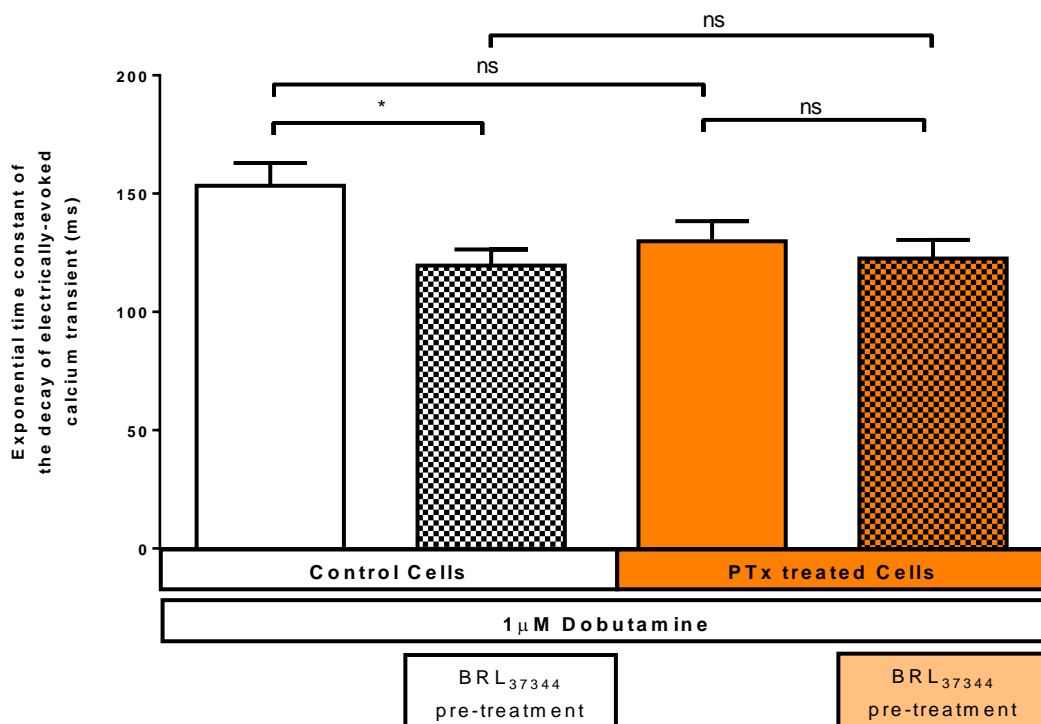
Figure 6.10 **The effect of PTx treatment on the reduction in relaxation time of the Ca^{2+} transient in response to β$_3$-ADR activation with BRL$_{37344}$ pre-treatment.**

Bar chart showing the exponential time constant of the electrically-induced Ca^{2+} transient of control and PTx-treated myocytes, stimulated at 1Hz by electrical field stimulation. Control cells; perfused with 1μM dobutamine (open white bar, n=5(10)) and pre-treated with 200nM BRL$_{37344}$ prior to dobutamine (hatched white bar; n=4(16)). PTx-treated cells; perfused with 1μM dobutamine (open orange bar, n=4(18)) and pre-treated with 200nM BRL$_{37344}$ prior to dobutamine (hatched orange bar, n=5(20)). Values are mean ± S.E.M. Number of hearts (number of experiments); $p < 0.05$, two-way ANOVA, Sidak's *post-hoc* test.

6.2.5 The role of nitric oxide in the anti-arrhythmic effect of β_3-ADR stimulation with BRL$_{37344}$

I have shown an anti-arrhythmic action of β_3-ADR stimulation by BRL$_{37344}$ against β_1-ADR induced arrhythmia. The β_3-ADR is coupled to the inhibitory G$_i$ protein; The G$_{i\alpha}$ activates PDE3 and PDE4, leading to hydrolysis of cAMP (Berthouze, Laurent et al. 2011), and the G$_{i\beta}$ subunit stimulates NO production by NOS, initiating its cGMP–dependent and cGMP–independent pathways which directly phosphorylate (cGMP–dependent) and S-nitrosylate (cGMP–independent) the components of E-C coupling (Hare 2003). The anti-arrhythmic action of β_3-ADR stimulation by BRL$_{37344}$ could be mediated by NO (G$_{i\beta}$ sub-unit), the action of PDE3 and PDE4 to reduce cAMP levels (G$_{i\alpha}$ sub-unit) or a combination of both. To investigate the role of NO in the anti-arrhythmic action of β_3-ADR stimulation by BRL$_{37344}$, we investigated arrhythmia generation and BRL$_{37344}$ cardio-protection during NOS inhibition with N^G-nitro-L-Arginine (L-NNA).

6.2.5.1 Inhibition of nitric oxide synthase removes the anti-arrhythmic effect of β_3-ADR stimulation with BRL$_{37344}$

To examine the role of NO in the anti-arrhythmic action of β_3-ADR activation with BRL$_{37344}$ pre-treatment, I compared the percentage of myocytes displaying spontaneous extra-contractions in response to β_1-ADR stimulation with 1uM dobutamine, and after pre-treatment of cells with 200nM BRL$_{37344}$ in the absence and presence of the non-specific NOS inhibitor 500µM L-NNA. L-NNA was present during BRL$_{37344}$ pre-treatment and perfusion with dobutamine. Arrhythmic activity was determined as previously described (See Methods 2.2.2).

Figure 6.11 shows the effect of NOS inhibition on the percentage of cells which displayed spontaneous arrhythmic activity in response to dobutamine, following BRL$_{37344}$ pre-treatment in the absence and presence of L-NNA. As previously shown in Figure 6.2B, superfusion of cells with dobutamine induced arrhythmic activity in 56.3 ± 2.9% (n=8(26/386) of myocytes and the pre-treatment of cells with BRL$_{37344}$ reduced this to 31.9 ± 2.7% (n=4(8/113);p<0.0001)). Inhibition of NOS during BRL$_{37344}$ pre-treatment abolished its ability to reduce arrhythmic activity in response to dobutamine, with 62.1 ± 2.4%
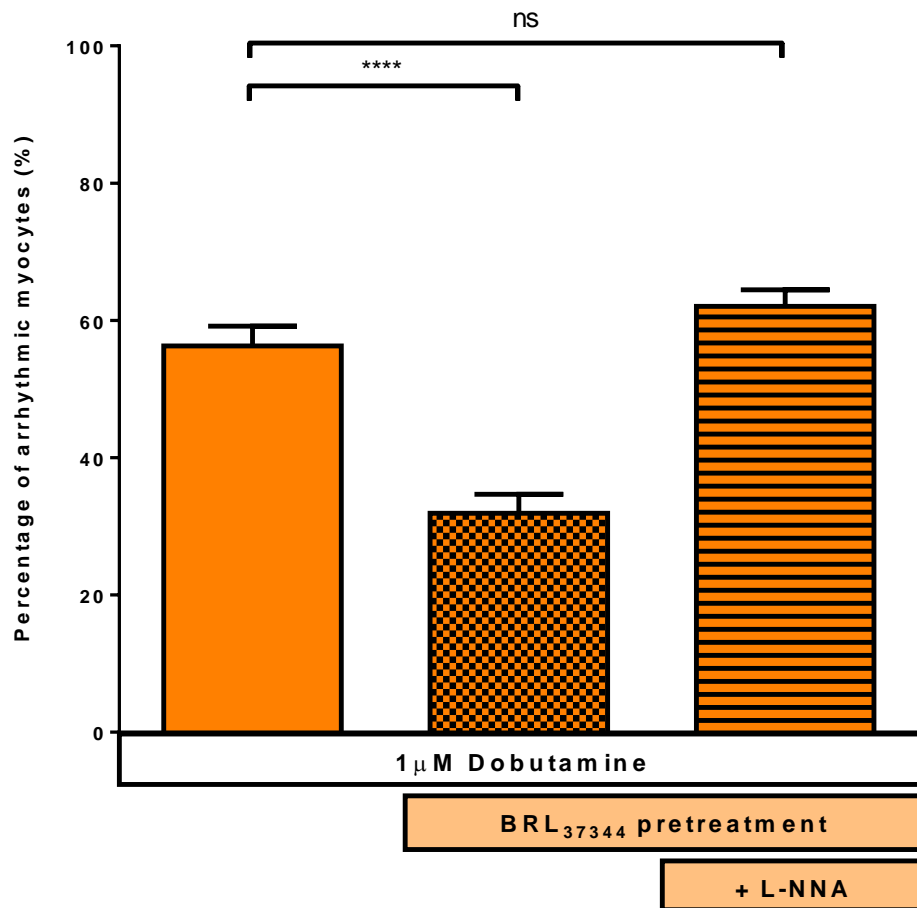
Figure 6.11 **The effect of Nitric Oxide Synthase Inhibition on the anti-arrhythmic effect of β_3-ADR activation with BRL$_{37344}$ in response to β_1-ADR stimulation with dobutamine.**

Bar chart showing the percentage of myocytes that develop spontaneous extra-contractions following superfusion with 1μM Dobutamine (open bar, n=8(26/386)), pre-treated with 200nM BRL$_{37344}$ prior to 1μM Dobutamine (hatched bar, n=4(8/113)) and pre-treated with 200nM BRL$_{37344}$ plus 500μM L-NNA prior to 1μM Dobutamine (striped bar, n=3(8/248)). Values are mean ± S.E.M. Number of hearts (number of experiments/number of cells); ****p<0.0001, one-way ANOVA, Sidak's *post-hoc* test.

(n=3(8/248)) of myocytes exhibiting spontaneous activity, which was not significantly different to dobutamine alone.

As a control, I also tested whether NOS inhibition had any effect on arrhythmic activity in the response to β_1-ADR stimulation with dobutamine. Arrhythmic activity in response to β_1-ADR stimulation with dobutamine, at 56.3 + 2.9% (n=8(24/386), did not change in response to NOS inhibition, 61.6 ± 2.5% (n=3(16/219);p=0.20).

These data show NOS inhibition abolishes the anti-arrhythmic actions of β_3-ADR activation with BRL_{37344} on arrhythmia generation during β_1-ADR activation, indicating that NO and its downstream pathway are responsible for this anti-arrhythmic activity.

6.2.5.2 Inhibition of nitric oxide synthase removes the additional increase in SERCA activity induced by β_3-ADR stimulation with BRL_{37344}

I have previously shown the anti-arrhythmic action of β_3-ADR stimulation with BRL_{37344} is accompanied by an additional increase in SERCA activity beyond the increase in response to β_1-ADR stimulation alone. As I have shown NOS inhibition abolishes the anti-arrhythmic actions of BRL_{37344} pre-treatment, I propose the additional increase in SERCA activity which accompanies BRL_{37344} pre-treatment will also be lost.

To determine the effect of NOS inhibition on the ability of BRL_{37344} to enhance the increase in SERCA activity by dobutamine, I compared the activity of SERCA (the exponential time constant of the electrically-induced Ca^{2+} transient) in response to β_1-ADR stimulation with 1uM dobutamine, and after pre-treatment of cells with 200nM $BRL_{37344,}$ in the absence and presence of the non-specific NOS inhibitor 500µM L-NNA. L-NNA was present during BRL_{37344} pre-treatment and perfusion with dobutamine. SERCA activity was determined as previously described (See Methods 2.2.3).

Figure 6.12 shows the exponential time constant of relaxation of the Ca^{2+} transients cells in response to dobutamine, following BRL_{37344} pre-treatment in the absence and presence of L-NNA. As previously shown in Figure 6.4C, superfusion of cells with dobutamine reduced relaxation time to 121.4 ± 5.6ms (n=3(14)) and the pre-treatment of cells with BRL_{37344} reduced this to 99.1 ± 5.6ms (n=3(22);p<0.05). Inhibition of NOS during BRL_{37344} pre-treatment did not fully abolish its ability to augment the increase in SERCA activity in
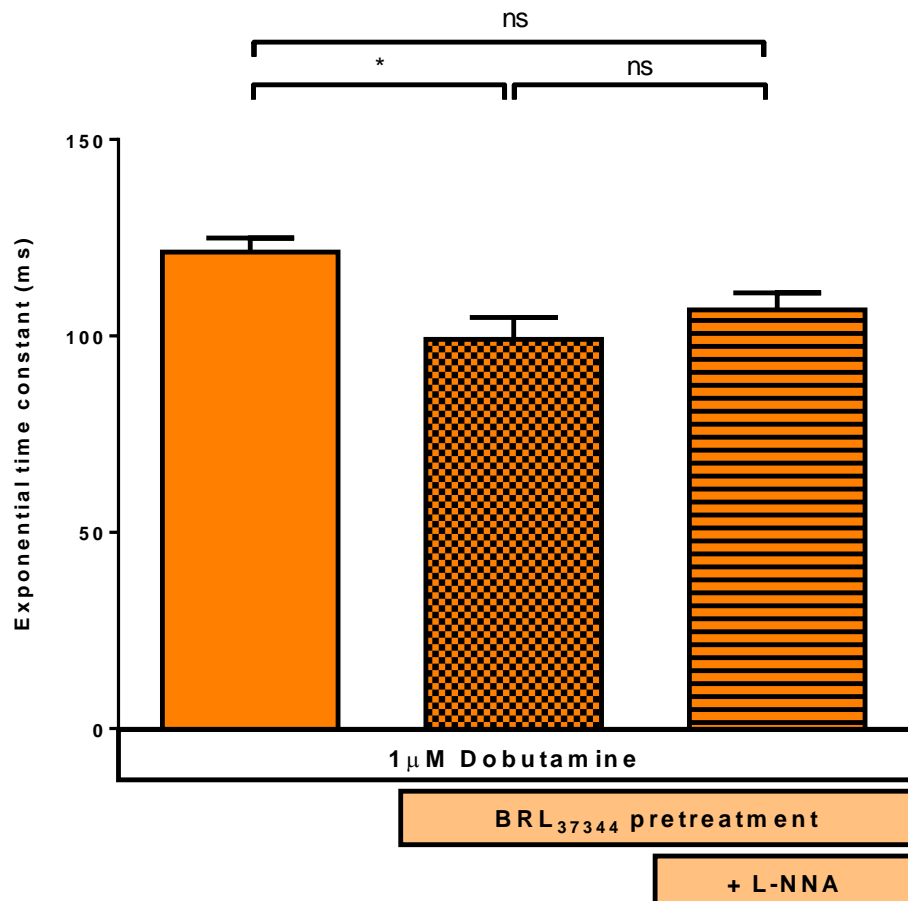
Figure 6.12 **The effect of Nitric Oxide Synthase Inhibition on the additional reduction in SERCA activity induced by β_3-ADR activation with BRL$_{37344}$ in response to β_1-ADR stimulation with dobutamine.**

Bar chart showing the exponential time constant of the decay of the electrically-induced Ca^{2+} transient recorded from ventricular myocytes stimulated at 1Hz by electrical field stimulation following superfusion with 1μM Dobutamine (open bar, n=3(14)), pre-treated with 200nM BRL$_{37344}$ prior to 1μM Dobutamine (hatched bar, n=3(22)) and pre-treated with 200nM BRL$_{37344}$ plus 500μM L-NNA prior to 1μM Dobutamine (striped bar, n=4(25)). Values are mean ± S.E.M. Number of hearts (number of experiments); *$p < 0.05$, one-way ANOVA, Sidak's *post-hoc* test.

response to dobutamine, at 106.6 ± 4.4ms (n=4(25)), however following BRL_{37344} pre-treatment SERCA activity was not significantly different to dobutamine alone (p=0.11).

As a control, I also tested whether NOS inhibition had any effect on SERCA activity in response to β_1-ADR stimulation with dobutamine. SERCA activity response to β_1-ADR stimulation with dobutamine, at 121.4 ± 3.6ms (n=3(14)), did not change in response to NOS inhibition, 115.2 ± 4.8ms (n=3(17);p=0.33)).

These data show NOS inhibition abolishes the augmented reduction in relaxation time during β_1-ADR activation, indicating that NO and its downstream pathway is involved in the increase in SERCA activity beyond the level of dobutamine alone.

6.2.6   Coupling of the β_2-ADR to G_i provides an anti-arrhythmic effect against specific β_2-ADR stimulation

I have shown β_2-ADR stimulation with a maximal concentration of salbutamol (1µM) did not induce arrhythmia in myocytes. The coupling of β_2-ADR to G_i leads to the activation of PDE3 and PDE4, limiting the diffusion of cAMP. The local increase in cAMP results in a reduced inotropic response to β_2-ADR stimulation as only targets of E-C coupling local to the β_2-ADR, such as LTCC and NCX, are affected by β_2-ADR derived cAMP.

In agreement with the literature, my data (Chapter 5.2.3) suggests that the compartmentalisation of cAMP signalling can be abolished by inhibition of PDE and PTx treatment to uncouple the G_i protein from the β_2-ADR. Abolishing the compartmentalisation of cAMP leads to global increases in cAMP and a greater inotropic response as targets of E-C coupling distal to the β_2-ADR, such as RyR2, PLB and TnI, are able to be targeted by β_2-ADR derived cAMP (Xiao, Ji et al. 1995; Xiao, Avdonin et al. 1999; Xiao 2001; Heijman, Volders et al. 2011; Cros and Brette 2013)

 I have previously shown that PTx treatment in the rat ventricular myocyte enhances the inotropic effect of β_2-ADR stimulation, augmenting the increase in systolic Ca^{2+} and the activity of SERCA (Chapter 5.2.3.2). Although SR Ca^{2+} content of PTx-treated myocytes was not measured previously, we propose SR Ca^{2+} content may have been increased following PTx treatment, as an increase in SERCA activity is associated with an increase in SR Ca^{2+} content as greater quantities of Ca^{2+} are re-sequestered to the SR during the relaxation

(Bers 2001). If SR Ca^{2+} content were to increase, this may act as a driver for DADs, and may enhance the ability of the β_2-ADR to induce arrhythmia.

I propose that coupling of the β_2-ADR to G_i and compartmentalised cAMP signalling, limits the ability of the β_2-ADR to induce arrhythmia and so we set out to investigate if the coupling to G_i provides a protective anti-arrhythmic action during β_2-ADR stimulation.

6.2.6.1   The β_2-ADR agonist salbutamol is pro-arrhythmic in the absence of G_i-coupling

β_2-ADR receptors are coupled to both the G_s and G_i proteins. In order to determine whether the Gi coupling, in addition to reducing the increase in systolic $[Ca^{2+}]_i$ in response to dobutamine and G_s-coupling, I set out to investigate if the coupling to G_i provides a protective anti-arrhythmic action, in PTX-treated cells which specifically uncouples G_i.

Comparison of basal arrhythmic activity between freshly isolated and control cells showed the no difference in arrhythmic activity (See Appendix 2).

To examine the impact of G_i protein uncoupling by PTx treatment on the development of spontaneous contractile activity following β_2-ADR activation with salbutamol, I compared the percentage of control myocytes and PTx-treated myocytes developing spontaneous extra-contractions in response to β_2-ADR stimulation with 1µM salbutamol. Arrhythmic activity was determined as previously described (See Methods 2.2.2).

Figure 6.13 is a bar chart of mean percentage of control and PTx-treated myocytes exhibiting spontaneous contractile activity in response to 1µM salbutamol. As previously described in Figure 6.1, salbutamol did not induce significant arrhythmic activity in freshly isolated cells, at 0.9 ± 0.3% (n=4(30/401)), however in control myocytes (3 hours incubation at 37°C in presence of Pen/strep) salbutamol did induce arrhythmic activity, at 7.7 + 1.7% (n=3(7/100)). The data shows a significant difference in the level of arrhythmic activity in response to β_2-ADR activation with salbutamol between control cells at 7.7 + 1.7% (n=3(7/100)) and PTx-treated cells at 27.3 ± 4.6% (n=3(7/66); p<0.001). G_i uncoupling with PTX-treatment, significantly increased the ability of salbutamol to produce arrhythmic activity; suggesting the dual coupling of β_2-ADR to G_i prevents arrhythmic activity in response to β_2-ADR activation by salbutamol.

Figure 6.13 **The effect of PTx treatment on the arrhythmic effect of β₂-ADR activation with salbutamol.**

Bar chart showing the percentage of control myocytes (white bar, n=3(7/100)) and PTx-treated myocytes (blue bar, n=3(7/66)) which developed spontaneous extra-contractions following perfusion with 1μM salbutamol, calculated from a field of 10-20.

Values are mean ± S.E.M. Number of hearts (number of experiments/number of cells); **p<0.01, unpaired t-test.

6.2.6.2 The β$_2$-ADR agonist salbutamol is pro-arrhythmic in the absence of PDE activity

My data has shown that G$_i$ uncoupling with PTX uncovers an arrhythmic actions of β$_2$-ADR stimulation with salbutamol which was absent in freshly isolated cells. The coupling of β$_2$-ADR to G$_i$ leads to the activation of PDE3 and PDE4, results in the compartmentalisation of cAMP signalling by limiting the diffusion of cAMP away from the β$_2$-ADR, thereby and limiting the positive inotropic response of β$_2$-ADR stimulation. Inhibition of PDE abolishes the compartmentalised signalling of the β$_2$-ADR as targets of E-C coupling distal to the β$_2$-ADR, such as RyR2, PLB and TnI, are able to be targeted by β$_2$-ADR derived cAMP. I therefore propose that inhibition of PDE and the resulting global increase in cAMP will lead to development of arrhythmic activity in rat ventricular myocytes.

To examine the impact of PDE inhibition on the development of spontaneous contractile activity following β$_2$-ADR activation with salbutamol, I compared the percentage myocytes developing spontaneous extra-contractions in response to β$_2$-ADR stimulation with 1μM salbutamol in the presence and absence of 30μM IBMX. Arrhythmic activity was determined as spontaneous extra-contractions in the absence of electrical field stimulation (As described in Methods 2.2.2).

Figure 6.14 is a bar chart of mean percentage of myocytes exhibiting spontaneous contractile activity in response to 1μM salbutamol and 1μM salbutamol plus 30μM IBMX. As previously described in Figure 6.1, salbutamol did not induce significant arrhythmic activity in freshly isolated cells, at 0.9 ± 0.3% (n=4(30/401)). However, inhibition of PDE with IBMX during salbutamol induced significant arrhythmic activity, at 50.6 ± 5.5% (n=3(6/112)) and so the data shows a significant difference in the percentage of myocytes developing arrhythmia in the absence and presence of PDE inhibition (p<0.0001).

PDE inhibition during salbutamol perfusion leads myocytes to become pro-arrhythmic; suggesting the dual coupling of β$_2$-ADR to G$_i$ and subsequent activation of PDE prevents arrhythmic activity in response to β$_2$-ADR activation by salbutamol.
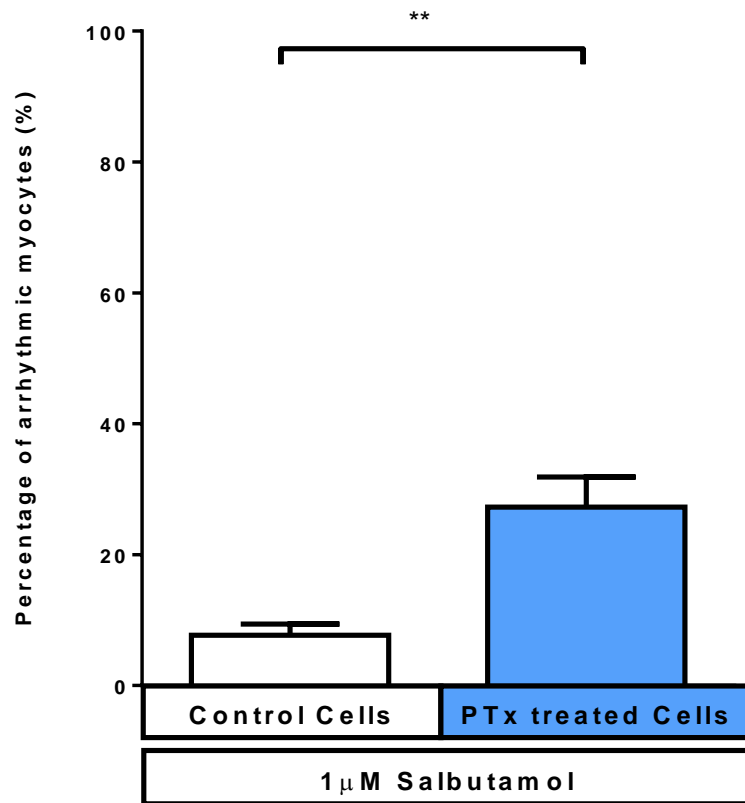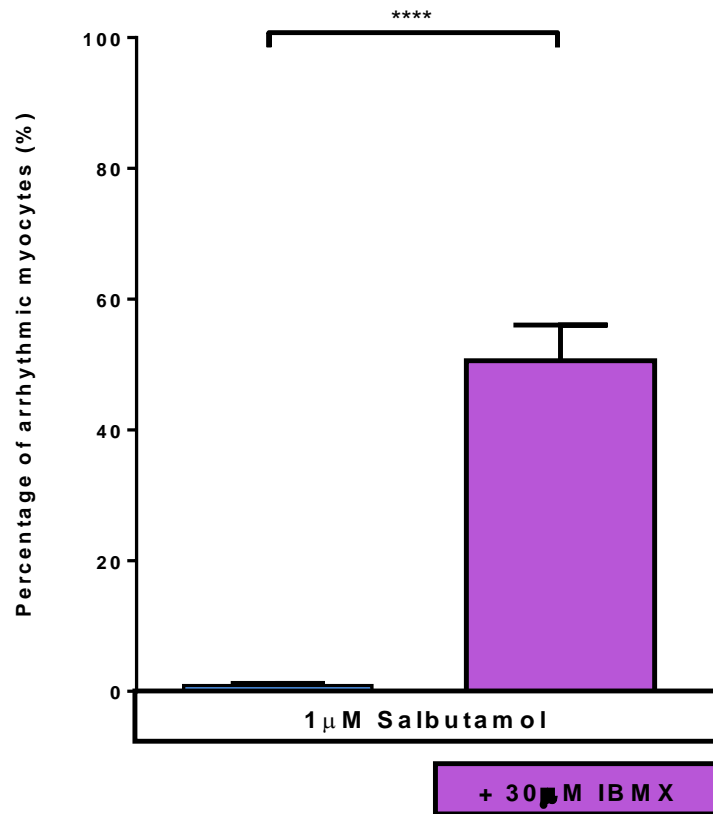
Figure 6.14   The effect of PDE inhibition on the arrhythmic effect of β_2-ADR activation with salbutamol.

Bar chart showing the percentage of myocytes which developed spontaneous extra-contractions following perfusion with 1μM salbutamol (blue bar, n=4(30/401)) and 1μM salbutamol and 30μM IBMX (purple bar, n=3(6/112)) calculated from a field of 10-20. Values are mean ± S.E.M. Number of hearts (number of experiments/number of cells); **p<0.01, unpaired t-test.

6.3   Discussion

In the present chapter I have investigated the potential anti-arrhythmic actions of β_3-ADR stimulation against sympathetic induced arrhythmia in rat ventricular myocytes, in particular in response to β_1-ADR and β_2-ADR stimulation using specific agonists. I have shown β_3-ADR activation by pre-treatment with the specific agonist BRL_{37344} prior to β_1-ADR stimulation reduces the development of β_1-ADR agonist-induced spontaneous arrhythmic activity of ventricular myocytes. This effect is paradoxically accompanied by an increase in SERCA activity over and above that seen by β_1-ADR activation alone. This anti-arrhythmic effect of BRL_{37344} pre-treatment is mediated by the G_i protein and NO signalling.

In addition, I have shown coupling of the β_2-ADR to the G_i protein reduces the propensity of β_2-ADR activation to generate arrhythmic activity in myocytes that is mediated by PDE and which may reflect compartmentalisation of cAMP.

The anti-arrhythmic actions of G_i coupling to both β_2-ADR and β_3-ADR may mediate an endogenous anti-arrhythmic action during excessive sympathetic activity.

6.3.1   The anti-arrhythmic action of β_3-ADR: Role of Nitric Oxide

It has been suggested that the β_3-ADR may act as a feedback mechanism in the heart, preventing Ca^{2+} overload damage from excessive $\beta_{1/2}$-ADR stimulation during periods of high levels of circulating catecholamines. This proposal was first based on the observation of a negative inotropic effect of β_3-ADR stimulation (Gauthier, Tavernier et al. 1996) and the need for greater concentration of circulating catecholamine required to stimulate the β_3-ADR as compared to the β_1/β_2-ADR (Strosberg 1997; Rozec and Gauthier 2006), and it has since been observed that genetic deletion of β_3-ADR results in a potentiation of cardiac contractility in response to sympathetic stimulation (Varghese, Harrison et al. 2000), providing evidence that the β_3-ADR act to oppose the positive inotropic effect of β_1/β_2-ADR stimulation. The negatively inotropic action of β_3-ADR may protect the myocardium during periods of excessive/prolonged $\beta_{1/2}$-ADR stimulation, and the action to reduce contractility and systolic $[Ca^{2+}]_i$ is likely to protect against arrhythmia generation.

An anti-arrhythmic effect of β_3-ADR signalling has been shown in a rabbit heart failure model, that 30 minutes pre-treatment with the β_3-ADR agonist BRL_{37344} reduced the incidence of β_1-ADR induced ventricular tachycardia (VT) by 50%, which was associated with an inhibition on the increase in the Ca^{2+} transient, SR Ca^{2+} load and I_{NCX} current density induced by β_1-ADR activation (Li, Liu et al. 2010). Zhou *et al.* have also shown β_3-ADR stimulation with BRL_{37344} is able to reduce the number of VT episodes in a canine model of VT after 1 month subcutaneous perfusion, which again was associated with changes in NCX, observed as reduced protein levels (Zhou, Tan et al. 2008). Although the investigators did not investigate the impact of NOS signalling on the anti-arrhythmic properties of β_3-ADR stimulation with BRL_{37344}, it is likely that eNOS and/or nNOS signalling impacted on the LTCC (eNOS) and SR Ca^{2+} content (nNOS) preventing Ca^{2+} overload and limiting arrhythmia generation.

In this chapter I have examined the ability of the β_3-ADR agonist BRL_{37344} to prevent arrhythmic activity in isolated ventricular myocytes in response to β_1-ADR stimulation with dobutamine. Due to the nature of the experimental set up, whereby arrhythmic activity was recorded as spontaneous extra-contractions in the absence of electrical field stimulation, any arrhythmic activity I observed was defined as a DAD. DADs occur after repolarisation is complete and are initiated by a spontaneous SR Ca^{2+} release from the RyR2, a "Ca^{2+} spark", initiating a Ca^{2+}-activated transient inward depolarising current, (INCX, $I_{Cl(Ca)}$ or $I_{NS(Ca)}$) depolarising the membrane (Venetucci, Trafford et al. 2008; Eisner, Kashimura et al. 2009) (See Introduction 1.1.5).

$\beta_{1/2}$-ADR stimulation activation has been shown to activate arrhythmias due to after-depolarisations; EAD's or DAD's (See Introduction 1.1.4). In the previous chapter (Chapter 5), I have shown $\beta_{1/2}$-ADR stimulation with ISO (global β-ADR) and dobutamine (β_1-ADR) lead to an increase in systolic $[Ca^{2+}]_i$, SR Ca^{2+} content, the LTCC and APD, which are likely to impact upon arrhythmia generation. Both the non-specific β-ADR agonist ISO and the specific β_1-ADR agonist dobutamine induced arrhythmic activity, in the form of delayed after-contractions, which fits with data previously shown in Chapter 5.2.1, in which ISO and dobutamine significantly increased SR Ca^{2+} content; which is known to be the main cause of DADs.

My data shows a clear reduction in the propensity of arrhythmic activity in response to both the non-specific β-ADR agonist ISO and the β_1-ADR agonist dobutamine, by prior β_3-

ADR activation with BRL_{37344} which could be abolished by NOS inhibition, indicating NO signalling in the anti-arrhythmic effect of β_3-ADR stimulation.

I previously showed (Chapter 5 Figure 5.6) that BRL_{37344} is able to reduce Ca^{2+} loading (SR Ca^{2+} content) and this would be expected to reduce the potential for DAD-induced arrhythmia (See Introduction 1.4). I had postulated that the anti-arrhythmic action of BRL_{37344} would result from a reduction in SR Ca^{2+} load, however, BRL_{37344} pre-treatment did not reduce the increase of the SR Ca^{2+} load in response to dobutamine. However, the anti-arrhythmic action of BRL_{37344} pre-treatment was instead associated with an additional increase in SERCA activity with no effect on the increase in SR Ca^{2+} content following β_1-ADR. Activation of β_1-ADR results in an increase in PKA activity which phosphorylates PLB at ser16 relieving inhibition and increasing SERCA activity, which increases the rate of decline in $[Ca^{2+}]_i$ during relaxation but also increasing SR Ca^{2+} content, which is considered to be pro-arrhythmic (Bers 2002). However, β_3-ADR activation results in an increase NOS signalling which also phosphorylates PLB, at Ser16 and but also at Thr17 (Pavlovic, Hall et al. 2013), and is therefore potentially increasing PLB phosphorylation above the level achieved by β_1-ADR stimulation.

However, despite this additional increase in SERCA activity in response to dobutamine, caused by β_3-ADR activation with BRL_{37344} pre-treatment, SR Ca^{2+} load was not increased beyond the levels driven by dobutamine alone. The apparent dissociation of an increase in SERCA activity and SR Ca^{2+} content was unexpected and difficult to reconcile. An additional effect of NO signalling on the SR is a result of changes to RyR2 function. As mentioned in Chapter 3 and 5, NO has been shown to increase RyR2 P_o by PKG phosphorylation (Lim, Venetucci et al. 2008) and S-nitrosylation (Stoyanovsky, Murphy et al. 1997; Xu, Eu et al. 1998) facilitating a diastolic leak (Lim, Venetucci et al. 2008). It may be that the additional $[Ca^{2+}]$ sequestered back to the SR by SERCA following BRL_{37344} pre-treatment is equal to a BRL_{37344} induced diastolic leak, which would have a null effect on the SR Ca^{2+} content.

It is also possible that NCX is involved in the lack of increase in SR Ca^{2+} content in the face of an increase in SERCA activity. Following BRL_{37344} pre-treatment, the activity of the NCX increased, although not significantly (p=0.26), however this would enable the NCX to compete with SERCA for Ca^{2+} removal, counteracting the additional increase in SERCA activity following BRL_{37344}, leading to a null effect on SR Ca^{2+} content. In addition, activation of β_3-ADR by BRL_{37344} has also been found to stimulate the Na^+/K^+ pump,

reducing $[Na^+]_i$ and promoting enhanced Ca^{2+} extrusion by NCX (Gauthier, Rozec et al. 2011). Contrary to my findings of an increase in NCX activity by BRL_{37344}, Li *et al.* observed an inhibition in the increase in I_{NCX} current density induced by β_1-ADR activation during BRL_{37344} perfusion (Li, Liu et al. 2010). Lim *et al.* suggest that other routes Ca^{2+} extrusion may be affected during conditions of enhanced RyR2 P_o and diastolic Ca^{2+} leak from the SR, such as the Na^+/H^+ exchanger (NHE). The NHE exchanges 1 Na^+ for 1 H^+, driven by the inward gradient of Na^+/K^+-ATPase, the NHE H^+ extrusion and Na^+ influx through the NHE. Given the electro-neutral coupling of 1Na:1H on the NHE, the inward flux of Na^+ via the NHE does not contribute to DAD generation, however, it may be that the increase in Na^+ by the NHE inhibits "forward-mode" NCX activity reducing the contribution of any inwardly direct NCX current to a DAD depolarising current (Lim, Venetucci et al. 2008), correlating with Li *et al.* findings of an inhibited NCX current.

In the present investigation, inhibition of NOS completely abolished the anti-arrhythmic effect of BRL_{37344} pre-treatment, demonstrating the role of NO in the anti-arrhythmic action of β_3-ADR stimulation.

My data also showed that the β_1-ADR specific agonist induced significantly greater level of arrhythmic activity in myocytes compared to the non-specific β-ADR agonist ISO. This observation may reflect the non-specific nature of ISO which stimulates β_1-ADR, β_2-ADR and β_3-ADR, and as I and others have shown β_3-ADR activation is anti-arrhythmic, it may be that stimulation of the β_3-ADR by ISO is preventing the development of arrhythmias. However, at higher concentrations of ISO (20-50nM) this difference in the incidence of arrhythmic activity was not observed (See Appendix 7), which suggests that the difference in arrhythmic action of ISO and dobutamine may have been due to the concentration of agonists used and the degree of activation of the receptors. It should however be noted that at these higher concentrations of ISO (20nM), BRL_{37344} was still able to reduce arrhythmic activity and provide protective effects against excessive β-ADR stimulation (See Appendix 8).

6.3.2   The anti-arrhythmic action of β_2-ADR coupling to G_i

In the present chapter I have shown a significantly greater propensity for arrhythmic activity in ventricular myocytes in response to maximal β_1-ADR stimulation than following maximal β_2-ADR stimulation. I have also shown that this is due to β_2-ADR coupling to the G_i protein, suggesting the compartmentalisation of cAMP signalling prevents arrhythmia generation, as uncoupling of the G_i protein from the β_2-ADR and inhibition of PDE enhances the arrhythmic action of β_2-ADR signalling.

DADs are triggered under conditions of increased $[Ca^{2+}]_i$ and high SR Ca^{2+} load and as I have shown in the previous chapter (Chapter 5.2.1) the positive effect of β_2-ADR stimulation on Ca^{2+} handling is modest this may explain the lack of DAD in response to salbutamol. In agreement with current reports in the literature, I have also shown the modest effect of β_2-ADR on Ca^{2+} handling to be due to dual coupling to the G_i protein and the resulting compartmentalised cAMP signalling due to activation of PDE, which limits increases in $[Ca^{2+}]_i$ and SR Ca^{2+} content; the drivers of DAD.

Following G_i uncoupling or PDE inhibition, the compartmentalisation of cAMP is abolished and a stimulation of the β_2-ADR leads to a global rise in cAMP, allowing targets of E-C coupling distal to the β_2-ADR to be phosphorylated by β_2-ADR derived PKA (Xiao, Ji et al. 1995; Xiao, Avdonin et al. 1999; Xiao 2001; Heijman, Volders et al. 2011; Cros and Brette 2013), and in the previous chapter (Chapter 5.2.3) I have shown G_i uncoupling or PDE inhibition lead to further increases in systolic $[Ca^{2+}]_i$, SR Ca^{2+} content and APD, which may affect arrhythmia generation as DAD's are triggered when SR Ca^{2+} content is high. If the increased SR Ca^{2+} load is sufficient, a spontaneous release of Ca^{2+} from the SR will fire, which can initiate the Ca^{2+} activated transient inward depolarising currents, which if sufficient in amplitude will fire an action potential; a DAD.

Under physiological conditions, the dual coupling of β_2-ADR to G_i limits the positive inotropic effect (SR Ca^{2+} accumulation) and provides a protective effect against DAD generation.

This protective action of G_i coupling to the β_2-ADR against arrhythmic activity differs from the anti-arrhythmic action of the β_3-ADR G_i coupling due to the involvement of NOS. The β_2-ADR and are both coupled to the inhibitory G-proteins, G_i, however the downstream signalling of each receptor differs. Stimulation of the β_3-ADR sets of α and β. Whereas β_2-

ADR stimulation leads to activation of the α subunit only, and there are no reports in the literature of the involvement of the beta subunit and NO in the signalling pathway of the β_2-ADR (See Introduction 1.2).

6.3.3 Conclusions

In the present study, I have shown β_3-ADR stimulation with BRL_{37344} is able to reduce the development of arrhythmic activity in isolated ventricular myocytes in response to β_1-ADR activation with dobutamine. This involves NOS signalling, which was also associated with an increased activity of SERCA, meaning faster decline in $[Ca^{2+}]$ during relaxation of the myocyte, but no increase in SR Ca^{2+} content. These findings were unexpected and difficult to resolve, and further investigation is required to fully understand the anti-arrhythmic action of β_3-ADR stimulation with BRL_{37344}.

I have also shown the dual coupling of the β_2-ADR to G_i provides a protective effect against DAD generation, likely to be due to the compartmentalisation of cAMP signalling limiting the inotropic effect at the SR preventing the driver for a DAD; Ca^{2+} overload of the SR.

Although not determined in this investigation, the action of β_3-ADR stimulation with BRL_{37344} to prevent against EAD induced arrhythmias should also be considered. Although in my hands, BRL_{37344} lead to a reduction in APD (Chapter 5, Figure 5.12), and although I did not observe a reduction in LTCC in response to BRL_{37344} reports in the literature suggest an inhibition and a reduced amplitude of LTCC following β_3-ADR stimulation (Gauthier, Rozec et al. 2011) which may impact upon EAD generation, and so further work is required.

Chapter 7: Physiological and Clinical implications of this investigation

Since the cloning of the β_3-ADR in 1989 (Emorine, Marullo et al. 1989) and subsequent identification in the heart (Gauthier, Tavernier et al. 1996), the role of the β_3-ADR in normal physiology and in particular in pathological conditions has been examined. The β_3-ADR exerts a negative inotropic action in the myocardium mediated by NO, by a cGMP-dependent increase in PKG phosphorylation of the key E-C coupling proteins (LTCC, RyR2, PLB), and/or via cGMP-independent direct S-nitrosylation of the same E-C coupling proteins (Hare 2003; Gonzalez, Fernandez et al. 2008). It has since been identified that alongside NO signalling, the β_3-ADR is also able to stimulate a number of PDE associated with the breakdown of cAMP, PDE2/PDE3/PDE4, providing a cross-talk between the positive inotropism of β_1/β_2-ADR stimulation and the negative inotropism of the β_3-ADR (Hammond and Balligand 2011).

The negative inotropic action of the β_3-ADR and the need for a greater concentration of the endogenous catecholamine required for its activation (Strosberg 1997) lead to the suggestion that the β_3-ADR may be preferentially activated during pathological conditions, such as heart failure (HF) due to the high levels of circulating catecholamines.

In HF, the smaller amplitude of Ca^{2+} transients, caused by reduced SR Ca^{2+} stores, reduces myofilament activation and depresses contractility in patients, even in the face of increased catecholamine levels (Pogwizd, Schlotthauer et al. 2001). The increased activation of the SNS acts initially to support the failing heart maintaining cardiac performance by increasing contractility and raising HR. However, long-term sustained increase in sympathetic outflow is ultimately damaging to the myocardium, leading to the down regulation of β_1-ADR and the uncoupling of β_2-ADR (Dessy and Balligand 2010). However, the β_3-ADR have been shown to be resistant to desensitisation or down regulation in both short-term (Rozec and Gauthier 2006) and long-term adrenergic activation (Gauthier, Langin et al. 2000), both *in vitro* and *in vivo*. The resistance to desensitisation or down regulation of the β_3-ADR is thought to occur due to the fact that unlike the β_1/β_2-ADR, β_3-ADR do not contain the binding site required for PKA or G protein-coupled receptor kinase (GRK) phosphorylation (Gauthier, Langin et al. 2000). Not only are the β_3-ADR resistant to down regulation, but in diseased states such as HF, β_3-ADR

expression appears to be upregulated, in both human patients (Rozec and Gauthier 2006; Moens, Yang et al. 2010) and animal models of HF (Zhou, Tan et al. 2008). Moniotte *et al.* report a 2-3 fold increase in β_3-ADR expression in the ventricle of failing human hearts compared to non-failing hearts (Moniotte, Kobzik et al. 2001) and Cheng *et al.* noted an up-regulation of function as well as expression of β_3-ADR in a canine HF model (Cheng, Zhang et al. 2001).

As the β_3-ADR response appears to be maintained, if not upregulated, in HF, it has been suggested that initially the maintained β_3-ADR response may be protective to the failing heart, allowing 'fine tuning' of the β_1/β_2-ADR positive inotropic response to heightened adrenergic stimulation, preventing damage to the myocardium and reducing arrhythmia generation (Gauthier, Langin et al. 2000), however, as HF progresses it is likely that long-term, the negative inotropic action of β_3-ADR stimulation would become maladaptive, as a constant negative inotropic effect would exert a progressively greater a cardio-depressive effect on an already failing heart, leading to further myocardial depression.

Due to the negative effect of β_3-ADR on contractility of the myocardium in the failing heart, it has been suggested that β_3-ADR antagonism would be an effective treatment in HF patients. Indeed, Morimoto *et al.* have shown that administration of the β_3-ADR antagonist, L$_{-748,337}$, improved left ventricular contraction in a canine model of HF at rest, both *in vivo* and *in vitro* in isolated left ventricular myocytes (Morimoto, Hasegawa et al. 2004). The same group have since found the increase in contractility at rest by β_3-ADR antagonism is maintained during exercise in the same canine HF model (Masutani, Cheng et al. 2013). Certainly data from this investigation would confer with the suggestion that β_3-ADR antagonist may provide effective therapeutic potential, by removing the negative inotropic action of β_3-ADR on Ca^{2+} handling and action potential duration that we have observed in isolated myocytes, this may be able to offer support to the failing heart.

However, in animal models of HF there is a high incidence of DADs (Baartscheer, Schumacher et al. 2003) due to a number of factors which increase the likelyhood of DAD generation, including an increased Ca^{2+} spark frequency, increased NCX function and the elevated β-adrenergic drive (Bers, Pogwizd et al. 2002; Bers, Despa et al. 2006; Eisner, Kashimura et al. 2009). In HF, the open probability of RyR2 is altered, tending to remain open for prolonged periods (Pogwizd, Schlotthauer et al. 2001; Bers 2002) which leads to a decrease in SR Ca^{2+} content, which should reduce the liklihood of Ca^{2+} induced arrhythmias

in the form of DADs. However, residual β-adrenergic response remains in HF, causing overstimulation of the β-ADR pathway driving local increases in SR Ca^{2+} content, reaching the threshold required for spontaneous RyR2 Ca^{2+} release (Janse 2004; Bers 2006), the net result being Ca^{2+} sparks at a lower SR Ca^{2+} content in HF (Eisner, Kashimura et al. 2009). The mRNA and protein expression of the NCX is increased in HF, as is the magnitude of the NCX current, creating a greater inward depolarising current for a given spontaneous Ca^{2+} release for the SR. Bers *et al.* have also shown that the size of the I_{K1} inward current is reduced, prolonging the plateau phase of the AP and reducing the stability of the RMP, and so allowing greater depolarisation following an inward NCX current triggered by a spontaneous release of Ca^{2+} from the SR. The combined result of an increase expression of the NCX, unstable RMP and residual β-adrenergic stimulation is an increased likelihood that an SR Ca^{2+} release induced DAD will trigger an arrhythmogenic action potential (Bers, Pogwizd et al. 2002).

In this investigation I have shown for the first time a time-of-day variation in the $β_3$-ADR signalling, observing a greater response in rest-period (ZT3) myocytes and also for the first time an anti-arrhythmic action of the $β_3$-ADR in rest-period (ZT3) myocytes against arrhythmias, specifically DADs, induced by high $β_1$-ADR stimulation in isolated ventricular myocytes. A role for $β_3$-ADR signalling to be protective against arrhythmia generation *in vivo* has been shown previously in a rabbit heart failure model. Li *et al.* observed that 30 minutes pre-treatment with the $β_3$-ADR agonist BRL_{37344} reduced the incidence of $β_1$-ADR induced ventricular tachycardia (VT) by 50% (Li, Liu et al. 2010) and Zhou *et al.* have also shown $β_3$-ADR stimulation with BRL_{37344} is able to reduce the number of VT episodes in a canine model of VT after 1 month subcutaneous perfusion (Zhou, Tan et al. 2008).

The anti-arrhythmic action of the $β_3$-ADR I have observed in this investigation, specifically against DAD arrhythmia, may convey a potential pharmacological treatment for HF patients', reducing the susceptibility to arrhythmia generation. However, current data suggesting antagonism of the $β_3$-ADR in HF patients to maintain contractility would inhibit the ability of the $β_3$-ADR to protect against DAD induced arrhythmias.

Sudden cardiac death (SCD) accounts for approximately 50% of death in HF patients (Tomaselli and Zipes 2004) and as the incidence of SCD is greatest during the transition from the resting to the active state (Muller, Ludmer et al. 1987; Willich, Levy et al. 1987;

Maron, Kogan et al. 1994) due to the morning surge in sympathetic activity (Dodt, Breckling et al. 1997).

The time-of-day variation in the effectiveness of β_3-ADR to induce a negative inotropic effect on Ca^{2+} handling I have shown in this investigation, has been mirrored by the work of Zhou *et al.*, who have observed that the mRNA expression of the β_3-ADR exhibits a time-of-day variation, with the expression of the β_3-ADR highest during the animals rest period (Zhou, Zhang et al. 2011) conferring with our data, and so it is possible that the ability of β_3-ADR activation to reduce arrhythmic activity in response to further sympathetic stimulation exhibits would also exhibit a time-of-day variation, although I was not able to investigate this.

The anti-arrhythmic action of β_3-ADR stimulation would offer therapeutic benefit during this vulnerable period when transitioning from the resting to the active state, especially under conditions of high sympathetic drive, such as HF, and so it may be possible to implement chrono-pharmacology in the use of β_3-ADR agonists/antagonists as a treatment option in HF and arrhythmia management. Administration of a short-acting β_3-ADR agonist during the vulnerable window, during transition from the resting to the active state, will confer protection against the inevitable surge in sympathetic activity, limiting Ca^{2+} overload and arrhythmia generation. However, it is essential to maintain support of the heart during the active-period (ZT15), especially as sympathetic stimulation is less effective at during this time, and so the short-acting β_3-ADR agonists could be followed by traditional β-blocker treatment /β_3-ADR antagonist, removing the negative inotropic effect on contractility during the active-period (ZT15) when the vulnerability to arrhythmia generation and SCD are lowest, whist improving contractility.
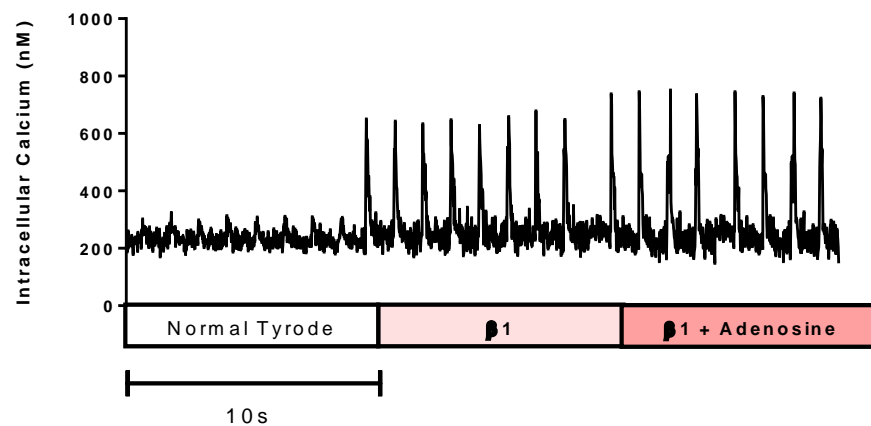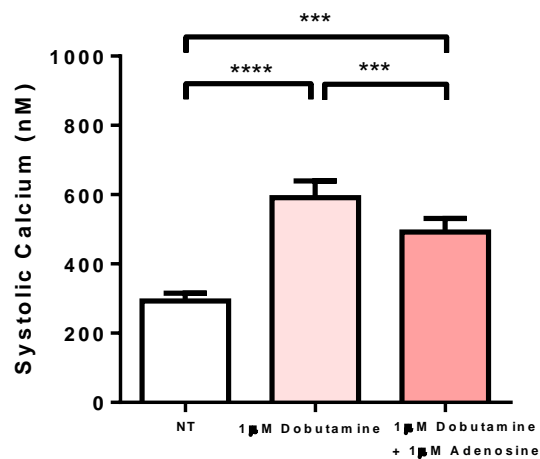
Appendix
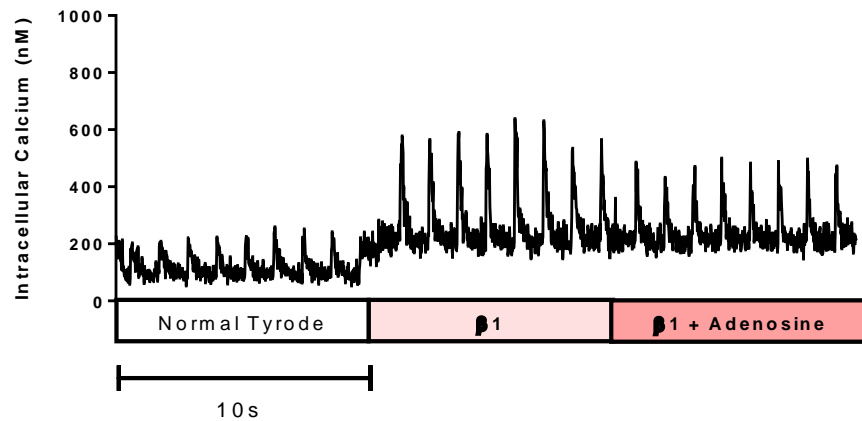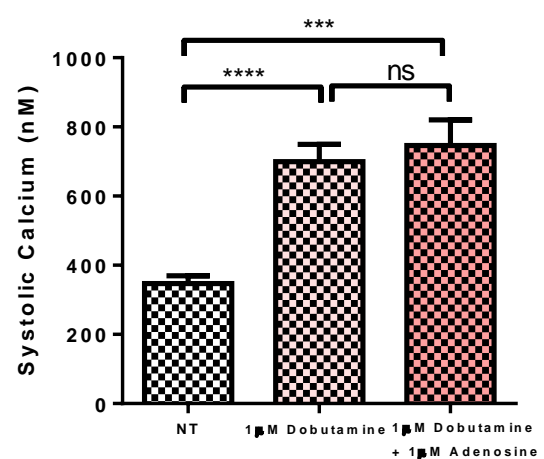
Appendix 1. The effect of PTx treatment on the antagonistic effect of adenosine on the β1 stimulatory response.

Traces of calcium transients recorded in normal Tyrode, 1μM dobutmaine and 1μM dobutmaine + 1μM Adenosine in **A.** Control cells and **B.** PTx-treated cells, displaying the inhibitory effects of adenosine on amplitude of calcium transients in the control cell, whereas following PTx treatment this effect is abolished. Mean systolic calcium levels from such experiments in **C.** control cells (n=15) and **D.** PTx-treated cells (n=17), (data analysed via one-way repeated measures ANOVA, Tukey's post hoc test,).

Appendix 2

|	Freshly isolated cells	Control cells	p-value
Systolic $[Ca^{2+}]_i$	341.0 ± 6.3nM (n=21(202))	312.6 ± 19.7nM (n=5(19))	*ns* p=0.32
Diastolic $[Ca^{2+}]_i$	81.6 ± 2.8nM (n=21(85))	115.6 ± 8.2nM (n=5(19))	*ns* p=0.13
Exponential time constant of the electrically-induced calcium transient	201.4 ± 4.8ms (n=21(224))	227.4 ± 23.5ms (n=5(18))	********* p<0.0001
APD_{30}	12.9 ± 0.6ms (n=21(82))	17.6 ± 1.8ms (n=5(31))	*ns* p=0.99
$APD5_{30}$	21.2 ± 0.9ms (n=21(82))	27.1 ± 3.0ms (n=5(31))	*ns* p=0.99
APD_{90}	66.9 ± 2.2ms (n=21(80))	73.4 ± 4.2ms (n=5(26))	*ns* p=0.99
Arrhythmic activity	0.4 ± 1.8 (n=8(95/1278))	0.5 ± 0.3 (n=6(42/462))	*ns* p=0.99

Appendix 2. Table of mean basal E-C coupling parameters measured from the freshly isolated and myocytes (incubated at 37°C with 2% Pen/Strep for 3 hours).
Table showing the mean Systolic $[Ca^{2+}]_i$, Diastolic $[Ca^{2+}]_i$, exponential time constant of the electrically-induced calcium transient). The table also shows mean electrophysiological parameters (APD_{30}, $APD5_{30}$ and APD_{90}) and mean arrhythmic activity of freshly isolated and control myocytes. Values are mean ± S.E.M. Number of hearts (number of experiments) or Number of hearts (number of experiments/number of cells); * p<0.05, **** p<0.0001, data analysed by one-way ANOVA, Sidak's *post-hoc* test.

Appendix 3
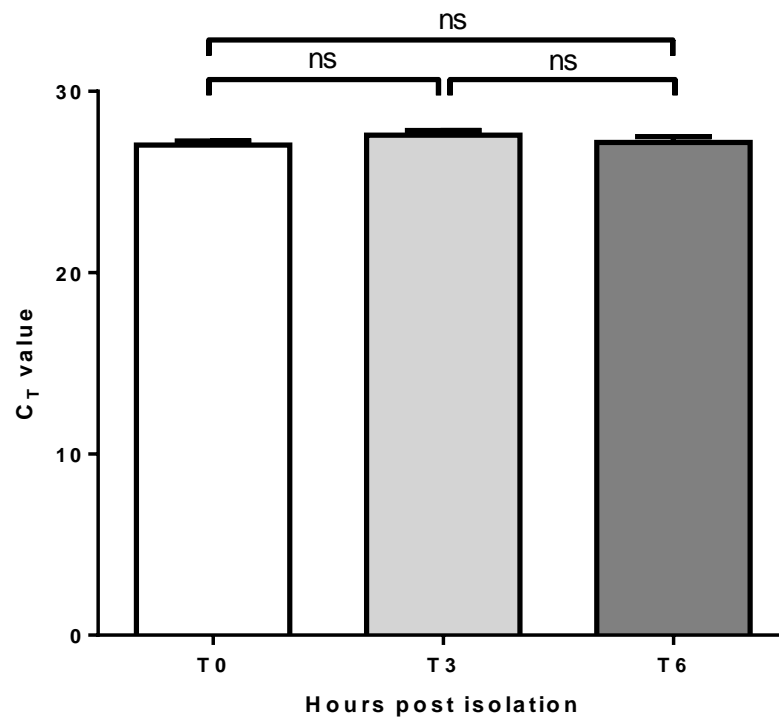
Appendix 3.   Absolute CT value of β-actin mRNA expression levels in ZT3 isolated ventricular cardiomyocytes.

Graph showing absolute CT value of β-actin mRNA expression levels in ZT3 isolated ventricular cardiomyocytes at time points corresponding to immediately following isolation (T0), 3 hours post isolation (T3) and 6 hours post isolation (T6). No significant difference was found between T0 (27.03 ± 0.24), T3 (27.58 ± 0.27) or T6 (27.19 ± 0.31), therefore providing evidence of stable β-actin mRNA expression levels in cardiomyocytes. n=4 (17-18), one-way ANOVA, Tukey's post-hoc test.

Appendix 4
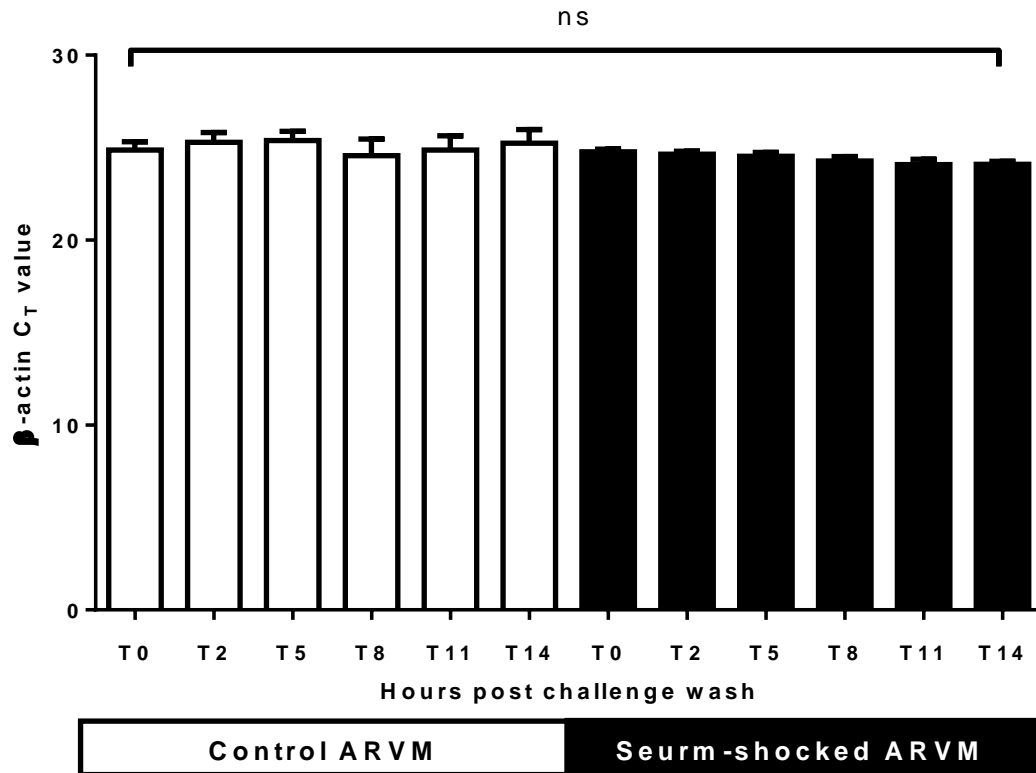
Appendix 4.   Absolute CT value of β-actin mRNA expression levels in control and serum-shocked cultured adult rat ventricular myocytes.

Graph showing absolute CT value of β-actin mRNA expression levels in control (white) and serum-shocked (black) cultured adult rat ventricular myocytes at time points corresponding to pre-challenge wash (T0), immediately post-challenge wash (T2) and 3 hour increments post challenge wash (T5, T8, T11, T14). No significant difference was found any time points, therefore providing evidence of stable β-actin mRNA expression levels in cardiomyocytes, both with-and without serum shock. Control n=3, Serum shock n = 5, two-way ANOVA, sidaks post-hoc test.

Appendix 5

Gene type	Gene name	Gene symbol	Standard curve slope value	Calculated gene efficiency (%)
Endogenous control gene	Beta-actin (**β-actin**)	Actb	-3.54	91.99
Circadian clock genes	Circadian locomotor output cycles kaput (**CLOCK**)	CLOCK	-3.34	99.25
	Period homolog 2 (**PER2**)	Per2	-3.23	104.43
	Aryl hydrocarbon receptor nuclear translocator-like (**BMAL1**)	Arntl	-3.15	107.87
	Nuclear receptor subfamily 1, group D, member 1 (**Rev-ErbA alpha** / Nr1d1)	Nr1d1	-3.91	80.16
β-adrenergic genes	β_1 adrenergic receptor (**β_1-ADR**)	Adrb1	-3.37	97.835
	β_3 adrenergic receptor (**β_3-ADR**)	Adrb3	N/A	N/A **
Nitric oxide synthase genes	Neuronal nitric oxide synthase 1 (**nNOS**)	NOS1	N/A	N/A **
	Endothelial nitric oxide synthase 3 (**nNOS**)	NOS3	-3.6	89.5

Appendix 5.   **Standard curve data assessed in ZT3 isolated ventricular cardiomyocytes**
Table showing the standard curve and efficiency values for ach TaqMan gene expression probe assay investigated in chapter4 of the results section using a 2-fold serial dilution. All TaqMan probes produced a linear standard curve with efficiency values of 80-100%. Data collected was analysed using the $2^{-\Delta\Delta CT}$ method.
**For the probes encoding β_3 adrenergic receptor (β_3-ADR) and Neuronal nitric oxide synthase 1 (nNOS) an amplifiable standard curve could not be produced due to the low abundance of β_3-ADR and nNOS in our samples. Therefore data collected was cautiously analysed using the $2^{-\Delta\Delta CT}$ method.
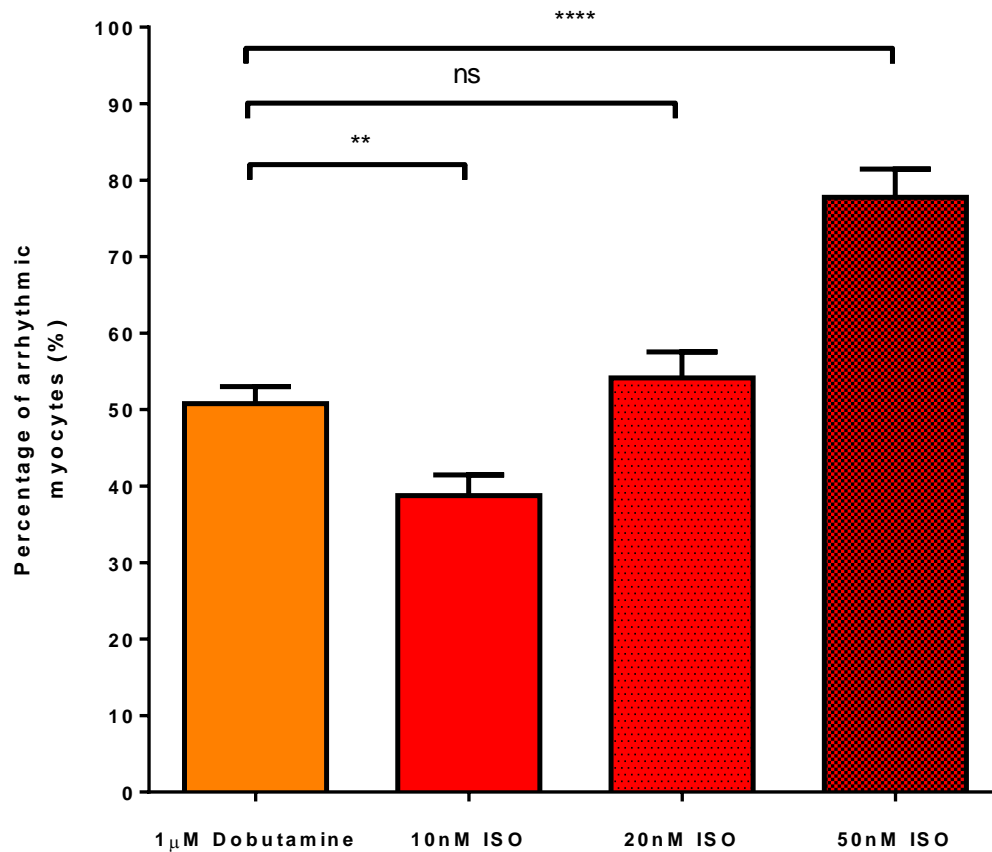
Appendix 6

	Normal Tyrode	30µM IBMX	p-value
Systolic $[Ca^{2+}]_i$ (n=5(27))	353.8 ± 14.8nM	397.3 ± 30.3nM	*ns* *p*=0.11
Diastolic $[Ca^{2+}]_i$ (n=5(24))	91.6 ± 5.1nM	94.5 ± 4.9nM	*ns* *p*=0.40
Exponential time constant of the electrically-induced calcium transient (n=5(25))	211.8 ± 14.5ms	191.6 ± 15.8ms	*ns* *p*=0.19
Peak SR calcium release (n=5(12))	505.0 ± 30.4nM	519.1 ± 58.1nM	*ns* *p*=0.80
Exponential time constant of the caffeine-induced calcium transient (n=5(8))	3653.0 ± 796.5ms	3118.0 ± 518.7ms	*ns* *p*=0.55
RMP (n=3(8))	-75.7 ± 0.82mV	-79.3 ± 0.75mV	*ns* *p*=0.23
APD_{30} (n=3(8))	15.6 ± 2.4ms	13.7 ± 1.9ms	*ns* *p*=0.08
$APD5_{30}$ (n=3(8))	25.0 ± 3.5ms	22.9 ± 2.8ms	*ns* *p*=0.44
APD_{90} (n=3(8))	71.0 ± 6.3ms	69.9 ± 6.5ms	*ns* *p*=0.97

Appendix 6.   Table of mean E-C coupling parameters measured from the rat myocyte showing superfusion of cells with 30µM IBMX alone had no effect on all parameters measured.
Table showing the mean calcium handling parameters (Systolic $[Ca^{2+}]_i$, Diastolic $[Ca^{2+}]_i$, exponential time constant of the electrically-induced calcium transient, peak SR calcium release and exponential time constant of the caffeine-induced calcium transient) and mean electrophysiological parameters (RMP, APD_{30}, $APD5_{30}$ and APD_{90}) in normal Tyrode and 30µM IBMX. Values are mean ± S.E.M. Number of hearts (number of experiments), data analysed by one-way ANOVA, Sidak's *post-hoc* test.

Appendix 7

Appendix 7. **Development of arrhythmic activity in rat ventricular myocytes in response to β-adrenergic stimulation.**

Bar chart showing the mean percentage of myocytes that develop spontaneous extra-contractions in response to 1μM dobutamine (orange bar, n=8(42/656)), 10nM ISO (red bar, n=3(23/221)), 20nM ISO (red bar, n=3(22/285)) and 50nM ISO (red bar, n=3(20/265)). Percentages were calculated from a field of 10-20 cells synchronously contracting cells stimulated at 1Hz by electrical field stimulation. Values are mean ± S.E.M. Number of hearts (number of experiments/number of cells); **p<0.01, ****p<0.0001, one-way ANOVA, sidak's *post-hoc* test.
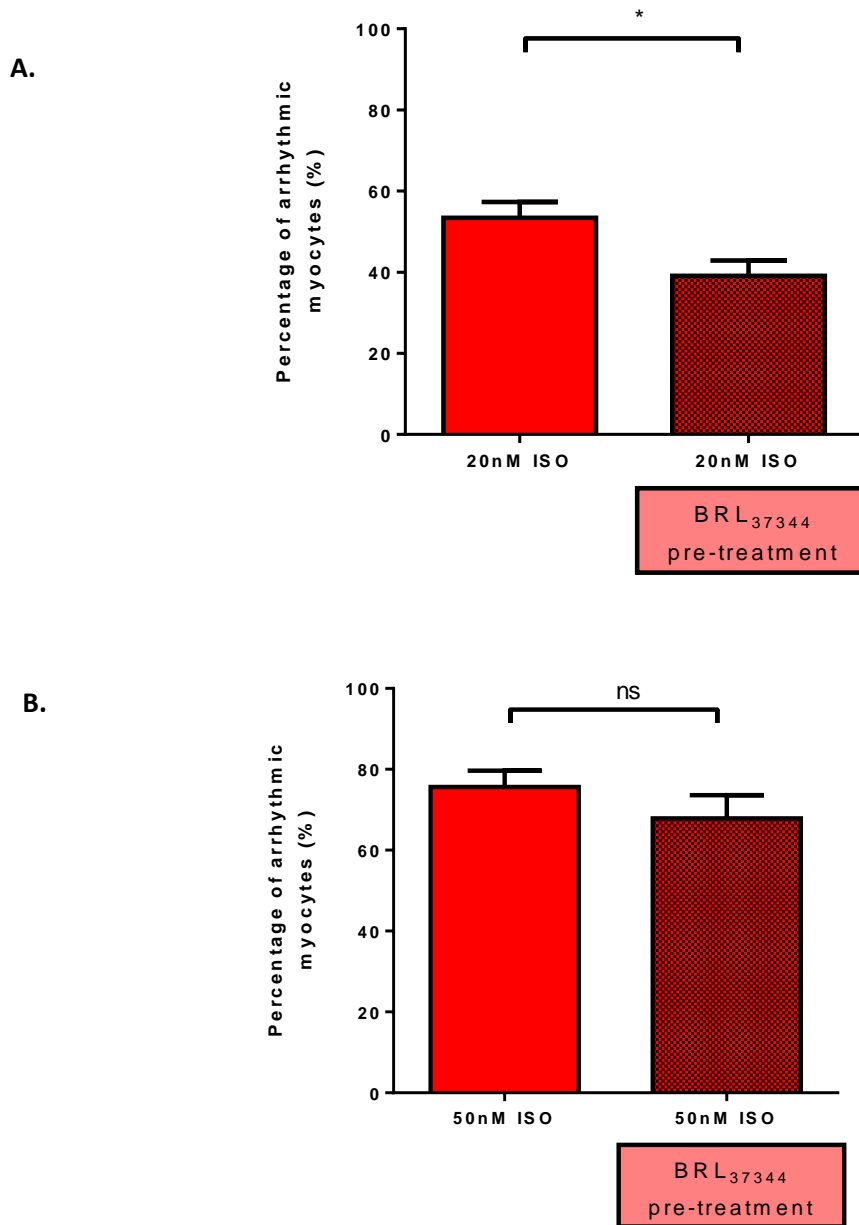
Appendix 8. **β₃-ADR activation with BRL$_{37344}$ pre-treatment reduces the development of arrhythmic activity in ventricular myocytes in response to β-adrenergic stimulation with high concentrations of ISO.**

Bar charts showing the effect of β₃-ADR stimulation by pre-treatment with BRL$_{37344}$ on the development of spontaneous extra-contractions in response to non-specific β-adrenergic stimulation with isoproterenol.

A. 20nM ISO (open bar, n=3(22/285)) and in cells pre-treated with 200nM BRL$_{37344}$ prior to 20nM ISO (hatched bar, n=4 (13/193)).

B. 50nM ISO (open bar, n=3(20/265))) and in cells pre-treated with 200nM BRL$_{37344}$ prior to 50nM ISO (hatched bar, n=3(12/152).

Values are mean ± S.E.M. Number of hearts (number of experiments/number of cells); *$p<0.05$, unpaired t-test.

Appendix 9

Drug	Log *Kd* β$_1$-ADR	Log *Kd* β$_2$-ADR	Log *Kd* β$_3$-ADR
Isoproterenol	-6.06 ± 0.08	-6.64 ± 0.09	-5.52 ± 0.08
Dobutamine	-5.23 ± 0.06	-5.84 ± 0.05	-5.09 ± 0.08
Salbutamol	-4.68 ± 0.03	-6.01 ± 0.03	-3.98 ± 0.06
BRL37344	-5.19 ± 0.07	-6.51 ± 0.06	-6.45 ± 0.06

Log K_D values obtained from [3H]-CGP 12177 whole-cell binding studies in CHO cells stably expressing the human β$_1$-, β$_2$- or β$_3$-adrenoceptors (Baker, 2010).

Bibliography

Aaronson, P. I. and J. P. T. Ward (2007). The cardiovascular system at a glance. Malden, Mass. ; Oxford, Blackwell.

Adachi-Akahane, S., L. Lu, et al. (1997). "Calcium signaling in transgenic mice overexpressing cardiac Na(+)-Ca2+ exchanger." J Gen Physiol **109**(6): 717-729.

Albrecht, U. (2012). "Timing to perfection: the biology of central and peripheral circadian clocks." Neuron **74**(2): 246-260.

Alexander, S. P., H. E. Benson, et al. (2013). "The Concise Guide to PHARMACOLOGY 2013/14: G protein-coupled receptors." Br J Pharmacol **170**(8): 1459-1581.

Altschafl, B. A., D. A. Arvanitis, et al. (2011). "Dual role of junctin in the regulation of ryanodine receptors and calcium release in cardiac ventricular myocytes." J Physiol **589**(Pt 24): 6063-6080.

Altschuld, R. A., R. C. Starling, et al. (1995). "Response of failing canine and human heart cells to beta 2-adrenergic stimulation." Circulation **92**(6): 1612-1618.

Antzelevitch, C. (2001). "Basic mechanisms of reentrant arrhythmias." Curr Opin Cardiol **16**(1): 1-7.

Aragon, J. P., M. E. Condit, et al. (2011). "Beta3-adrenoreceptor stimulation ameliorates myocardial ischemia-reperfusion injury via endothelial nitric oxide synthase and neuronal nitric oxide synthase activation." J Am Coll Cardiol **58**(25): 2683-2691.

Asada, K., J. Kurokawa, et al. (2009). "Redox- and calmodulin-dependent S-nitrosylation of the KCNQ1 channel." J Biol Chem **284**(9): 6014-6020.

Ashpole, N. M., A. W. Herren, et al. (2012). "Ca2+/calmodulin-dependent protein kinase II (CaMKII) regulates cardiac sodium channel NaV1.5 gating by multiple phosphorylation sites." J Biol Chem **287**(24): 19856-19869.

Audigane, L., B. G. Kerfant, et al. (2009). "Rabbit, a relevant model for the study of cardiac beta 3-adrenoceptors." Exp Physiol **94**(4): 400-411.

Auffermann, W., T. Stefenelli, et al. (1989). "Influence of positive inotropic agents on intracellular calcium transients. Part I. Normal rat heart." Am Heart J **118**(6): 1219-1227.

Baartscheer, A., C. A. Schumacher, et al. (2003). "SR calcium handling and calcium after-transients in a rabbit model of heart failure." Cardiovasc Res **58**(1): 99-108.

Bai, C. X., I. Namekata, et al. (2005). "Role of nitric oxide in Ca2+ sensitivity of the slowly activating delayed rectifier K+ current in cardiac myocytes." Circ Res **96**(1): 64-72.

Balijepalli, R. C., J. D. Foell, et al. (2006). "Localization of cardiac L-type Ca(2+) channels to a caveolar macromolecular signaling complex is required for beta(2)-adrenergic regulation." Proc Natl Acad Sci U S A **103**(19): 7500-7505.

Balligand, J. L., L. Kobzik, et al. (1995). "Nitric oxide-dependent parasympathetic signaling is due to activation of constitutive endothelial (type III) nitric oxide synthase in cardiac myocytes." J Biol Chem **270**(24): 14582-14586.

Balsalobre, A., F. Damiola, et al. (1998). "A serum shock induces circadian gene expression in mammalian tissue culture cells." Cell **93**(6): 929-937.

Baltas, L. G., P. Karczewski, et al. (1997). "The endogenous cardiac sarcoplasmic reticulum Ca2+/calmodulin-dependent kinase is activated in response to beta-adrenergic stimulation and becomes Ca2+-independent in intact beating hearts." FEBS Lett **409**(2): 131-136.

Barhanin, J., F. Lesage, et al. (1996). "K(V)LQT1 and lsK (minK) proteins associate to form the I(Ks) cardiac potassium current." Nature **384**(6604): 78-80.

Barman, P., S. C. Choisy, et al. (2011). "beta-Adrenoceptor/PKA-stimulation, Na(+)-Ca(2+) exchange and PKA-activated Cl(-) currents in rabbit cardiomyocytes: a conundrum." Cell Calcium **49**(4): 233-239.

Barouch, L. A., R. W. Harrison, et al. (2002). "Nitric oxide regulates the heart by spatial confinement of nitric oxide synthase isoforms." Nature **416**(6878): 337-339.

Bartel, S., D. Vetter, et al. (2000). "Phosphorylation of phospholamban at threonine-17 in the absence and presence of beta-adrenergic stimulation in neonatal rat cardiomyocytes." J Mol Cell Cardiol **32**(12): 2173-2185.

Bass, J. and J. S. Takahashi (2010). "Circadian integration of metabolism and energetics." Science **330**(6009): 1349-1354.

Bassani, J. W., W. Yuan, et al. (1995). "Fractional SR Ca release is regulated by trigger Ca and SR Ca content in cardiac myocytes." Am J Physiol **268**(5 Pt 1): C1313-1319.

Beca, S., R. Aschars-Sobbi, et al. (2011). "Regulation of murine cardiac function by phosphodiesterases type 3 and 4." Curr Opin Pharmacol **11**(6): 714-719.

Belge, C., J. Hammond, et al. (2014). "Enhanced expression of beta3-adrenoceptors in cardiac myocytes attenuates neurohormone-induced hypertrophic remodeling through nitric oxide synthase." Circulation **129**(4): 451-462.

Belge, C., P. B. Massion, et al. (2005). "Nitric oxide and the heart: update on new paradigms." Ann N Y Acad Sci **1047**: 173-182.

Bender, A. T. and J. A. Beavo (2006). "Cyclic nucleotide phosphodiesterases: molecular regulation to clinical use." Pharmacol Rev **58**(3): 488-520.

Bers, D. M. (2001). Excitation-contraction coupling and cardiac contractile force. Dordrecht ; London, Kluwer Academic.

Bers, D. M. (2002). "Calcium and cardiac rhythms: physiological and pathophysiological." Circ Res **90**(1): 14-17.

Bers, D. M. (2002). "Cardiac excitation-contraction coupling." Nature **415**(6868): 198-205.

Bers, D. M. (2006). "Altered cardiac myocyte Ca regulation in heart failure." Physiology (Bethesda) **21**: 380-387.

Bers, D. M. (2008). "Calcium cycling and signaling in cardiac myocytes." Annu Rev Physiol **70**: 23-49.

Bers, D. M., S. Despa, et al. (2006). "Regulation of Ca2+ and Na+ in normal and failing cardiac myocytes." Ann N Y Acad Sci **1080**: 165-177.

Bers, D. M., S. M. Pogwizd, et al. (2002). "Upregulated Na/Ca exchange is involved in both contractile dysfunction and arrhythmogenesis in heart failure." Basic Res Cardiol **97 Suppl 1**: I36-42.

Berthouze, M., A. C. Laurent, et al. (2011). "New perspectives in cAMP-signaling modulation." Curr Heart Fail Rep **8**(3): 159-167.

Borea, P. A., S. Amerini, et al. (1992). "Beta 1- and beta 2-adrenoceptors in sheep cardiac ventricular muscle." J Mol Cell Cardiol **24**(7): 753-763.

Bosch, R. F., A. C. Schneck, et al. (2002). "beta3-Adrenergic regulation of an ion channel in the heart-inhibition of the slow delayed rectifier potassium current I(Ks) in guinea pig ventricular myocytes." Cardiovasc Res **56**(3): 393-403.

Bray, M. S., C. A. Shaw, et al. (2008). "Disruption of the circadian clock within the cardiomyocyte influences myocardial contractile function, metabolism, and gene expression." Am J Physiol Heart Circ Physiol **294**(2): H1036-1047.

Brodde, O. E., H. Bruck, et al. (2006). "Cardiac adrenoceptors: Physiological and pathophysiological relevance." Journal of Pharmacological Sciences **100**(5): 323-337.

Bundgaard, H., C. C. Liu, et al. (2010). "beta(3) Adrenergic Stimulation of the Cardiac Na(+) -K(+) Pump by Reversal of an Inhibitory Oxidative Modification." Circulation **122**(25): 2699-U2209.

Burkard, N., A. G. Rokita, et al. (2007). "Conditional neuronal nitric oxide synthase overexpression impairs myocardial contractility." Circ Res **100**(3): e32-44.

Bustin, S. A. (2000). "Absolute quantification of mRNA using real-time reverse transcription polymerase chain reaction assays." J Mol Endocrinol **25**(2): 169-193.

Bustin, S. A. and R. Mueller (2005). "Real-time reverse transcription PCR (qRT-PCR) and its potential use in clinical diagnosis." Clin Sci (Lond) **109**(4): 365-379.

Bustin, S. A. and T. Nolan (2004). "Pitfalls of quantitative real-time reverse-transcription polymerase chain reaction." J Biomol Tech **15**(3): 155-166.

Calvert, J. W., M. E. Condit, et al. (2011). "Exercise protects against myocardial ischemia-reperfusion injury via stimulation of beta(3)-adrenergic receptors and increased nitric oxide signaling: role of nitrite and nitrosothiols." Circ Res **108**(12): 1448-1458.

Cannell, M. B. and C. H. Kong (2012). "Local control in cardiac E-C coupling." J Mol Cell Cardiol **52**(2): 298-303.

Casadei, B. (2006). "The emerging role of neuronal nitric oxide synthase in the regulation of myocardial function." Exp Physiol **91**(6): 943-955.

Chen-Izu, Y., R. P. Xiao, et al. (2000). "G(i)-dependent localization of beta(2)-adrenergic receptor signaling to L-type Ca(2+) channels." Biophys J **79**(5): 2547-2556.

Cheng, H. and W. J. Lederer (2008). "Calcium sparks." Physiol Rev **88**(4): 1491-1545.

Cheng, H. J., Z. S. Zhang, et al. (2001). "Upregulation of functional beta(3)-adrenergic receptor in the failing canine myocardium." Circ Res **89**(7): 599-606.

Chou, M. T., S. H. Lo, et al. (2012). "Activation of beta-adrenoceptors by dobutamine may induce a higher expression of peroxisome proliferator-activated receptors delta (PPARdelta) in neonatal rat cardiomyocytes." ScientificWorldJournal **2012**: 248320.

Collins, H. E. and G. C. Rodrigo (2010). "Inotropic response of cardiac ventricular myocytes to beta-adrenergic stimulation with isoproterenol exhibits diurnal variation: involvement of nitric oxide." Circ Res **106**(7): 1244-1252.

Conti, M., D. Mika, et al. (2014). "Cyclic AMP compartments and signaling specificity: role of cyclic nucleotide phosphodiesterases." J Gen Physiol **143**(1): 29-38.

Coumel, P., B. Escoubet, et al. (1984). "Beta-blocking therapy in atrial and ventricular tachyarrhythmias: experience with nadolol." Am Heart J **108**(4 Pt 2): 1098-1108.

Cros, C. and F. Brette (2013). "Functional subcellular distribution of beta1- and beta2-adrenergic receptors in rat ventricular cardiac myocytes." Physiol Rep **1**(3): e00038.

Curran, J., M. J. Hinton, et al. (2007). "Beta-adrenergic enhancement of sarcoplasmic reticulum calcium leak in cardiac myocytes is mediated by calcium/calmodulin-dependent protein kinase." Circ Res **100**(3): 391-398.

Danson, E. J., J. K. Choate, et al. (2005). "Cardiac nitric oxide: emerging role for nNOS in regulating physiological function." Pharmacol Ther **106**(1): 57-74.

Danson, E. J., Choate, J.K. and Paterson, D.J. (2005). "Cardiac nitric oxide: Emerging role for nNOS in regulating physiological function." Pharmacology and Therapeutics **106**: 57 - 74.

Dawson, D., C. A. Lygate, et al. (2005). "nNOS gene deletion exacerbates pathological left ventricular remodeling and functional deterioration after myocardial infarction." Circulation **112**(24): 3729-3737.

De Ferrari, G. M., M. C. Viola, et al. (1995). "Distinct patterns of calcium transients during early and delayed afterdepolarizations induced by isoproterenol in ventricular myocytes." Circulation **91**(10): 2510-2515.

de Tombe, P. P. (2003). "Cardiac myofilaments: mechanics and regulation." J Biomech **36**(5): 721-730.

Dedkova, E. N., Y. G. Wang, et al. (2002). "Nitric oxide signalling by selective beta(2)-adrenoceptor stimulation prevents ACh-induced inhibition of beta(2)-stimulated Ca(2+) current in cat atrial myocytes." J Physiol **542**(Pt 3): 711-723.

Defer, N., M. Best-Belpomme, et al. (2000). "Tissue specificity and physiological relevance of various isoforms of adenylyl cyclase." Am J Physiol Renal Physiol **279**(3): F400-416.

Deng, Y. J., W. Wu, et al. (2009). "[Regulation of resting intracellular Ca(2+) concentration of ventricular myocytes by beta(3)-adrenoceptor and its signaling pathway in rats with experimental heart failure]." Nan Fang Yi Ke Da Xue Xue Bao **29**(8): 1635-1637.

Denniff, M., H. E. Turrell, et al. (2014). "The time-of-day variation in vascular smooth muscle contractility depends on a nitric oxide signalling pathway." J Mol Cell Cardiol **66**: 133-140.

Dessy, C. and J. L. Balligand (2010). "Beta3-adrenergic receptors in cardiac and vascular tissues emerging concepts and therapeutic perspectives." Adv Pharmacol **59**: 135-163.

Dheda, K., J. F. Huggett, et al. (2004). "Validation of housekeeping genes for normalizing RNA expression in real-time PCR." Biotechniques **37**(1): 112-114, 116, 118-119.

Diaz, M. E., A. W. Trafford, et al. (1997). "Measurement of sarcoplasmic reticulum Ca2+ content and sarcolemmal Ca2+ fluxes in isolated rat ventricular myocytes during spontaneous Ca2+ release." J Physiol **501 (Pt 1)**: 3-16.

Dibner, C., U. Schibler, et al. (2010). "The mammalian circadian timing system: organization and coordination of central and peripheral clocks." Annu Rev Physiol **72**: 517-549.

Dimsdale, J. E. and J. Moss (1980). "Plasma catecholamines in stress and exercise." JAMA **243**(4): 340-342.

Dodt, C., U. Breckling, et al. (1997). "Plasma epinephrine and norepinephrine concentrations of healthy humans associated with nighttime sleep and morning arousal." Hypertension **30**(1 Pt 1): 71-76.

Dorak, M. T. (2006). Real-time PCR. New York, N.Y. ; Abingdon, Taylor & Francis.

Dudzinski, D. M. and T. Michel (2007). "Life history of eNOS: partners and pathways." Cardiovasc Res **75**(2): 247-260.

Durgan, D. J., M. A. Hotze, et al. (2005). "The intrinsic circadian clock within the cardiomyocyte." Am J Physiol Heart Circ Physiol **289**(4): H1530-1541.

Durgan, D. J., N. A. Trexler, et al. (2006). "The circadian clock within the cardiomyocyte is essential for responsiveness of the heart to fatty acids." J Biol Chem **281**(34): 24254-24269.

Durgan, D. J., J. Y. Tsai, et al. (2011). "Evidence suggesting that the cardiomyocyte circadian clock modulates responsiveness of the heart to hypertrophic stimuli in mice." Chronobiol Int **28**(3): 187-203.

Edery, I. (2000). "Circadian rhythms in a nutshell." Physiol Genomics **3**(2): 59-74.

Eisner, D. A., T. Kashimura, et al. (2009). "What role does modulation of the ryanodine receptor play in cardiac inotropy and arrhythmogenesis?" J Mol Cell Cardiol **46**(4): 474-481.

Eisner, D. A., T. Kashimura, et al. (2009). "From the ryanodine receptor to cardiac arrhythmias." Circ J **73**(9): 1561-1567.

El-Armouche, A. and T. Eschenhagen (2009). "beta-Adrenergic stimulation and myocardial function in the failing heart." Heart Fail Rev **14**(4): 225-241.

Emorine, L. J., S. Marullo, et al. (1989). "Molecular characterization of the human beta 3-adrenergic receptor." Science **245**(4922): 1118-1121.

Evans, B. A., M. Papaioannou, et al. (1996). "Expression of beta 3-adrenoceptor mRNA in rat tissues." Br J Pharmacol **117**(1): 210-216.

Fan, J., Y. M. Shuba, et al. (1996). "Regulation of cardiac sodium-calcium exchanger by beta-adrenergic agonists." Proc Natl Acad Sci U S A **93**(11): 5527-5532.

Farrell, R. E. (2005). RNA methodologies : a laboratory guide for isolation and characterization. Amsterdam ; Boston, Elsevier/Academic Press.

Ferrero, P., M. Said, et al. (2007). "Ca2+/calmodulin kinase II increases ryanodine binding and Ca2+-induced sarcoplasmic reticulum Ca2+ release kinetics during beta-adrenergic stimulation." J Mol Cell Cardiol **43**(3): 281-291.

Florea, S. M. and L. A. Blatter (2012). "Regulation of cardiac alternans by beta-adrenergic signaling pathways." Am J Physiol Heart Circ Physiol **303**(8): H1047-1056.

Francis, S. H., M. A. Blount, et al. (2011). "Mammalian cyclic nucleotide phosphodiesterases: molecular mechanisms and physiological functions." Physiol Rev **91**(2): 651-690.

Furchgott, R. F. and J. V. Zawadzki (1980). "The obligatory role of endothelial cells in the relaxation of arterial smooth muscle by acetylcholine." Nature **288**(5789): 373-376.

Gaine, S. P., Naeije, R., Peacock, A.J. (2014). The Right Heart. A. J. Peacock. London, Springer-Verlag London**:** 323.

Gauthier, C., D. Langin, et al. (2000). "Beta3-adrenoceptors in the cardiovascular system." Trends Pharmacol Sci **21**(11): 426-431.

Gauthier, C., V. Leblais, et al. (1998). "The negative inotropic effect of beta3-adrenoceptor stimulation is mediated by activation of a nitric oxide synthase pathway in human ventricle." J Clin Invest **102**(7): 1377-1384.

Gauthier, C., B. Rozec, et al. (2011). "Beta-3 adrenoceptors as new therapeutic targets for cardiovascular pathologies." Curr Heart Fail Rep **8**(3): 184-192.

Gauthier, C., G. Tavernier, et al. (1996). "Functional beta3-adrenoceptor in the human heart." J Clin Invest **98**(2): 556-562.

Gauthier, C., G. Tavernier, et al. (1999). "Interspecies differences in the cardiac negative inotropic effects of beta(3)-adrenoceptor agonists." J Pharmacol Exp Ther **290**(2): 687-693.

Ginsburg, K. S. and D. M. Bers (2005). "Isoproterenol does not enhance Ca-dependent Na/Ca exchange current in intact rabbit ventricular myocytes." J Mol Cell Cardiol **39**(6): 972-981.

Golan, D. E. (2008). Principles of pharmacology : the pathophysiologic basis of drug therapy. Philadelphia, Pa. ; London, Wolters Kluwer/Lippincott Williams & Wilkins.

Goldhaber, J. I. (1999). "Sodium-calcium exchange: the phantom menace." Circ Res **85**(11): 982-984.

Golowasch, J., G. Thomas, et al. (2009). "Membrane capacitance measurements revisited: dependence of capacitance value on measurement method in nonisopotential neurons." J Neurophysiol **102**(4): 2161-2175.

Gomez, R., R. Caballero, et al. (2009). "Nitric oxide increases cardiac IK1 by nitrosylation of cysteine 76 of Kir2.1 channels." Circ Res **105**(4): 383-392.

Gomez, R., L. Nunez, et al. (2008). "Nitric oxide inhibits Kv4.3 and human cardiac transient outward potassium current (Ito1)." Cardiovasc Res **80**(3): 375-384.

Gonzalez-Munoz, C., T. Fuente, et al. (2009). "Phosphodiesterases inhibition unmask a positive inotropic effect mediated by beta2-adrenoceptors in rat ventricular myocardium." Eur J Pharmacol **607**(1-3): 151-155.

Gonzalez, D. R., F. Beigi, et al. (2007). "Deficient ryanodine receptor S-nitrosylation increases sarcoplasmic reticulum calcium leak and arrhythmogenesis in cardiomyocytes." Proc Natl Acad Sci U S A **104**(51): 20612-20617.

Gonzalez, D. R., I. C. Fernandez, et al. (2008). "Differential role of S-nitrosylation and the NO-cGMP-PKG pathway in cardiac contractility." Nitric Oxide **18**(3): 157-167.

Granneman, J. G. and C. J. Whitty (1991). "CGP 12177A modulates brown fat adenylate cyclase activity by interacting with two distinct receptor sites." J Pharmacol Exp Ther **256**(2): 421-425.

Grant, A. O. (2009). "Cardiac ion channels." Circ Arrhythm Electrophysiol **2**(2): 185-194.

Grimm, M. and J. H. Brown (2010). "Beta-adrenergic receptor signaling in the heart: role of CaMKII." J Mol Cell Cardiol **48**(2): 322-330.

Groden, D. L., Z. Guan, et al. (1991). "Determination of Fura-2 dissociation constants following adjustment of the apparent Ca-EGTA association constant for temperature and ionic strength." Cell Calcium **12**(4): 279-287.

Guo, Y. F. and P. K. Stein (2003). "Circadian rhythm in the cardiovascular system: chronocardiology." Am Heart J **145**(5): 779-786.

Gyorke, S. and D. Terentyev (2008). "Modulation of ryanodine receptor by luminal calcium and accessory proteins in health and cardiac disease." Cardiovasc Res **77**(2): 245-255.

Hammond, J. and J. L. Balligand (2011). "Nitric oxide synthase and cyclic GMP signaling in cardiac myocytes: From contractility to remodeling." J Mol Cell Cardiol.

Han, X., I. Kubota, et al. (1998). "Muscarinic cholinergic regulation of cardiac myocyte ICa-L is absent in mice with targeted disruption of endothelial nitric oxide synthase." Proc Natl Acad Sci U S A **95**(11): 6510-6515.

Hare, J. M. (2003). "Nitric oxide and excitation-contraction coupling." J Mol Cell Cardiol **35**(7): 719-729.

Heijman, J., P. G. Volders, et al. (2011). "Local control of beta-adrenergic stimulation: Effects on ventricular myocyte electrophysiology and Ca(2+)-transient." J Mol Cell Cardiol **50**(5): 863-871.

Heusch, G. (2011). "Beta3-adrenoceptor activation just says NO to myocardial reperfusion injury." J Am Coll Cardiol **58**(25): 2692-2694.

Hille, B. (2001). Ion channels of excitable membranes. Sunderland, Mass., Sinauer Associates.

Hund, T. J., O. M. Koval, et al. (2010). "A beta(IV)-spectrin/CaMKII signaling complex is essential for membrane excitability in mice." J Clin Invest **120**(10): 3508-3519.

Janse, M. J. (2004). "Electrophysiological changes in heart failure and their relationship to arrhythmogenesis." Cardiovasc Res **61**(2): 208-217.

Janssens, S., P. Pokreisz, et al. (2004). "Cardiomyocyte-specific overexpression of nitric oxide synthase 3 improves left ventricular performance and reduces compensatory hypertrophy after myocardial infarction." Circ Res **94**(9): 1256-1262.

January, C. T. and J. M. Riddle (1989). "Early afterdepolarizations: mechanism of induction and block. A role for L-type Ca2+ current." Circ Res **64**(5): 977-990.

Jeyaraj, D., S. M. Haldar, et al. (2012). "Circadian rhythms govern cardiac repolarization and arrhythmogenesis." Nature **483**(7387): 96-99.

Jiang, L. H., D. J. Gawler, et al. (2000). "Regulation of cloned cardiac L-type calcium channels by cGMP-dependent protein kinase." J Biol Chem **275**(9): 6135-6143.

Jin, R. C. and J. Loscalzo (2010). "Vascular Nitric Oxide: Formation and Function." J Blood Med **2010**(1): 147-162.

Jurevicius, J. and R. Fischmeister (1996). "cAMP compartmentation is responsible for a local activation of cardiac Ca2+ channels by beta-adrenergic agonists." Proc Natl Acad Sci U S A **93**(1): 295-299.

Kamp, T. J. and J. W. Hell (2000). "Regulation of cardiac L-type calcium channels by protein kinase A and protein kinase C." Circ Res **87**(12): 1095-1102.

Kass, D. A. (2008). "Message delivered: how myocytes control cAMP signaling." Circ Res **102**(9): 1002-1004.

Kaumann, A. J. and P. Molenaar (1997). "Modulation of human cardiac function through 4 beta-adrenoceptor populations." Naunyn Schmiedebergs Arch Pharmacol **355**(6): 667-681.

Kerfant, B. G., D. Zhao, et al. (2007). "PI3Kgamma is required for PDE4, not PDE3, activity in subcellular microdomains containing the sarcoplasmic reticular calcium ATPase in cardiomyocytes." Circ Res **101**(4): 400-408.

Khan, S. A., M. W. Skaf, et al. (2003). "Nitric oxide regulation of myocardial contractility and calcium cycling: independent impact of neuronal and endothelial nitric oxide synthases." Circ Res **92**(12): 1322-1329.

Kilts, J. D., M. A. Gerhardt, et al. (2000). "Beta(2)-adrenergic and several other G protein-coupled receptors in human atrial membranes activate both G(s) and G(i)." Circ Res **87**(8): 705-709.

Kitamura, T., K. Onishi, et al. (2000). "The negative inotropic effect of beta3-adrenoceptor stimulation in the beating guinea pig heart." J Cardiovasc Pharmacol **35**(5): 786-790.

Klabunde, R. E. (2005). Cardiovascular physiology concepts. Philadelphia, Pa. ; London, Lippincott Williams & Wilkins.

Knowles, R. G., M. Palacios, et al. (1989). "Formation of nitric oxide from L-arginine in the central nervous system: a transduction mechanism for stimulation of the soluble guanylate cyclase." Proc Natl Acad Sci U S A **86**(13): 5159-5162.

Ko, C. H. and J. S. Takahashi (2006). "Molecular components of the mammalian circadian clock." Hum Mol Genet **15 Spec No 2**: R271-277.

Kobayashi, T. and R. J. Solaro (2005). "Calcium, thin filaments, and the integrative biology of cardiac contractility." Annu Rev Physiol **67**: 39-67.

Kuschel, M., P. Karczewski, et al. (1999). "Ser16 prevails over Thr17 phospholamban phosphorylation in the beta-adrenergic regulation of cardiac relaxation." Am J Physiol **276**(5 Pt 2): H1625-1633.

Lambert, D. G. (2006). Calcium Signaling Protocols. New Jersey, Humana Press Inc.

Lawrence, C. and G. C. Rodrigo (1999). "A Na+-activated K+ current (IK,Na) is present in guinea-pig but not rat ventricular myocytes." Pflugers Arch **437**(6): 831-838.

Layland, J., J. M. Li, et al. (2002). "Role of cyclic GMP-dependent protein kinase in the contractile response to exogenous nitric oxide in rat cardiac myocytes." J Physiol **540**(Pt 2): 457-467.

Layland, J., R. J. Solaro, et al. (2005). "Regulation of cardiac contractile function by troponin I phosphorylation." Cardiovasc Res **66**(1): 12-21.

Levick, J. R. (2003). An introduction to cardiovascular physiology. London, Arnold.

Levick, J. R. (2013). An introduction to cardiovascular physiology. London, Arnold.

Li, H., Y. Liu, et al. (2010). "Activation of beta 3-Adrenergic Receptor Inhibits Ventricular Arrhythmia in Heart Failure through Calcium Handling." Tohoku Journal of Experimental Medicine **222**(3): 167-174.

Li, L., J. Desantiago, et al. (2000). "Phosphorylation of phospholamban and troponin I in beta-adrenergic-induced acceleration of cardiac relaxation." Am J Physiol Heart Circ Physiol **278**(3): H769-779.

Lim, G., L. Venetucci, et al. (2008). "Does nitric oxide modulate cardiac ryanodine receptor function? Implications for excitation-contraction coupling." Cardiovasc Res **77**(2): 256-264.

Lin, X., H. Jo, et al. (2006). "Beta-adrenergic stimulation does not activate Na+/Ca2+ exchange current in guinea pig, mouse, and rat ventricular myocytes." Am J Physiol Cell Physiol **290**(2): C601-608.

Lohse, M. J., S. Engelhardt, et al. (2003). "What is the role of beta-adrenergic signaling in heart failure?" Circ Res **93**(10): 896-906.

Loscalzo, J. and J. A. Vita (2000). Nitric Oxide and the Cardiovascular System, Humana Press.

Lu, Z. (2004). "Mechanism of rectification in inward-rectifier K+ channels." Annu Rev Physiol **66**: 103-129.

Main, M. J., C. J. Grantham, et al. (1997). "Changes in subsarcolemmal sodium concentration measured by Na-Ca exchanger activity during Na-pump inhibition and beta-adrenergic stimulation in guinea-pig ventricular myocytes." Pflugers Arch **435**(1): 112-118.

Manis, P. B. (2014). Delayed Rectifier and A-Type Potassium Channels. Encyclopedia of Computational Neuroscience. D. Jaeger and R. Jung, Springer New York**: 1-16.

Maron, B. J., J. Kogan, et al. (1994). "Circadian variability in the occurrence of sudden cardiac death in patients with hypertrophic cardiomyopathy." J Am Coll Cardiol **23**(6): 1405-1409.

Martin, S. R., K. Emanuel, et al. (2006). "Are myocardial eNOS and nNOS involved in the beta-adrenergic and muscarinic regulation of inotropy? A systematic investigation." Cardiovasc Res **70**(1): 97-106.

Martino, T., S. Arab, et al. (2004). "Day/night rhythms in gene expression of the normal murine heart." J Mol Med (Berl) **82**(4): 256-264.

Martino, T. A. and M. E. Young (2015). "Influence of the Cardiomyocyte Circadian Clock on Cardiac Physiology and Pathophysiology." J Biol Rhythms **30**(3): 183-205.

Marx, S. O., S. Reiken, et al. (2000). "PKA phosphorylation dissociates FKBP12.6 from the calcium release channel (ryanodine receptor): defective regulation in failing hearts." Cell **101**(4): 365-376.

Massion, P. B., C. Dessy, et al. (2004). "Cardiomyocyte-restricted overexpression of endothelial nitric oxide synthase (NOS3) attenuates beta-adrenergic stimulation and reinforces vagal inhibition of cardiac contraction." Circulation **110**(17): 2666-2672.

Massion, P. B., M. Pelat, et al. (2005). "Regulation of the mammalian heart function by nitric oxide." Comp Biochem Physiol A Mol Integr Physiol **142**(2): 144-150.

Masutani, S., H. J. Cheng, et al. (2013). "beta(3)-Adrenergic receptor antagonist improves exercise performance in pacing-induced heart failure." American Journal of Physiology-Heart and Circulatory Physiology **305**(6): H923-H930.

Matsui, K., T. Kiyosue, et al. (1999). "Effects of pimobendan on the L-type Ca2+ current and developed tension in guinea-pig ventricular myocytes and papillary muscle: comparison with IBMX, milrinone, and cilostazol." Cardiovasc Drugs Ther **13**(2): 105-113.

Mattiazzi, A. and E. G. Kranias (2011). "CaMKII regulation of phospholamban and SR Ca2+ load." Heart Rhythm **8**(5): 784-787.

Meredith, I. T., A. Broughton, et al. (1991). "Evidence of a selective increase in cardiac sympathetic activity in patients with sustained ventricular arrhythmias." N Engl J Med **325**(9): 618-624.

Mery, P. F., S. M. Lohmann, et al. (1991). "Ca2+ current is regulated by cyclic GMP-dependent protein kinase in mammalian cardiac myocytes." Proc Natl Acad Sci U S A **88**(4): 1197-1201.

Mika, D., J. Leroy, et al. (2012). "PDEs create local domains of cAMP signaling." J Mol Cell Cardiol **52**(2): 323-329.

Moens, A. L., R. Yang, et al. (2010). "Beta 3-adrenoreceptor regulation of nitric oxide in the cardiovascular system." J Mol Cell Cardiol **48**(6): 1088-1095.

Mohawk, J. A., C. B. Green, et al. (2012). "Central and peripheral circadian clocks in mammals." Annu Rev Neurosci **35**: 445-462.

Moniotte, S., L. Kobzik, et al. (2001). "Upregulation of beta(3)-adrenoceptors and altered contractile response to inotropic amines in human failing myocardium." Circulation **103**(12): 1649-1655.

Morimoto, A., H. Hasegawa, et al. (2004). "Endogenous beta3-adrenoreceptor activation contributes to left ventricular and cardiomyocyte dysfunction in heart failure." Am J Physiol Heart Circ Physiol **286**(6): H2425-2433.

Movsesian, M. A. (2002). "PDE3 cyclic nucleotide phosphodiesterases and the compartmentation of cyclic nucleotide-mediated signalling in cardiac myocytes." Basic Res Cardiol **97 Suppl 1**: I83-90.

Muller, J. E., P. L. Ludmer, et al. (1987). "Circadian variation in the frequency of sudden cardiac death." Circulation **75**(1): 131-138.

Napp, A., K. Brixius, et al. (2009). "Effects of the beta3-adrenergic agonist BRL 37344 on endothelial nitric oxide synthase phosphorylation and force of contraction in human failing myocardium." J Card Fail **15**(1): 57-67.

Nerbonne, J. M. and R. S. Kass (2005). "Molecular physiology of cardiac repolarization." Physiol Rev **85**(4): 1205-1253.

Nikolaev, V. O., A. Moshkov, et al. (2010). "Beta2-adrenergic receptor redistribution in heart failure changes cAMP compartmentation." Science **327**(5973): 1653-1657.

Niu, X., V. L. Watts, et al. (2012). "Cardioprotective effect of beta-3 adrenergic receptor agonism: role of neuronal nitric oxide synthase." J Am Coll Cardiol **59**(22): 1979-1987.

Nolan, T., R. E. Hands, et al. (2006). "Quantification of mRNA using real-time RT-PCR." Nat Protoc **1**(3): 1559-1582.

Oestreich, E. A., H. Wang, et al. (2007). "Epac-mediated activation of phospholipase C(epsilon) plays a critical role in beta-adrenergic receptor-dependent enhancement of Ca2+ mobilization in cardiac myocytes." J Biol Chem **282**(8): 5488-5495.

Ogden, D. (1994). Microelectrode techniques : the Plymouth Workshop handbook. Cambridge, Company of Biologists.

Osadchii, O. E. (2007). "Cardiac hypertrophy induced by sustained beta-adrenoreceptor activation: pathophysiological aspects." Heart Fail Rev **12**(1): 66-86.

Pabbathi, V. K., Y. H. Zhang, et al. (2002). "Comparison of Na(+)/Ca(2+) exchanger current and of its response to isoproterenol between acutely isolated and short-term cultured adult ventricular myocytes." Biochem Biophys Res Commun **297**(2): 302-308.

Palmer, R. M., D. S. Ashton, et al. (1988). "Vascular endothelial cells synthesize nitric oxide from L-arginine." Nature **333**(6174): 664-666.

Pavlovic, D., A. R. Hall, et al. (2013). "Nitric oxide regulates cardiac intracellular Na(+) and Ca(2)(+) by modulating Na/K ATPase via PKCepsilon and phospholemman-dependent mechanism." J Mol Cell Cardiol **61**: 164-171.

Penna, L. B. and R. A. Bassani (2010). "Increased spontaneous activity and reduced inotropic response to catecholamines in ventricular myocytes from footshock-stressed rats." Stress **13**(1): 73-82.

Pennartz, C. M., M. T. de Jeu, et al. (2002). "Diurnal modulation of pacemaker potentials and calcium current in the mammalian circadian clock." Nature **416**(6878): 286-290.

Pereira, L., M. Metrich, et al. (2007). "The cAMP binding protein Epac modulates Ca2+ sparks by a Ca2+/calmodulin kinase signalling pathway in rat cardiac myocytes." J Physiol **583**(Pt 2): 685-694.

Podrid, P. J. and P. R. Kowey (2001). Cardiac Arrhythmia: Mechanisms, Diagnosis, and Management, Lippincott Williams & Wilkins.

Pogwizd, S. M., K. Schlotthauer, et al. (2001). "Arrhythmogenesis and contractile dysfunction in heart failure: Roles of sodium-calcium exchange, inward rectifier potassium current, and residual beta-adrenergic responsiveness." Circ Res **88**(11): 1159-1167.

Port, J. D. and M. R. Bristow (2001). "Altered beta-adrenergic receptor gene regulation and signaling in chronic heart failure." J Mol Cell Cardiol **33**(5): 887-905.

Portman, M. A. (2001). "Molecular clock mechanisms and circadian rhythms intrinsic to the heart." Circ Res **89**(12): 1084-1086.

Poteser, M., C. Romanin, et al. (2001). "S-nitrosation controls gating and conductance of the alpha 1 subunit of class C L-type Ca(2+) channels." J Biol Chem **276**(18): 14797-14803.

Rochais, F., A. Abi-Gerges, et al. (2006). "A specific pattern of phosphodiesterases controls the cAMP signals generated by different Gs-coupled receptors in adult rat ventricular myocytes." Circ Res **98**(8): 1081-1088.

Rozec, B. and C. Gauthier (2006). "beta3-adrenoceptors in the cardiovascular system: putative roles in human pathologies." Pharmacol Ther **111**(3): 652-673.

Ruiz-Hurtado, G., E. Morel, et al. (2013). "Epac in cardiac calcium signaling." J Mol Cell Cardiol **58**: 162-171.

Sabri, A., E. Pak, et al. (2000). "Coupling function of endogenous alpha(1)- and beta-adrenergic receptors in mouse cardiomyocytes." Circ Res **86**(10): 1047-1053.

Said, M., C. Mundina-Weilenmann, et al. (2002). "The relative relevance of phosphorylation of the Thr(17) residue of phospholamban is different at different levels of beta-adrenergic stimulation." Pflugers Arch **444**(6): 801-809.

Schlotthauer, K. and D. M. Bers (2000). "Sarcoplasmic reticulum Ca(2+) release causes myocyte depolarization. Underlying mechanism and threshold for triggered action potentials." Circ Res **87**(9): 774-780.

Schmitt, N., M. Grunnet, et al. (2014). "Cardiac potassium channel subtypes: new roles in repolarization and arrhythmia." Physiol Rev **94**(2): 609-653.

Schmittgen, T. D. and K. J. Livak (2008). "Analyzing real-time PCR data by the comparative C(T) method." Nat Protoc **3**(6): 1101-1108.

Schram, G., M. Pourrier, et al. (2002). "Differential distribution of cardiac ion channel expression as a basis for regional specialization in electrical function." Circ Res **90**(9): 939-950.

Schulz, R., T. Rassaf, et al. (2005). "Recent advances in the understanding of the role of nitric oxide in cardiovascular homeostasis." Pharmacol Ther **108**(3): 225-256.

Scriven, D. R., P. Dan, et al. (2000). "Distribution of proteins implicated in excitation-contraction coupling in rat ventricular myocytes." Biophys J **79**(5): 2682-2691.

Sears, C. E., E. A. Ashley, et al. (2004). "Nitric oxide control of cardiac function: is neuronal nitric oxide synthase a key component?" Philos Trans R Soc Lond B Biol Sci **359**(1446): 1021-1044.

Sears, C. E., S. M. Bryant, et al. (2003). "Cardiac neuronal nitric oxide synthase isoform regulates myocardial contraction and calcium handling." Circ Res **92**(5): e52-59.

Seddon, M., A. M. Shah, et al. (2007). "Cardiomyocytes as effectors of nitric oxide signalling." Cardiovasc Res **75**(2): 315-326.

Sher, A. A., P. J. Noble, et al. (2008). "The role of the Na+/Ca2+ exchangers in Ca2+ dynamics in ventricular myocytes." Prog Biophys Mol Biol **96**(1-3): 377-398.

Solaro, R., J. (2011). Regulation of Cardiac Contractility. San Rafael (CA), Morgan & Claypool Life Sciences.

Song, Q., J. J. Saucerman, et al. (2008). "Differential integration of Ca2+-calmodulin signal in intact ventricular myocytes at low and high affinity Ca2+-calmodulin targets." J Biol Chem **283**(46): 31531-31540.

Song, Y., J. C. Shryock, et al. (2001). "Selective attenuation by adenosine of arrhythmogenic action of isoproterenol on ventricular myocytes." Am J Physiol Heart Circ Physiol **280**(6): H2789-2795.

Stefenelli, T., J. Wikman-Coffelt, et al. (1990). "Calcium-dependent fluorescence transients during ventricular fibrillation." Am Heart J **120**(3): 590-597.

Storch, K. F., O. Lipan, et al. (2002). "Extensive and divergent circadian gene expression in liver and heart." Nature **417**(6884): 78-83.

Stoyanovsky, D., T. Murphy, et al. (1997). "Nitric oxide activates skeletal and cardiac ryanodine receptors." Cell Calcium **21**(1): 19-29.

Strosberg, A. D. (1997). "Structure and function of the beta 3-adrenergic receptor." Annu Rev Pharmacol Toxicol **37**: 421-450.

Sun, J., E. Picht, et al. (2006). "Hypercontractile female hearts exhibit increased S-nitrosylation of the L-type Ca2+ channel alpha1 subunit and reduced ischemia/reperfusion injury." Circ Res **98**(3): 403-411.

Sun, J., C. Steenbergen, et al. (2006). "S-nitrosylation: NO-related redox signaling to protect against oxidative stress." Antioxid Redox Signal **8**(9-10): 1693-1705.

Sun, J., N. Yamaguchi, et al. (2008). "Regulation of the cardiac muscle ryanodine receptor by O(2) tension and S-nitrosoglutathione." Biochemistry **47**(52): 13985-13990.

Takimoto, E. (2012). "Cyclic GMP-dependent signaling in cardiac myocytes." Circ J **76**(8): 1819-1825.

Tamargo, J., R. Caballero, et al. (2004). "Pharmacology of cardiac potassium channels." Cardiovasc Res **62**(1): 9-33.

Tang, L., H. Wang, et al. (2014). "Targeting NOS as a therapeutic approach for heart failure." Pharmacol Ther **142**(3): 306-315.

Tomaselli, G. F. and D. P. Zipes (2004). "What causes sudden death in heart failure?" Circ Res **95**(8): 754-763.

Treuer, A. V. and D. R. Gonzalez (2015). "Nitric oxide synthases, S-nitrosylation and cardiovascular health: from molecular mechanisms to therapeutic opportunities (review)." Mol Med Rep **11**(3): 1555-1565.

Tristani-Firouzi, M., J. Chen, et al. (2001). "Molecular biology of K(+) channels and their role in cardiac arrhythmias." Am J Med **110**(1): 50-59.

Umar, S. and A. van der Laarse (2010). "Nitric oxide and nitric oxide synthase isoforms in the normal, hypertrophic, and failing heart." Mol Cell Biochem **333**(1-2): 191-201.

Vallance, P. and N. Chan (2001). "Endothelial function and nitric oxide: clinical relevance." Heart **85**(3): 342-350.

van der Heyden, M. A., T. J. Wijnhoven, et al. (2005). "Molecular aspects of adrenergic modulation of cardiac L-type Ca2+ channels." Cardiovasc Res **65**(1): 28-39.

Van Hove, C. E., C. Van der Donckt, et al. (2009). "Vasodilator efficacy of nitric oxide depends on mechanisms of intracellular calcium mobilization in mouse aortic smooth muscle cells." Br J Pharmacol **158**(3): 920-930.

Vandsburger, M. H., B. A. French, et al. (2007). "Multi-parameter in vivo cardiac magnetic resonance imaging demonstrates normal perfusion reserve despite severely attenuated beta-adrenergic functional response in neuronal nitric oxide synthase knockout mice." Eur Heart J **28**(22): 2792-2798.

Vandsburger, M. H., B. A. French, et al. (2012). "Displacement-encoded and manganese-enhanced cardiac MRI reveal that nNOS, not eNOS, plays a dominant role in modulating contraction and calcium influx in the mammalian heart." Am J Physiol Heart Circ Physiol **302**(2): H412-419.

Varghese, P., R. W. Harrison, et al. (2000). "beta(3)-adrenoceptor deficiency blocks nitric oxide-dependent inhibition of myocardial contractility." J Clin Invest **106**(5): 697-703.

Varro, A., D. A. Lathrop, et al. (1993). "Ionic currents and action potentials in rabbit, rat, and guinea pig ventricular myocytes." Basic Res Cardiol **88**(2): 93-102.

Veldkamp, M. W., A. C. van Ginneken, et al. (1995). "Delayed rectifier channels in human ventricular myocytes." Circulation **92**(12): 3497-3504.

Venetucci, L. A., A. W. Trafford, et al. (2008). "The sarcoplasmic reticulum and arrhythmogenic calcium release." Cardiovasc Res **77**(2): 285-292.

Vrydag, W. and M. C. Michel (2007). "Tools to study beta3-adrenoceptors." Naunyn Schmiedebergs Arch Pharmacol **374**(5-6): 385-398.

Wallukat, G. (2002). "The beta-adrenergic receptors." Herz **27**(7): 683-690.

Walsh, K. B., T. B. Begenisich, et al. (1988). "Beta-adrenergic modulation in the heart. Independent regulation of K and Ca channels." Pflugers Arch **411**(2): 232-234.

Walsh, K. B. and R. S. Kass (1988). "Regulation of a heart potassium channel by protein kinase A and C." Science **242**(4875): 67-69.

Wang, H., M. J. Kohr, et al. (2008). "Neuronal nitric oxide synthase signaling within cardiac myocytes targets phospholamban." Am J Physiol Cell Physiol **294**(6): C1566-1575.

Wang, H., M. J. Kohr, et al. (2008). "Endothelial nitric oxide synthase decreases beta-adrenergic responsiveness via inhibition of the L-type Ca2+ current." Am J Physiol Heart Circ Physiol **294**(3): H1473-1480.

Wang, W., W. Zhu, et al. (2004). "Sustained beta1-adrenergic stimulation modulates cardiac contractility by Ca2+/calmodulin kinase signaling pathway." Circ Res **95**(8): 798-806.

Weiss, J. N., A. Garfinkel, et al. (2010). "Early afterdepolarizations and cardiac arrhythmias." Heart Rhythm **7**(12): 1891-1899.

Wier, W. G., T. M. Egan, et al. (1994). "Local control of excitation-contraction coupling in rat heart cells." J Physiol **474**(3): 463-471.

Willich, S. N., D. Levy, et al. (1987). "Circadian variation in the incidence of sudden cardiac death in the Framingham Heart Study population." Am J Cardiol **60**(10): 801-806.

Witte, K., R. Parsa-Parsi, et al. (1995). "Mechanisms of the circadian regulation of beta-adrenoceptor density and adenylyl cyclase activity in cardiac tissue from normotensive and spontaneously hypertensive rats." J Mol Cell Cardiol **27**(5): 1195-1202.

Wrobel, J. and G. Nagel (1979). "Diurnal rhythm of active calcium transport in rat intestine." Experientia **35**(12): 1581-1582.

Wu, Y. and M. E. Anderson (2000). "Ca2+-activated non-selective cation current in rabbit ventricular myocytes." J Physiol **522 Pt 1**: 51-57.

Xiao, B., M. T. Jiang, et al. (2005). "Characterization of a novel PKA phosphorylation site, serine-2030, reveals no PKA hyperphosphorylation of the cardiac ryanodine receptor in canine heart failure." Circ Res **96**(8): 847-855.

Xiao, B., G. Zhong, et al. (2006). "Ser-2030, but not Ser-2808, is the major phosphorylation site in cardiac ryanodine receptors responding to protein kinase A activation upon beta-adrenergic stimulation in normal and failing hearts." Biochem J **396**(1): 7-16.

Xiao, R. P. (2001). "Beta-adrenergic signaling in the heart: dual coupling of the beta2-adrenergic receptor to G(s) and G(i) proteins." Sci STKE **2001**(104): re15.

Xiao, R. P., P. Avdonin, et al. (1999). "Coupling of beta2-adrenoceptor to Gi proteins and its physiological relevance in murine cardiac myocytes." Circ Res **84**(1): 43-52.

Xiao, R. P., X. Ji, et al. (1995). "Functional coupling of the beta 2-adrenoceptor to a pertussis toxin-sensitive G protein in cardiac myocytes." Mol Pharmacol **47**(2): 322-329.

Xiao, R. P. and E. G. Lakatta (1993). "Beta 1-adrenoceptor stimulation and beta 2-adrenoceptor stimulation differ in their effects on contraction, cytosolic Ca2+, and Ca2+ current in single rat ventricular cells." Circ Res **73**(2): 286-300.

Xu, K. Y., D. L. Huso, et al. (1999). "Nitric oxide synthase in cardiac sarcoplasmic reticulum." Proc Natl Acad Sci U S A **96**(2): 657-662.

Xu, L., J. P. Eu, et al. (1998). "Activation of the cardiac calcium release channel (ryanodine receptor) by poly-S-nitrosylation." Science **279**(5348): 234-237.

Yamada, M., K. Ohta, et al. (2008). "Contribution of L-type Ca2+ channels to early afterdepolarizations induced by I Kr and I Ks channel suppression in guinea pig ventricular myocytes." J Membr Biol **222**(3): 151-166.

Yamashita, T., A. Sekiguchi, et al. (2003). "Circadian variation of cardiac K+ channel gene expression." Circulation **107**(14): 1917-1922.

Yan, Z. Y., T. Ban, et al. (2015). "Na+-induced Ca2+ influx through reverse mode of Na+-Ca2+ exchanger in mouse ventricular cardiomyocyte." Oncotarget.

Yang, L., G. Liu, et al. (2007). "Protein kinase G phosphorylates Cav1.2 alpha1c and beta2 subunits." Circ Res **101**(5): 465-474.

Young, M. E. (2003). "Circadian rhythms in cardiac gene expression." Curr Hypertens Rep **5**(6): 445-453.

Young, M. E. (2006). "The circadian clock within the heart: potential influence on myocardial gene expression, metabolism, and function." Am J Physiol Heart Circ Physiol **290**(1): H1-16.

Young, M. E., P. Razeghi, et al. (2001). "Intrinsic diurnal variations in cardiac metabolism and contractile function." Circ Res **89**(12): 1199-1208.

Young, M. E., P. Razeghi, et al. (2001). "Clock genes in the heart: characterization and attenuation with hypertrophy." Circ Res **88**(11): 1142-1150.

Zhang, Y. H. and B. Casadei (2012). "Sub-cellular targeting of constitutive NOS in health and disease." J Mol Cell Cardiol **52**(2): 341-350.

Zhang, Y. H., M. H. Zhang, et al. (2008). "Reduced phospholamban phosphorylation is associated with impaired relaxation in left ventricular myocytes from neuronal NO synthase-deficient mice." Circ Res **102**(2): 242-249.

Zhang, Z. S., H. J. Cheng, et al. (2005). "Enhanced inhibition of L-type Ca2+ current by beta3-adrenergic stimulation in failing rat heart." J Pharmacol Exp Ther **315**(3): 1203-1211.

Zhou, L., P. Zhang, et al. (2011). "Altered circadian rhythm of cardiac beta3-adrenoceptor activity following myocardial infarction in the rat." Basic Res Cardiol **106**(1): 37-50.

Zhou, S., A. Y. Tan, et al. (2008). "Antiarrhythmic effects of beta3-adrenergic receptor stimulation in a canine model of ventricular tachycardia." Heart Rhythm **5**(2): 289-297.

Ziolo, M. T. (2008). "The fork in the nitric oxide road: cyclic GMP or nitrosylation?" Nitric Oxide **18**(3): 153-156.

Ziolo, M. T., M. J. Kohr, et al. (2008). "Nitric oxide signaling and the regulation of myocardial function." J Mol Cell Cardiol **45**(5): 625-632.

Zipes, D. P., and Jalife, J. (2014). Cardiac Electrophysiology: From Cell to Bedside. Philadelphia, Elsevier.

Zipes, D. P., Libby, P., Bonow, R.O. and Braunwald, E. (2012). Braunwald's Heart Disease: A Textbook of Cardiovascular Medicine. BRAUNWALD'S HEART DISEASE: A TEXTBOOK OF CARDIOVASCULAR MEDICINE, Chapter 25: Pathophysiology of Heart Disease. Philadelphia, USA, Elsevier Saunders**:** 487-503.